UNIVERSITY OF SOUTHAMPTON
Faculty of Engineering and Applied Science
School of Electronics and Computer Science
Southampton SO17 1BJ

Interference Suppression in Single- and Multi-Carrier CDMA Systems

by

Hua Wei
B.Eng.

A doctoral thesis submitted in partial fulfilment of the requirements for the award of Doctor of Philosophy at the University of Southampton

April 2005

SUPERVISOR: Professor Lajos Hanzo
FREng, FIEEE, FIEE, DSc
Chair of Telecommunications
School of Electronics and Computer Science
University of Southampton
Southampton SO17 1BJ
United Kingdom.

Dedicated to my parents.

UNIVERSITY OF SOUTHAMPTON

ABSTRACT

Faculty of Engineering and Applied Science
School of Electronics and Computer Science

Doctor of Philosophy

Interference Suppression in Single- and Multi-Carrier CDMA Systems

by Hua Wei

In this dissertation we aimed for investigating numerous interference suppressing techniques designed for CDMA communications systems, which include *chip-waveform optimization, spreading code optimization*, and *multiuser detection*. We investigated the achievable performance in conjunction with the various time-limited and band-limited chip-waveforms. Our study showed that the *raised cosine chip-waveform* based DS-CDMA scheme was capable of achieving a similar performance to that of the so-called optimum waveform based DS-CDMA arrangement, when aiming for an energy containment in excess of 99%. In the context of *spreading code optimization*, we comparatively studied LAS-CDMA and traditional DS-CDMA systems communicating over a Nakagami-m fading channel. The employment of LAS spreading codes is capable of suppressing both the multiple access interference (MAI) and multi-path interference (MPI), hence LAS-CDMA exhibited a significantly better performance than that of the traditional random code based DS-CDMA system in a quasi-synchronous channel. Considering the *receiver optimization* techniques, we investigated several multiuser detectors, which include iterative multiuser detectors, genetic algorithm (GA) aided multiuser detectors, M-algorithm (MA) assisted multiuser detectors, blind multiuser detectors, as well as combined GA and Radial Basis Function (GA-RBF) assisted multiuser detectors. Following the philosophy of turbo equalization, the iterative multiuser detector investigated utilized the soft outputs of the channel decoder for soft interference cancellation. This specific detector was capable of significantly improving the achievable performance. We comparatively investigated both GA aided and M-algorithm assisted multiuser detectors designed for DS-CDMA systems. Furthermore, we studied an RBF based multiuser detector and invoked a GA for reducing its complexity. The GA-RBF assisted MUD exhibited a significantly lower complexity than that of the conventional RBF network based multiuser detector. We also proposed GA assisted multiuser detectors designed for MC-CDMA systems, which constitute a low-complexity suboptimal MUD technique applicable to both synchronous and asynchronous MC-CDMA systems communicating over frequency selective fading channels. Our simulation results showed that the GA assisted multiuser detector achieves a significant complexity reduction in comparison to Verdu's optimum MUD, which may be as high as a factor of 1000, when the number of user is $K = 20$. We also investigated the family of subspace based blind multiuser detectors designed for MC-CDMA systems using antenna arrays, which only require the prior knowledge of the signature waveform and the timing of the reference user, but not of the interfering users. Finally, we studied joint time- and frequency-domain spreading assisted MC DS-CDMA.

Acknowledgements

First, I would like thank to my supervisor Professor Lajos Hanzo for his continual encouragement and enthusiasm. Over the past three years or so, his enthusiasm in searching for new ideas in mobile communications has always inspired and motivated me to reach new peaks, which I never dreamed of accomplishing. What I have learned from him is not just a range of solutions to the mobile communication problems, but his inspirational insights, his way of conducting research and his art of living. I guess I will never forget the nights when we solved problems at 12:00pm. I could hardly ask for more from a supervisor. My sincere thanks go to the Mobile VCE, UK and to the British Council for supporting my research financially. My research could not have been finished without the aid of my friends in our group. Mong Suan Yee introduced me to my first research project and Lie Liang Yang answered many of my ignorant questions. I am also indebted to Byoung Jo Choi, Xing Yao Wu, Feng Guo, Song Ni, Bin Hu, Jin Wang, Soon Xin Ng, Bee Leong Yeap, Ming Jiang, Xiang Liu, Wei Liu, Sohail Ahmed, Nurul Nadia Ahmad, Mohamad Yusoff Alias, Jin Yee Chung for their wonderful friendship and their warm encouragement. I want to say a big thank you to Denise Harvey and Rebecca Earl for providing us with practical day-to-day assistance. I would also like to thank my parents and my sisters in China for the invaluable understanding and encouragement. Finally, I would like to thank my wife Jing Wang, you are the best.

List of Publications

1. H. Wei, S. X. Ng and L. Hanzo, "Coded Modulation Assisted Iterative Parallel Interference Cancellation Aided CDMA", *In Proceedings of the IEEE Vehicular Technology Conference (VTC) 2003 Fall*, pp. 1109-1113, Orlando, Florida, USA.
2. L-L. Yang, H. Wei and L. Hanzo, "A Multicarrier DS-CDMA System Using Both Time-Domain and Frequency-Domain Spreading", *In Proceedings of the IEEE Vehicular Technology Conference (VTC) 2003 Fall*, pp. 2426-2430, Orlando, Florida, USA.
3. L-L. Yang, H. Wei and L. Hanzo, "Multiuser Detection in Multicarrier CDMA Systems Employing Both Time-Domain and Frequency-Domain Spreading", *In Proceedings of PIMRC'2003*, pp. 1840-1844, Beijing, China.
4. S. Ni, H. Wei, J. S. Blogh and L. Hanzo, "Network Performance of Asynchronous UTRA-like FDD/CDMA Systems using Loosely Synchronized Spreading Codes." *In Proceedings of the IEEE Vehicular Technology Conference (VTC) 2003 Fall*, pp. 1359-1363, Orlando, Florida, USA.
5. H. Wei and L. Hanzo, "Reduced-Complexity Near-Optimum Genetic Algorithm Assisted Multiuser Detection for Synchronous Multicarrier CDMA", *In Proceedings of the IEEE Vehicular Technology Conference (VTC) 2004 Spring*, Milan, Italy.
6. H. Wei and L. Hanzo, "Semi-Blind and Group-Blind Multiuser Detection for the Uplink MC-CDMA", *In Proceedings of the IEEE Vehicular Technology Conference (VTC) 2004 Spring*, Milan, Italy.
7. B.L. Yeap, F. Guo, E.L. Kuan, H. Wei and L. Hanzo, "Blind Per-Survivor Processing-Based Multiuser Detection for Channel-coded Multicarrier DS-CDMA Systems", *In Proceedings of the IEEE Vehicular Technology Conference (VTC) 2004 Spring*, Milan, Italy.
8. H. Wei and L. Hanzo, "Genetic Algorithm Assisted Multiuser Detection for Asynchronous Multicarrier CDMA", *In Proceedings of the IEEE Vehicular Technology Conference (VTC) 2004 Fall*, Los Angeles, USA.

9. H. Wei, L-L. Yang and L. Hanzo, "Time- and frequency-domain spreading assisted MC DS-CDMA using interference rejection spreading codes for quasi-synchronous communications", *In Proceedings of the IEEE Vehicular Technology Conference (VTC) 2004 Fall*, Los Angeles, USA.
10. H. Wei and L. Hanzo "Reduced-Complexity Genetic Algorithm Aided and Radial Basis Function Assisted Multiuser Detection for Synchronous CDMA", *European Signal Processing Conference (EUSIPCO)* Sep. 2004, pp. 157-160, Vienna, Austria.
11. J.Y. Chung, H. Wei and L. Hanzo, "Space-Time Spreading Assisted Adaptive QAM Aided Multicarrier DS-CDMA VideoTelephony", *IEE International Conference on 3G Mobile Communication Technologies (3G 2004)*, 18 - 20 October 2004, pp. 148-152, London, UK
12. H. Wei and L. Hanzo, "On the Uplink Performance of RAKE-Receiver Assisted Band-Limited DS-CDMA Systems Over Nakagami Channels", *IEE International Conference on 3G Mobile Communication Technologies (3G 2004)*, 18 - 20 October 2004, pp. 312-316, London, UK
13. J.Y. Chung, H. Wei and L. Hanzo, "Iterative Parallel Interference Cancellation Aided CDMA Based MPEG-4 Video Telephony", *IEE International Conference on 3G Mobile Communication Technologies (3G 2004)*, 18 - 20 October 2004, pp. 307-311, London, UK
14. H. Wei and L. Hanzo, "Chapter 6: Iterative PIC using Turbo Codes, LDPC codes, TCM and TTCM" in L. Hanzo, L-L. Yang, E-L. Kuan and K. Yen, *"Single- and Multi-Carrier DS-CDMA"*, New York, USA: John Wiley, IEEE Press, 2003, pp. 227-250.
15. H. Wei and L. Hanzo, "Chapter 14: GA-Assisted Multiuser Detection for MC-CDMA" in L. Hanzo, L-L. Yang, E-L. Kuan and K. Yen, *"Single- and Multi-Carrier DS-CDMA"*, New York, USA: John Wiley, IEEE Press, 2003, pp. 433-459.
16. H. Wei, L-L. Yang and L. Hanzo, "Interference-Free Broadband Single- and Multi-Carrier DS-CDMA", *IEEE Communication Magazine*, pp. 68-72, Feb, 2005.
17. H. Wei and L. Hanzo, "On the Uplink Performance of LAS-CDMA", *To appear in the Proceedings of IEEE VTC'05 Spring.*
18. S. Ni, H. Wei and L. Hanzo, "Loosely Synchronized Spreading Code Aided Network Performance of Quasi-Synchronous UTRA-like TDD/CDMA Systems", *To appear in the Proceedings of IEEE VTC'05 Spring.*,
19. H. Wei and L. Hanzo, "On the Performance Benefits of Large Area Synchronized Multicarrier DS-CDMA", *submitted to Electronics Letters.*
20. H. Wei and L. Hanzo, "On the Performance of LAS-CDMA", *To appear in IEEE Transactions on Wireless Communications*
21. H. Wei and L. Hanzo, "On the Uplink Performance of Band-Limited DS-CDMA Over Nakagami-m Channels", *submitted to IEEE Transactions on Wireless Communications*

22. L-L. Yang, H. Wei and L. Hanzo, "Low-Complexity Multiuser Detection of Time- and Frequency-Domain Spread Multicarrier Code-Division Multiple-Access", *submitted to IEEE Transactions on Vehicular Technology.*
23. H. Wei and L. Hanzo, "Downlink Spreading Assisted DS-CDMA Using Interference Rejection Codes", *submitted to IEEE Transactions on Vehicular Technology.*
24. H. Wei and L. Hanzo, "Time- and Frequency-Domain Spreading Assisted MC DS-CDMA Using Interference Rejection Codes" *submitted to IEEE Transactions on Vehicular Technology.*
25. H. Wei and L. Hanzo, "A Space-Time Spreading Assisted Multicarrier DS-CDMA System Using OVSF codes and Adaptive Modulation", *submitted to IEEE VTC'05 Fall.*
26. X. Liu, H. Wei and L. Hanzo, "Analytical BER Performance of Asynchronous DS-CDMA Ad Hoc Networks Using Large Area Synchronized Spreading Codes Having an Interference-Free Window", *submitted to IEEE VTC'05 Fall.*

Contents

CHAPTER 1

Introduction

1.1 Introduction to Wireless Access Technology

Traditional wireless access techniques are constituted by Frequency Division Multiple Access (FDMA) [1], Time Division Multiple Acess (TDMA) [1], Code Division Multiple Access (CDMA) [2, 3], and Space Division Multiple Access (SDMA) [4, 5]. The multiple access philosophy of all these access techniques is depicted in Figure 1.1. In FDMA, as seen in Figure 1.1(a), we partition the available frequency bandwidth into a number of sub-bands, where each user has a dedicated frequency-band for its communications. The first generation analogue mobile system, which was known as the Advanced Mobile Phone System (AMPS), employed the FDMA principle as its access technology. In the TDMA regime of Figure 1.1(b) the time-dimension is divided into a number of time slots, where each user is assigned to a dedicated time slot when it communicates. A combination of TDMA and frequency-division uplink/downlink duplexing was used in the digital mobile standard, known as Global System of Mobile (GSM) [6], which was the first representative of the family of second generation (2G) mobile communication systems.

As shown in Figure 1.1(c) in a CDMA system, all the users share the same frequency bandwidth, all the time, when they transmit, but each user is distinguished by its unique, user-specific Pseudo-random Noise (PN) based spreading code. The philosophy of CDMA originates from the military Spread Spectrum (SS) communication principle, where the term "spread" implies that the transmission bandwidth is significantly higher than that required by the information signal. According to the specific procedure used for spreading the information signal to the high-bandwidth spread signal, there exist numerous different CDMA systems, which are classified in Figure 1.2. The family of spread spectrum communication systems includes three basic techniques, namely Directly Sequence

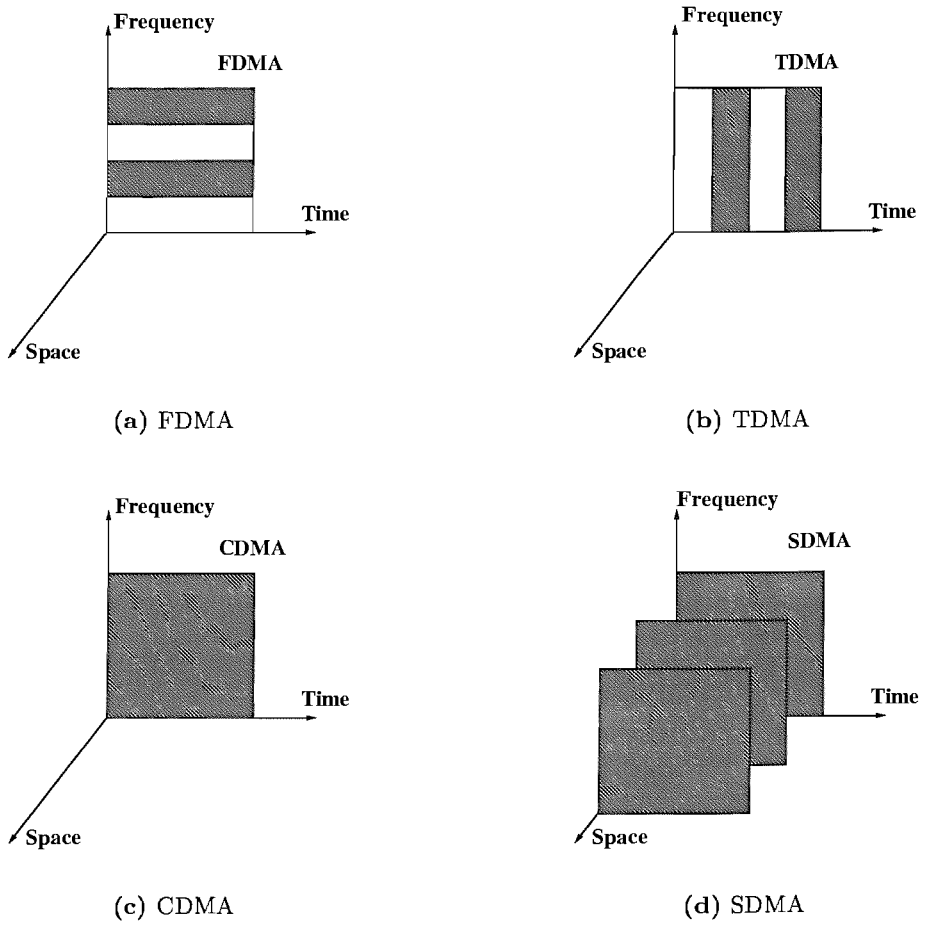

Figure 1.1: Wireless access schemes

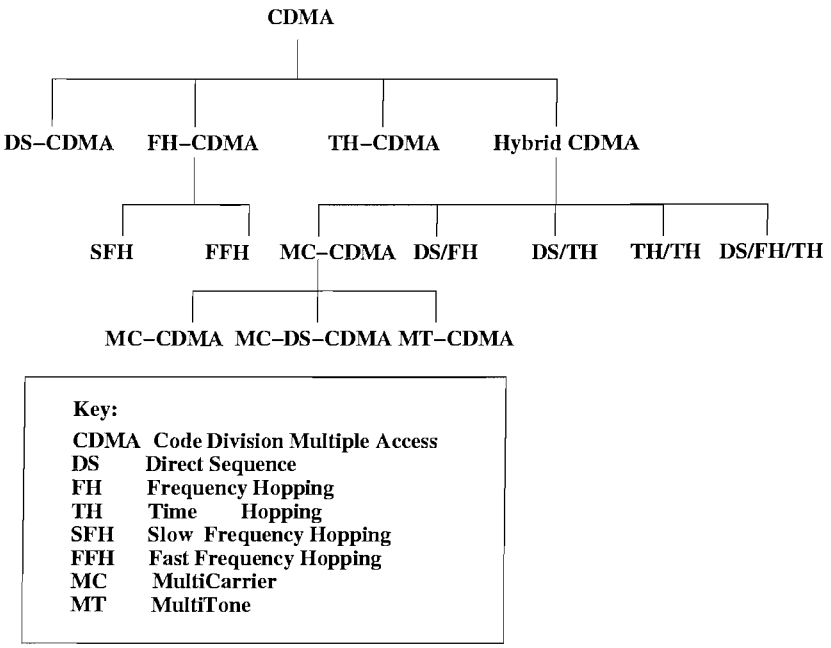

Figure 1.2: Classification of CDMA schemes according to the modulation method used for obtaining the spread signal.

CDMA (DS-CDMA) [3], Frequency Hopping aided CDMA (FH-CDMA) [4] and Time Hopping CDMA (TH-CDMA) [7]. Furthermore, as seen in Figure 1.2, numerous hybrid CDMA systems can be created by combining the above techniques. In DS-CDMA, a pseudo-random noise sequence is used for directly modulating the information bits, which results in a high-bandwidth DS-spread signal. In a FH-CDMA system the total transmission bandwidth is divided into a number of sub-bands, which have a bandwidth that is equal to the bandwidth of the original information signal. Then a pseudo-noise code is used for selecting a set of consecutive sub-bands for the transmission of information during successive hops, which are controlled by the so-called Frequency Hopping Pattern (FHP). There are two categories of FH-CDMA, namely Slow Frequency Hopping (SFH) and Fast Frequency Hopping (FFH). In SFH, the rate of frequency hopping is lower than the symbol rate, hence typically several symbols are transmitted in each FH sub-band. In contrast to SFH, the rate of frequency hopping in FFH is higher than the rate of the transmission symbol stream, resulting in several hops across a number of sub-bands during the transmission of a single information bit. DS-CDMA and FH-CDMA constitute the most common forms of spread spectrum signalling techniques. Another spread spectrum based signalling method, which is analogous to FH, is the so-called Time Hopping (TH) technique [7]. In TH, a time interval, which is selected to be significantly longer than the reciprocal of the information rate, is subdivided into a number of time slots. The information symbols are transmitted in pseudo-randomly selected time slots as a block of one or more symbols. The terminology of hybrid CDMA encompasses a group of techniques that combine two or more of the above-mentioned spread spectrum techniques. One of these hybrid techniques, known as MultiCarrier CDMA (MC-CDMA), enjoyed growing interest in recent years. Prasad and Hara [8] provided an excellent overview of MC-CDMA systems. Briefly, MC-CDMA schemes may be classified into three categories, namely frequency domain spreading MultiCarrier CDMA (MC-CDMA) [4], MultiCarrier Direct Sequence CDMA (MC-DS-CDMA) [3] and MultiTone (MT-CDMA) [8]. Their common characteristic is that a spreading code is used for spreading a user's signal either in the time or in the frequency domain, and that more than one carrier frequency is used for transmission. In recent years, a number of novel hybrid CDMA schemes were proposed. For example, in reference [9], a novel SFH assisted MC-CDMA scheme was proposed by Yang and Hanzo. For more detailed information on a range of other multiple access schemes, the reader is referred to the excellent monographs by Viterbi [10], Prasad [11], Glisic and Leppänen [1], as well as Glisic and Vucetic [2].

CDMA techniques have been standardized in the context of several second generation (2G) [12] and third generation (3G) mobile systems [3]. More explicitly, the DS-CDMA technique was first ratified in the context of the Interim Standard-95 (IS-95) [3, 12] in the United States in 1995. In June 1998, the Wideband-CDMA (W-CDMA) [3, 13] and UMTS Terrestrial Radio Access (UTRA) [3, 14] were selected for employment in the 3G mobile radio systems by the International Telecommunications Union (ITU), both of which are based on DS-CDMA techniques. The cdma2000 standard [3, 15], which is based on MC-CDMA using three subcarriers, was also accepted as a candidate for 3G mobile

communications by the ITU. Furthermore, the Time-Duplex (TD), smart antenna aided CDMA (TD-SCDMA) [16] system proposed by China was also ratified by the ITU.

Finally, at the time of writing the least exploited wireless access method is Space Division Multiple Access (SDMA) [3, 4]. The spatial dimension can be utilized for partitioning the users, where according to the terminology of spatial access users are spatially separated from each other. As an example, in the TD-SCDMA [16] standard, SDMA techniques are invoked for reducing the multiple access interference. The basic principles of SDMA may be augmented with the aid of two specific examples. In the context of beamforming techniques [5] spatially selective beams are created for the sake of forming a high-gain antenna beam in the direction of several multipath components arriving from the wanted user. This allows the receiver to coherently combine all the useful signal energy arriving from the wanted user via a multiplicity of propagation path. By contrast, the beamformer creates spatially selective beams for nulling the multipath components of the interfering users. Whilst this technique potentially reduces the number of resolvable multipath components combined by the beamformer and hence reduces the achievable diversity gain, it reduces the effects of multiuser interference quite significantly and hence has the potential of doubling the achievable user capacity [5]. As a second application of SDMA principles, in [4] multiple antenna elements were exploited for supporting multiple users in the uplink of OFDM based Multicarrier CDMA. The operating philosophy of these systems is that provided we have an accurate channel estimator, the individual users may be distinguished even within the same bandwidth on the basis their unique user-specific Channel Impulsive Response (CIR) or channel transfer function.

Each of the above access techniques has its advantages and disadvantages. For example, GSM, requires sophisticated frequency/time management for monitoring, which users are supported in which frequency/time slot combination. The benefit of this is that the channels are intended to be orthogonal, hence the effects of cochannel interference can be readily controlled. Channel equalization and frequency hopping is utilized in GSM for minimizing the Inter-Symbol Interference (ISI) and fading effects. By contrast, an advantage of DS-CDMA is that it has the ability of resolving multipath components with the aid of a RAKE receiver as discussed in [10]. More specifically, the RAKE-fingers coherently combine the differently delayed, attenuated and phase-rotated signal components, hence achieving a diversity gain, which can be increased upon increasing the number of RAKE-fingers combined. However, Rake-combining aided CDMA requires strict power control, so that the "near-far" effect is minimized. This effect occurs, when users near the transmitter benefit from a higher received power than those far away. Hence the distant users suffer a performance degradation owing the high-power co-channel interferers. CDMA exploits the orthogonality of the spreading codes, provided that the codes' orthogonality is not destroyed by fading. However, in realistic mobile environments, the codes' orthogonality is rarely maintained, especially in an uplink scenario, since the mobiles transmit asynchronously and from different distances. Therefore, owing to the multipath effects and as a consequence of the difficulties in maintaining perfect chip synchronization of all users in the uplink, the orthogonality of the spreading codes is typically destroyed.

Hence, CDMA systems suffer from Multiple Access Interference (MAI) and the capacity of CDMA is typically "interference-limited". In the next section, we will consider a range of methods designed for reducing the effects of MAI. More specifically, numerous methods have been proposed for reducing the amount of MAI imposed on the received signal, such as for example power control [17], the optimization of user signature sequences [18–20] and the employment of sectorised antennas [21] or sophisticated beamforming techniques [5]. Nevertheless, these techniques have their limitations in combating the effects of MAI, especially in conjunction with conventional single-user detectors. The inherent reason is that single-user detectors treat the MAI as "noise", rather than useful "information", even though the base station has to demodulate the signals received for all the users supported within the propagation cell considered. In order to avoid this impediment and to efficiently utilize all the information received, numerous multiuser detectors [22] were proposed in literature [3], some of which are reviewed in the forthcoming sections.

1.2 Interference Suppression Techniques Designed for CDMA Systems

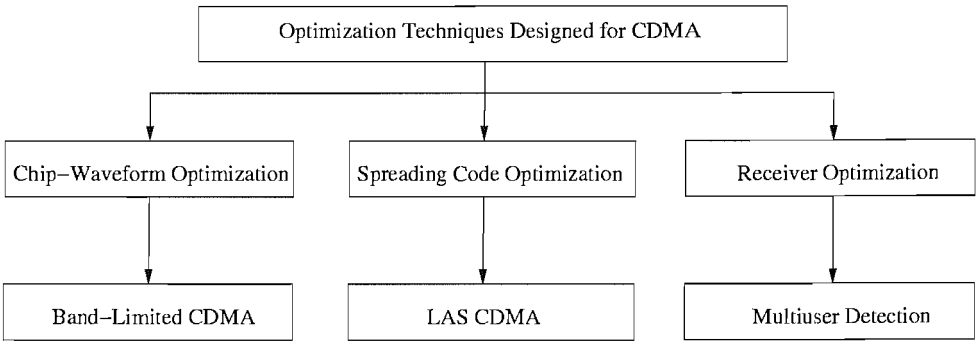

Figure 1.3: Optimization of CDMA systems

Reducing the effect of MAI and MPI plays a crucial role in CDMA communications systems. In this dissertation we discuss a range of CDMA transceiver techniques, which are summarized in Figure 1.3, namely the chip-waveform optimization problem, the spreading code optimization problem and multiuser detection. More explicitly, in Chapter 2 we studied the problem of chip-waveform optimization, investigating which chip-waveform exhibits the best performance in the context of having a fixed bandwidth and bit error rate. For example, we often investigated the DS-CDMA system in conjunction with the rectangular chip-waveform. However, the rectangular chip-waveform requires an infinite bandwidth and owing to its high out-of-band emission it induces adjacent channel interference, also inflicting a high amount of MAI. Hence, in Chapter 2 we investigated the performance of DS-CDMA using various chip-waveforms in the context of the same fixed bandwidth. The waveforms considered include the rectangular chip-waveform, half-sine chip-waveform, time-limited raised-cosine chip-waveform, band-limited raised-cosine chip-waveform [7] and the bandlimited optimum chip-waveform of [23]. We determined the best chip-waveform in different scenarios.

Furthermore, the choice of a suitable spreading code is also important for the sake of attaining a good performance in the CDMA communication system considered. Hence, the second optimization problem studied in this dissertation is related to the choice of a suitable spreading code for employment in quasi-synchronous DS-CDMA systems. Traditional spreading sequences, such as m-sequences [3], Gold codes [3] and Kasami codes [3] exhibit non-zero off-peak auto-correlations and cross-correlations, which result in a high MAI in case of asynchronous uplink transmissions. Another family of spreading codes is constituted by classic orthogonal Walsh codes [3] and orthogonal Gold codes, which however retain their orthogonality only in case of perfectly synchronous transmissions, while exhibiting non-zero off-peak auto-correlations and cross-correlations in asynchronous scenarios. Consequently, these imperfect correlation properties limit their achievable performance in asynchronous scenarios. Hence traditional DS-CDMA cellular systems are interference limited and suffer from the well-known 'near-far' effects, unless complex and 'power-hungry' interference cancellers [3] or multi-user detectors (MUD) [3] are employed for combating these adverse effects. Most of the above-mentioned system performance limitations are circumvented by the attractive family of Large Area Synchronized (LAS) CDMA spreading sequences, which are constituted by the combination of the so-called Large Area (LA) codes [19, 24] and Loosely Synchronous (LS) codes [19, 24]. The resultant Large Area Synchronized (LAS) codes exhibit a so-called Interference Free Window (IFW), where the off-peak aperiodic autocorrelation values as well as the aperiodic cross-correlation values become zero, resulting in both zero Inter-Symbol Interference (ISI) and zero MAI, provided that the time-offset of the asynchronously received codes is within the IFW.

Finally, for the sake of suppressing the interference at the receiver side, multiuser detection was used in Chapters [4 - 9]. The multiuser detector considers the other users' signals also as useful "information" rather than as "noise", and hence it is capable of significantly improving the BER performance of CDMA communications systems. However, the complexity of multiuser detectors is typically high, may even be irrealistic for employment in practical implementations. Over the past decade the topic of reducing the complexity of MUDs has captured a growing interest in the wireless communication community. In Chapters 4 - 9 of this dissertation we investigated numerous MUDs, which include linear MUDs, genetic algorithm assisted MUDs, the M-Algorithm assisted MUD, turbo MUD and blind MUD for employment in different CDMA communication systems, respectively. We also investigated multiuser detection in conjunction with spreading code optimization.

1.3 Organization and Novel Contributions of the Thesis

The outline of the dissertation is as follows :

- **Chapter 2**: In this chapter, we investigated the performance of band-limited DS-CDMA systems in conjunction with different chip-waveform designs, when communicating over a dispersive Nakagami-m channel. The required bandwidth W of a

DS-CDMA communication system is $W = \frac{1+\beta}{2T_c} = \frac{G(1+\beta)}{2T_s}$, where T_c and T_s represent the chip duration and data symbol duration respectively, while β is the Nyquist *roll-off* factor, which determines the excess bandwidth and G is the processing gain. We studied the trade-offs between the processing gain G and the excess bandwidth β in the context of various chip-waveforms. More specifically, owing to the fact that we have $G(1+\beta) = 2WT_s$, we will investigate how to harmonize the processing gain G and the excess bandwidth β for the sake of achieving the best possible BER performance, when the system's bandwidth and the bit rate are fixed.

- **Chapter 3**: Large Area Synchronized (LAS)-CDMA is investigated in this chapter, which exhibits a significantly better performance than the traditional random code based DS-CDMA system. Closed-form formulas are derived for characterizing the BER performance of LAS-CDMA as a function of the number of resolvable paths L_p, the maximum delay difference τ_{max} and the number of users K, when communicating over a Nakagami-m fading channel. Furthermore, we studied the family of LAS MC DS-CDMA systems in case of a high-chip rate scenario. More specifically, we appropriately select the number of subcarriers U in the proposed broadband LAS MC DS-CDMA system so that we can guarantee that the LAS codes remain capable of suppressing both the MAI and the MPI, as well as maintaining the highest possible multipath diversity order. Finally, we will investigate the performance of an LS code based STS scheme in comparison to that of the STS scheme of [25], when communicating over dispersive Nakagami-m multipath channels in a downlink scenario.
- **Chapter 4**: Assuming a fixed complexity, we comparatively studied an iterative PIC assisted MUD in conjunction with various channel codecs, such as convolutional coding, turbo coding, LDPC coding, as well as Trellis Coded Modulation (TCM) and Turbo Trellis Coded Modulation (TTCM). Parallel Interference Cancellation (PIC) constitutes a powerful interference rejection technique, which becomes particularly attractive, when the CDMA system benefits from accurate power control. Additionally, the principle of turbo equalization is invoked, where the receiver jointly carries out soft interference cancellation and channel decoding. The attraction of this combined operation is that the channel decoder refrains from making premature "hard" decisions concerning the transmitted data. Instead, it provides soft information for the PIC scheme and after a few iterations a substantially improved performance may be achieved, which may approach the single-user bound at the cost of a moderate implementational complexity.
- **Chapter 5**: In this chapter, we first introduce the concept and architecture of the subspace based multiuser detector. Then the family of space-time blind multiuser detectors is investigated in conjunction with antenna arrays. Furthermore, we investigated the application of subspace-based semi-blind and group-blind multiuser detectors designed for the MC-CDMA uplink, while a short cyclic prefix, rather than differential encoding was used for removing the phase ambiguity encountered. Additionally, the Akaike Information theoretic Criterion (AIC) [26] was invoked for

the estimation of the rank of the signal space. Finally, we studied the performance of a blind MMSE multiuser detector and a form-II group-blind multiuser detector in conjunction with Zadoff-Chu spreading codes [27], Gold codes [28] and Walsh codes [28].

- **Chapter 6**: Here we focus our attention on comparatively studying a Genetic Algorithm (GA) aided MUD and an M-Algorithm (MA) assisted MUD in the context of a synchronous DS-CDMA system, when transmitting over non-dispersive AWGN channels. We will evaluate their complexity and their achievable performance. Furthermore, we will compare their near-far resistance in the case of imperfect power control. The implementation of RBF based MUDs has been initially proposed by the Edinburgh team [29]. However, until recently its high complexity has hindered its wide-spread implementation. For the sake of reducing its complexity, in this chapter we propose the employment of GAs in the context of an RBF assisted MUD and investigate its attainable performance. We will demonstrate that the GA-RBF assisted MUD exhibits a significantly lower complexity than the traditional RBF based MUD.
- **Chapter 7**: In this chapter we will employ a GA assisted MUD scheme as a suboptimal MUD technique applicable to both bit-synchronous and asynchronous MC-CDMA systems communicating over broadband frequency selective fading channels. We assume that each subcarrier obeys independent Rayleigh fading. More explicitly, we will investigate the performance of this specific GA-assisted MUD as a function of the affordable detection complexity.
- **Chapter 8**: Time- and Frequency- (TF)-domain spreading assisted MC DS-CDMA MUD schemes are investigated in this chapter for the sake of reducing the complexity of the MUD. We will consider the employment of two different interference rejection spreading codes as the T-domain spreading code, where both of these codes exhibit a so-called Interference Free Window (IFW). The benefit of employing these specific codes as the T-domain code is that we are capable of reducing the complexity of the MUD, while achieving a frequency diversity gain. Specifically, the MUD's complexity is reduced because only a small fraction of the total number of users has to be separated and detected by the MUD, which belong to a given MUD group. By contrast, the set of users which are differentiated with the aid of unique user-specific spreading codes having an IFW do not interfere with each other, as a benefit of the IFW provided by the T-Domain codes used. Another advantage of the proposed scheme is that we can significantly extend the width of the IFW in comparison to a single-carrier DS-CDMA system, because as a benefit of distributing the bits to several subcarriers MC DS-CDMA has the potential of significantly reducing the chip rate, thereby extending the duration T_c of the chips.
- **Chapter 9**: Here we propose a novel STS assisted MC DS-CDMA system for supporting a wide range of bit rates with the aid of advantageously combining Adaptive Quadrature Amplitude Modulation (AQAM) [30] and Orthogonal Variable Spreading Factor (OVSF) based DS spreading codes [31]. Since OVSF codes exhibit

variable *Spreading Factors* (SFs), we can adjust the transmitted bit rate both with the aid of different SFs and different modulation schemes.

The novel contributions of this dissertation are listed below:

- Comparatively studied DS-CDMA systems using various chip-waveforms for transmission over a Nakagami-m fading channel in the context of the same fixed bandwidth [32,33].
- Investigated the performance of LAS-CDMA over a Nakagami-m channel as a function of the maximum time difference τ_{max}, the number of users K and the number of resolvable paths L_p [34,35].
- Studied an LS-code based STS schemes in comparison to a traditional STS scheme in a downlink scenario [36].
- Designed a PIC assisted iterative MUD in conjunction with numerous channel coding schemes [37].
- Investigated the performance of both blind and group-blind multiuser detection in conjunction with antenna arrays in the CDMA uplink [38].
- Proposed a GA assisted MUD for MC-CDMA systems [39,40].
- Comparatively studied the M-algorithm assisted MUD and a GA assisted MUD in the context of DS-CDMA. A GA-aided and RBF-assisted MUD was proposed for DS-CDMA [41].
- Investigated the performance of time-domain and frequency-domain spreading aided MC DS-CDMA using interference rejection codes [42,43].
- Investigated the performance of a novel AQAM assisted MC DS-CDMA system designed for supporting multirate communications [44].

1.4 Basic Multiuser Detector Structures

In this section we will consider some basic Multiuser Detector (MUD) structures. In discussing multiuser detection, it is convenient to introduce a matrix-vector notation based system model for describing the output of the conventional detector. We commence with a simple example considering a three-user synchronous system communicating over a non-dispersive AWGN channel. The matched filter output related to each of the users can be written as:

$$\begin{aligned} z_1 &= A_1 b_1 + \rho_{21} A_2 b_2 + \rho_{31} A_3 b_3 + n_1 \\ z_2 &= \rho_{12} A_1 b_1 + A_2 b_2 + \rho_{32} A_3 b_3 + n_2 \\ z_3 &= \rho_{13} A_1 b_1 + \rho_{23} A_2 b_2 + A_3 b_3 + n_3, \end{aligned} \tag{1.1}$$

where $A_1 \ldots A_3$ denotes the received signal amplitudes owing to the bits $b_1 \ldots b_3$ transmitted by the three users, $n_1 \ldots n_3$ are the corresponding noise samples and ρ_{ij}, $i = 1 \ldots 3$, $j = 1 \ldots 3$ represent the cross-correlation coefficients amongst the user-specific

spreading codes. Equation 1.1 may be expressed in a more compact from as follows:

$$\begin{bmatrix} z_1 \\ z_2 \\ z_3 \end{bmatrix} = \begin{bmatrix} 1 & \rho_{21} & \rho_{31} \\ \rho_{12} & 1 & \rho_{32} \\ \rho_{13} & \rho_{32} & 1 \end{bmatrix} \begin{bmatrix} A_1 & 0 & 0 \\ 0 & A_2 & 0 \\ 0 & 0 & A_3 \end{bmatrix} \begin{bmatrix} b_1 \\ b_2 \\ b_3 \end{bmatrix} + \begin{bmatrix} n_1 \\ n_2 \\ n_3 \end{bmatrix} \tag{1.2}$$

or as:

$$\mathbf{Z} = \mathbf{RAb} + \mathbf{n}. \tag{1.3}$$

In the context of a K-user system, the real vectors $\mathbf{b}$, $\mathbf{n}$ and are K-dimensional vectors that hold the users' transmitted data, the noise and the matched-filter output of all K users, respectively. The matrix $\mathbf{A}$ is a diagonal matrix containing the corresponding received signal amplitudes, while the matrix $\mathbf{R}$ is a real $K \times K$-dimensional cross-correlation matrix, whose entries contain the cross-correlation coefficient of every pair of spreading codes. Note that since the correlation coefficient of the codes satisfy $\rho_{jk} = \rho_{kj}$, the matrix $\mathbf{R}$ is clearly symmetric. Below we will briefly consider a number of multiuser detector structures in a little more detail.

1.4.1 Maximum Likelihood Sequence Estimator

The Maximum Likelihood Sequence Estimator (MLSE) detects the most likely transmitted K-bit vector $\mathbf{b}$ of the K users. The vector $\mathbf{b}$ is chosen by maximizing the *posteriori probability* of $P(\mathbf{b}|r(t))$, where $r(t)$ denotes the received channel-impaired signal during a bit interval. Under the assumption that all 2^K possible vectors $\mathbf{b}$ are equally probable, this detector is referred to as the MLSE. Therefore, this detector does not minimize the bit error probability of any of the K users, it rather minimizes the probability of encountering erroneous K-bit vectors. The problem associated with the MLSE approach is its high complexity. In general, there are 2^K possible vectors $\mathbf{b}$. An exhaustive search is clearly impractical for a high number of users. Hence, despite its optimum performance, owing to its excessive complexity the employment of the MLSE detector becomes impractical for real-time implementations. Therefore, numerous reduced-complexity sub-optimum multiuser detectors have been proposed in literature [3, 22].

1.4.2 Decorrelating Multiuser Detectors

As shown in Figure 1.4, the decorrelating multiuser detector applies the inverse of the Cross-Correlation (CCL) matrix $L_{dec} = \mathbf{R}^{-1}$ of the K users' spreading codes at the output of the conventional matched filter based detector in order to remove the "cross-talk" among the K users' spreading codes. Hence, the decoupled output vector $\hat{\mathbf{b}}$ of the decorrelating detector is given by:

$$\hat{\mathbf{b}} = \mathbf{R}^{-1}\mathbf{Z} = \mathbf{Ab} + \mathbf{R}^{-1}\mathbf{n}, \tag{1.4}$$

which is constituted by the decoupled data plus a noise term. Thus, we can see that the decorrelating detector completely eliminates the MAI. The philosophy of this detector

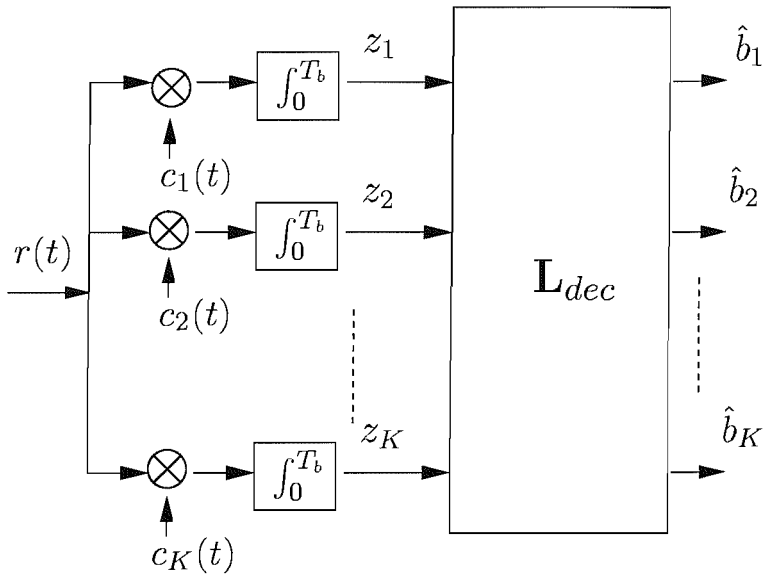

Figure 1.4: Schematic of the decorrelating multiuser detector.

is very similar to that of the Zero-Forcing (ZF) equalizer [30]. The advantages of the decorrelating detector are that it:

- provides substantial performance improvements over the conventional single-user detector;
- does not have to estimate the received signal's amplitude;
- it exhibits a significantly lower complexity than the MLSE detector;
- it exhibits near-far resistance.

However, a disadvantage of this detector is that it imposes noise amplification. More explicitly, the power of the noise associated with the term $\mathbf{R}^{-1}\mathbf{n}$ at the output of the decorrelating detector is always higher than that of the original noise term $\mathbf{n}$. Another disadvantage of the decorrelating detector is that the complexity of inverting the CCL matrix $\mathbf{R}$ is high, in particular when the number of users K is high.

1.4.3 Linear MMSE Multiuser Detector

The noise amplification problem of the decorrelating detector is circumvented by the linear MMSE MUD, which jointly minimizes the effect of the background noise and that of the MAI by exploiting the knowledge of the received signal power of the K users. More explicitly, this detector minimizes the expected value of $E[\| \mathbf{Ly} - \mathbf{b} \|^2]$, and hence the decoupled matrix becomes [22]:

$$\mathbf{L}_{MMSE} = [\mathbf{R} + \sigma_n^2 \mathbf{A}^{-2}]^{-1}. \tag{1.5}$$

As seen from Equation 1.5, the MMSE detectors invokes a modified inverse of the correlation matrix, where the adjustment term of Equation 1.5 is proportional to the background noise power σ_n^2. From a physical perspective, the MMSE detector balances the desire to

completely eliminate the MAI with the desire of avoiding the background noise enhancement problem. Since it takes the effects of the background noise into account, the MMSE detector generally provides a better performance than the decorrelating detector. As the background noise reduces, the MMSE detector's noise-related term of Equation 1.5 diminishes and hence the solution in Equation 1.5 converges to the decorrelating detector of solution of Equation 1.4.

An important disadvantage of this detector is that unlike the decorrelating detector, it requires the estimation of the K users received signal amplitude. Furthermore, like the decorrelating detector, the MMSE detector also has to invoke matrix inversion.

Finally, Figure 1.5 exhibits the performance of the linear decorrelating and MMSE detectors. The system considered supported $K = 20$ users and random spreading codes having a length of $N_c = 31$ were employed for communicating over the AWGN channel.

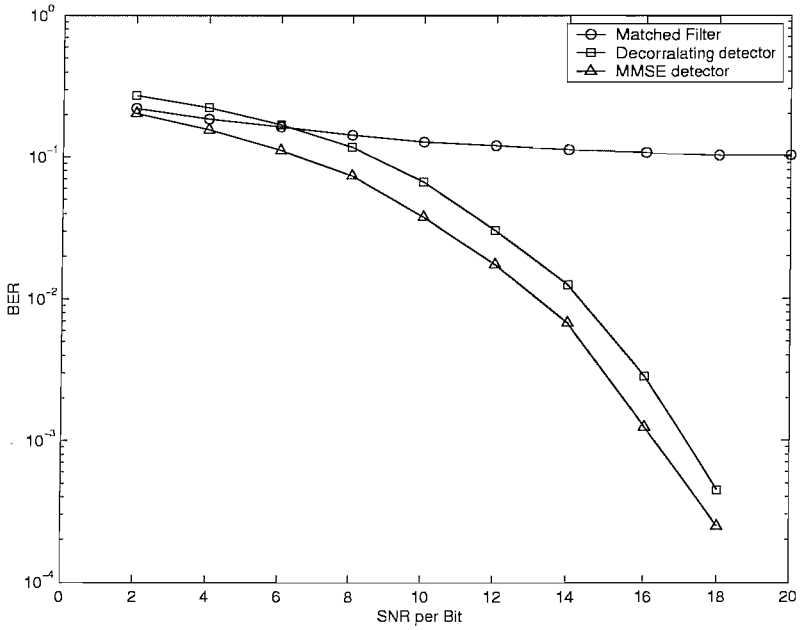

Figure 1.5: BER performance of the family of linear MUDs. Random codes of length $N_c = 31$ were used and $K = 20$ users were supported in the system communicating over an AWGN channel.

1.4.4 Successive Interference Cancellation

The schematic of the Successive Interference Canceller (SIC) is depicted in Figure 1.6, where all the K users have been ranked according to their received signal power, with the highest-power user being labelled as user 1 and the lowest-power one labelled as user K. After power ranking, the received composite signal is processed by the matched filter or RAKE receiver of user 1 for the sake of obtaining the initial data estimates. The transmitted signal of this user is then reconstructed using both the hard decision bits/symbols, as well as the estimates of the CIR and the spreading sequence. Then the estimated reconstructed signal of this user is subtracted from the composite multiuser received signal. The remaining signal is then processed by the matched filter or RAKE receiver of user 2 in order to obtain its data estimate. Upon employing the estimate of the

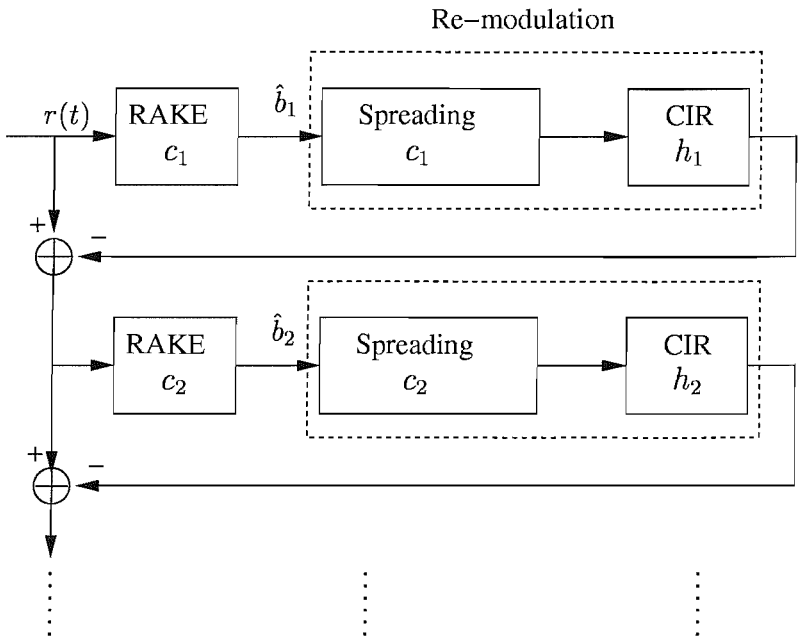

Figure 1.6: Schematic of the successive interference canceller.

transmitted data, as well as the CIR and spreading sequence of user 2, the corresponding modulated signal is reconstructed and subtracted from the remaining composite signal that has already had the highest-power user's signals cancelled from it. This process is repeated, until the lowest-power user, namely the Kth user's signal is processed. The SIC detector imposes only modest additional complexity and has the potential of providing a significant performance improvement over the conventional single-user RAKE detector. It does, however, pose a couple of implementation difficulties. Firstly, one additional bit delay is imposed by each cancellation stage. Thus, a trade-off has to be found between the number of users and the amount of tolerable delay. Secondly, all the users must be ranked according to their received signal power, which must be updated after each cancellation stage. A trade-off must be found between the precision of power ranking and the acceptable processing complexity. Another potential problem associated with the SIC detector occurs, if the initial data estimate of user k is unreliable. In this case, even if the timing, power and phase estimates are perfect, but the bit estimate is wrong, the interference imposed on the remaining users indexed from $(k+1)$ to K will be enhanced, rather than reduced. Thus, a certain minimum performance threshold must be exceeded by the matched filter based conventional detector for the SIC multiuser detector to achieve a further performance improvement.

1.4.5 Parallel Interference Cancellation Multiuser Detector

In contrast to the SIC based multiuser detector, the parallel interference cancellation (PIC) aided detector estimates and subtracts the MAI imposed by all interfering users from the signal of the desired user in parallel. Figure 1.7 shows a single cancellation stage of one user. In each cancellation stage, the signal of each user is reconstructed by invoking the data estimates from the previous cancellation stage. Then, for each

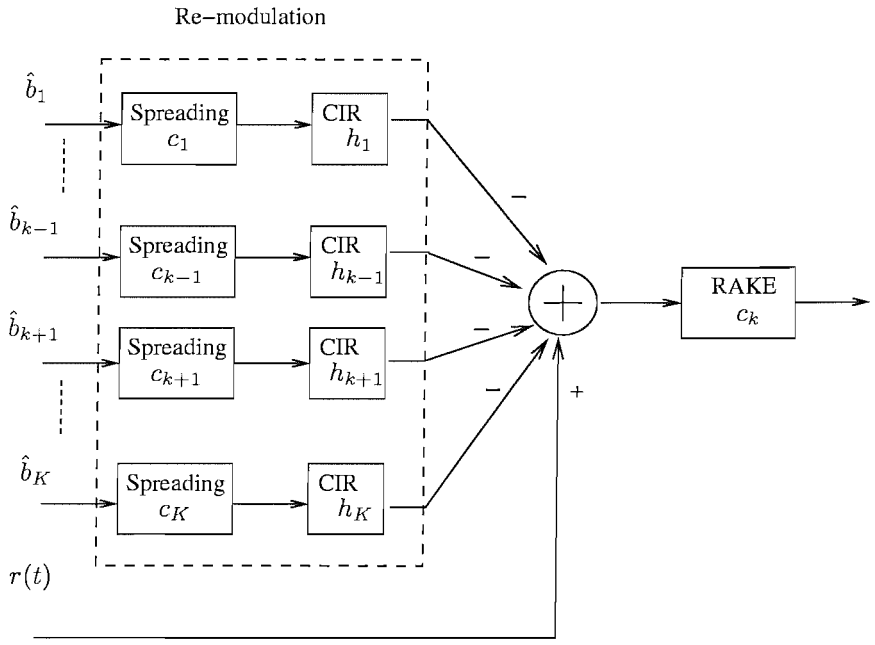

Figure 1.7: Schematic of the parallel interference canceller.

user, the reconstructed signals of all the other users are subtracted from the received composite signal and the resultant signal is processed by the matched filter or RAKE receiver, in order to obtain a new set of data for each of the K users to be used in the next interference cancellation stage. The reconstruction, cancellation and re-estimation operations are repeated as many times as the affordable complexity of system allows. The advantage of PIC in comparison to SIC is that it does not require the power estimates of all users to be updated after each cancellation stage, and that all the users have the same processing delay. However, again, a certain minimum performance threshold has to be exceeded by the conventional detector in the context of the PIC multiuser detector for the sake of attaining a further performance improvement.

1.4.6 Genetic Algorithm Assisted Multiuser Detector

Verdú's optimum multiuser detector is capable of achieving a near-single user performance by maximizing the following likelihood function [22]:

$$\Omega(\mathbf{b}) = 2\mathbf{b}^T\mathbf{AZ} - \mathbf{bARA}^H\mathbf{b}^T, \tag{1.6}$$

where the variables are defined as before. In other words, the multiuser detector will achieve the optimum single-user performance, if it carries out an exhaustive search over the entire search space of the vector $\mathbf{b}$. Unfortunately, the associated complexity is excessive, even in case of the non-dispersive synchronous scenario of supporting K BPSK users, which is on the order of $O(2^K)$. Hence genetic algorithms have been proposed for reducing the associated complexity [3].

The basic flowchart of a Genetic Algorithm (GA) is shown in Figure 1.8. Let us first assume that the current bit of interest is the ith bit of all the K synchronous users. GAs

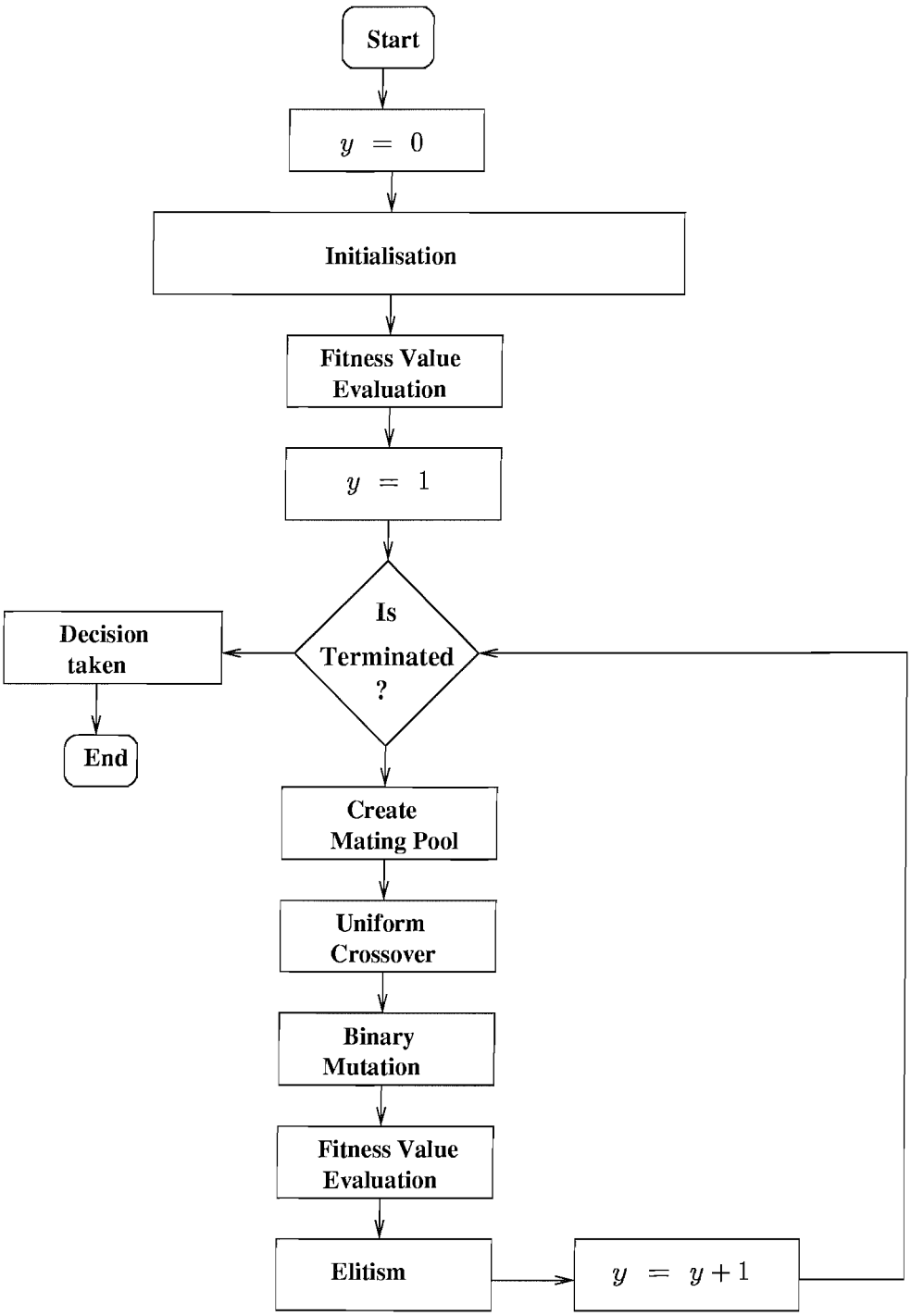

Figure 1.8: Flowchart of a GA-based multiuser detector.

commence their search for the optimum solution at the so-called $y = 0$th *generation* with an initial population of so-called *individuals*, each consisting of K antipodal bits. The number of K-bit individuals in the population is given by the *population size* P. Hence, we can express the pth individual here as $\tilde{\boldsymbol{b}}_p(y)$. A *fitness* value, denoted as $f\left[\tilde{\boldsymbol{b}}_p(y)\right]$ for $p = 1, \ldots, P$ is associated with each K-bit individual, which is computed by substituting the corresponding elements $\tilde{\boldsymbol{b}}_p(y)$ into Equation 1.6. Based on the evaluated fitness, a new population of P individuals is created for the $(y+1)$th generation through a series of genetic processes to be defined below, which are referred to in GA parlance as *selection*, *crossover*, *mutation* and *elitism* [3,45]. Let us now highlight the processes that are involved in the GA [3, 45]. These processes are repeated, until the Yth generation's individuals are generated. In most cases, the GA is capable of approaching the optimum single-user performance at a fraction of the complexity in comparison to Verdu's optimum MUD.

Selection - As suggested by the terminology, the *selection* process [45] selects two so-called K-bit *parent* vectors from a *mating pool* consisting of T number of K-bit individuals – where we have $2 \leq T < P$ – in order to produce two so-called *offspring* for the next generation population of K-bit individuals. Individuals having the T highest fitness values in the population of K-bit vectors are placed in the mating pool. We shall denote the K-bit individuals in the mating pool as $\check{\boldsymbol{b}}_q(y)$ for $q = 1, \ldots, T$. The K-bit individuals in the mating pool are selected as K-bit parent vectors according to a probabilistic function to be specified below, which is based on their corresponding fitness values $f\left[\check{\boldsymbol{b}}_q(y)\right]$. In [3], the so-called *sigma scaling* [45] was employed, where the selection probability $p\left(\check{\boldsymbol{b}}_q(y)\right)$ for a K-bit individual to become a parent is a function of both its own fitness $f[b_q(y)]$ as well as that of the mating pool's mean fitness $\bar{f}$ and that of its associated standard deviation σ_f, which is formulated below as [45]:

$$p\left(\check{\boldsymbol{b}}_q(y)\right) = \begin{cases} 1.0 - \frac{f\left[\check{\boldsymbol{b}}_q(y)\right] - \bar{f}}{2\sigma_f} & \text{if } \sigma_f \neq 0 \\ 1.0 & \text{if } \sigma_f = 0, \end{cases} \tag{1.7}$$

where we have:

$$\bar{f} = \frac{1}{T}\sum_{q=1}^{T} f\left[\check{\boldsymbol{b}}_q(y)\right]; \ \sigma_f = \sqrt{\frac{\sum_{q=1}^{T}\left\{f\left[\check{\boldsymbol{b}}_q(y)\right] - \bar{f}\right\}^2}{T-1}}.$$

Crossover - The antipodal K-bit parent vectors are then appropriately combined using the so-called *uniform crossover* [45] process, in order to produce two K-bit offspring vectors. The process of uniform crossover invokes a so-called *crossover mask*, which is a sequence consisting of K randomly generated binary 1s and 0s. The bits of the K-bit parent vectors are exchanged between the pair of parents at the particular bit locations corresponding to a binary 1 in the crossover mask. The selection of K-bit parents from the mating pool of K-bit vectors is repeated, until a new population of P number of K-bit offspring is produced, in order to perform the crossover process.

Mutation - The *mutation* process [45] refers to the alteration of the value of an antipodal bit in the K-bit antipodal offspring vectors from 1 to -1 or vice versa, with a

probability of p_m. This mutation is invoked for the sake of increasing the diversity of the population, in an effect to avoid premature convergence to a local minimum.

Elitism - Finally, upon invoking the process of elitism [45], we identify the lowest-merit K-bit offspring in the population and replace it with the highest-merit K-bit individual from the mating pool. This will ensure that the highest-merit K-bit individual is propagated throughout the evolution process to further generations.

GAs are not guaranteed to find the optimal solution and their efficiency is determined essentially by the population size P, i.e. by the number of individuals in a population, and the number of generations invoked. Hence, the size of the population in a GA is a major factor in determining the accuracy of convergence. As the population size increases, the GA has a better chance of finding the global optimum solution, but the computational cost also increases as a function of the population size. The GA-based MUD has to compute the objective functions of Equation 1.6 $(P \cdot Y)$ number of times.

1.5 Survey of Bandlimited CDMA and LAS-CDMA

First, we briefly portray the history of bandlimited CDMA systems. In [46], Amoroso introduced various definitions of the bandwidth of digital signalling schemes. Numerous valuable studies have been conducted [23, 47–50] for the sake of finding various attractive chip waveforms for CDMA communication systems. In [48], Dallas and Pavlidou investigated the impact of the signalling pulse shape using several time-limited waveforms, such as rectangular, half-sine and raised cosine chip-waveforms. Cho and Lehnert [23] considered the performance of several band-limited chip-waveforms in the context of DS-CDMA systems, when communicating over a non-dispersive AWGN channel and the authors of [23] defined the so-called normalized interference factor for the sake of characterizing the interference-related effects of a specific chip-pulse shape. Beaulieu and Cheng [51] provided a precise error-rate analysis for band-limited binary phase-shift keying, when communicating over dispersive Nakagami-m channels, although no direct sequence spreading was used. In [50], Yang and Hanzo studied the performance of generalized multicarrier DS-CDMA using various time-limited chip-waveforms, namely the rectangular, half-sine, as well as the raised-cosine chip-waveforms and closed-form formulae were derived for evaluating the attainable BER performance, when communicating over a dispersive Nakagami-m channel.

By contrast, the literatures of LAS spreading sequences is sparse. Li [24] first studied various LA code construction schemes and their application in CDMA systems. However, the LS code construction scheme has not been public until recently. In 2001 Stańczak, Boche and Haardt [18] also investigated the construction of various schemes designed for the generation of various LS codes. They developed a systematic way of constructing so-called LS-like codes. Recently, Choi and Hanzo [19] revised the methods of LA code construction in [24], thereby increasing the number of codes generated in comparison to Li's original design [52], which results in a considerable capacity increase. Furthermore, Fan [53] proposed the family of so-called generalized orthogonal spreading codes, which also exhibited an IFW.

1.6 Survey of Multiuser Detection Techniques

1.6.1 Survey of Multiuser Detectors for DS-CDMA

The brief history of multiuser detectors designed for DS-CDMA is summarized in Table 1.1. Verdú's seminal work [54] published in 1986 proposed and analyzed the optimal multiuser detector, which invoked the maximum likelihood sequence detector. Again, unfortunately, this detector is too complex for practical CDMA systems, when the number of users is high. Therefore, over the last decade or so, most of the related research has focused on contriving suboptimal multiuser detector solutions, which are feasible to implement in complexity terms. To elaborate a litter further, the classic linear MMSE detector and the decorrelating multiuser detector was investigated in [54, 55]. Varanasi and Aazhang proposed the family of interference cancellers [56]. Recently, a novel linear multiuser detector proposed by Chen *et al.* [67] was investigated, which obeys the so-called Minimum Bit Error Rate (MBER) design criterion, rather than the MMSE criterion. The rationale of the MBER MUD is that it is better to directly minimise the BER if possible, rather than the MSE, since the MSE solution fails to achieve the minimum BER as a consequence of optimizing the MSE, which is not directly related to the BER. The results of [67] show that the MBER multiuser detector is capable of achieving a better BER performance than that of the MMSE MUD. Another class of multiuser detectors based on the tree-search aided M-algorithm [59], T-algorithm [59], hybrid MT-algorithm [59] as well as on the Viterbi Algorithm (VA) [59] These detectors have been proposed in the literature in order to reduce the complexity of the original ML detectors, and they are capable of achieving a near-optimum performance. Motivated by the fact that the VA often discards relatively high-probability paths, since it can only retain a single survival path, in the M-algorithm M paths per trellis-stage are retained, which are typically the highest-metric M number of paths. As M increases, the achievable performance also improves at the cost of an increased complexity. Alternatively, in the T-algorithm all the trellis paths may be retained, which exceed a certain path-metric threshold T. At the decision stage, the path associated with the highest metric was selected as the most likely transmitted sequence.

The interference cancellation based multiuser detectors of Section 1.4.4 and Section 1.4.4 typically achieve an attractive performance versus complexity trade-off and they can be divided into three basic categories, SIC, PIC, and various hybrids of both. Reed *et al.* [60] proposed an iterative MUD enhanced by turbo coding. After processing the received signal in a bank of matched filters, the matched filters' outputs were processed using turbo-style iterative decoding [77, 78]. In this process, a multiuser decoder was used for producing the Logarithmic Likelihood Ratios (LLR) which constituted the soft inputs to the single-user Soft-In Soft-Out (SISO) channel decoders. These single-user decoders then provided similar SISO LLRs for the iterative multiuser detectors. This iterative process continued, until no further performance improvement was achieved or the affordable complexity was exhausted. However, this iterative multiuser detector's complexity is on the order of $O(2^K)$, hence its implementation is complex, when the

Year	Author	Contribution
1986	Verdú [54]	The optimum MUD as well as a number of sub-optimum linear MUDs were proposed.
1989	Lupas and Verdú [55]	Linear MUDs were further investigated.
1990	Varanasi and Aazhang [56]	Interference cancellers were proposed and investigated.
	Verdu and Lupas [57]	The near-far resistance was investigated in the context of MUDs.
1992	Aazhang, Paris and Orsak	Neural network based MUDs were proposed and investigated.
1995	Honig, Madhow and Poor [58]	The minimum output energy (MOE) algorithm based blind MUD was investigated.
1997	Wei [59]	Tree-search based MUDs such as the M-algorithm and T-algorithm were proposed.
1998	Reed [60]	Iterative multiuser detection was proposed.
	Divsalar, Simon [61]	The PIC assisted iterative MUD employed a novel tentative decision, and supported a high-user load.
	Wang and Poor [62]	Subspace algorithm based linear blind detectors were introduced.
1999	Wang and Host-Madsen [63]	Subspace algorithm based linear group-blind MUDs were investigated.
	Reed and Alexander [64]	Iterative MUDs invoking antenna arrays were investigated.
2000	Ergün and Hacioglu [65]	GA assisted MUDs were proposed and investigated.
2001	Peng [66]	Multiuser detection was contrived for asynchronous CDMA subject to frequency offset.
	Chen and Hanzo [67]	The Adaptive Minimum Bit Error Ratio (AMBER) linear MUD was proposed and investigated.
2002	Reynolds and Wang [68]	Blind iterative MUDs were investigated in the context of unknown interference.
	Poor and Tanda [69]	Multiuser detection in flat fading non-Gaussian channels was investigated.
	Lampe [66]	Iterative MUD combined with integrated channel estimation was proposed.
2003	Sfar, Murch and Letaief [70]	Layered space-time multiuser detection was proposed and studied.
	Kapur and Varanasi [71]	Multiuser detectors invoked in the context of overloaded CDMA systems were studied.
	Kocian and Fleury [72]	Expectation-Maximization based MUDs designed for joint data detection and channel estimation were proposed.
2004	Honig and Woodward [73]	Adaptive iterative multiuser decision feedback detection designed for CDMA was proposed and studied.
	Yen and Hanzo [74]	GA assisted MUDs contrived for asynchronous CDMA were investigated.
	Das and Varanasi [75]	Optimum noncoherent multiuser decision feedback detection was designed.
	Li, Georghiades and Wang [76]	Sequential expectation-maximization (EM) algorithm based blind multiuser detectors were advocated.

Table 1.1: Contributions on the multiuser detection for the DS-CDMA systems.

number of users K is high. For the sake of reducing the complexity, Zhang *et al.* [79] and Reed *et al.* [80] proposed PIC based iterative multiuser detectors. These PIC based iterative multiuser detectors were capable of exploiting the emerging soft decision values during the parallel interference cancellation process. Divsalar *et al.* [61] further improved the achievable performance of the family of PIC based iterative multiuser detectors by incorporating a tentative decision device invoking only the reliably estimated data symbols for the generation and cancellation of the MAI. This measure prevented the error propagation. Recently, Lampe *et al.* [81] proposed an iterative multiuser detector combined with channel estimation. Its main feature is that channel estimation was based on tentative pilot symbol aided estimation combined with interference cancellation and with the adaptation of estimation filters invoked for decreasing the effect of MAI. With the advent of this receiver, near-optimum channel estimation can be achieved, resulting in a near-single-user performance.

Year	Author	Contribution
1997	Juntti, Schlösser and Lilleberg [82]	The earliest contribution on GA-assisted DS-CDMA multiuser detection.
1998	Wang, Liu and Antoniou [83]	GA assisted MUD designed for asynchronous DS-CDMA in conjunction with the Viterbi Algorithm.
2000	Ergün and Hacioglu [65]	A hybrid approach combining a GA and a multistage detector.
2001	Yen and Hanzo [3,84]	GA based joint multiuser detection and fading channel estimation for synchronous systems.
2003	Yen and Hanzo [3,85]	Antenna-diversity assisted GA based multiuser detection schemes.
2004	Yen and Hanzo [74]	GA assisted MUDs based on a truncated window and designed for asynchronous DS-CDMA communicating over multipath fading channels.

Table 1.2: Contributions on GA-assisted multiuser detection.

Following a similar approach, in Table 1.2, we summarized the history of the GA-assisted multiuser detection. An iterative hybrid genetic algorithm based search technique has been first proposed by Juntti [82] in 1997. The following year, Wang *et al.* [83] proposed a GA aided MUD for an asynchronous CDMA system communicating over AWGN channels. The users' bits were successively detected in conjunction with the modified Viterbi algorithm. Ergün *et al.* [65] proposed a hybrid GA-based approach that employs a GA and a Multi Stage Detector (MSD) for multiuser detection, in order to mitigate the irreducible error floor imposed by the conventional MSD detectors. More recently, Yen and Hanzo [3, 84, 86, 87] further investigated the performance of GA-based multiuser detectors. In [86], they investigated the performance of a synchronous GA-based multiuser detector. The authors studied *sigma scaling, fitness-proportionate, linear-ranking* as well as *tournament* [45] based GA selection schemes. Furthermore, several crossover methods were studied including *single-point, double-point, uniform* crossover [45]. A range of

other optimization schemes such as *incest prevention*, as well as *elitism* were also invoked. Furthermore, the effects of crossover probability and mutation probability on the GA-based multiuser detector were investigated. In [84], Yen and Hanzo studied GA-based joint multiuser detection integrated with channel estimation. The simulation results provided showed that the GA was capable of tracking the variations of the fading channel, while achieving a channel gain estimation Mean Square Error (MSE) as low as 10^{-3} in a noiseless channel having a Doppler frequency of $f_d = 200$Hz. The proposed channel estimator and multiuser detector were capable of achieving a BER as low as 2×10^{-3} at an SNR value of 30dB in a 10-user CDMA environment without channel coding or diversity. Since channel estimation and symbol detection were performed simultaneously, no pilot or training sequence was necessary, which resulted in a higher throughput and shorter detection time, than that of a conventional trained CDMA multiuser detector. In [87], Yen and Hanzo proposed a GA assisted multiuser detector for transmission over a dispersive Rayleigh fading channel, which invoked a *truncated observation window*. The desired bits residing within the *truncated observation window* were detected using GAs, and two different strategies were evaluated for providing tentative decisions concerning the *edge bits*. These detectors were capable of achieving a near-optimal BER performance, while attaining a substantial complexity reduction. Finally, in [85] Yen and Hanzo presented a novel approach to the problem of multiuser detection designed for transmission over flat Rayleigh-fading channels assisted by the antenna diversity. The proposed detectors have resolved the optimization conflict arising from the different correlation metrics provided by the different antennas by selecting only the so-called non-dominated individuals of a given population for the mating pool [45] on the basis of exploiting the so-called Pareto optimality [45]. The authors showed that the detectors based on Pareto optimality exhibited a lower BER than conventional diversity selection schemes.

Year	Author	Contribution
1995	Honig, Madhow and Poor [58]	Minimum Output Energy (MOE) algorithm based blind multiuser detectors.
1998	Wang and Poor [62]	Subspace algorithm based linear blind detectors.
1999	Wang and Host-Madsen [63]	Subspace algorithm based linear group-blind multiuser detectors
2001	Spasojevic Wang and Host-Madsen [88]	Nonlinear group-blind multiuser detectors.
	Yen and Hanzo [84]	Genetic algorithm assisted blind multiuser detectors. for synchronous CDMA.
2003	Reynolds Wang [89]	Transmitter optimization for blind and group-blind multiuser detectors.
2004	Li, Georghiades and Wang [76]	Sequential expectation-maximization (EM) algorithm based blind multiuser detectors.

Table 1.3: Contributions on the blind multiuser detection

The history of blind multiuser detectors designed for DS-CDMA is summarized in Table 1.3. The blind multiuser detector was first proposed and investigated by Honig *et al.* [58]. However, this specific Minimum Output Energy (MOE) based blind multiuser detector exhibited a relatively poor performance in the high SNR region. Wang and Poor [62] proposed and investigated the family of subspace based blind multiuser detectors, when communicating over a non-dispersive AWGN channel, which exhibited a significantly better performance than that of the MOE based blind multiuser detector. Wang and Poor [90] later extended their work to dispersive asynchronous CDMA environments. In [63, 91], Wang and Host-Madsen proposed group-blind multiuser detectors for uplink single-carrier DS-CDMA, which exploited the prior knowledge of all known signature waveforms of the users communicating in the reference cell, rather than only that of the reference user. With the advent of this extra information their group-blind multiuser detector exhibited a substantial performance improvement over that of a blind multiuser detector. Furthermore, Spasojevic and Wang *et al.* [88] proposed a nonlinear group-blind multiuser detector for DS-CDMA systems. The GA based blind multiuser detector was proposed and investigated by Yen and Hanzo [84]. Recently, a novel expectation-maximization (EM) algorithm based blind multiuser detector was proposed by Li, Georghiades and Wang [76], which exhibited a low computational complexity, that was on the order of $O(K^2)$ per bit, where K is the number of users.

Year	Author	Contribution
1996	Schnell and Kaiser [92]	Maximum likelihood MUDs are proposed.
2000	Miller and Rainbolt [93]	Linear MMSE multiuser detection was proposed for MC-CDMA.
	Namgoong, Wong and Lehnert [94]	Subspace based blind multiuser detection for MC DS-CDMA.
2001	Zong, Wang and Bar-Ness [95]	Partial sampling MMSE interference suppression multiuser detection for MC-CDMA.
	Yang, Lu and Wang [96]	Blind Bayesian Monte Carlo Multiuser detectors for coded MC-CDMA system.
2003	Kalofonos, Stojanovic [97]	Adaptive MUD for MC-CDMA systems.
	Kafle and Sesay [98]	Iterative semi-blind multiuser detection for coded MC-CDMA uplink system was investigated.
2004	Zhang, Bi and Zhang [99]	Blind multiuser detection for MC-CDMA was investigated.

Table 1.4: Contributions on multiuser detection designed for MC-CDMA systems.

1.6.2 Survey of Multiuser Detectors for MC-CDMA

Finally, a brief historical prospective of the family of multiuser detectors designed for MC-CDMA was provided in Table 1.4. Schnell and Kaiser [92] considered the employment of a Maximum Likelihood Sequence Estimator (MLSE) for MC-CDMA communications.

However, this multiuser detector exhibits an excessive complexity. Following the philosophy of the corresponding single carrier DS-CDMA multiuser detector, a linear MMSE multiuser detector was proposed by Miller*et al.* [93] for MC-CDMA systems. In this chapter, the authors considered the employment of a chip-based matched filter in the context of the MMSE optimization criterion, and two different MMSE detection strategies were investigated and compared. According to first strategy, the MMSE multiuser detector was designed separately for each subcarrier, while in the second case, the optimization of the MMSE multiuser detector was carried out jointly for all the subcarriers. Naturally, the joint optimization produces a substantially better performance. Namgoong, Wang and Lehnert [94] proposed a subspace based MMSE detector for MC DS-CDMA, invoking a blind algorithm [62, 63] for channel estimation in conjunction with the MMSE decision criterion. More specifically, the channel estimation and multiuser detection were both carried out blindly. Zhong, Wang and Bar-Ness [95] considered Partial Sampling MMSE aided (PS-MMSE) multiuser detectors for employment in MC-CDMA. This was justified by the fact that the conventional MMSE receiver required perfect timing estimation of the desired signal before commencing multiuser detection. The error incurred in estimating the timing of the desired signal inflicts both intersymbol interference and inter-subcarrier interference, which severely degrades the system's performance. The PS-MMSE multiuser detector eliminated this problem, since it required no timing estimation. Unlike the conventional MMSE MUD, which demodulates the received signal of each subcarrier at the symbol rate, the PS-MMSE multiuser detector demodulates this signal at an increased sampling rate, which is significantly higher than the symbol rate. An iterative multiuser detector contrived for MC-CDMA was also proposed by Kafle and Sesay [100], where the authors considered two prototype schemes, namely the MMSE based iterative multiuser detector and a PIC based iterative multiuser detector. Adaptive MC-CDMA multiuser detectors were considered by Kalofonos *et al.* in [97], where the performance of both the Least Mean Square (LMS) and Recursive Least Square (RLS) adaptation principles was quantified. The resultant multiuser detectors exhibited a low complexity and high robustness against parameter variations, while maintaining a good performance.

Recently, Kafle and Sesay [98] advocated an iterative semi-blind multiuser detector designed for the turbo coded MC-CDMA uplink, which employed a cyclic prefix. These iterative receivers were derived using a subspace approach, which was capable of blindly suppressing the unknown interference. Zhang, Bi and Zhang [99] presented a blind adaptive decorrelating detector designed for asynchronous MC-CDMA systems communicating over Rayleigh-fading channels. This detector was derived by making use of the cross-correlation matrix between the consecutively received signals. The main attraction of the detection algorithm was its simplicity, since the detector can be implemented without channel estimation, except for the indispensible synchronization of the desired user.

CHAPTER 2

Bandlimited CDMA

2.1 Introduction

The signalling pulse design or waveform design plays an important role in determining the properties of digital communication systems. In [46], Amoroso introduced various definitions of the bandwidth of digital signalling schemes. In the context of CDMA based communications, numerous valuable studies have been conducted [23, 47–50] for the sake of finding various attractive chip waveforms. In [48], the authors investigated the impact of the signalling pulse shape for several time-limited waveforms, such as rectangular, half-sine and raised cosine chip-waveforms. More specifically, the different chip-waveform designs are expected to incur different amounts of multiple access interference (MAI), while requiring different signalling bandwidths. However, the authors of [48] did not consider the bandwidth requirement of the different chip-waveform, although the different chip-waveforms occupy different bandwidths. Hence in this chapter we will investigate the BER performance of these time-limited chip-waveforms in the context of a DS-CDMA system, when they occupy the same bandwidth.

Cho and Lehnert [23] investigated the performance of several band-limited chip-waveforms in the context of DS-CDMA systems, when communicating over a non-dispersive AWGN channel. For example, a time-domain chip-waveform associated with a raised cosine spectrum was studied in [7, 23]. More specifically, the authors of [23] defined the so-called normalized interference factor for the sake of characterizing the interference-related effects of a specific chip-pulse shape and hence for analyzing the achievable performance of band-limited waveform based DS-CDMA systems, as it will be discussed in detail throughout this chapter. The novel contribution of [51] was that the authors provided

a precise error-rate analysis for band-limited binary phase-shift keying, when communicating over dispersive Nakagami-m channels, although no direct sequence spreading was used. In [50], Yang and Hanzo investigated the performance of generalized multicarrier DS-CDMA using various time-limited chip-waveforms, namely the rectangular, half-sine, as well as the raised-cosine chip-waveforms, and the closed-form formulae were derived for evaluating the BER performance, when communicating over a dispersive Nakagami-m channel. Based on the above-mentioned studies, in this chapter we investigate the performance of band-limited DS-CDMA systems in conjunction with different chip-waveform designs, when communicating over a dispersive Nakagami-m channel. The required baseband bandwidth W of a DS-CDMA communication system is $W = \frac{1+\beta}{2T_c} = \frac{G(1+\beta)}{2T_s}$, where T_c and T_s represent the chip duration and data symbol duration respectively, while β is the Nyquist *roll-off* factor, which determines the excess bandwidth and G is the processing gain. It is plausible that a system using different chip-waveforms requires a different excess bandwidth. For example, the third generation wideband-CDMA system [13] employs square-root raised cosine spectral-domain shaping having a Nyquist *roll-off* factor of $\beta = 0.22$[1]. Furthermore, in the context of band-limited chip-waveform, the interference factor associated with a specific pulse shape is expected to decrease as the excess bandwidth β increases. In other words, we are capable of reducing the MAI imposed on other users at the cost of decreasing the attainable spectral efficiency, as it will be demonstrated in Section 2.4. It is possible to strike a trade-off between the processing gain G and the excess bandwidth β. Hence in this chapter we investigated the design of band-limited DS-CDMA systems, as a function of the processing gain G and the excess bandwidth β. More specifically, owing to the fact that we have $G(1+\beta) = 2WT_s$, we will investigate how to harmonize the processing gain G and the excess bandwidth β for the sake of achieving a good performance, when the system's bandwidth and the bit rate are fixed.

This chapter is organized as follows. Section 2.2 describes the CDMA communication system designed for communicating over a dispersive Nakagami-m channel, while Section 2.3 will analyze the BER performance of the band-limited DS-CDMA system in conjunction with different waveforms, which include both time-limited and band-limited chip-waveforms. Finally, Section 2.4 provides our numerical results and Section 2.5 offers our conclusions.

2.2 System Model

2.2.1 System Model

Let us consider an asynchronous K-user DS-CDMA communication system, where each user is assigned a unique signature waveform $\mathbf{c}_k(t) = \sum_{i=0}^{G-1} c_{ki}\psi_{T_c}(t - iT_c)$. The sequence $c_{ki} \in \frac{1}{\sqrt{G}}\{+1, -1, +j, -j\}$ represents the random Pseudo-Noise (PN) spreading sequence

[1]Sine the Nyquist *roll-off* factor β and the excess bandwidth are directly linked to each other, both terminologies will be used interchangeable throughout this chapter. This is justified, because we will be investigating not only Nyquist signalling, but a range of other bandlimited signalling pulses

of the kth user and G is the processing gain, which obeys $G = T_s/T_c$, and $\psi_{T_c}(t)$ represents the chip-waveform having an energy of $\int_{-\infty}^{+\infty} \psi_{T_c}^2(t)dt = T_c$. For convenience, we define the normalized chip-waveform $\hat{\psi}(t) = \psi_{T_c}(t/T_c)$. For the band-limited system considered, the normalized chip-waveform $\hat{\psi}(t)$ satisfies:

$$\int_{-\infty}^{+\infty} \hat{\psi}(t - n_1)\hat{\psi}^*(t - n_2)dt = \delta(n_1, n_2), \tag{2.1}$$

where $\delta(n_1, n_2) = 1$ for $n_1 = n_2$, and 0 for $n_1 \neq n_2$. From Eq.(2.1), we have:

$$\sum_{n=-\infty}^{\infty} \hat{\psi}^2(n) = 1. \tag{2.2}$$

Consequently, when the K users' signals are transmitted over a frequency-selective fading channel, the received complex-valued low-pass equivalent signal at a given base station can be expressed as:

$$R(t) = \sum_{k=1}^{K} \sum_{l=0}^{L_p-1} \sqrt{2P_k}\mathbf{c}_k(t - lT_c - \tau_k)b_k(t - lT_c - \tau_k)h_{kl}\exp(j\theta_{kl}) + n(t), \tag{2.3}$$

where $n(t)$ is the complex-valued low-pass-equivalent AWGN having a double-sided spectral density of $N_0/2$ and τ_k is the propagation delay of user k, while L_p is the total number of resolvable paths.

2.2.2 Channel Model

The DS-CDMA signal experiences independent frequency-selective Nakagami-m fading. The complex low-pass equivalent representation of the Channel Impulse Response (CIR) encountered by the kth user is given by [7]:

$$h_k(t) = \sum_{l=0}^{L_p-1} h_{kl}\delta(t - lT_c)\exp\left(j\theta_{kl}\right), \tag{2.4}$$

where h_{kl} represents the Nakagami-distributed fading envelope, lT_c is the relative delay of the lth path of user k with respect to the main path, while L_p is the total number of resolvable multipath components. Furthermore, θ_{kl} is the uniformly distributed phase-shift of the lth multipath component of the channel and $\delta(t)$ is the Kronecker Delta-function. More explicitly, the L multipath attenuations $\{h_{kl}\}$ are independent Nakagami distributed random variables having a Probability Density Function (PDF) of [101–103]:

$$\begin{aligned} p(h_{kl}) &= M(h_{kl}, m_{kl}, \Omega_{kl}), \\ M(R, m, \Omega) &= \frac{2m^m R^{2m-1}}{\Gamma(m)\Omega^m} e^{(-m/\Omega)R^2}, \end{aligned} \tag{2.5}$$

where $\Gamma(\cdot)$ is the gamma function [7], and m_{kl} is the Nakagami-m fading parameter, which characterizes the severity of the fading for the l-th resolvable path of user k [104].

Specifically, $m_{kl} = 1$ represents Rayleigh fading, $m_{kl} \to \infty$ corresponds to the conventional Gaussian scenario and $m_{kl} = 1/2$ describes the so-called one-sided Gaussian fading, i.e. the worst-case fading condition. The Rician and log-normal distributions can also be closely approximated by the Nakagami distribution in conjunction with values of $m_{kl} > 1$. The parameter Ω_{kl} in Eq.(2.5) is the second moment of h_{kl}, i.e. we have $\Omega_{kl} = E[(h_{kl})^2]$. We assume a negative exponentially decaying multipath intensity profile (MIP) given by $\Omega_{kl} = \Omega_{k0}e^{-\eta l}$, $\eta \geq 0, l = 0, \ldots, L_p - 1$, where Ω_{kl} is the average signal strength corresponding to the first resolvable path and η is the rate of average power decay. In general, the user-index is dropped from Ω_{kl}, since we assume that $\Omega_{k0} = \Omega_0$ for $k = 1 \ldots K$.

2.3 BER Analysis

Let the first user be the user-of-interest and consider a receiver using de-spreading as well as multipath diversity combining. The conventional matched filter based RAKE receiver using MRC may be invoked for detection, where we assume that the RAKE receiver is capable of combining L_r number of diversity paths.

Let us assume that we have achieved time synchronization and perfect estimates of the channel magnitudes and phases are available. The individual matched filter outputs are appropriately delayed, in order to coherently combine the L_r number of path signals processed by the RAKE combiner. The lth RAKE combiner finger's output Z_{kl} is sampled at $t = T + lT_c + \tau_k$, in order to detect the kth user's transmitted symbol $b_k[0]$, which is expressed as:

$$Z_{kl} = D_{kl} + I_{kl}, \tag{2.6}$$

where D_{kl} represents the desired direct Line-of-Sight (LOS) component, which can be expressed as:

$$D_{kl} = \sqrt{2P}T_s b_k[0]h_{kl}^2. \tag{2.7}$$

In Eq.(2.7) $b_k[0]$ is the first bit transmitted by the kth BPSK user and we have $b_k[0] \in \{+1, -1\}$. Hence, the interference plus noise term I_k in Eq.(2.6) may be expressed as:

$$I_{kl} = I_{kl}[S] + I_{kl}[M] + N_{kl}, \tag{2.8}$$

where $I_{kl}[S]$ represents the multipath interference imposed by the user-of-interest. Explicitly, $I_{kl}[S]$ may be expressed as:

$$I_{kl}[S] = \sqrt{2P}T_s h_{kl} \sum_{\substack{l_p=0 \\ l_p \neq l}}^{L_p-1} h_{kl_p} \exp(j\theta_{kl_p}) \left\{ \sum_{n=-\infty}^{\infty} \rho_{kk}(n)\hat{\psi}(n) \right\}, \tag{2.9}$$

where the term $\rho_{kk}(n)$ is formulated as:

$$\rho_{kk}(n) = \frac{1}{G}\sum_{i=0}^{G-1} c_k[i]^* c_k[i - nG - l_p]. \tag{2.10}$$

Furthermore, $I_{kl}[M]$ of Eq.(2.8) represents the multiuser interference inflicted by the $K-1$ interfering users, which is expressed as:

$$\begin{aligned} I_{kl}[M] &= \sqrt{2P}T_s h_{kl} \sum_{\substack{k'=1 \\ k'\neq k}}^{K} \sum_{l_p=0}^{L_p-1} h_{k'l_p} \exp(j\theta_{kl_p}) \\ &\quad \times \left\{ \sum_{n=-\infty}^{\infty} \rho_{kk'}(n)\hat{\psi}(n-\tau_k) \right\}, \end{aligned} \tag{2.11}$$

and we have:

$$\rho_{kk'}(n) = \frac{1}{G}\sum_{i=0}^{G-1} c_k[i]^* c_{k'}[i - nG - l_p]. \tag{2.12}$$

It was shown in [23, 105] for a random PN spreading sequence that the random variables $\rho_{kk}(n)$ and $\rho_{kk'}(n)$ may be modelled as complex Gaussian random variables having a mean of zero and a variance of $1/G$. Therefore, the variance of the term $I_{kl}[S]$ of Eq.(2.8), which was explicitly formulated in Eq.(2.9) can be expressed as:

$$\mathrm{Var}\{I_{kl}[S]\} = 2PT_s^2 h_{kl}^2 \Omega_0 [q(L_p,\eta) - 1]\frac{1}{G}\sum_{n=-\infty}^{\infty} \hat{\psi}^2(n), \tag{2.13}$$

which may be simplified with the aid of Eq.(2.2) to:

$$\mathrm{Var}\{I_{kl}[S]\} = 2PT_s^2 h_{kl}^2 \frac{1}{G}\Omega_0 [q(L_p,\eta) - 1]. \tag{2.14}$$

Similarly, the variance of the term $I_{kl}[M]$ formulated in Eq.(2.11) can be expressed as:

$$\begin{aligned} \mathrm{Var}\{I_{kl}[M]\} &= 2PT_s^2 h_{kl}^2 \Omega_0 K q(L_p,\eta)\frac{1}{G}E[\sum_{n=-\infty}^{\infty} \hat{\psi}^2(n-\tau)] \\ &= 2PT_s^2 h_{kl}^2 \Omega_0 K q(L_p,\eta)\frac{1}{G}E[\phi(\beta,\tau)], \end{aligned} \tag{2.15}$$

where $E[\phi(\beta,\tau)] = E[\sum_{n=-\infty}^{\infty} \hat{\psi}^2(n-\tau)]$ defines the *interference factor* associated with a specific chip pulse shape, which predetermines the amount of the MAI imposed by different chip-waveforms, while τ is a random variable uniformly distributed in $[0, 1]$, and $E[\phi(\beta,\tau)]$ can be expressed as a function of the excess bandwidth β, as we mentioned before.

Finally, the noise term of Eq.(2.8) can be expressed as:

$$N_{kl} = h_{kl}\int_0^{T_s} n(t)c[t]dt, \tag{2.16}$$

which is a Gaussian random variable having zero mean and a variance of $2N_0T_sh_{kl}^2$.

The MRC's decision variable Z_k, is constituted by the sum of the RAKE fingers' output, which can be expressed as:

$$Z_k = \sum_{l=0}^{L_r-1} Z_{kl}. \tag{2.17}$$

In the analysis of this section we employ the Gaussian approximation and hence model the multiuser interference and the self-interference terms of Eq.(2.8) as an AWGN process having zero mean and a variance equal to the corresponding variances. More explicitly, the assumptions made in this section are as follows. The RAKE fingers' output signal Z_{kl} is a Gaussian distributed random variable having a mean of D_{kl}. Consequently, according to the analysis of the previous sections –for the random spreading codes and BPSK modulation considered, the variance of the lth RAKE finger's output samples Z_{kl} for a given set of channel amplitudes $\{h_{kl}\}$ may be approximated as:

$$\begin{aligned}\sigma_{kl}^2 &= \frac{1}{2} \times \{\mathrm{Var}\{I_{kl}[S]\} + \mathrm{Var}\{N_{kl}\} + \mathrm{Var}\{I_{kl}[N]\}\} \\ &= 2PT_s^2 \left[\frac{Kq(L_p,\eta)E[\phi(\beta,\tau)]}{2G} + \frac{q(L_p,\eta)-1}{2G} + \left(\frac{2\Omega_0 E_b}{N_0}\right)^{-1}\right] \cdot \Omega_0 h_{kl}^2,\end{aligned} \tag{2.18}$$

where $E_b = PT_s$ is the energy per bit and we have $q(L_p,\eta) = \sum_{l=0}^{L_p-1} e^{-\eta l}$. Furthermore, the MRC's output sample Z_k can be approximated by an AWGN variable having a mean value of $\mathrm{E}[Z_k] = \sum_{l=0}^{L_r-1} D_{kl}$ and a variance of $\mathrm{Var}[Z_k] = \sum_{l=0}^{L_r-1} \sigma_{kl}^2$ [102, 106]. To expound further, upon using Eq.(2.7) and Eq.(2.18) we have:

$$\mathrm{E}[Z_k] = \sum_{l=0}^{L_r-1} \sqrt{2P}T_s b_k[0] h_{kl}^2, \tag{2.19}$$

$$\mathrm{Var}[Z_k] = 2PT_s^2 \left[\frac{Kq(L_p,\eta)E[\phi(\beta,\tau)]}{2G} + \frac{q(L_p,\eta)-1}{2G} + \left(\frac{2\Omega_0 E_b}{N_0}\right)^{-1}\right] \cdot \Omega_0 \sum_{l=0}^{L_r-1} h_{kl}^2. \tag{2.20}$$

Therefore, the BER of BPSK modulation conditioned on the set of fading magnitudes $\{h_{kl}, l = 0, 1, \ldots, L_r - 1\}$ can be expressed as:

$$P_b(\gamma) = Q\left(\sqrt{\frac{(\mathrm{E}[Z_k])^2}{\mathrm{Var}[Z_k]}}\right) = Q\left(\sqrt{\sum_{l=0}^{L_r-1} 2\gamma_l}\right), \tag{2.21}$$

where $Q(x)$ represents the Gaussian Q-function, which can also be represented in its

less conventional form as [104, 106] $Q(x) = \frac{1}{\pi}\int_0^{\pi/2} \exp\left(-\frac{x^2}{2\sin^2\theta}\right) d\theta$, where $x \geq 0$. Furthermore, $2\gamma_l$ in Eq.(2.21) represents the output Signal to Interference plus Noise Ratio (SINR) at the lth finger of the RAKE receiver, while γ_l is given by:

$$\gamma_l = \gamma_c \cdot \frac{h_{kl}^2}{\Omega_0}. \tag{2.22}$$

Let us now substitute Eq.(2.22) into Eq.(2.21) and Eq.(2.19) as well as Eq.(2.20) also into Eq.(2.22). We can see then that the expressions under the square-root functions must be equal, which allows us to express γ_c as follows:

$$\gamma_c = \left[\frac{Kq(L_p,\eta)E[\phi(\beta,\tau)]}{G} + \frac{q(L_p,\eta)-1}{G} + \left(\frac{\Omega_0 E_b}{N_0}\right)^{-1}\right]^{-1}. \tag{2.23}$$

The average BER $P_b(E)$ at a given value of E_b/N_0 can be obtained by the weighted averaging of the output γ_l, i.e. upon integrating the conditional BER of Eq.(2.21) after weighting it by the probability of occurrence of a specific instantaneous value of γ_l, which is quantified by the joint PDF of the instantaneous γ_l values corresponding to the L_r multipath components $\{\gamma_l : l = 0, 2, \ldots, L_r - 1\}$. Since the random variables $\{\gamma_l : l = 1, 2, \ldots, L_r - 1\}$ are assumed to be statistically independent, the average BER expressed in Eq.(2.21) can be formulated as [107]:

$$P_b(E) = \frac{1}{\pi}\int_0^{\pi/2} \prod_{l=0}^{L_r-1} I_l\left(\overline{\gamma}_l, \theta\right) d\theta, \tag{2.24}$$

where $I_l\left(\overline{\gamma}_l, \theta\right)$ is given by:

$$I_l\left(\overline{\gamma}_l, \theta\right) = \int_0^{\infty} \exp\left(-\frac{\gamma_l}{\sin^2\theta}\right) p_{\gamma_l}(\gamma_l) d\gamma_l. \tag{2.25}$$

Since we have $\gamma_l = \gamma_c \cdot \frac{h_l^2}{\Omega_0}$ and h_l obeys the Nakagami-m distribution characterized by Eq.(2.5), it can be shown that the PDF of γ_l can be formulated as [104, 107]:

$$p_{\gamma_l}(\gamma_l) = \left(\frac{m}{\overline{\gamma}_l}\right)^m \frac{\gamma^{m-1}}{\Gamma(m)} \exp\left(-\frac{m\gamma_l}{\overline{\gamma}_l}\right), \quad \gamma_l \geq 0, \tag{2.26}$$

where $\overline{\gamma}_l = \gamma_c e^{-\eta l}$ for $l = 0, 1, \ldots, L_r - 1$.

Upon substituting Eq.(2.26) into Eq.(2.25) it can be shown that we have [104]:

$$I_l\left(\overline{\gamma}_l, \theta\right) = \left(\frac{m\sin^2\theta}{\overline{\gamma}_l + m\sin^2\theta}\right)^m. \tag{2.27}$$

Finally, upon substituting Eq.(2.27) into Eq.(2.24), the average BER of the CDMA system considered can be written as:

$$P_b(E) = \frac{1}{\pi}\int_0^{\pi/2}\prod_{l=0}^{L_r-1}\left(\frac{m\sin^2\theta}{\overline{\gamma}_l + m\sin^2\theta}\right)^m d\theta. \tag{2.28}$$

2.3.1 Time-Limited Waveforms

In this section, we will consider three widely-used time-limited chip-waveforms, which are the rectangular, half-sine and raised-cosine time-domain chip-waveforms, respectively. Explicitly, the time domain shape of these waveforms is formulated as follows.

1) Rectangular:

$\psi^r_{T_c}(t) = u(t)$;

2) Half-Sine:

$\psi^s_{T_c}(t) = \sqrt{2}\sin(\frac{\pi t}{T_c})u(t)$;

3) Raised Cosine:

$\psi^c_{T_c}(t) = \sqrt{\frac{2}{3}}\left[1-\cos(\frac{2\pi t}{T_c})\right]u(t)$.

Figure 2.1 portrays the associated chip-pulse shapes in the time domain, while the

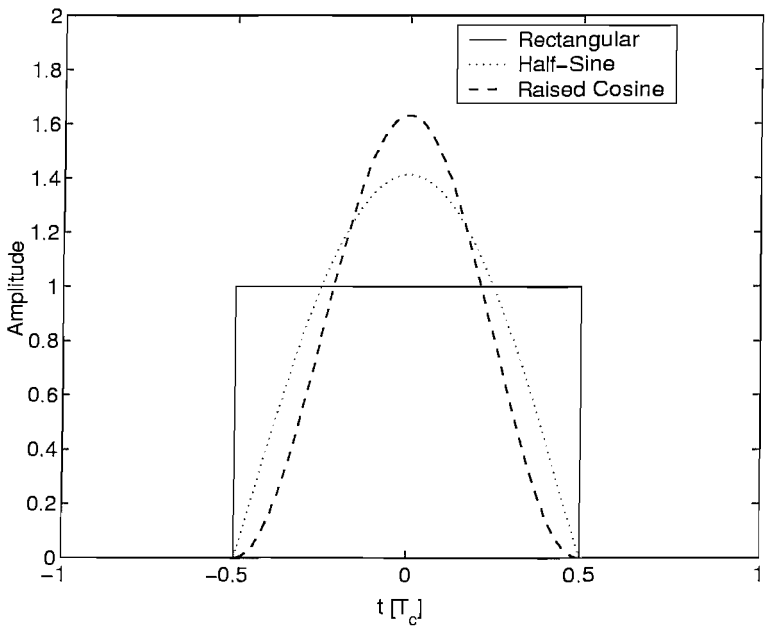

Figure 2.1: The pulse shape of the time-limited waveforms.

corresponding frequency-domain spectral density function $Q(f)$ may be expressed with the aid of the Fourier transform $Q(f) = \mathcal{F}\{\psi_{T_c}(t)\}$. More specifically, the spectral density function $Q(f)$ of these waveforms can be expressed as a function of the normalized frequency fT_c, and for notational convenience we denote the normalized frequency fT_c as f. Then we have:

1) Rectangular:

$Q^r(f) = \mathrm{sinc}(f)$;

2) Half-Sine:

$Q^s(f) = \frac{\cos(\pi f)}{1-4(f)^2}$;

3) Raised Cosine:

$Q^c(f) = \text{sinc}(f) + \frac{1}{2}\text{sinc}(f-1) + \frac{1}{2}\text{sinc}(f+1)$.

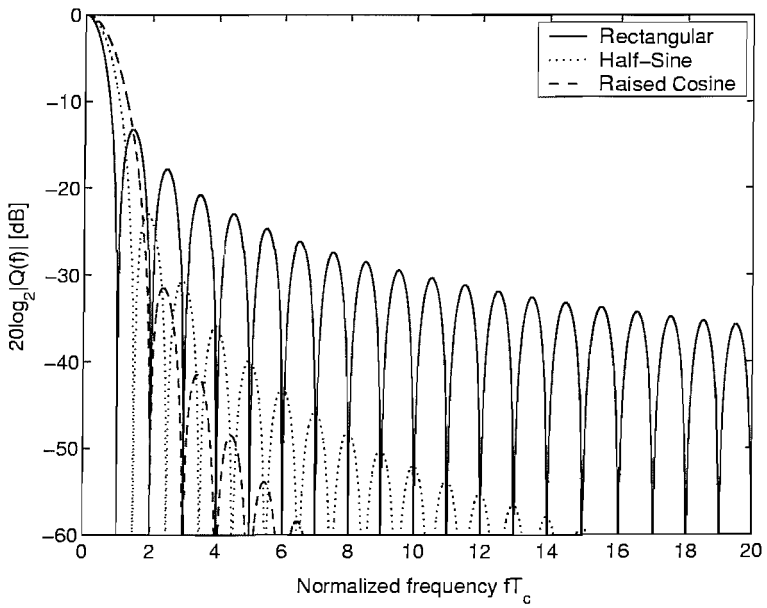

Figure 2.2: The logarithmic energy density spectrum $|Q(f)|^2$ of the rectangular, half-sine and raised cosine time-limited chip-waveforms.

Figure 2.2 portrays the corresponding energy spectral density function $|Q(f)|^2$. We considered two different fractional energy containment bandwidth definitions [46, 49] for the sake of characterizing these time-limited waveforms. It is conceptually appealing to define the fractional energy containment bandwidth [46] as the normalized frequency W that satisfies $\frac{\int_{-W}^{W} Q^2(f)df}{\int_{-\infty}^{\infty} Q^2(f)df} \geq 99\%$. In [46], the similar but more stringent definition of $\frac{\int_{-W}^{W} Q^2(f)df}{\int_{-\infty}^{\infty} Q^2(f)df} \geq 99.995\%$ was used, especially in the context of finite time duration signalling pulses. In terms of the Nyquist excess bandwidth β, we have:

$$\beta = 2WT_c - 1. \tag{2.29}$$

In [23, 48], Dallas and Pavlidou investigated the interference factor, $E[\phi(\beta, \tau)]$ defined in the context of Eq.(2.15), which was found to be 0.666, 0.596 and 0.582 for the rectangular, half-sine and raised cosine chip-waveforms, respectively. Therefore, following Eq.(2.29) and the above definition of the energy containment bandwidth, the required excess bandwidths are summarized in Table 2.1 for both of the above mentioned energy containment factors, along with the corresponding interference factors for the three time-limited chip-waveforms considered.

Waveform	Energy containment bandwidth $\geq 99\%$	Energy containment bandwidth $\geq 99.995\%$	Interference factor $E[\phi(\beta,\tau)]$
Rectangular	$\beta = 12.22$	$\beta = 38.34$	0.666
Half-Sine	$\beta = 1.36$	$\beta = 12.90$	0.596
Raise Cosine	$\beta = 1.82$	$\beta = 5.58$	0.482

Table 2.1: The required excess bandwidth β and the corresponding interference factors $E[\phi(\beta,\tau)]$ for various time-domain chip-pulse shapes.

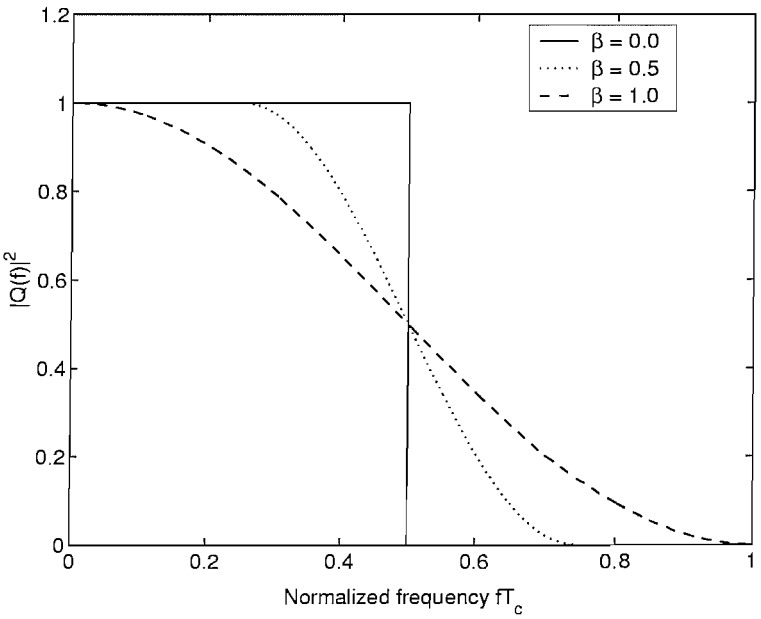

Figure 2.3: The energy spectral density function of three different BRC waveforms, when the excess bandwidth was $\beta = 0, 0.5$ and 1, respectively.

2.3.2 Band-Limited Waveforms

Having considered three time-limited waveforms in the previous section, in this section we will consider two different band-limited waveforms. The first is the well-known frequency-domain raised cosine Nyquist spectrum [7], whose energy spectral density function $Q^2(f)$ is shown in Figure 2.3, where β represents the Nyquist *roll-off* factor, quantifying the excess Nyquist bandwidth. We will refer to this Nyquist signalling pulse as a Band-limited Raised Cosine (BRC) signalling waveform, which is characterized by the spectral domain representation given by [30]:

$$|Q(f)|^2 = \begin{cases} 0, & \text{for } |f| \geq \frac{1+\beta}{2} \\ 1, & \text{for } |f| \leq \frac{1-\beta}{2} \\ \frac{1}{2}\left\{1 + \cos\left(\frac{\pi}{\beta}(|f| - \frac{1}{2})\right)\right\}, & \text{elsewhere.} \end{cases} \tag{2.30}$$

Furthermore, the corresponding chip-pulse shape in time domain can be expressed as [30]:

$$\psi_{T_c}(t) = \text{sinc}(\pi t/T_c)\frac{\cos(\pi\beta t/T_c)}{1 - 4\beta^2 t^2/T_c^2}. \tag{2.31}$$

In Figure 2.4 we plotted the chip-pulse shapes of three different BRC waveforms in the time-domain for the *roll-off* factors of $\beta = 0, 0.5$ and 1.0.

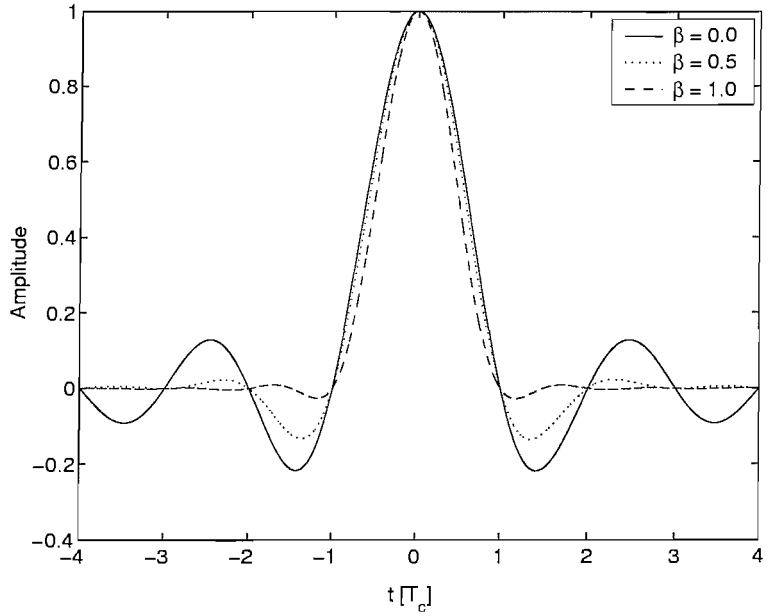

Figure 2.4: The chip-pulse shape of the BRC waveform in the time-domain for *roll-off* factors of $\beta = 0, 0.5, 1$, respectively.

Another band-limited chip-waveform is the so-called optimum waveform [23][2], which was proposed by Cho and Lehnert [23] for the BER performance analysis of band-limited DS-CDMA systems communicating over an AWGN channels, which is given by:

$$|Q(f)|^2 = \begin{cases} 1, & \text{for } |f| < \frac{1-\beta}{2} \\ \frac{1}{2}, & \text{for } \frac{1-\beta}{2} \leq |f| \leq \frac{1+\beta}{2} \\ 0, & \text{elsewhere.} \end{cases} \tag{2.32}$$

Observe in Figure 2.5 that the optimum pulse shapes exhibit an ideal low-pass spectral-domain representation for both $\beta = 0$ and $\beta = 1$. Both of these ideal low-pass spectra are associated with an ideal sinc-shaped time-domain signalling waveform, which has equidistant zero-crossings in the time-domain and hence imposes no inter-symbol interference. However, since the system associated with $\beta = 1$ has twice as high a bandwidth as the scheme having $\beta = 0$, the time-domain zero-crossings of the latter are twice as far as apart as those of the former. This property was similar to that of the Nyquist signalling pulse of Figure 2.4, which exhibited two extra zero-crossing between $[T_c, 2T_c]$. This Given the excess bandwidth values of $0 \leq \beta \leq 1$, Cho and Lehnert [23] investigated the associated interference factors $E[\phi(\beta, \tau)]$ for both the BRC waveform and for the optimum waveform. Explicitly, they found that the interference factor of the pulse shape for the

[2]The terminology 'optimum' is this context implies that the best BER performance was achieved by the system considered, when communicating over an AWGN channel.

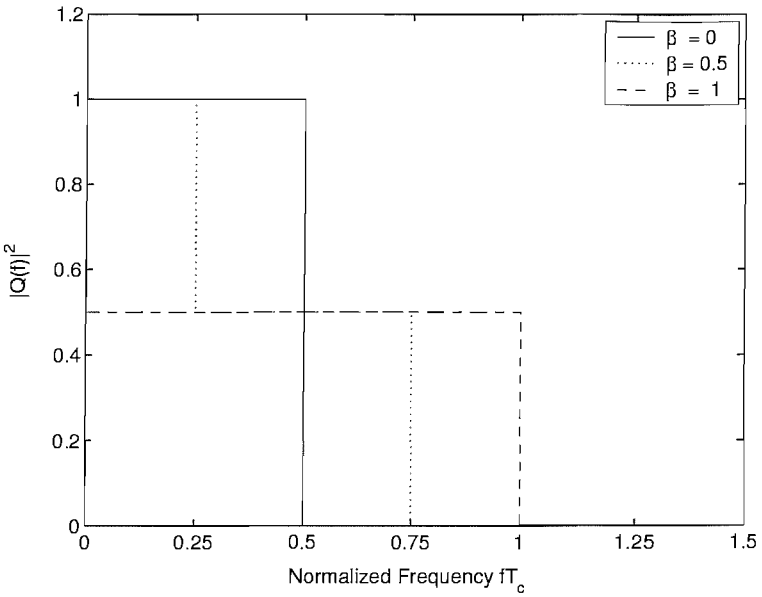

Figure 2.5: Frequency-domain representation of the optimum chip-waveform designed by Cho and Lehnert [23] for the excess bandwidth values of $\beta = 0, 0.5$ anb 1, respectively.

BRC waveform can be expressed as [23]:

$$\begin{aligned} \phi(\beta,\tau) &= 1 - \frac{\beta}{4} + \frac{\beta}{4}\cos(2\pi\tau), \\ E[\phi(\beta,\tau)] &= 1 - \frac{\beta}{4}, \end{aligned} \tag{2.33}$$

while that for the optimum bandlimited waveform as [23]:

$$\begin{aligned} \phi(\beta,\tau) &= 1 - \frac{\beta}{2} + \frac{\beta}{2}\cos(2\pi\tau), \\ E[\phi(\beta,\tau)] &= 1 - \frac{\beta}{2}. \end{aligned} \tag{2.34}$$

Having considered the associated interference factors of the BRC and optimum chip-pulse shape for the family of the band-limited waveforms, in next section we will consider the optimization of the processing gain G and the excess bandwidth β.

2.3.3 Jointly Optimizing the Processing Gain G and the Excess Bandwidth β for Band-Limited Waveforms

Given a bandwidth W and a transmitted bit rate of $\frac{1}{T_s}$, according to Eq.(2.23) we have to minimize $\frac{E[\phi(\beta,\tau)]}{G}$ under the constraint that the total system's bandwidth of $G(1+\beta) = 2WT_s$ is a constant. More explicitly, the inteference factor $E[\phi(\beta,\tau)]$ is divided by G for the sake of optimising the system, because the increased amount of MAI imposed by a chip-waveform having higher spectral-domain side-lobes manifests itself in terms of an increased interference factor. The effects of this increased MAI maybe compensated by employing a higher spreading factor or spreading gain, hence their joint optimum is sought. This optimisation problem can be solved with the aid of Lagrange multipliers.

Hence for the sake of finding the optimum bandlimited chip-waveform, let

$$\Omega(G,\beta) = \frac{E[\phi(\beta,\tau)]}{G} + \lambda[G(1+\beta) - 2WT_s]. \tag{2.35}$$

Then, upon using the optimum bandlimited waveform of Cho and Lehnert [23], we have:

$$\Omega(G,\beta) = \frac{1-\frac{\beta}{2}}{G} + \lambda[G(1+\beta) - 2WT_s]. \tag{2.36}$$

Owing to the fact that $\Omega(G,\beta)$ is a strictly convex function of G and β, for the optimum waveform the worst possible configuration of the variables G and β satisfies:

$$\frac{\partial\Omega(G,\beta)}{\partial G} = -\frac{1-\beta/2}{G^2} + \lambda(1+\beta) = 0, \tag{2.37}$$

$$\frac{\partial\Omega(G,\beta)}{\partial\beta} = -\frac{1}{2G} + \lambda G = 0, \tag{2.38}$$

and from Eq.(2.37) we arrive at $\beta = 1/2$.

$$\Omega(G,\beta) = \frac{1-\frac{\beta}{4}}{G} + \lambda[G(1+\beta) - 2WT_s]. \tag{2.39}$$

Similarly, for the BRC waveform it may be readily shown by evaluating Eq.(2.39) that a choice of $\beta = 3/2$ achieved the worst-case performance. However, in our case β is limited to the interval of $[0,1]$, hence $\beta = 1$ achieved the worst possible performance in the context of the BRC waveform. In the next section we will discuss the choice of β required for achieving the best possible performance for band-limited chip-waveform based DS-CDMA systems.

2.4 Numerical Results

In this section we will investigate the achievable BER performance of band-limited DS-CDMA. As mentioned before, the normalized bandwidth can be expressed as $G(1+\beta) = 2WT_s$. Hence upon stipulating a specific $G(1+\beta)$ value, the system's bandwidth as well as the bit rate has been fixed. The parameters employed in our investigations were $L_p = 10, L_r = 4, \eta = 0.2$, and $K = 10$. Figure 2.6 portrays the attainable BER performance of DS-CDMA in conjunction with the previously mentioned three time-limited waveforms at $G(1+\beta) = 1000$[3]. These results were plotted by evaluating Eq.(2.28). We can observe that in Figure 2.6 the raised cosine waveform based DS-CDMA system is capable of achieving the best performance, since its frequency-domain spectral side-lobe seen in Figure 2.2 is relatively low, and the corresponding excess bandwidth values are listed in Table 2.1. By contrast, the performance of the rectangular chip-waveform based DS-CDMA scheme is the worst amongst the three chip-waveforms investigated. When considering an energy containment in excess of 99%, the half-sine signalling chip-waveform based DS-CDMA system achieves a similar performance to that of the scheme using a time-domain raised

[3]In all the following figures, E_b/N_0= average SNR per bit.

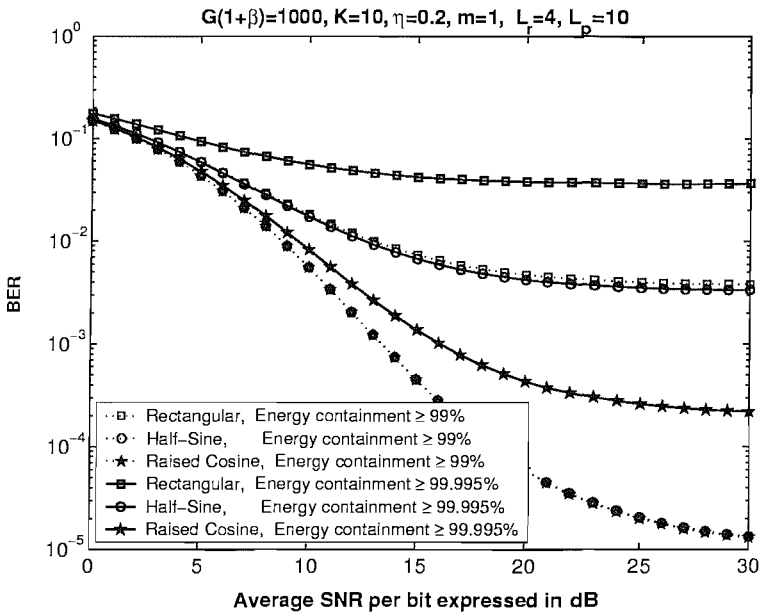

Figure 2.6: BER performance comparisons of various band-limited DS-CDMA systems as a function of E_b/N_0 when communicating over a Rayleigh channel associated with $m = 1$ in conjunction with three time-limited chip-waveforms, where two different energy containment factors, namely $\geq$ 99% and $\geq$ 99.995% were considered. A negative-exponentially decaying Multipath Intensity Profile (MIP) having a decay factor of $\eta = 0.2$ was used, the total number of resolvable paths was $L_p = 10$, but the RAKE-receiver's complexity was limited to combining only $L_r = 4$ paths. A total of $K = 10$ users were supported.

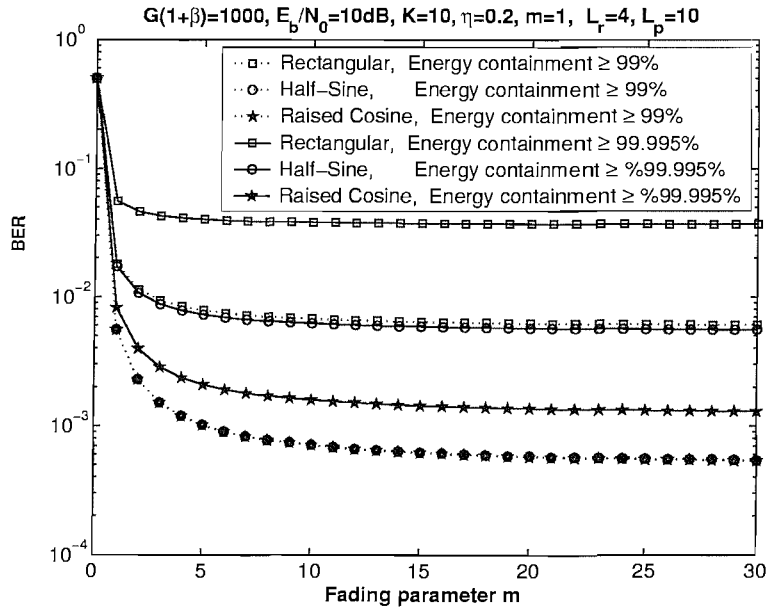

Figure 2.7: BER performance comparisons of various band-limited DS-CDMA systems as a function of the Nakagami fading parameter m in conjunction with three time-limited chip-waveforms, where two different energy containment factors, namely $\geq$ 99% and $\geq$ 99.995% were considered. A negative-exponentially decaying Multipath Intensity Profile (MIP) having a decay factor of $\eta = 0.2$ was used, the total number of resolvable paths was $L_p = 10$, but the RAKE-receiver's complexity was limited to combining only $L_r = 4$ paths. A total of $K = 10$ users were supported.

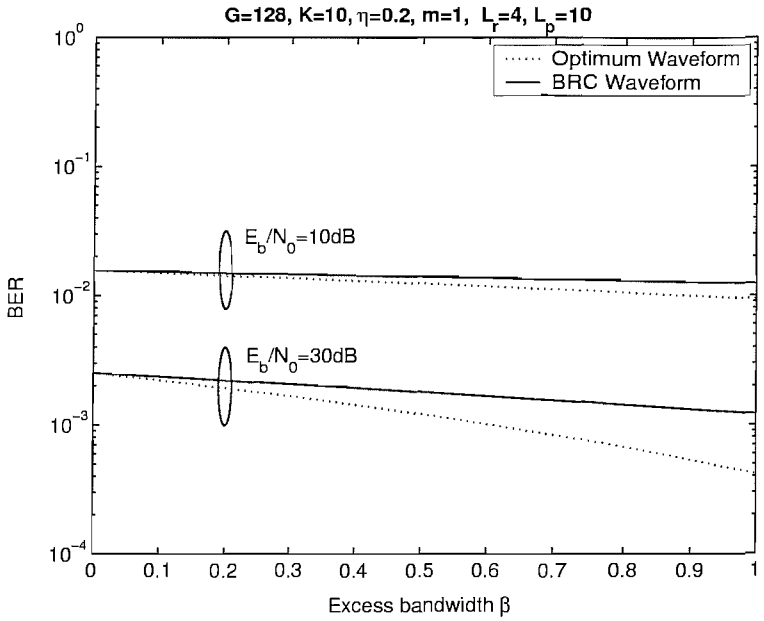

Figure 2.8: BER performance comparison of band-limited DS-CDMA as a function of the excess bandwidth β in conjunction with the BRC and the optimum [23] waveforms, when the processing gain was fixed to $G = 128$. A negative-exponentially decaying Multipath Intensity Profile (MIP) having a decay factor of $\eta = 0.2$ was used, the total number of resolvable paths was $L_p = 10$, but the RAKE-receiver's complexity was limited to combining only $L_r = 4$ paths, and a total of $K = 10$ users were supported. The total bandwidth requirement obeyed the relationship of $G(1+\beta)$, varying over the range of $128 \ldots 256$. The BER reduction observed is a consequence of a higher excess bandwidth β.

cosine chip-waveform. This is because as seen in Table 2.1, the half-sine chip-waveform based DS-CDMA system requires a smaller excess bandwidth β than that of the raised cosine chip-waveform based system, when the energy containment is in excess of 99%, while at the same time exhibiting a higher interference factor of $E[\phi(\beta, \tau)]$. Figure 2.7 portrays the attainable BER performance of band-limited DS-CDMA as a function of the Nakagami fading parameter m. From this figure we may infer similar conclusions to those accruing from Figure 2.6, when communicating over different fading channels characterised by various Nakagami fading parameters.

Figure 2.8 depicts the achievable performance of the band-limited chip-waveform based DS-CDMA system as a function of the excess bandwidth β, where we have $G = 128$ and β is limited $[0, 1]$. Both the BRC chip-waveform and the optimum chip-waveform of Cho and Lehnert [23] were used. From this figure, we may conclude that the system is capable of achieving an improved BER performance, as the excess bandwidth β increases. More specifically, we are capable of reducing the interference factor $E[\phi(\beta, \tau)]$ at the cost of increasing β and hence reducing the bandwidth efficiency. In Figure 2.9 we investigated the trade-offs between the different values of the spreading gain G and the excess bandwidth β at a fixed bandwidth requirement of $G(1+\beta) = 256$. From this figure we can observe that the BER performance of the optimum chip-waveform based DS-CDMA system is at its worst, when we have $\beta = 0.5$, although this trend is only visible at $E_b/N_0 = 30$dB.

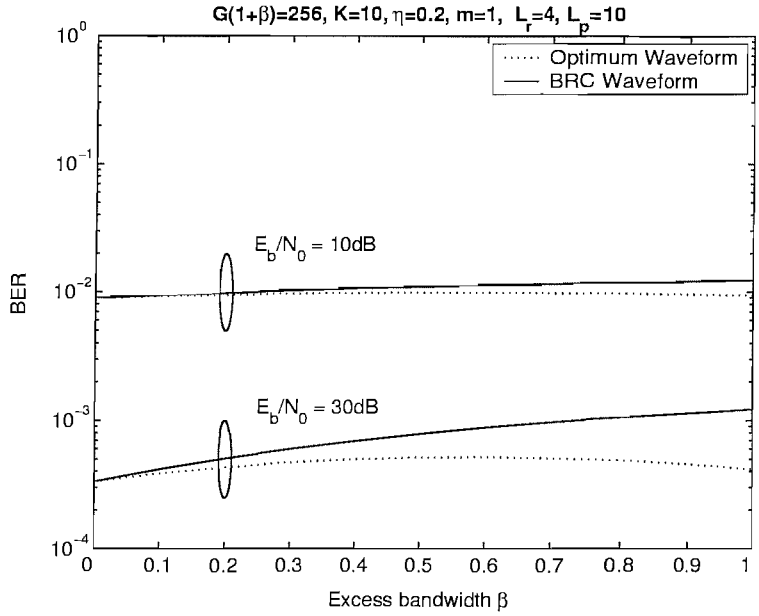

Figure 2.9: BER performance comparison of band-limited DS-CDMA as a function of the excess bandwidth β in conjunction with the BRC and the optimum waveforms [23], when the bandwidth required was fixed to $G(1+\beta) = 256$. A negative-exponentially decaying Multipath Intensity Profile (MIP) having a decay factor of $\eta = 0.2$ was used, the total number of resolvable paths was $L_p = 10$, but the RAKE-receiver's complexity was limited to combining only $L_r = 4$ paths, and a total of $K = 10$ users were supported.

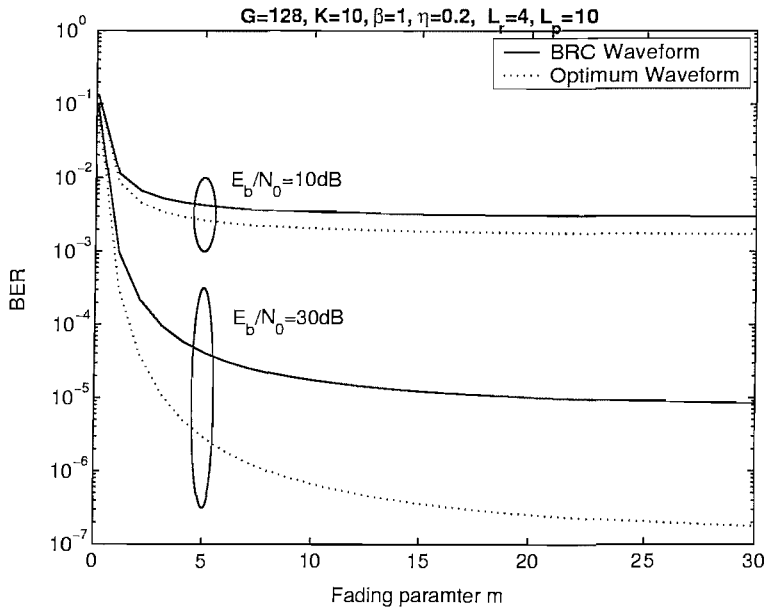

Figure 2.10: BER performance comparison of band-limited DS-CDMA as a function of the Nakagami fading parameter m in conjunction with the BRC and the optimum [23] waveforms, where the excess bandwidth was fixed to $\beta = 1$, and the processing gain was $G = 128$. A negative-exponentially decaying Multipath Intensity Profile (MIP) having a decay factor of $\eta = 0.2$ was used, the total number of resolvable paths was $L_p = 10$, but the RAKE-receiver's complexity was limited to combining only $L_r = 4$ paths, and a total of $K = 10$ users were supported. As m increases, the channel becomes a dispersive AWGN-like transmission medium, resulting in a reduced BER.

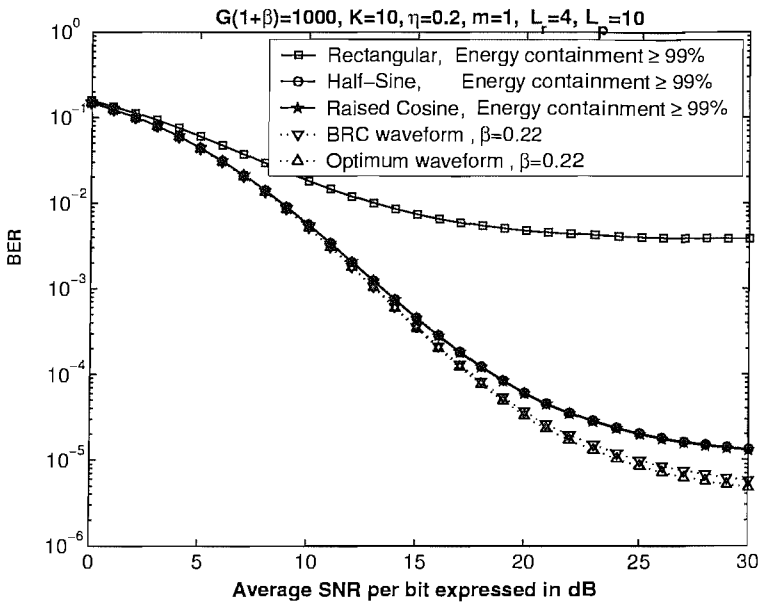

Figure 2.11: BER performance comparison of band-limited DS-CDMA as a function of E_b/N_0 in conjunction with the three time-limited and two band-limited chip-waveforms studied, when the required bandwidth was fixed to $G(1+\beta) = 1000$. A negative-exponentially decaying Multipath Intensity Profile (MIP) having a decay factor of $\eta = 0.2$ was used, the total number of resolvable paths was $L_p = 10$, but the RAKE-receiver's complexity was limited to combining only $L_r = 4$ paths, and a total of $K = 10$ users were supported.

This performance trend is in line with our discussions provided in Section 2.3.3. By contrast, when we have $\beta \to 0$ and $\beta \to 1$, the system is capable of achieving its best possible performance, although again, these trends are only perceivable at $E_b/N_0 = 30$dB. Furthermore, for the BRC waveform, when we have $\beta \to 0$ the system attains its best possible performance. Figure 2.10 comparatively studied the performance of the BRC waveform and the optimum chip-waveform of [23] as a function of the Nakagami fading parameter m. From this figure we may conclude that the optimum waveform is capable of achieving a significantly better performance than that of the BRC waveform, when we have $\beta \to 1$.

In Figure 2.11 we investigated the BER performance of band-limited DS-CDMA in conjunction with the tree different time-limited and two band-limited chip-waveforms considered, when the bandwidth occupied was fixed to $G(1+\beta) = 1000$. From this figure we infer that a frequency-domain BRC waveform based DS-CDMA system employing $\beta = 0.22$ is capable of achieving a similar performance to that of using the optimum waveform [23] associated with $\beta = 0.22$, when communicating over a Rayleigh fading channel. Furthermore, the time-domain raised-cosine waveform aided CDMA system of Figure 2.11 was also capable of approaching the BER of both the frequency-domain BRC and optimum chip-waveform, although at $E_b/N_0 = 30$dB it exhibited an approximately factor two higher residual BER. Finally, Figure 2.12 portrays the BER performance of the band-limited DS-CDMA system investigated as a function of the number of users K supported.

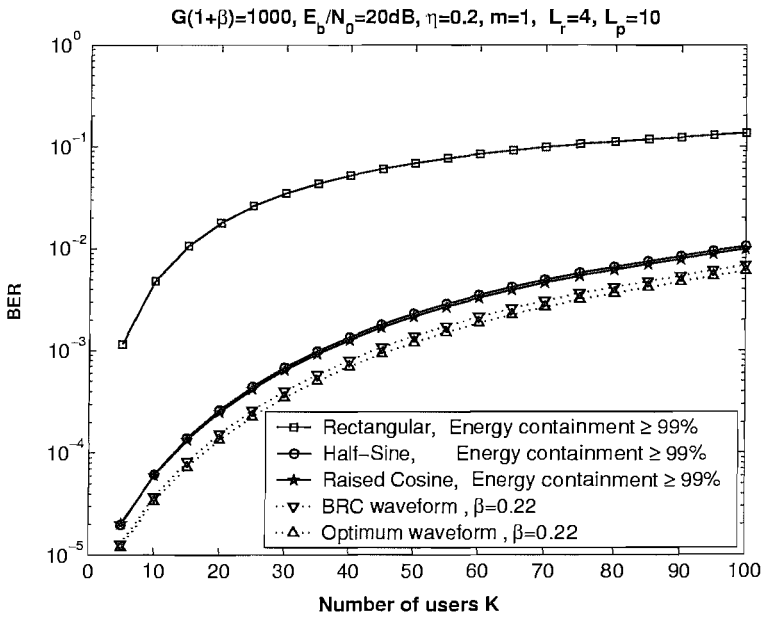

Figure 2.12: BER performance comparison of band-limited DS-CDMA as a function of the number of users K supported in conjunction with the three time-limited and two band-limited chip-waveforms studied, when the required bandwidth was fixed to $G(1+\beta) = 1000$. A negative-exponentially decaying Multipath Intensity Profile (MIP) having a decay factor of $\eta = 0.2$ was used, the total number of resolvable paths was $L_p = 10$, but the RAKE-receiver's complexity was limited to combining only $L_r = 4$ paths, and the SNR of each user was fixed to $E_b/N_0 = 20$dB.

2.5 Chapter Conclusions

Pulse Shape	Bit Error Ratio P_b
Rectangular waveform (energy containment $\geq 99\%$)	1.1×10^{-2}
Half Sine waveform (energy containment $\geq 99\%$)	6.5×10^{-5}
Raised Cosine waveform (energy containment $\geq 99\%$)	6.5×10^{-5}
Rectangular waveform (energy containment $\geq 99.99\%$)	9.5×10^{-2}
Half Sine waveform (energy containment $\geq 99.99\%$)	7.5×10^{-3}
Raised Cosine waveform (energy containment $\geq 99.99\%$)	6.2×10^{-4}
BRC waveform ($\beta = 0.22$)	3.1×10^{-5}
Optimum waveform($\beta = 0.22$)	3.0×10^{-5}

Table 2.2: BER performance in conjunction with various chip-waveforms, when we have the bandwidth of $G(1+\beta) = 1000$ and $E_b/N_0 = 20$dB, while $K = 10$ users are supported.

In this chapter, we have investigated the achievable performance of band-limited DS-CDMA in conjunction with three different time-limited and two band-limited chip-waveforms. In the context of the time-limited waveforms the raised cosine waveform based DS-CDMA system achieved the best performance, because its frequency-domain spectral side-lobe seen in Figure 2.2 is relatively low. By contrast, when we considered band-limited waveforms, we investigated the BER performance of both the optimum [23] and BRC waveform based DS-CDMA systems. Both of these band-limited waveform based DS-CDMA schemes exhibited a better BER performance than that of the time-limited

waveforms. When aiming for an energy containment in excess of 99%, the raised cosine waveform based DS-CDMA scheme was capable of achieving a similar performance to that of the optimum waveform based DS-CDMA arrangement. Finally, Table 2.2 summarizes the BER performance of DS-CDMA in conjunction with various chip-waveforms, when communicating over a $L_p = 10$-path Rayleigh fading channel. The number of users supported was $K = 10$ and the E_b/N_0 value was 20dB.

CHAPTER 3

LAS-CDMA

3.1 Introduction

In Direct Sequence Code Division Multiple Access (DS-CDMA) systems, the spreading sequences characterize the associated Inter Symbol Interference (ISI) as well as the Multiple Access Interference (MAI) properties [3]. Traditional spreading sequences, such as m-sequences [3], Gold codes [3] and Kasami codes [3] exhibit non-zero off-peak auto-correlations and cross-correlations, which results in a high MAI in case of asynchronous uplink transmissions. Another family of orthogonal codes is constituted by Walsh codes [3] and orthogonal Gold codes [4], which retain their orthogonality only in case of perfect synchronization, but they also exhibit non-zero off-peak auto-correlations and cross-correlations in asynchronous scenarios. Consequently, these correlation properties limit the achievable performance in asynchronous scenarios. Hence traditional DS-CDMA cellular systems are interference limited and suffer from the so-called 'near-far' effects, unless complex interference cancellers [3] or multi-user detectors [3] are employed for combating these adverse effects. This results in costly and 'power-hungry' implementations. All these limitations are imposed by the imperfect correlation properties of the spreading sequences employed.

Hence, considerable research efforts have been invested in designing spreading sequences, which exhibit zero correlation values, when the relative delay-induced code offset is in the so-called Zero Correlation Zone (ZCZ) or Interference Free Window (IFW) of the spreading code [53]. The attractive family of Large Area Synchronized (LAS) CDMA spreading sequences is constituted by the combination of the so-called Large Area (LA) codes [24, 52] and Loosely Synchronous (LS) codes [18]. The resultant LAS codes exhibit an IFW , where the off-peak aperiodic autocorrelation values as well as the aperiodic

cross-correlation values become zero, resulting in zero ISI and zero MAI, provided that the time-offset of the codes is within the IFW. In order to ensure that the relative time-offsets between the codes are within the IFW, the mobiles are expected to operate in a quasi-synchronous manner. More specifically, interference-free CDMA communications become possible, when the total time-offset expressed in terms of the number of chip intervals, which is the sum of the time-offset of the mobiles plus the maximum channel-induced delay spread is within the designed IFW. In case of high transmission-delay differences accurate timing-advance control has to be used [108], as it was also advocated in the GSM system [6]. Provided that these conditions are satisfied, a major benefit of the LAS codes is that they are capable of achieving a near-single-user performance without multi-user detectors.

The disadvantage of LAS codes is that the number of codes having an IFW is limited. For example, we will show that when we consider a spreading factor of 151, we only have 32 LAS codes exhibiting an IFW of width $3T_c$, where T_c is the chip duration. Furthermore, the auto-correlation and cross-correlation function of LAS codes typically exhibits a higher value outside the IFW than traditional random codes. More explicitly, when the LAS-CDMA system operates in an asynchronous manner, such as for example the third-generation W-CDMA system [3, 13], it will encounter more serious MAI and Multipath Interference (MPI) than traditional DS-CDMA.

In this chapter, we will investigate the performance of LAS-CDMA in a quasi-synchronous uplink scenario when communicating over a Nakagami-m channel and characterize its BER performance as a function of the number of resolvable paths L_p, the maximum delay difference τ_{max}, the number of users K and the Nakagami fading parameter m. Furthermore, we will comparatively study LAS-CDMA and traditional DS-CDMA systems.

Furthermore, when we consider a Space-Time Spreading (STS) [25] assisted DS-CDMA scheme communicating over a non-dispersive downlink channel, the employment of orthogonal spreading codes such as Walsh codes and orthogonal Gold codes [4] is ideal for the non-dispersive synchronous downlink (DL) channel, since the channel will not destroy the orthogonality of the codes, when we invoke a matched filter based RAKE receiver at the receiver side. However, classic orthogonal codes – such as for example Walsh codes – will lose their orthogonality, when communicating over a dispersive multipath channel. More specifically, when the RAKE receiver coherently combines the different paths' energy, it will inevitably combine both the multiple access interference (MAI) as well as the multipath interference (MPI) in case of communicating over a dispersive multipath channel. In order to circumvent this problem, the family of LS codes [18, 19] has been proposed for the downlink scenario. More specifically, when the dispersive channel's delay spread does not exceed the width of IFW, we can combine all the paths' energy without imposing any MAI and MPI interference. Hence, in this chapter we will also investigate the performance of an LS code based STS scheme in comparison to that of the STS scheme of [25], when communicating over dispersive Nakagami-m multipath channels. Since LS codes were described in [18, 19], while the philosophy of STS was detailed

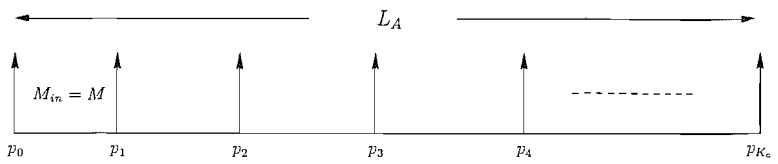

Figure 3.1: Stylized pulse-positions in the LA(L_A, M, K_c) code having K_c number of binary ± 1 pulses, and exhibiting a minimum spacing of M chip durations between non-zero pulses, while having a total code length of L_A chips.

in [3, 25], here we refrain from their detailed description.

This chapter is organized as follows. Section 3.2 will introduce the family of LAS codes, while Section 3.3 will describe the LAS-CDMA system model. In Section 3.3.3 we will characterize the BER performance of LAS-CDMA, and in Section 3.3.4 we will discuss our findings. Section 3.4 describes the Multi-Carrier LAS-code based DS-CDMA (MC LAS DS-CDMA) for broadband communications systems, while Section 3.4.3 illustrates the performances of MC LAS DS-CDMA communicating in diverse propagation environments. Section 3.5 characterizes the downlink performance of space-time spreading using the LS code. Finally, in Section 3.6 we will offer our conclusion.

3.2 Generation of LAS-Codes

3.2.1 LA Codes

LA codes [24, 52] belong to a family of ternary codes having elements of ± 1 or 0. Their maximum correlation magnitude is unity and they also exhibit an IFW. Let us denote the family of the K_c number of orthogonal ternary codes employing K_c number of binary ± 1 pulses by LA(L_A, M, K_c), which exhibit a minimum spacing of M chip durations between non-zero pulses, while having a total code length of L_A chips, as shown in Figure 3.1. All the codes corresponding to an LA code family share the same legitimate pulse positions. However, a specific drawback of this family of sequences is their relatively low duty ratio, quantifying the density of the non-zero pulses, since this limits the number of codes available and hence the number of users supported. Li [24] characterized the pulse positions of the LA code family, while Choi and Hanzo [19] further improved the achievable duty ratio of the LA codes. In the LAS-CDMA 2000 system [109], the LA codes used constitute a modified version of the LA(L_A, M, K_c)=LA(2552, 136, 17) code, where the $K_c = 17$ non-zero pulse positions, p_k, $k = 0, \cdots, 16$, are given by:

$$\begin{aligned}\{p_k\} &= \{0, 136, 274, 414, 556, 700, 846, 994, 1144, \\ &\quad 1296, 1450, 1606, 1764, 1924, 2086, 2250, 2416\}.\end{aligned}$$

Again, observe in this code construction that the pulse positions are not exactly equidistant. For example, the distance between the second, third and fourth pulses is 274-138=138 and 414-174=140, respectively, which is larger than $M = 136$, since M is the minimum spacing. For a specific procedure concerning the design of LA-code based LAS

codes, please refer to [19], where the associated correlation properties and the IFW width of the codes were also characterized.

3.2.2 Loosely Synchronized Codes

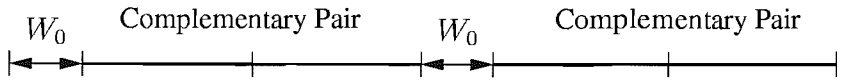

(a) The LS code structure

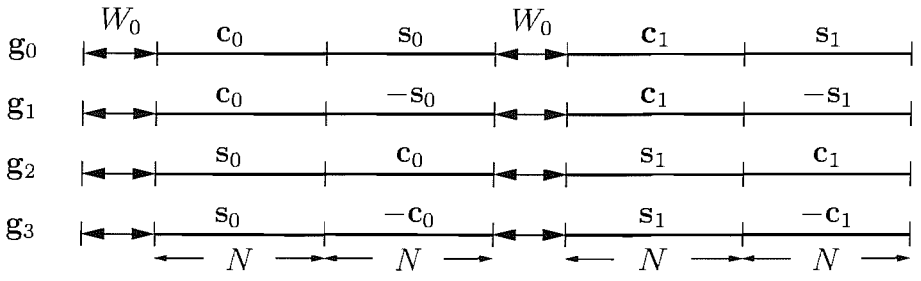

(b) Generating four LS codes.

Figure 3.2: Generating the LS(N, P, W_0) code using the ($P \times P$) = (4 × 4) Walsh-Hadamard matrix components (1, 1, 1, 1) and (1, −1, 1, −1).

Apart from the LA codes of Section 3.2.1, there exists another specific family of spreading codes, which also exhibits an IFW. Specifically, Loosely Synchronized (LS) codes [18] exploit the properties of the so-called orthogonal complementary sets [18, 110]. To expound further, let us introduce the notation of LS(N, P, W_0) for denoting the family of LS codes generated by applying a ($P \times P$)-dimensional Walsh-Hadamard (WH) matrix to an orthogonal complementary code set of length N, as it is exemplified in the context of Figure 3.2. More specifically, we generate a complementary code pair inserting W_0 number of zeros both in the center and at the beginning of the complementary pair, as shown in Figure 3.2(a), using the procedure described in [18]. As mentioned above, the polarity of the codes c_0 and s_0 seen in Figure 3.2(b) during the constitution of the LS codes is determined by the polarity of the components of a Walsh-Hadamard matrix, namely by (1, 1, 1, 1) and (1, −1, 1, −1). Then, the total length of the LS(N, P, W_0) code is given by $L_S = NP + 2W_0$ and later we will demonstrate that the total number of codes available is given by $4P$. The number of these codes having an IFW of W_0 chips is P, which limits the number of users that can be supported without imposing multiuser interference. Hence the number of codes having as long an IFW as possible has to be maximized for a given code length $L_S = NP + 2W_0$.

Since the construction method of binary LS codes was described in [18], here we refrain from providing an indepth discourse and we will focus our attention on the employment of orthogonal complementary sets [111, 112] for the generation of LS codes.

For a given complementary code pair $\{\mathbf{c}_0, \mathbf{s}_0\}$ of length N, one of the corresponding so-called mate pairs can be written as $\{\mathbf{c}_1, \mathbf{s}_1\}$, where we have:

$$\mathbf{c}_1 = \tilde{\mathbf{s}}_0^*, \tag{3.1}$$

$$\mathbf{s}_1 = -\tilde{\mathbf{c}}_0^*, \tag{3.2}$$

and where the superscript $*$ denotes the conjugation and $\tilde{\mathbf{s}}_0$ denotes the reverse-ordered sequence and $-\mathbf{s}_0$ is the negated version of $\mathbf{s}_0$, respectively. Note that in Equation 3.1 and Equation 3.2 additional complex conjugation of the polyphase complementary sequences $\{\mathbf{c}_0, \mathbf{s}_0\}$ is required for deriving the corresponding mate pair $\{\mathbf{c}_1, \mathbf{s}_1\}$ in comparison to binary complementary sequences [18]. Having obtained a complementary pair and its corresponding mate pair, we may employ the construction method of [18] for generating a whole family of LS codes. The LS codes generated exhibit an IFW of length W_0. Hence, we may adopt the choice of $W_0 = N-1$ in order to minimize the total length of the LS codes generated, while providing as long an IFW as possible.

For example, the LS(N, P, W_0)=LS(4,4,3) codes can be generated based on the complementary pair of [111]:

$$\mathbf{c}_0 = + + + - \tag{3.3}$$

$$\mathbf{s}_0 = + + - + . \tag{3.4}$$

Upon substituting Equation 3.1 and Equation 3.2 into Equation 3.3 and Equation 3.4, the corresponding mate pair can be obtained as:

$$\mathbf{c}_1 = \tilde{\mathbf{s}}_0^* = + - + + \tag{3.5}$$

$$\mathbf{s}_1 = -\tilde{\mathbf{c}}_0^* = + - - - . \tag{3.6}$$

The first set of four LS codes can be generated using the first two rows of a $(P \times P) = (4 \times 4)$-dimensional Walsh-Hadamard matrix, namely using $\mathbf{w}_0 = (+1, +1, +1, +1)$ and $\mathbf{w}_1 = (+1, -1, +1, -1)$, as shown in Figure 3.2(b). Another set of four LS codes can be obtained by exchanging the subscripts 0 and 1. Finally, eight additional LS codes can be generated by applying the same principle, but with the aid of the last two rows of the (4×4)-dimensional Walsh-Hadamard matrix, namely using $\mathbf{w}_2 = (+1, +1, -1, -1)$ and $\mathbf{w}_3 = (+1, -1, -1, +1)$. Hence, the total number of available codes in the family of LS(N, P, W_0) is given by $4P$. More explicitly, there are four sets of P number of LS codes. Each set has four LS codes, and the LS codes in the same set exhibit an IFW length of $[-\iota, +\iota]$, where we have $\iota = \min\{W_0, N-1\}$. The aperiodic auto-correlation and cross-correlation function $\rho_{kk}(\tau)$, $\rho_{jk}(\tau)$ of the codes belonging to the same set will be zero, provided that we have $\tau \leq \iota T_c$. Furthermore, the LS codes belonging to the four different sets are still orthogonal to each other at zero offset, namely in a perfectly synchronous environment. However, the LS codes belonging to the four different sets will lose their orthogonality, when they have a non-zero code-offset.

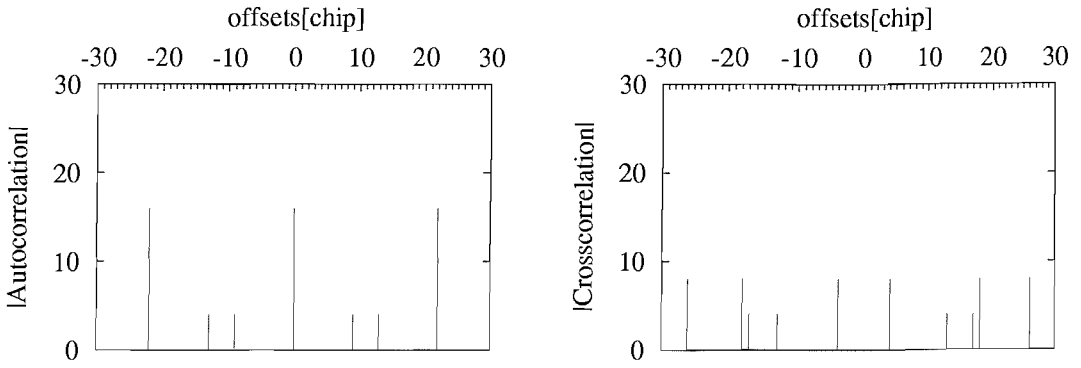

(a) Autocorrelation (b) Crosscorrelations

Figure 3.3: correlation magnitudes of the LS(4, 4, 3) codes. (a) All four codes exhibit the same autocorrelation magnitude. (b) The crosscorrelation magnitudes of $\mathbf{g}_0$ and $\mathbf{g}_2$.

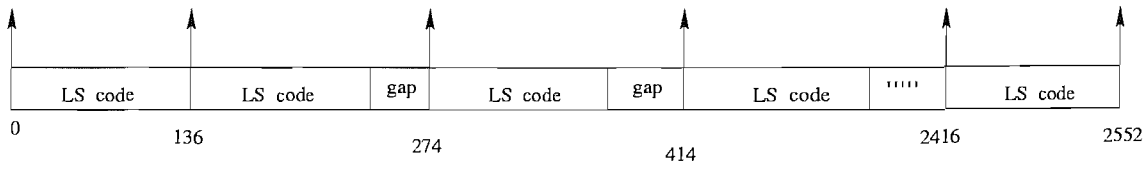

Figure 3.4: LAS($L_A, M, K_c; N, P, W_0$)=LAS(2552,136,17;4,32,4) spreading, inserting the LS codes of Figure 3.2 into the zero-space of the LA codes seen Figure 3.1. The gap seen in the figure indicates that the M = 136-chip LS code does not always fill the spacing between the consecutive pulse of the constituent LA code.

All four different codes in same set of the LS(4,4,3) code family exhibited the same autocorrelation magnitudes, namely that seen in Figure 3.3(a). It can be observed in Figure 3.3(a) that the off-peak autocorrelation $R_p[\tau]$ becomes zero for $|\tau| \leq W_0 = 3$. The crosscorrelation magnitudes $|R_{j,k}(\tau)|$ depicted in Figure 3.3(b) are also zero for $|\tau| \leq W_0 = 3$. Based on the observations made as regards to the aperiodic correlations we may conclude that the LS(4,4,3) codes exhibit an IFW of ± 3 chip durations.

In this section we have demonstrated that the family of LS(N, P, W_0) codes can be constructed for almost any arbitrary code-length related parameter N by employing binary sequences. Having discussed the construction of LA and LS codes, let us now consider how LS codes are implanted at the non-zero pulse-positions of the LA codes for the sake of generating LAS codes.

3.2.3 Seeding LS Codes in LA Codes to Generate LAS codes

We observed in Section 3.2.1 that the main problems associated with applying LA codes in practical CDMA systems are related to their low duty ratio and to the resultant small number of available codes. A specific family of LAS codes [18] mitigates this problem by combining the LA codes of Section 3.2.1 and the LS codes of Section 3.2.2. More specifically, LS codes are inserted between the non-zero pulses of the LA code sequence of Figure 3.1, in an effort to generate an increased number of spreading codes having an

increased duty ratio, while maintaining attractive correlation properties. For example, in the LAS-2000 system [109], the LS spreading codes are inserted into the LA code's zero space, as shown in Figure 3.4.

Let us denote the combined code generated from the LA(L_A,M,K_c) and LS(N,P,W_0) codes as LAS($L_A, M, K; N, P, W_0$), which is generated by employing the so-called absolute encoding method [19, 24]. For the sake of preserving the original IFW size of the constituent LS(N,P,W_0) code when combined with an LA(L_A,M,K_c) code employing the absolute encoding scheme, the length of the LS code - including W_0 number of trailing zeros - should not exceed the minimum pulse spacing M of the LA code, requiring that we have:

$$PN + 2W_0 \leq M. \tag{3.7}$$

In the LAS-CDMA 2000 system [109], a modified version of the LA(2552,136,17) and LS(4,32,4) codes was combined for the sake of generating the LAS($L_A = 2552, L_S = M = 136, K = 17; N = 4, P = 32, W_0 = 4$) code. As we mentioned in Section 3.2.2, from the total set of $4P = 128$ LS codes, only 32 LS codes exhibited an IFW width of $\iota = 3$, and different permutations of the LA codes were employed in the different cells for the sake of mitigating the inter-cell interferences imposed [1]. Recall that this measure was necessary because the LAS codes from different set, which were generated from the different WH matrix row remain orthogonal only in a synchronous scenario.

3.3 LAS-CDMA System Model

3.3.1 Channel Model

The DS-CDMA signal experiences independent frequency-selective Nakagami-m fading. The complex low-pass equivalent representation of the Channel Impulse Response (CIR) encountered by the kth user is given by [7]:

$$h_k(t) = \sum_{l=0}^{L_p-1} h_{kl}\delta(t - lT_c)\exp\left(j\theta_{kl}\right), \tag{3.8}$$

where h_{kl} represents the Nakagami-distributed fading envelope, lT_c is the relative delay of the lth path of user k with respect to the main path, while L_p is the total number of resolvable multipath components. Furthermore, θ_{kl} is the uniformly distributed phase-shift of the lth multipath component of the channel and $\delta(t)$ is the Kronecker Delta-function. More explicitly, the l multipath attenuations $\{h_{kl}\}$ are independent Nakagami distributed random variables, which is depicted in Section 2.2.2.

[1] For example, the LA code [1,1,1,1,...,-1,1-1] may be used in cell 1, wile the LA code [1,-1,1,-1,...,1,1 1] can be used in cell 2. This specific permutation of the code-allocation mitigates the inter-cell interference, because using the same codes in different cells would result in an increased inter-cell interference due to their high cross-correlation.

3.3.2 System Model

We support K asynchronous CDMA users in the system and each user is assigned an unique signature waveform $\mathbf{c}_k(t) = \sum_{i=0}^{G-1} c_{ki}\psi_{T_c}(t - iT_c)$, where G is the spreading gain and $\psi_{T_c}(t)$ is the rectangular chip waveform, which is defined over the interval $[0, T_c)$. Consequently, when the K users' signals are transmitted over the frequency-selective fading channel considered, the complex low-pass equivalent signal received at a given base station can be expressed as:

$$R(t) = \sum_{k=1}^{K} \sum_{l=0}^{L_p-1} \sqrt{2P}\mathbf{c}_k(t - lT_c - \tau_k)b_k(t - lT_c - \tau_k)h_{kl}\exp(j\theta_{kl}) + n(t), \tag{3.9}$$

where b_k is the transmitted bit of user k, while $n(t)$ is the complex-valued low-pass-equivalent AWGN having a double-sided spectral density of $N_0/2$ and τ_k is the propagation delay of user k, while τ_k is assumed to be a random variable uniformly distributed in the range of $[0, \tau_{max}]$, and L_p is the total number of resolvable paths.

3.3.3 BER Analysis

Random Spreading Code Based CDMA

Let the kth user be the user-of-interest and consider a receiver using de-spreading as well as multipath diversity combining. The conventional matched filter based RAKE receiver using MRC can be invoked for detection, where we assume that the RAKE receiver combines a total of L_r number of diversity paths, which may be more or possibly less than the actual number of resolvable components available at the current chip-rate. The value of L_r is typically restricted by the affordable receiver complexity.

Let us assume that we have achieved perfect time synchronization and that perfect estimates of the channel tap weights as well as phases are available. Then, after appropriately delaying the individual matched filter outputs, in order to coherently combine the L number of path signals with the aid of the RAKE combiner, the output Z_{kl} of the RAKE receiver's lth finger sampled at $t = T + lT_c + \tau_k$, can be expressed as:

$$Z_{kl} = D_{kl} + I_{kl}, \tag{3.10}$$

where D_{kl} represents the desired direct component, which can be expressed as:

$$D_{kl} = \sqrt{2P}T_s b_k[0]h_{kl}^2. \tag{3.11}$$

In Equation 3.11 $b_k[0]$ is the first bit transmitted by the kth user, where we have $b_k[0] \in \{+1, -1\}$. Hence, the interference plus noise term I_{kl} in Equation 3.10 can be expressed as:

$$I_{kl} = I_{kl}[S] + I_{kl}[M] + N_k, \tag{3.12}$$

where $I_{kl}[S]$ represents the multipath interference imposed by the user-of-interest, which can be expressed as:

$$I_{kl}[S] = \sqrt{2P}T_s h_{kl} \sum_{\substack{l_p=0 \\ l_p \neq l}}^{L_p-1} \frac{h_{kl_p} \cos\theta_{kl_p}}{T_s} \times \int_0^{T_s} b_k[t-(l_p-l)T_c] \cdot c_k[t-(l_p-l)T_c] c_k[t] dt. \quad (3.13)$$

Furthermore, $I_{kl}[M]$ represents the multiuser interference inflicted by the $K-1$ number of interfering signals, which can be expressed as:

$$I_{kl}[M] = \sqrt{2P}T_s h_{kl} \sum_{\substack{k'=1 \\ k' \neq k}}^{K} \sum_{l_p=0}^{L_p-1} \frac{h_{k'l_p} \cos\theta_{k'l_p}}{T_s} \cdot \int_0^{T_s} b_{k'}[t-(l_p-l)T_c-(\tau_{k'}-\tau_k)] \times c_{k'}[t-(l_p-l)T_c-(\tau_{k'}-\tau_k)] c_k[t] dt. \quad (3.14)$$

In Equation 3.13 and Equation 3.14 the $\cos(\cdot)$ terms are contributed by the phase differences between the incoming carrier and the locally generated carrier used in the demodulation. Finally, the noise term in Equation 3.12 can be expressed as:

$$N_{kl} = h_{kl} \int_0^{T_s} n(t) c_k[t] \cos(2\pi f_c t + \theta_{kl}) dt, \quad (3.15)$$

which is a Gaussian random variable having a zero mean and a variance of $N_0 T_s h_{kl}^2$, where $\{h_{kl}\}$ represents the path attenuations.

The MRC's decision variable Z_k, which is given by the sum of all the RAKE fingers' outputs, can be expressed as:

$$Z_k = \sum_{l=0}^{L_r-1} Z_{kl}. \quad (3.16)$$

Having obtained the decision variables of the MRC's output samples, let us now analyze the BER performance of the proposed LAS-CDMA system and benchmark it against a random code based CDMA system using hard-detection by invoking the often-used classic Gaussian approximation. We employ the standard Gaussian approximation and hence model both the multiuser interference and the self-interference terms of Equation 3.12 as an AWGN process having a zero mean and a variance equal to the corresponding variances. Consequently, for a given set of channel amplitudes $\{h_{kl}\}$ – according to the analysis of the previous sections – for the random spreading codes and BPSK modulation considered, the RAKE fingers' output signal Z_{kl} is a Gaussian distributed random variable having a mean of D_{kl}.

Let us first consider the random code based DS-CDMA system, the variance of the lth RAKE finger's output samples Z_{kl} for a given set of channel amplitudes $\{h_{kl}\}$ may be

approximated as [104, 106]:

$$\sigma_{kl}^2 = 2PT_s^2 \left[\frac{Kq(L_p,\eta)}{3G} + \frac{q(L_p,\eta)-1}{2G} + \left(\frac{2\Omega_0 E_b}{N_0}\right)^{-1} \right] \cdot \Omega_0 h_{kl}^2, \tag{3.17}$$

where $E_b = PT_s$ is the energy per bit and we have $q(L_p,\eta) = \sum_{l=0}^{L_p-1} e^{-\eta l}$. Furthermore, the MRC's output sample Z_k can be approximated by an AWGN variable having a mean value of $\mathrm{E}[Z_k] = \sum_{l=0}^{L_r-1} D_{kl}$ and a variance of $\mathrm{Var}[Z_k] = \sum_{l=0}^{L_r-1} \sigma_{kl}^2$ [102, 106], where we have:

$$\mathrm{E}[Z_k] = \sum_{l=0}^{L_r-1} \sqrt{2P}T_s b_k[0] h_{kl}^2, \tag{3.18}$$

$$\mathrm{Var}[Z_k] = 2PT_s^2 \left[\frac{Kq(L_p,\eta)}{3G} + \frac{q(L_p,\eta)-1}{2G} + \left(\frac{2\Omega_0 E_b}{N_0}\right)^{-1} \right] \cdot \Omega_0 \sum_{l=0}^{L_r-1} h_{kl}^2. \tag{3.19}$$

Therefore, the BER using BPSK modulation conditioned on a set of fading attenuations $\{h_{kl}, l = 0, 1, \ldots, L_r - 1\}$ can be expressed as:

$$P_b(\gamma) = Q\left(\sqrt{\frac{(\mathrm{E}[Z_k])^2}{\mathrm{Var}[Z_k]}}\right) = Q\left(\sqrt{\sum_{l=0}^{L_r-1} 2\gamma_l}\right), \tag{3.20}$$

where $Q(x)$ represents the Gaussian Q-function, which can also be represented in its less conventional form as [104, 106] $Q(x) = \frac{1}{\pi}\int_0^{\pi/2} \exp\left(-\frac{x^2}{2\sin^2\theta}\right) d\theta$, where $x \geq 0$. Furthermore, $2\gamma_l$ in Equation 3.20 represents the output Signal to Interference plus Noise Ratio (SINR) at the lth finger of the RAKE receiver, while γ_l is given by:

$$\gamma_l = \gamma_c \cdot \frac{h_{kl}^2}{\Omega_0}. \tag{3.21}$$

Let us now substitute Equation 3.21 into Equation 3.20 and Equation 3.18 as well as Equation 3.19 also into Equation 3.20. We can see then that the expressions under the square-root functions must be equal, which allows us to express γ_c as follows:

$$\gamma_c = \left[\frac{q(L_p,\eta)-1}{G} + \frac{2Kq(L_p,\eta)}{3G} + \left(\frac{\Omega_0 E_b}{N_0}\right)^{-1} \right]^{-1}. \tag{3.22}$$

Therefore, for a random code based DS-CDMA system we may argue that all paths of the interfering users will impose MAI on the reference user, and all multipath components of the reference user will additionally inflict MPI upon the reference user's desired signal.

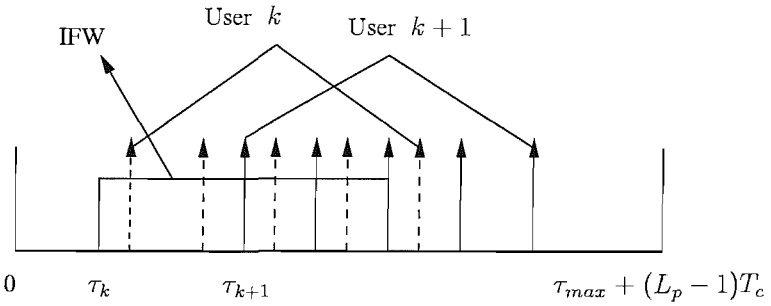

Figure 3.5: Illustration of the interference suppression capability of the LAS codes for the first finger of the RAKE receiver, when the width of the IFW is $\iota = 2$.

LAS Spreading Code Based CDMA

Let us now consider the interference suppression achieved with the aid of the IFW of LAS codes. In this scenario, only the paths arriving from the interfering users outside the IFW will inflict MAI upon the reference user, and this user's own delayed paths arriving outside the IFW will additionally impose MPI. Observe in Figure 3.5, for example that both the kth user and the $(k+1)$st user encounter five multipath components. When we considered the kth user's first RAKE receiver finger and an IFW of $\iota = 2$, only those two paths of the kth user will impose MPI, which fall outside the code's IFW. Similarly, the $(k+1)st$ user imposed only one interfering path on the kth user's first RAKE finger's decision variable, since four of the five path fall within the IFW. Hence, we will investigate the interference suppression capability of the IFW, as shown in a stylized fashion in Figure 3.5.

As argued above, in the context of LAS-CDMA, not all the $(L_p - 1)$ paths will impose MPI and for the lth finger's output sample Z_{kl} of the RAKE receiver only the rays arriving outside the IFW will impose MPI, where we have:

$$|l_p - l| > \iota. \tag{3.23}$$

Hence, for the lth finger of the RAKE receiver, the corresponding MPI term $I_{kl}[S]$ can be expressed as:

$$\begin{aligned} I_{kl}[S] &= \sqrt{2P}T_s h_{kl} \sum_{\substack{l_p=0 \\ |l_p-l|>l}}^{L_p-1} \frac{h_{kl_p}\cos\theta_{kl_p}}{T_s} \\ &\quad \cdot \int_0^{T_s} b_k[t-(l_p-l)T_c]\cdot c[t-(l_p-l)T_c]c[t]dt. \end{aligned} \tag{3.24}$$

We introduce the notation $\xi = l_p - l$ for the path length difference between the l_pth and the lth path, and when the delay spread exceeds ι, the integral seen in Equation 3.24 can be expressed as:

$$\frac{1}{T_s}\int_0^{T_s} b_k[t-\xi T_c]\cdot c[t-\xi T_c]c[t]dt = \rho_{kk}(\xi)b_k[-1] + \varrho_{kk}(\xi)b_k[0], \tag{3.25}$$

where we define the partial auto-correlation $\rho_{kk}(\xi)$ and $\varrho_{kk}(\xi)$ as:

$$\rho_{kk}(\xi) = \frac{1}{T_s}\int_0^{|\xi|T_c} c_k[t]c_k[t-|\xi|T_c]dt, \tag{3.26}$$

$$\varrho_{kk}(\xi) = \frac{1}{T_s}\int_{|\xi|T_c}^{T_s} c_k[t]c_k[t-|\xi|T_c]dt, \tag{3.27}$$

and we have $E\{h_{kl_p}^2\} = \Omega_0 e^{-\eta l_p}$. Hence the lth finger's MPI variance can be expressed as:

$$\mathrm{Var}\{I_{kl}[S]\} = 2P\cdot T_s^2 h_{kl}^2 \sum_{\substack{l_p=0 \\ |l_p-l|>\iota}}^{L_p-1} \Omega_0 e^{-\eta l_p}[\rho_{kk}^2(\xi)+\varrho_{kk}^2(\xi)]. \tag{3.28}$$

Similarly, for the multiuser interference term $I_{kl}[M]$ of Equation 3.12, only the rays arriving outside the IFW will impose MAI in Equation 3.14. Therefore, only the paths satisfying

$$|(l_p-l)T_c+(\tau_{k'}-\tau_k)| > \iota T_c, \tag{3.29}$$

will impose MAI. Let us now define $\xi = Int\{(l_p-l)T_c+(\tau_{k'}-\tau_k)/T_c\}$, where $Int\{x\}$ denotes the integer part of the arbitrary value x, while $x - Int\{x\}$ represents the non-integer part of the value x, hence we have:

$$\xi = Int\{(l_p-l)T_c+(\tau_{k'}-\tau_k)/T_c\}, \tag{3.30}$$

$$\tau_c = (l_p-l)T_c+(\tau_{k'}-\tau_k)-\xi T_c. \tag{3.31}$$

Furthermore, we define the partial cross-correlation of the spreading codes $\rho_{k'k}(\xi)$ and $\varrho_{k'k}(\xi)$ as:

$$\rho_{k'k}(\xi) = \frac{1}{T_s}\int_0^{|\xi|T_c} c_k(t)c_{k'}(t-|\xi|T_c)dt, \tag{3.32}$$

$$\varrho_{k'k}(\xi) = \frac{1}{T_s}\int_{|\xi|T_c}^{T_s} c_k(t)c_{k'}(t-|\xi|T_c)dt. \tag{3.33}$$

According to [113], the integral in Equation 3.14 can be expressed as:

$$\begin{aligned}&\tfrac{1}{T_s}\cdot\textstyle\int_0^{T_s} b_{k'}[t-(l_p-l)T_c-(\tau_{k'}-\tau_k)]c_{k'}[t-(l_p-l)T_c-(\tau_{k'}-\tau_k)]c[t]dt \\ &\quad= b_{k'}[-1]\{\rho_{k'k}(\xi)\hat{R}_\psi(\tau_c)+\rho_{k'k}(\xi+1)R_\psi(\tau_c)\}+ \\ &\quad\quad b_{k'}[0]\{\varrho_{k'k}(\xi)\hat{R}_\psi(\tau_c)+\varrho_{k'k}(\xi+1)R_\psi(\tau_c)\},\end{aligned} \tag{3.34}$$

where $\hat{R}_\psi(\tau_c)$ and $R_\psi(\tau_c)$ are the partial autocorrelation functions of the chips waveform, which are defined as [113]:

$$R_\psi(\tau_c) = \int_0^{\tau_c} \psi_{T_c}(t)\psi_{T_c}(t+T_c-\tau_c)dt, \tag{3.35}$$

$$\hat{R}_\psi(\tau_c) = \int_{\tau_c}^{T_c} \psi_{T_c}(t)\psi_{T_c}(t-\tau_c)dt. \tag{3.36}$$

For a rectangular chip waveform we have $R_\psi(\tau_c) = \tau_c$ and $\hat{R}_\psi(\tau_c) = (T_c - \tau_c)$.

For convenience, we define the asynchronous partial cross-correlations $\hat{\rho}_{k'k}(\tau_c)$ and $\hat{\rho}_{k'k}(\tau_c)$ as:

$$\hat{\rho}_{k'k}(\tau_c) = \rho_{k'k}(\xi)\hat{R}_\psi(\tau_c) + \rho_{k'k}(\xi+1)R_\psi(\tau_c), \tag{3.37}$$

$$\hat{\varrho}_{k'k}(\tau_c) = \varrho_{k'k}(\xi)\hat{R}_\psi(\tau_c) + \varrho_{k'k}(\xi+1)R_\psi(\tau_c), \tag{3.38}$$

and we assume that τ_k and $\tau_{k'}$ are random variables uniformly distributed in $[0, \tau_{max}]$. Therefore, the average variance of the MAI imposed by the k'th user at the lth finger of RAKE receiver can expressed as:

$$V_{k'k}(l) = 2PT_s h_{kl}^2 \int_0^{\tau_{max}} \int_0^{\tau_{max}} \frac{1}{\tau_{max}} \frac{1}{\tau_{max}} \times \sum_{\substack{l_p=0 \\ |(l_p-l)T_c+(\tau_{k'}-\tau_k)|>\iota T_c}}^{L_p-1} \Omega_0 e^{-\eta l_p} (\hat{\rho}_{k'k}^2(\tau_c) + \hat{\varrho}_{k'k}^2(\tau_c)) d\tau_k d\tau_{k'}. \tag{3.39}$$

Finally, the variance of the MAI term $I_{kl}[M]$ of Equation 3.12 can be expressed as:

$$\mathrm{Var}(I_{kl}[M]) = \sum_{\substack{k'=1 \\ k' \neq k}}^{K} V_{k'k}(l). \tag{3.40}$$

For the sake of convenient comparison to the random code based system, we will introduce the MPI and MAI interference reduction factors of $\Upsilon_S(l)$ and $\Upsilon_M(l)$, respectively, which are defined as:

$$\Upsilon_S(l) = \frac{2G \cdot \mathrm{Var}\{I_{kl}[S]\}}{2PT_s^2 \Omega_0 h_{kl}^2}, \tag{3.41}$$

$$\Upsilon_M(l) = \frac{3G \cdot \mathrm{Var}\{I_{kl}[M]\}}{2PT_s^2 \Omega_0 h_{kl}^2}. \tag{3.42}$$

Hence, upon substituting Equation 3.28 into Equation 3.41, the corresponding MPI reduction factor $\Upsilon_S(l)$ can be expressed as:

$$\Upsilon_S(l) = 2G \cdot \sum_{\substack{l_p=0 \\ |l_p-l|>\iota}}^{L_p-1} e^{-\eta l_p} [\rho_{kk}^2(\xi) + \varrho_{kk}^2(\xi)]. \tag{3.43}$$

Similarly, upon substituting Equation 3.40 into Equation 3.42, the corresponding MUI reduction factor $\Upsilon_M(l)$ can be expressed as:

$$\Upsilon_M(l) = \frac{3G}{K} \sum_{\substack{k'=1 \\ k' \neq k}}^{K} \int_0^{\tau_{max}} \int_0^{\tau_{max}} \frac{1}{\tau_{max}} \frac{1}{\tau_{max}} \times \sum_{\substack{l_p=0 \\ |(l_p-l)T_c+(\tau_{k'}-\tau_k)|>\iota T_c}}^{L_p-1} e^{-\eta l_p} (\hat{\rho}^2_{k'k}(\tau_c) + \hat{\varrho}^2_{k'k}(\tau_c)) d\tau_k d\tau_{k'}. \quad (3.44)$$

Having obtained $\Upsilon_S(l)$ and $\Upsilon_M(l)$, now we are ready to calculate the γ_c and the average bit error probability, which we synonymously refer to as the BER $P_b(E)$.

For the LAS-CDMA system, given a fading attenuation set of $\{h_{kl}, l = 0, 1, \ldots, L_r - 1\}$, the BER is given by:

$$P_b(\gamma) = Q\left(\sqrt{\sum_{l=0}^{L_r-1} 2\gamma_l}\right), \quad (3.45)$$

where γ_l may be expressed as:

$$\gamma_l = \gamma_c \cdot \frac{h^2_{kl}}{\Omega_0}. \quad (3.46)$$

Following a similar approach to that used in the context of the random code based CDMA system, the corresponding γ_c expression can be formulated as:

$$\gamma_c = \left[\frac{\Upsilon_S(l)}{G} + \frac{2K\Upsilon_M(l)}{3G} + \left(\frac{\Omega_0 E_b}{N_0}\right)^{-1}\right]^{-1}. \quad (3.47)$$

The average BER, $P_b(E)$ can be obtained by the weighted averaging of the conditional BER expression of Equation 3.20 and Equation 3.45 over the joint PDF of the instantaneous SNR values corresponding to the L_r multipath components $\{\gamma_l : l = 1, 2, \ldots, L_r\}$. Since the random variables $\{\gamma_l : l = 1, 2, \ldots, L_r\}$ are assumed to be statistically independent, the average BER expression of Equation 3.20 and Equation 3.45 can be formulated as [107]:

$$P_b(E) = \frac{1}{\pi} \int_0^{\pi/2} \prod_{l=0}^{L_r-1} I_l\left(\overline{\gamma}_l, \theta\right) d\theta, \quad (3.48)$$

where we have

$$I_l\left(\overline{\gamma}_l, \theta\right) = \int_0^{\infty} \exp\left(-\frac{\gamma_l}{\sin^2\theta}\right) p_{\gamma_l}(\gamma_l) d\gamma_l. \quad (3.49)$$

Since $\gamma_l = \gamma_c \cdot \frac{(h_l)^2}{\Omega_0}$ and h_l obeys the Nakagami-m distribution characterized by Equation 2.5, it can be shown that the PDF of γ_l can be formulated as:

$$p_{\gamma_l}(\gamma_l) = \left(\frac{m_l}{\overline{\gamma}_l}\right)^{m_l} \frac{\gamma^{m_l-1}}{\Gamma(m_l)} \exp\left(-\frac{m_l\gamma_l}{\overline{\gamma}_l}\right), \quad \gamma_l \geq 0, \tag{3.50}$$

where $\overline{\gamma}_l = \gamma_c e^{-\eta l}$ for $l = 0, 1, \ldots, L_r - 1$.

Upon substituting (3.50) into (3.49) it can be shown that we have [104]:

$$I_l\left(\overline{\gamma}_l, \theta\right) = \left(\frac{m_l \sin^2\theta}{\overline{\gamma}_l + m_l \sin^2\theta}\right)^{m_l}. \tag{3.51}$$

Finally, upon substituting (3.51) into (3.48), the average BER of the both the random and las codes based CDMA system can be written as:

$$P_b(E) = \frac{1}{\pi} \int_0^{\pi/2} \prod_{l=0}^{L_r-1} \left(\frac{m_l \sin^2\theta}{\overline{\gamma}_l + m_l \sin^2\theta}\right)^{m_l} d\theta. \tag{3.52}$$

3.3.4 Performance of LAS DS-CDMA

In our investigations we compared a traditional and a LAS-code based CDMA system, both of which have the same chip-rate and bandwidth. However, both their effective spreading gain as well as their correlation functions are different. Therefore these two systems are affected differently by the MAI and MPI and hence their expected performance will differ. In the LAS-CDMA 2000 system, the LA(2552,136,17) and LS(4,32,4) codes are combined, as seen in Figure 3.4. More explicitly, the total length of the LS(N, P, W_0) =LS(4,32,4) code is $L_s = NP+2W_0 = 136$ chips, which is incorporated into the LA(L_A, M, K)=LA(2552,136,17) code, again, as seen in Figure 3.4, for the sake of creating the LAS($L_A, M, K_c; N, P, W_0$)=LAS(2552,136,17;4,32,4) code. Since this LAS code has certain zero-valued gaps after inserting the LS code into the LA code as portrayed in Figure 3.4, as well as the $2W_0$ number of zeros constituting the IFW, its spreading factor maybe calculated by simply noting each bit to be transmitted is spread by one of the constituent LS(4,32,4) codes. Although the length of this LS code is $L_S = NP + 2W_0 = 136$, the effective spreading gain of the LAS code is identical to that of its constituent LS codes, namely $G_{\text{LAS}} = G_{\text{LS}} = 128$. By contrast, a traditional random code based CDMA system having the same $L_A = 2552$ chips would have a higher spreading gain, since it doest not have any zero-valued gaps, nor has an IFW. Hence the corresponding spreading gain becomes $G_{\text{Random}} = 2552/17 = 151$, since in Figure 3.4 $K = 17$ bits are mapped to $L_A = 2552$ chips. This spreading gain difference was taken into account in our results, again, assuming that the LAS-code and random code based systems considered have the same bandwidth. We will compare these two system's performance based on these two different effective spreading gains. For simplicity's sake, we assume that all paths have the same Nakagami fading parameter, *i.e.* we have $m_l = m$, $l = 0, \ldots, L_r - 1$.

In Figure 3.6, we assumed that the LAS-CDMA system operated in a quasi-synchronous scenario, which can be achieved for example with the aid of a Global Positioning System (GPS) assisted synchronization protocol. We assume that we have a maximum propagation delay of $\tau_{max} = 2T_c$. The channel's delay spread is negative exponentially distributed in the range of $[0.3, 3]\mu s$ [114], and we assume that both the random and LAS-code based systems have a chip rate of $1.2288M$chips. The number of resolvable paths is $L_p = \lfloor \frac{\tau}{T_c} \rfloor + 1 = 4$, where $\tau = 3\mu s$. Both the random code based CDMA system and the LAS-CDMA system supported $K = 32$ users, and the width of the IFW was $3T_c$ for the LAS-CDMA system, *i.e* we had $\iota = 3$. From Figure 3.6, we can observe that the LAS-CDMA system has a significantly better BER performance than the traditional DS-CDMA system, when communicating over a quasi-synchronous channel, provided that both these two systems combine the same $L_r = 1, 2, 3 \leq L_p$ number of resolvable paths, respectively. The reason that the LAS-CDMA scheme outperforms the traditional DS-CDMA system is that the MAI and MPI is reduced, as a benefit of using LAS codes.

Figure 3.7 exhibits the performance of these two systems communicating over different fading channels associated with different Nakagami fading parameters. More explicitly, when we have $m = 1$, we model a Rayleigh fading channel, $m = 2$ represents a Rician fading channel, while $m \to \infty$ corresponds to an AWGN channel. We can observe from Figure 3.7 that the LAS-CDMA system exhibited a significantly better BER performance than the traditional DS-CDMA system, regardless of the value of m. More specifically, provided that all these uplink users are in a quasi-synchronous state, *i.e* we have $\tau_{max} = 2T_c$ and $L_p = 4$, the LAS-CDMA scheme outperformed the traditional DS-CDMA system, when communicating over different Nakagami multipath fading channels.

Figure 3.8 shows the performance of these two systems for transmission over different dispersive channels having $L_p = 4 \ldots 12$ resolvable multipath components and assuming that $L_r = 3$ of these components were combined by the RAKE receiver. We can observe from Figure 3.8 that when the channel became more dispersive, the LAS-CDMA system's performance was significantly degraded and its gain over the traditional DS-CDMA system was eroded. Nonetheless, the LAS-CDMA scheme still outperformed the traditional DS-CDMA system, provided that the users were in a quasi-synchronous state, *i.e* when we had $\tau_{max} = 2T_c$. However, when L_p was increased to 12, the LAS-CDMA system retained only a moderate gain over the traditional DS-CDMA arrangement even if the LAS-CDMA operated in a quasi-synchronous scenario. The reason for this performance erosion is that many of the paths will be located outside IFW when L_p is high and the auto-correlation as well as cross-correlation of LS codes outside the IFW is higher than that of the random codes. Hence, when L_p is high, LAS-CDMA inevitably encounters serious MAI and MPI. However, for a high chip-rate system we may consider the employment of MC DS-CDMA [3], which is capable of ensuring that each subcarrier encounters only $L_p = 4$ resolvable paths. In this scenario, LAS MC DS-CDMA may be expected to retain its ability to effectively suppress both the MAI and MPI.

In Figure 3.9 we can observe that as the maximum time difference τ_{max} increases, the

performance of LAS-CDMA degrade significantly. When we have $\tau_{max} \geq 10T_c$, the LAS-CDMA system's performance becomes even worse than that of traditional DS-CDMA. This is because the insertion of zeros in the LAS codes reduces the effective spreading gain of the LAS-CDMA system and when the propagation delay τ_{max} increases, the MAI suppression capability will be inevitably reduced. Hence we may conclude that LAS-CDMA systems are suitable for operating in a quasi-synchronous CDMA environment.

Stańczak *et al.* [18] concluded that the width ι of the IFW and the number of users K will obey: $K(\iota + 1) \leq G$. In the LAS-CDMA 2000 system [109], when the number of users K exceeds 32, or more explicitly, when all the four different sets of LS codes as we mentioned in Section 3.2.2 are employed, the width of the IFW will be reduced to zero for the codes belonging to different sets associated with different rows of the corresponding WH matrix. For example, when we have $K = 128$, all the 128 users' signals are orthogonal to each other in case of perfect synchronization. However, the width of the IFW of LS codes belonging different LAS code sets generated using different rows of the WH matrix becomes zero. In this scenario, serious MAI and MPI will be incurred, when the inter-set orthogonality of the LAS-codes generated with the aid of difference row of the WH matrix is destroyed by the multipath channel. Therefore, the performance of LAS-CDMA will significantly degrade, when the number of users supported becomes $K > 32$. In Figure 3.10, we can observe that for $K \geq 60$ the LAS-CDMA system will have no advantage in comparison to the traditional DS-CDMA scheme, or even may perform worse than the traditional DS-CDMA arrangement, although all users operate in a quasi-synchronous manner. Hence, we may conclude that the employment of LAS-CDMA is beneficial in low user load scenarios, where the delay spread is also limited.

In order to circumvent the performance limitation of the proposed system, we finally introduce the concept of multicarrier LAS DS-CDMA, which allows us to extend the IFW duration by a factor of the number subcarriers [34] because the chip-duration of each subcarrier is increased according to the number of subcarriers, which will be discussed in Section 3.4. Figure 3.11 demonstrated the achievable performance of Single-carrier LAS DS-CDMA and MC LAS CDMA for a single-carrier $3.84M$chips/s system. From this figure we may conclude that the MC LAS DS-CDMA is capable of achieving the best performance trade-off by selecting the optimum number of subcarriers U according to the channel delay dispersion τ_{ch} and the delay difference τ_{max}. For example, From Figure 3.11, we may conclude that $U = 8$ MC LAS DS-CDMA system exhibited the best trade-off in a scenario of $\tau_{ch} = 3\mu s$ and $\tau_{max} = 5\mu s$

Finally, Figure 3.12 portrays the achievable performance both as a function of the propagation delay τ_{max} and the SNR per bit, E_b/N_0. From Figure 3.12 we infer that LAS-CDMA exhibits advantages, when we have $\tau_{max} \leq 5T_c$.

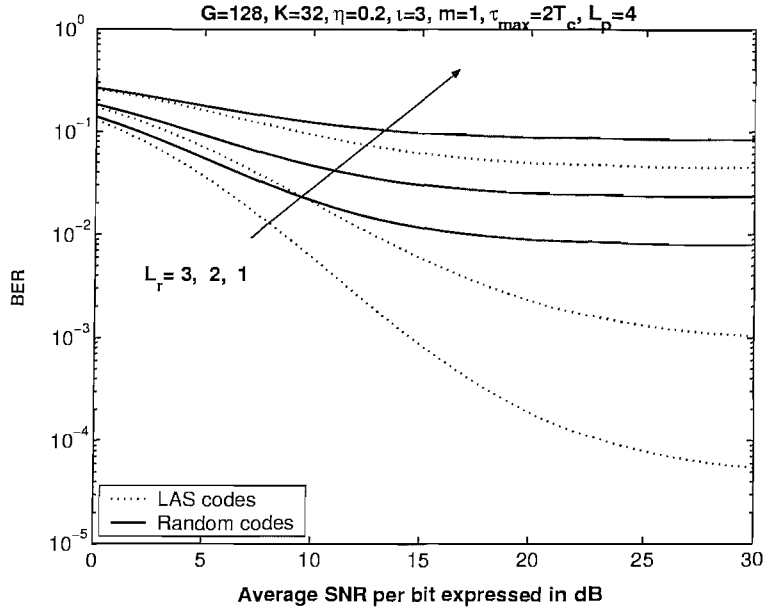

Figure 3.6: BER versus channel SNR performance comparison of random code based classic CDMA and LAS CDMA, when communicating over a Nakagami-m channel having $m = 1$. $K = 32$ users were supported, and the negative exponential Multipath Intensity Profile (MIP) decay factor was $\eta = 0.2$. The IFW width was $\iota = 3$, and the maximum delay difference was $\tau_{max} = 2T_c$. The number of resolvable paths was $L_p = 4$ and the RAKE receiver combined $L_r = 1, 2, 3$ paths, respectively.

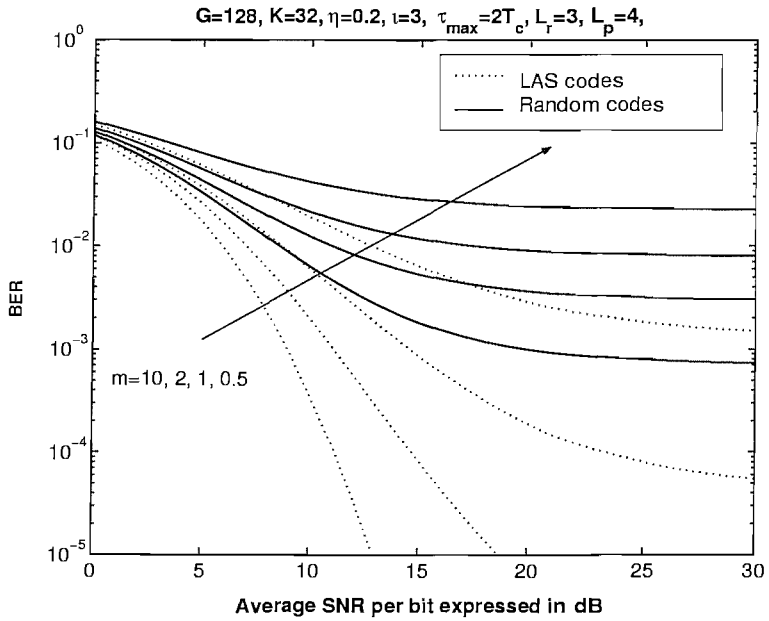

Figure 3.7: BER versus channel SNR performance comparison of random code based classic CDMA and LAS CDMA, when communicating over different Nakagami fading channels. $K = 32$ users were supported and the negative exponential MIP decay factor was $\eta = 0.2$. The IFW width was $\iota = 3$, and the maximum delay difference was $\tau_{max} = 2T_c$. The number of resolvable paths was $L_p = 4$ and the RAKE receiver combined $L_r = 3$ paths.

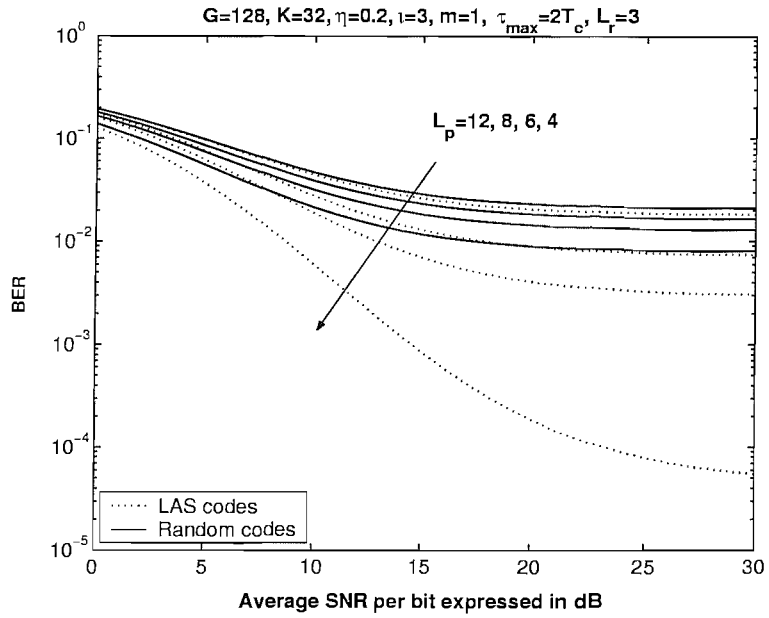

Figure 3.8: BER versus channel SNR performance comparison of random code based classic CDMA and LAS CDMA, when communicating over a dispersive Rayleigh-fading channel having $m = 1$. The number of resolvable paths was $L_p = 4, 6, 8, 12$, respectively. $K = 32$ users were supported, and the negative exponential MIP decay factor was $\eta = 0.2$. The IFW width was $\iota = 3$ and the maximum delay difference was $\tau_{max} = 2T_c$. The RAKE receiver combined $L_r = 3$ paths.

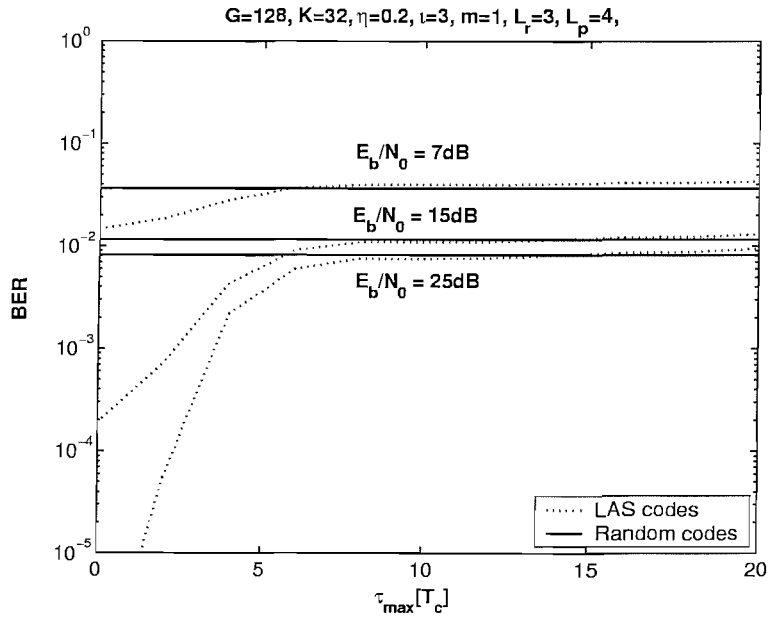

Figure 3.9: BER performance comparison of random code based classic CDMA and LAS CDMA as a function of the maximum delay difference τ_{max}, when communicating over a dispersive Rayleigh-fading channel having $m = 1$. $K = 32$ users were supported, and the negative exponential MIP decay factor was $\eta = 0.2$. The IFW width was $\iota = 3$. The number of resolvable path was $L_p = 4$ and the RAKE receiver combined $L_r = 3$ paths.

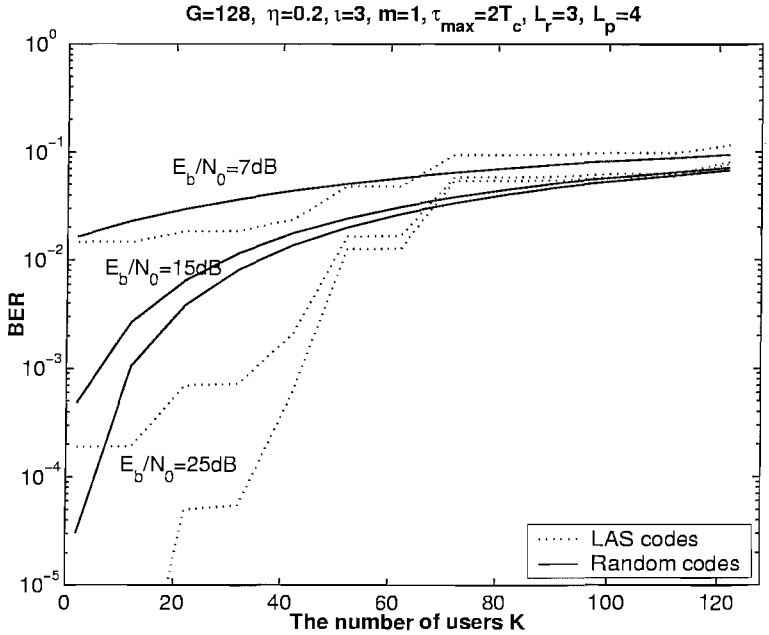

Figure 3.10: BER performance comparison of random code based classic CDMA and LAS CDMA as a function of the number of users K supported, when communicating over a dispersive Rayleigh fading channel having $m = 1$. The negative exponential MIP decay factor was $\eta = 0.2$, and the number of resolvable paths was $L_p = 4$. The RAKE receiver combined $L_r = 3$ paths.

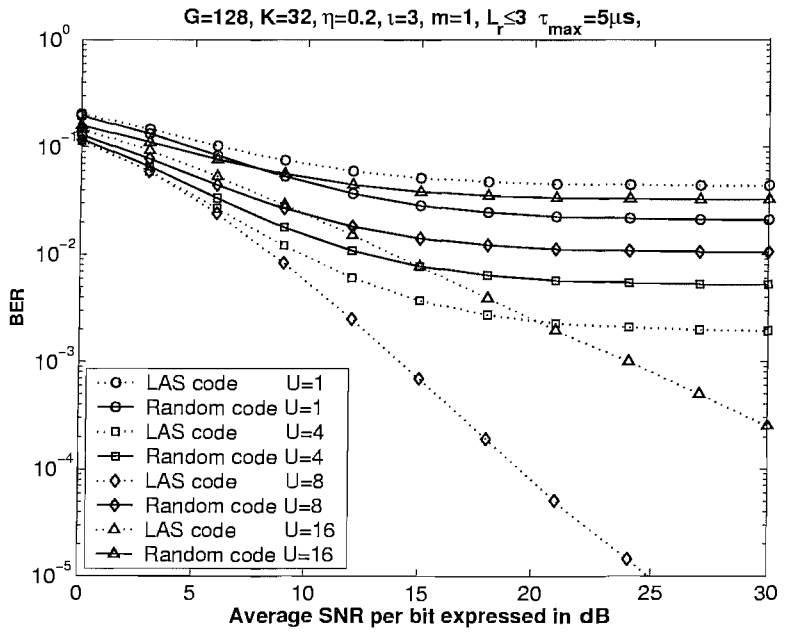

Figure 3.11: BER versus E_b/N_0 performance comparison of two MC DS-CDMAs based on Equation 3.52 when we considered LAS codes and random spreading codes. The RAKE receiver was configured for combining $L_r \leq 3$ paths' energy. The channel dispersion was $\tau_{ch} = 3\mu s$, Hence the number of resolvable multipath components for $U = 1, 4, 8, 16$ was $L_p = 12, 3, 2, 1$, and the dispersion of the propagation environment considered was $\tau_{max} = 5\mu s$.

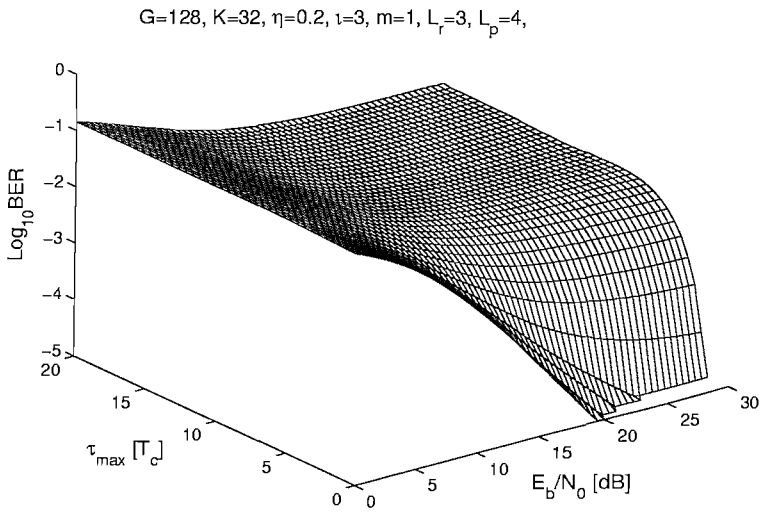

Figure 3.12: BER performance of LAS CDMA as a function of the maximum delay difference τ_{max} and E_b/N_0, when communicating over a Rayleigh fading channel having $m = 1$. $K = 32$ users were supported. The negative exponential MIP decay factor was $\eta = 0.2$, the IFW width was $\iota = 3$, and the number of resolvable paths was $L_p = 4$. The RAKE receiver combined $L_r = 3$ paths.

3.4 LAS MC DS-CDMA for Broadband Communications

3.4.1 Drawbacks of Single-Carrier DS-CDMA for High Chip-Rate System

In the context of broadband wireless mobile systems communicating in diverse propagation environments, both single-carrier DS-CDMA and MC-CDMA exhibit certain limitations. Specifically, in the context of broadband wireless systems that may have a bandwidth of the order of 100MHz. A classic single-carrier DS-CDMA would encounter the following problems.

(a) The number of resolvable paths to be processed by the RAKE receiver may become excessive. Assuming binary transmissions using BPSK modulation as an example, the symbol duration and bit duration are the same. Propagation measurements of typical wireless channels including indoor, open rural, suburban and urban areas indicate that the delay-spread is typically distributed over the range of $[0.1\mu s, 3\mu s]$ [114]. When communicating at 20 Mchips/s, for example, these schemes cannot maintain a high integrity in environments exhibiting a delay-spread in excess of $1\mu s$, since severe inter-symbol interference (ISI) will be imposed on the adjacent symbols due to the delayed paths having a delay spread higher than $1\mu s$. A single-carrier DS-CDMA scheme designed using a high number of RAKE fingers for environments having a high delay-spread may in reality combine noise, rather than useful signal energy, if the number of resolvable paths is low in environments having a low delay-spread. This phenomenon would degrade the system's performance. By contrast, a low-complexity single-carrier DS-CDMA scheme designed using a low number of RAKE fingers for employment in low-dispersive environments inevitable would waste some of the useful signal energy delivered by multipath in highly

dispersive environments. However, the high complexity imposed by the estimation of a high number of resolvable paths or the potentially sub-optimum RAKE-receiver performance owing to the received signal energy loss associated with the uncombined paths in a low-complexity receiver maybe unavoidable. In order to mitigating these problems, a highly efficient combining arrangement has to invoke an adaptive MRC scheme, which is capable of combining a time-variant number of resolvable paths encountered in various communication environments. However, the cost of such a combining scheme is the associated increased the receiver complexity.

(b) In Section 3.3.4, we have investigated the achievable performance of Single-Carrier LAS-code based DS-CDMA (SC LAS DS-CDMA) and showed that LAS codes may fail to suppress the MAI and MPI, when the number of resolvable paths becomes high. This was graphically demonstrated in Figure 3.5 for five paths, where two resolvable paths arrived outside the IFW, which would inevitably impose both MAI and MPI, when we invoke a traditional RAKE receiver. More explicitly, for a SC LAS DS-CDMA system, the achievable performance is expected to significantly degrade, as the chip rate increases to 20 $Mchips/s$, for example. It was also mentioned in Section 3.3.4 that in case of a high-chip-rate single-carrier LAS-CDMA system, the tolerable asynchronous uplink delay-difference of the users are limited, which requires the accurate adaptive timing advance control.

Based on these arguments, we propose the employment of LAS code based Multi-Carrier DS-CDMA (MC LAS DS-CDMA) for a high chip-rate system, where the chip-rate of the individual subcarriers may be reduced by a factor corresponding to the number of subcarriers, hence extending the chip-duration the same factor. This measure allows us to avoid having multipath components outside the IFW. Further more, it has the potential to guarantee that the RAKE receiver will achieve path-diversity when communicating over a dispersive channel as well as suppressing both the MAI and MPI.

3.4.2 Broadband MC DS-CDMA for Diverse Propagation Environments

First of all, to a certain extent MC DS-CDMA constitutes a trade-off between SC DS-CDMA and MC-CDMA in terms of the system's architecture and performance. MC DS-CDMA typically requires lower chip rate spreading codes, than SC DS-CDMA due to employing multiple subcarriers, while necessitating a lower number of subcarriers than MC-CDMA due to imposing DS spreading on each subcarrier's signal. Consequently, MC DS-CDMA typically requires lower-rate signal processing, than SC DS-CDMA and has a lower worst-case peak-to-average power fluctuation than MC-CDMA. However, MC DS-CDMA is more attractive than an arbitrary ad-hoc compromise multiple-access scheme, positioned between SC DS-CDMA and MC-CDMA, since it exhibits a number of advantageous properties, which can be exploited in the context of broadband MC DS-CDMA designed for diverse propagation environments. In [3] it was shown that MC DS-CDMA has the highest degree of freedom in the family of CDMA schemes and this property can be beneficially exploited during the system design procedure. Below we investigate, how the specific parameters of MC DS-CDMA, which determine the degree

of design freedom can be adjusted for satisfying the requirements of diverse propagation environments.

The channels are assumed to be slowly varying frequency-selective fading channels and the delay-spreads are assumed to be limited to the range of $[T_m, T_M]$, where T_m corresponds to the environment having the minimum delay-spread considered, experienced for example in an indoor environment. By contrast, T_M is associated with an environment having the maximum possible delay-spread, as in an urban area. Hence, given $[T_m, T_M]$, the number of resolvable paths encountered by both SC DS-CDMA and MC DS-CDMA is summarized in Table 3.1. Hence, when the number of subcarriers is low, the corresponding number of resolvable paths will be high, hence the orthogonality of the LAS codes may be destroyed, rendering them unable to suppress MAI and MPI. By contrast, when the number of subcarrier is high, for example, then we have a high chip-duration and hence we may have $T_M < T_c$. In this case we can maintain the orthogonality of the LAS codes, but we cannot achieve the multipath diversity despite communicating in a dispersive scenario. Hence, in this chapter, we will optimize the number of subcarriers U for broadband communications. More specifically, we can guarantee that the IFW of LAS codes retains its ability to suppress both the MAI and MPI as well as maintaining a sufficiently high multipath diversity gain.

Multiple-access scheme	Number of subcarriers	Number of resolvable paths
SC DS-CDMA	1	$\lfloor \frac{T_m}{T_{c1}} \rfloor + 1, \lfloor \frac{T_M}{T_{c1}} \rfloor + 1$
MC DS-CDMA	U	$\lfloor \frac{T_m}{T_c} \rfloor + 1, \lfloor \frac{T_M}{T_c} \rfloor + 1$

U: Number of bits involved in S-P conversion;
T_{c1}: Chip-duration of spreading codes in SC DS-CDMA;
T_c: Chip-duration of spreading codes in MC DS-CDMA, obeying: $T_c = U \cdot T_{c1}$
T_m: Delay-spread of the environment having the minimum delay-spread;
T_M: Delay-spread of the environment having the maximum delay-spread;

Table 3.1: Typical signal and receiver characteristics associated with SC DS-CDMA and MC DS-CDMA Systems communicating over wireless channels [114]

The above philosophy might be augmented with the aid of an example. Let us assume that the total bandwidth of the broadband MC DS-CDMA system is about 40MHz. The delay-spread is assumed to be limited to the range of $[T_m = 0.1\mu s, T_M = 3\mu s]$, which includes the typical delay-spread values experienced in indoor, open rural, suburban and urban areas. Furthermore, we assume that all the users are synchronized at the base station and the chip rate of the SC DS-CDMA system considered is 20 $Mchips/s$. As in section 3.2, the width of the IFW of the LAS codes is $3T_c$, which allows them to suppress both the MAI and the MPI completely, provided that the number of resolvable paths satisfies $L_p \leq 3$. Hence, we can set the number of resolvable paths to $L_p = 3$, and we have $L_p = \lfloor T_M/(UT_{c1}) \rfloor + 1$, and we can set $T_M/(UT_{c1}) = 2.5$. Thus we have to configure the system to use $U = T_M/T_{c1} = \frac{3\mu s}{2.5 \times 0.05\mu s} = 24$ subcarriers. Consequently, this MC DS-CDMA system will operate efficiently over a wide range communication environments and will achieve a multipath diversity order of three, as well as suppressing both the MAI and MPI, provided that the delay-spread of the specific environment encountered is in the range of $[0.1\mu s, 3\mu s]$.

Advantages - Based on the above rules of selecting the system parameters, broadband MC DS-CDMA is capable of mitigating the problems encountered by both SC DS-CDMA and MC-CDMA. Specifically, broadband MC DS-CDMA has the following advantages:

- MC DS-CDMA is capable of communicating in propagation environments as diverse as indoor, open rural, suburban and urban areas. This is achieved by avoiding or at least mitigating the problems imposed by the different-dispersion fading channels associated with the above propagations environments.
- Broadband MC DS-CDMA is capable of mitigating the requirements of high-chip-rate based broadband SC DS-CDMA systems. This is achieved by introducing computationally efficient Discrete Fourier Transform (DFT) based parallel processing, carrying out modulation for all subcarriers in a single DFT-step, when the number of subcarriers is in excess of 64, the FFT becomes more efficient than the DFT.
- In the broadband LAS MC DS-CDMA system, provided that we appropriately select the number of subcarriers U, we can guarantee that the LAS codes remain capable of suppressing the MAI and the MPI as well as maintaining a multipath diversity order identical to the number of resolvable multipath components.

Disadvantages - However, MC DS-CDMA also has to obey certain design trade-offs. Two main deficiencies associated with broadband MC DS-CDMA are as follows.

- The Doppler frequency shift of the lowest and highest frequency subcarriers may be substantially different. This is because broadband MC DS-CDMA may occupy a high system bandwidth, potentially on the order of tens or even hundreds of MHz. The different Doppler frequency shifts of the different subcarriers will destroy the orthogonality of the subcarriers and a given subcarrier signal will experience interference imposed by the adjacent subcarrier signals. However, the interference imposed by the surrounding subcarrier signals becomes relatively low, when the vehicular speed is low. This is because the orthogonality between the desired subcarrier and the adjacent subcarriers remains relatively intact due to their similar frequencies, while the distant subcarriers impose a relatively low Inter-Subcarrier Interference (ICI) on the desired subcarrier, since the ICI between the subcarriers decays inverse-proportionally with their frequency-domain separation.
- The peak factor [4] of MC DS-CDMA is higher than that of the corresponding SC DS-CDMA system. The main drawback of multicarrier systems is their high peak-to-mean envelope power fluctuation or, synonymously, high-crest factors. Hence expensive linear power amplifiers having a high dynamic range are required in order to reduce the nonlinear distortion of the signal, which would results in a high out-of-band emission, *i.e* adjacent-channel interference.

3.4.3 Performance of MC LAS DS-CDMA

Bit Error Rate of MC LAS DS-CDMA

Having outline the benefits of LAS-code based MC DS-CDMA, let us now characterize its achievable performance. We support K asynchronous CDMA users in the system and each user is assigned a unique signature waveform $\mathbf{c}_k(t) = \sum_{i=0}^{G-1} c_{ki}\psi_{T_c}(t-iT_c)$, while $\psi_{T_c}(t)$ is the rectangular chip waveform, which is defined over the interval $[0, T_c)$. Consequently, when the K users' signals are transmitted over the frequency-selective fading channel, the received complex low-pass equivalent signal at a given base station can be expressed as:

$$R(t) = \sum_{k=1}^{K}\sum_{u=0}^{U-1}\sum_{l=0}^{L_p-1}\sqrt{2P_k}\mathbf{c}_k(t-lT_c-\tau_k)b_{ku}(t-lT_c-\tau_k)h_{ku}^l\exp(j\theta_{ku}^l)+n(t), \quad (3.53)$$

where $n(t)$ is the complex valued low-pass-equivalent AWGN having a double-sided spectral density of $N_0/2$, and τ_k is the propagation delay of user k. We define the τ_k as a random variable uniformly distributed in the range of $[0, \tau_{max}]$, L_p is the total number of resolvable paths.

In Section 3.3.3, the average BER of the LAS CDMA system was derived, which can be written as:

$$P_b(E) = \frac{1}{\pi}\int_0^{\pi/2}\prod_{l=0}^{L_r-1}\left(\frac{m_l\sin^2\theta}{\overline{\gamma}_l+m_l\sin^2\theta}\right)^{m_l}d\theta, \quad (3.54)$$

where L_r is the number of Rake receiver fingers and $\overline{\gamma}_l = \gamma_c e^{-\eta l}$ is the average output SNR at the lth finger of the RAKE receiver, $l = 0, 1, \ldots, L_r - 1$, where η is the negative exponential MIP decay factor, and γ_c can be expressed as:

$$\gamma_c = \left[\frac{\Upsilon_S(l)}{G}+\frac{2K\Upsilon_M(l)}{3G}+\left(\frac{\Omega_0 E_b}{N_0}\right)^{-1}\right]^{-1}, \quad (3.55)$$

where the $\Upsilon_S(l)$ and $\Upsilon_M(l)$ are the corresponding MPI and MAI reduction factors as defined in the context of Equation 3.41 and Equation 3.42 of Section 3.3.3 achieved by the employment of LAS codes.

3.4.4 Numerical Results

Let us assuming that in our MC LAS DS-CDMA system, the bandwidth is 40 MHz. This bandwidth is sufficiencies high for supporting a 20 $Mchips/s$ SC DS-CDMA system when using a rectangular waveform and Nyquist sampling, but employing no excess bandwidth. The LA(2552,136,17) and LS(4,32,4) of Figure 3.4 are invoked, and as in the SC system of Section 3.3.4, the spreading gain of LAS MC DS-CDMA is $G = 128$. As argued in Section 3.3.4, for the sake of maintaining the same bandwidth requirement as the MC LAS DS-CDMA system, the traditional MC DS-CDMA system's spreading gain was $G' = 2552/17 = 151$. We will compare the achievable performance of these two systems

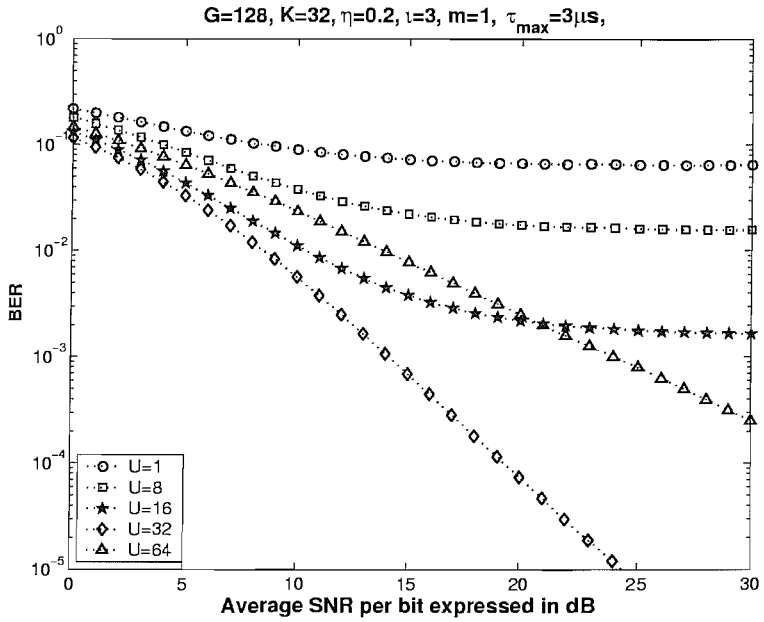

Figure 3.13: BER versus E_b/N_0 Performance of MC LAS DS-CDMA, when we considered different number of subcarriers, U. The RAKE receiver combines $L_r \leq 3$ number of paths. The dispersion of the propagation environment considered was $T_M = 3\mu s$. Hence the number of resolvable multipath components for $U = 1, 8, 16, 32, 64$ was $L_p = 61, 8, 4, 2, 1$. The results were computed from Equation 3.54.

based on their different spreading gains. As in our SC LAS DS-CDMA investigations in Section 3.3.4, we assume that all paths have the same fading parameter, *i.e.* $m_l = m$, $l = 0, \ldots, L_r - 1$, and we have $\tau_{max} = 3\mu s$.

From Figure 3.13 we can conclude that the MC LAS DS-CDMA system having $U = 32$ subcarriers will achieve the best performance trade-off in this scenario. Furthermore, Figure 3.13 demonstrated that the performance of the SC LAS DS-CDMA is significantly worse than that of the LAS MC-DS-CDMA. This is because that the SC system encountered a total number of $L_p = 61$ uniform distributed multipath components and 57 of these were outside the IFW. By contrast for $U = 8, 16, 32, 64$, the corresponding $L_p = 8, 4, 2, 1$. The best performance is achieved by the system having $U = 32$ subcarriers, because the number resolvable multipath components matches the number of RAKE receiver fingers.

From Figure 3.14 we can observe that when we consider $U \leq 8$ and $L_r \leq 3$, the random code based classic MC DS-CDMA system outperforms the MC LAS DS-CDMA. However, when U is greater than 8, the MC LAS DS-CDMA have a significantly better performance than that of the random code based MC DS-CDMA system in the investigated scenario. These performance trends are justified, because $U = 32$ and $U = 64$ the chip-duration became sufficiently long for the MC LAS DS-CDMA system to avoid any multipath components falling outside the IFW and yet having a sufficiently high number of resolvable multipath components for attaining a diversity of 2 and 1, respectively. This justified that the $U = 32$ scenario achieves the best performance.

In Figure 3.15 we configured the RAKE receiver for combining all available paths' energy, *i.e.* we had $L_r = L_p$. In this scenario, the MC LAS DS-CDMA system always outperformed classic random code based MC DS-CDMA scheme when the number of

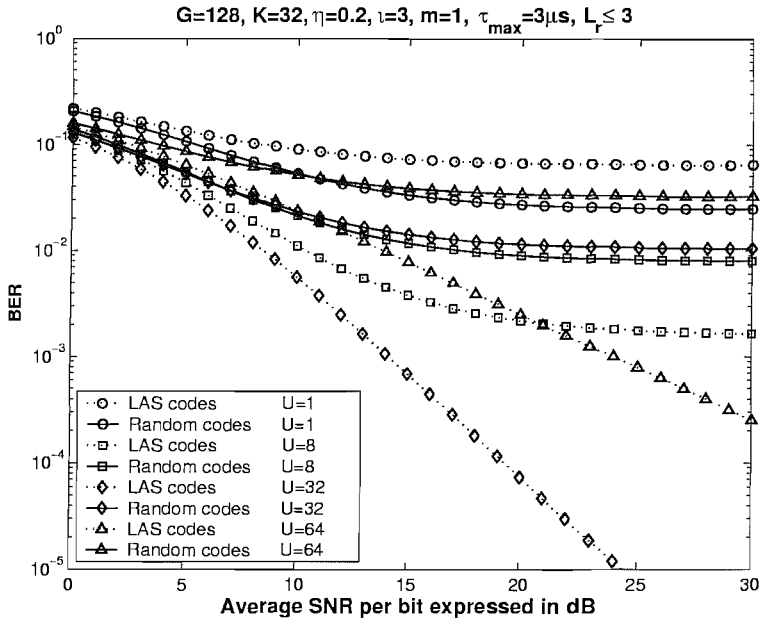

Figure 3.14: BER versus E_b/N_0 performance comparison of two MC DS-CDMAs when we considered LAS codes and random spreading codes. The RAKE receiver was configured for combining $L_r \leq 3$ paths' energy. The dispersion of the propagation environment considered was $T_M = 3\mu s$. Hence the number of resolvable multipath components for $U = 1, 8, 32, 64$ was $L_p = 61, 4, 2, 1$. The results were computed from Equation 3.54.

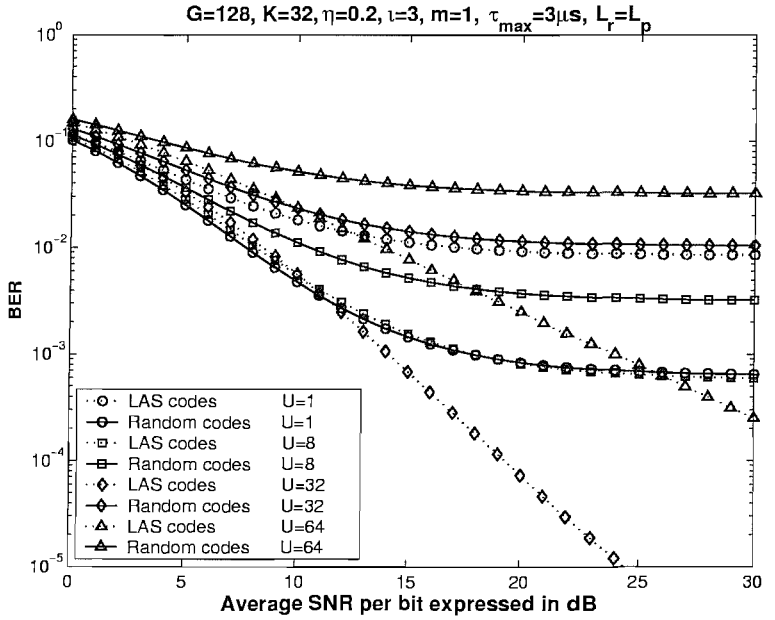

Figure 3.15: BER versus E_b/N_0 performance comparison of two MC DS-CDMAs when we considered LAS codes and random spreading codes. The RAKE receiver was configured for combining all paths' energy, *i.e.* we had $L_r = L_p$. The dispersion of the propagation environment considered was $T_M = 3\mu s$. Hence the number of resolvable multipath components for $U = 1, 32, 64$ was $L_p = 61, 2, 1$. The results were computed from Equation 3.54.

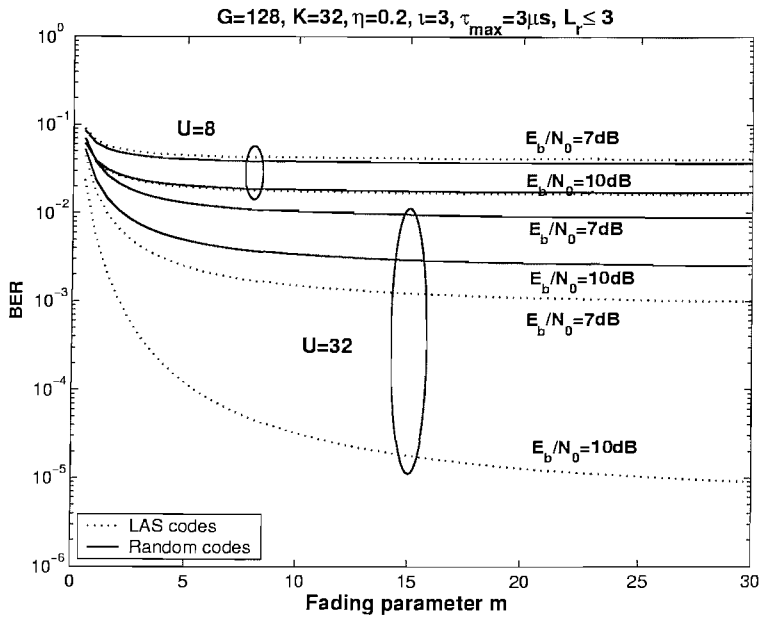

Figure 3.16: BER versus Nakagami fading parameter performance comparison of MC DS-CDMA when we considered LAS codes and random spreading codes. The RAKE receiver combined $L_r \leq 3$ paths, when communicating over different Nakagami fading channel. The dispersion of the propagation environment considered was $T_M = 3\mu s$. Hence the number of resolvable multipath components for $U = 8, 32$ was $L_p = 8, 2$. The results were computed from Equation 3.54.

users supported was $K = 32$. As before, $U = 32$ MC LAS DS-CDMA system exhibited the best performance, as argued before.

In Figure 3.16 we plotted the attainable BER performance as a function of the fading parameter m. More explicitly, we compared the performance of MC LAS DS-CDMA to that of random code based MC DS-CDMA when communicating over different Nakagami fading channels. From Figure 3.16 we may conclude that when the number of subcarriers is $U = 8$, these two systems achieve a similar performance. However, when the number of subcarriers is increased to $U = 32$, the MC LAS DS-CDMA system significantly outperformed random code based MC DS-CDMA arrangement in the investigated scenario.

As argued before, the LAS CDMA system is expected to be operated in a quasi-synchronous manner. When operates in an asynchronous manner, its achievable performance may become inferior in comparison to that of random code based DS-CDMA. Form Figure 3.17 we may conclude that even when we optimized the number of subcarriers resulting in $U = 32$, for asynchronous propagation delay difference in excess of $\tau_{max} \geq 12\mu s$, the MC LAS DS-CDMA will have no advantage in comparison to the random code based MC DS-CDMA. Hence the MC LAS DS-CDMA systems require accurate adaptive timing advance control [108]. As a benefit, they are capable of outperforming the family of the traditional random codes and can dispense with the employment of multiuser detectors.

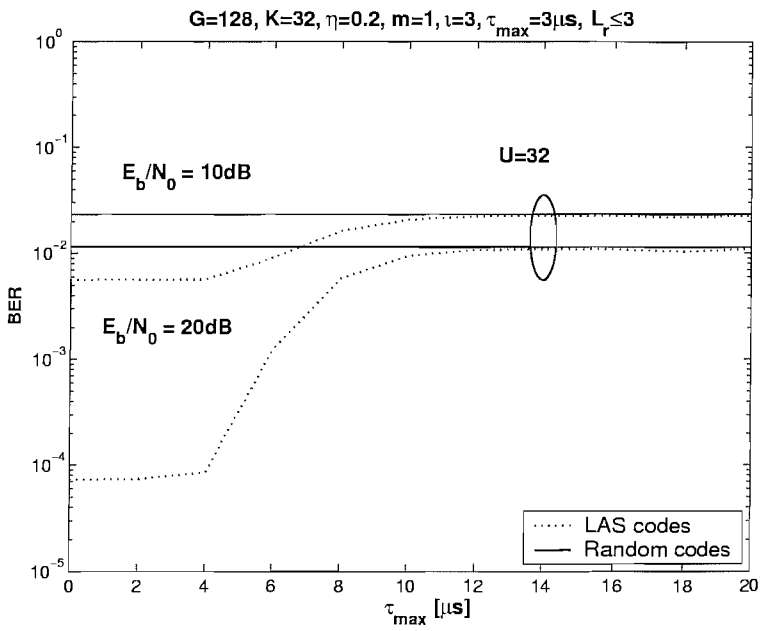

Figure 3.17: BER versus maximum asynchronous delay difference τ_{max} performance comparison of MC DS-CDMA when we considered LAS codes and random spreading codes. The RAKE receiver combined $L_r \leq 3$ paths. The dispersion of the propagation environment considered was $T_M = 3\mu s$. Hence the number of resolvable multipath components for $U = 32$ was $L_p = 2$. The results were computed from Equation 3.54.

3.5 Space-Time Spreading Using Interference Rejection Codes

3.5.1 Transmitted Signal

As seen in Figure 3.18, the system considered in this chapter consists of U antennas located at the transmitter side. The binary input data stream having a bit duration of T_b is serial-to-parallel (S/P) converted to U parallel sub-streams. The new bit duration of each reduced-rate parallel sub-stream, which we refer to as the symbol duration becomes $T_s = UT_b$. After S/P conversion, the U number of parallel bits which have a U-fold higher bit duration are direct-sequence spread using the STS schemes proposed in [25] with the aid of U number of orthogonal spreading sequences - for example, Walsh codes - having a period of UG, where $G = T_b/T_c$ represents the number of chips per bit and T_c is the chip-duration of the orthogonal spreading sequences.

As described above, we have assumed that the number of parallel data sub-streams, the number of orthogonal spreading sequences used by the STS block of Figure 3.18 and the number of transmission antennas is the same, namely U. This specific STS scheme constitutes a sub-class of the generic family of STS schemes, where the number of parallel data sub-streams, the number of orthogonal spreading sequences required by the STS block and the number of transmission antennas may take different values. However, the study conducted in [25] has shown that the number of orthogonal spreading sequences required by STS is usually higher, than the number of parallel sub-streams. The STS scheme having an equal number of parallel sub-streams, orthogonal STS-related spreading sequences as well as transmission antennas constitutes an attractive scheme, since this STS

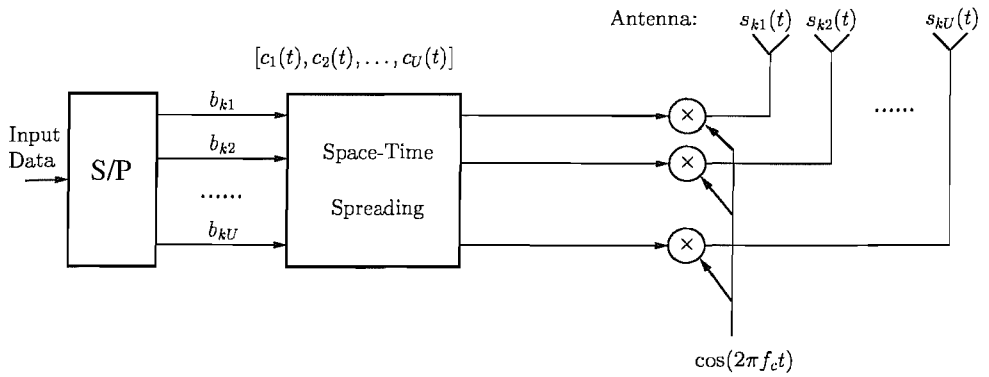

(a) Transmitter

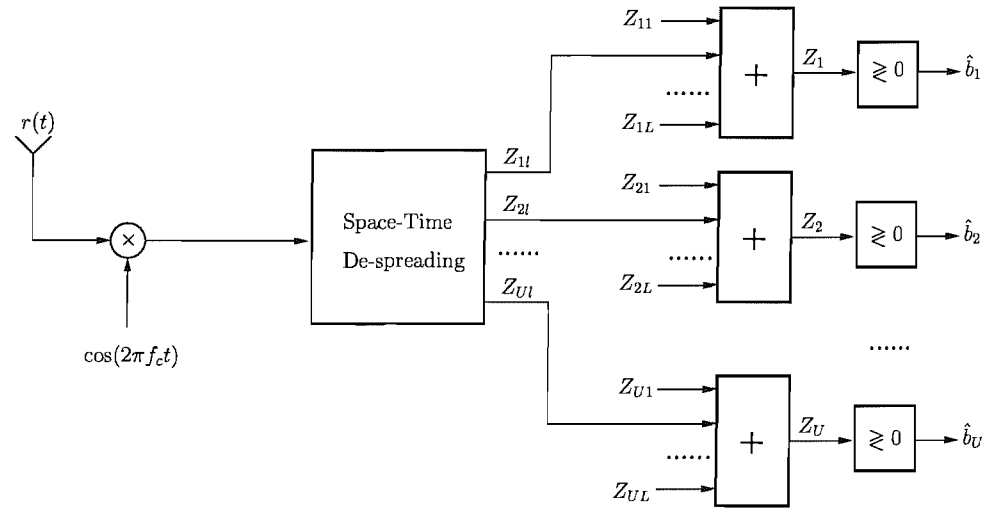

(b) Receiver

Figure 3.18: Transmitter and receiver block diagram of the W-CDMA system using space-time spreading.

scheme is capable of providing maximal transmit diversity without requiring extra STS codes. Note that for the specific values of $U = 2, 4, 8$ the above-mentioned attractive STS schemes have been specified in [25]. In this section, we only investigate these attractive STS schemes.

Based on the philosophy of STS as discussed in [25] and referring to Figure 3.18(a), the transmitted signal of the kth user can be written as:

$$\mathbf{s}_k(t) = \sqrt{\frac{2P}{U^2}}\mathbf{c}(t)^T\mathbf{B}_U(t)\cos(2\pi f_c t), \tag{3.56}$$

where P represents each user's transmitted power, which is constant for all users, $\mathbf{s}_k(t) = [s_{k1}(t)\ s_{k2}(t)\ \ldots\ s_{kU}(t)]^T$ represents the transmitted signal vector of the U transmission antennas, while $\mathbf{c}(t)$ and f_c represent the DS scrambling-based spreading waveform and the carrier frequency, respectively. In Eq(3.56) the vector $\mathbf{c}(t) = [c_1(t)\ c_2(t)\ \ldots\ c_U(t)]^T$ is constituted by the U number of spreading waveforms assigned for the STS block, where

$c_i(t) = \sum_{j=0}^{UG} c_{ij} P_{T_c}(t - jT_c)$, $i = 1, 2, \ldots, U$ denotes the individual components of the STS-based spread signals, and $\{c_{ij}\}$ represents a spreading sequence of period UG for each index i, while $P_{T_c}(t)$ is the rectangular chip-waveform spanning the chip-interval $[0 - T_c]$. **In this chapter, we will consider two different STS schemes. The benchmarker arrangement is the traditional STS scheme of [25], employed for example in W-CDMA.** In this scheme, $c_i(t)$ can be expressed as: $c_i(t) = w_i(t) \otimes \mathrm{PN}(t) = \sum_{j=0}^{UG} (w_{ij} \otimes p_{ij}) P_{T_c}(t - jT_c)$, where $w_i(t) = \sum_{j=0}^{UG} w_{ij} P_{T_c}(t - jT_c)$ denotes the unique user-specific Walsh spreading sequence used by the STS scheme of Figure 3.18, while $\mathrm{PN}(t) = \sum_{j=0}^{UG} p_{ij} P_{T_c}(t - jT_c)$ is the random cell-specific pseduo-noise scrambling sequence. Hence we have $c_{ij} = w_{ij} \otimes p_{ij}$ and c_{ij} may also be modelled as a random spreading sequence. The employment of the PN scrambling sequence in combination with the Walsh code allows the system to reuse the user-specific Walsh codes in adjacent cells and reduce the MAI. **In contrast to the benchmarker, in our proposed scheme space-time spreading is carried out using the family of interference rejection LS codes.** In this scheme, the spreading signature waveform $c_i(t)$ can be expressed as: $c_i(t) = \mathrm{LS}_i(t) = \sum_{j=0}^{UG} \mathrm{LS}_{ij} P_{T_c}(t - jT_c)$, where $\mathrm{LS}_i(t)$ denotes the ith LS spreading signature waveform. **Moreover, we do not impose PN-code based scrambling on the LS STS codes, because this would destroy their IFW. Hence for the sake of maintaining the IFW of the spreading codes, the STS scheme using LS codes does not invoke the conventional scheme's scrambling operation.** It is worth noting that the omission of the PN-code based spreading does not constitute a problem in conjunction with LS codes, since they exhibit an IFW and hence they are more immune to both MAI and MPI that the Walsh codes. It has to be noticed however that the owing to the absence of the PN scrambling code the amount of inter-cell interference is expected to be higher, especially, because the adjacent-cell interference is likely to arrive outside the IFW, where the cross-correlation of the LS codes is higher than that of the cell-specific PN scrambling codes. Still considering Eq(3.56), $\mathbf{B}_U(t)$ represents the $(U \times U)$-dimensional transmitted data matrix created by mapping U input data bits to the U parallel sub-streams according to the specific design rules of [25], so that the maximum possible transmit diversity is achieved, while using relatively low-complexity signal detection algorithms. Specifically, $\mathbf{B}_U(t)$ can be expressed as [25]:

$$\mathbf{B}_U(t) = \begin{pmatrix} a_{11} b_{k,11} & a_{12} b_{k,12} & \ldots & a_{1U} b_{k,1U} \\ a_{21} b_{k,21} & a_{22} b_{k,22} & \ldots & a_{2U} b_{k,2U} \\ \vdots & \vdots & \ddots & \vdots \\ a_{U1} b_{k,U1} & a_{U2} b_{k,U2} & \ldots & a_{UU} b_{k,UU} \end{pmatrix} (t), \tag{3.57}$$

where the time dependence of the (i, j)th element is indicated at the right of the matrix for simplicity. In Eq.(3.57) a_{ij} represents the sign of the element at the ith row and

the jth column, which is determined by the STS design rule, while $b_{k,ij}$ is the data bit assigned to the (i,j)th element, which is one of the U input data bits $\{b_{k1}, b_{k1}, \ldots, b_{kU}\}$ of user k. Each input data bit of $\{b_{k1}, b_{k2}, \ldots, b_{kU}\}$ appears only once in any given row and in any given column. For $U = 2$ and 4, $\mathbf{B}_2(t)$ and $\mathbf{B}_4(t)$ may be expressed as [25]:

$$\mathbf{B}_2(t) = \begin{pmatrix} b_1 & b_2 \\ b_2 & -b_1 \end{pmatrix}(t), \quad \mathbf{B}_4(t) = \begin{pmatrix} b_1 & b_2 & b_3 & b_4 \\ b_2 & -b_1 & b_4 & -b_3 \\ b_3 & -b_4 & -b_1 & b_2 \\ b_4 & b_3 & -b_2 & -b_1 \end{pmatrix}(t). \tag{3.58}$$

Based on Equations (3.56) and (3.57) the signal transmitted by the uth antenna to the kth user can be explicitly formulated as:

$$s_{ku}(t) = \sqrt{\frac{2P}{U^2}} \sum_{i=1}^{U} c_i(t) a_{iu} b_{k,iu}(t) \cos(2\pi f_c t), \; u = 1, 2, \ldots, U. \tag{3.59}$$

3.5.2 Channel Model

The U number of parallel signals $\mathbf{s}_k(t) = [s_{k1}(t)\ s_{k2}(t)\ \ldots\ s_{kU}(t)]$ are transmitted by the U number of antennas over frequency-selective fading channels, where each parallel signal experiences independent frequency-selective Nakagami-m fading. The complex low-pass equivalent representation of the impulse response experienced by the uth parallel signal of all users is given by [7]:

$$h^u(t) = \sum_{l=0}^{L_p-1} h_l^u \delta(t - \tau_l) \exp\left(j\phi_l^u\right), \tag{3.60}$$

where h_l^u, τ_l and ψ_l^u represent the attenuation, delay and phase-shift of the lth multipath component of the channel, respectively. Without loss of generality, we assume that we have $\tau_l = lT_c$, while L_p is the total number of resolvable multipath components and $\delta(t)$ is the Kronecker Delta-function. We assume that the phases $\{\psi_l^u\}$ in Eq.(3.60) are independent identically distributed (iid) random variables uniformly distributed in the interval $[0, 2\pi)$, while the l multipath attenuations $\{h_l^u\}$ in Eq.(3.60) are independent Nakagami random variables having a Probability Density Function (PDF), which is depicted in section 2.2.2.

We support K synchronous CDMA users in the system and assume perfect power control. Consequently, when the K users' signals obeying the form of Eq.(3.56) are transmitted over the frequency-selective fading channels characterized by Eq.(3.60), the received complex low-pass equivalent signal at a given mobile station can be expressed as:

$$R(t) = \sum_{k=1}^{K} \sum_{l=0}^{L_p-1} \sqrt{\frac{2P}{U^2}} \mathbf{c}(t - \tau_l)^T \mathbf{B}_U(t - \tau_l) \mathbf{h}_l + n(t), \tag{3.61}$$

where $n(t)$ is the complex-valued low-pass-equivalent AWGN having a double-sided spectral density of $N_0/2$, while

$$\mathbf{h}_l = \begin{pmatrix} h_l^1 \exp(j\psi_l^1) \\ h_l^2 \exp(j\psi_l^2) \\ \cdots \\ h_l^U \exp(j\psi_l^U) \end{pmatrix}, \; l = 0, 1, \ldots, L_p - 1 \tag{3.62}$$

represents the channel's complex impulse response in the context of the kth user and the lth resolvable path, where $\psi_l^u = \phi_l^u - 2\pi f_c \tau_l$. Furthermore, in Eq.(3.61) we assumed that the signals transmitted by the U number of transmission antennas arrive at the receiver antenna after experiencing the same set of delays. This assumption is justified by the fact that in the frequency band of cellular systems the propagation delay differences among the transmission antenna elements is on the order of nanoseconds, while the multipath delays are of the order of microseconds [25], provided that U is a relatively low number.

3.5.3 Receiver Model

Let the first user be the user-of-interest and consider a receiver using space-time despreading as well as diversity combining, as shown in Figure 3.18(b), where the subscript of the reference user's signal has been omitted for notational convenience. The receiver of Figure 3.18(b) carries out the inverse processing of Figure 3.18(a), in addition to multipath diversity combining. In Figure 3.18(b) the received signal is first down-converted using the carrier frequency f_c, and we assumed that the receiver is capable of achieving near-perfect multipath-delay estimation for the reference user. The de-scrambled signal associated with the lth resolvable path is space-time de-spread using the approach of [25] - which will be further discussed in Section 3.5.4, in order to obtain U separate variables, $\{Z_{1l}, Z_{2l}, \ldots, Z_{Ul}\}$, corresponding to the U parallel data bits $\{b_1, b_2, \ldots, b_U\}$, respectively. Following space-time de-spreading, a decision variable is formed for each parallel transmitted data bit of $\{b_1, b_2, \ldots, b_U\}$ by Equal-Gain (EG) diversity combining the corresponding variables associated with the L_r number of resolvable paths, which can be written as:

$$Z_u = \sum_{l=0}^{L_r-1} Z_{ul}, \; u = 1, 2, \ldots, U. \tag{3.63}$$

Finally, the U number of transmitted data bits $\{b_1, b_2, \ldots, b_U\}$ can be decided based on the decision variables $\{Z_u\}_{u=1}^{U}$ using the conventional decision rule of a BPSK scheme.

Above we have described the transmitter model, the channel model as well as the receiver model of W-CDMA using STS. Let us now describe the detection procedure of the W-CDMA scheme using STS.

3.5.4 Detection of Space-Time Spread Signals

Let $\mathbf{d}_l = [d_{1l}\ d_{2l}\ \ldots\ d_{Ul}]^T$, $l = 1, 2, \ldots, L_r - 1$ - where T denotes the vector transpose - represent the correlator's output variable vector in the context of the lth ($l = 1, 2, \ldots, L$) resolvable path, where

$$d_{ul} = \int_{\tau_l}^{UT_b+\tau_l} R(t)c_u(t-\tau_l)dt. \tag{3.64}$$

When substituting Eq.(3.61) into Eq.(3.64), it can be shown that:

$$\begin{aligned} d_{ul} = \sqrt{2P}T_b \left[a_{u1}b_{u1}h_l^1 \exp\left(j\psi_l^1\right) + a_{u2}b_{u2}h_l^2 \exp\left(j\psi_l^2\right) + \ldots \right. \\ \left. \ldots + a_{uU}b_{uU}h_l^U \exp\left(j\psi_l^U\right)\right] + J_u(l), \quad u = 1, 2, \ldots, U, \end{aligned} \tag{3.65}$$

where

$$J_u(l) = J_{Su}(l) + J_{Mu}(l) + N_u(l), \ u = 1, 2, \ldots, U \tag{3.66}$$

and $J_{Su}(l)$ is due to the multipath-induced self-interference of the signal-of-interest inflicted upon the lth path signal, where $J_{Su}(l)$ can be expressed as:

$$\begin{aligned} J_{Su}(l) = \sum_{j=0, j\neq l}^{L_p-1} \sqrt{\frac{2P}{U^2}} \int_{\tau_l}^{UT_b+\tau_l} \mathbf{c}(t-\tau_j)^T \mathbf{B}_U(t-\tau_j)\mathbf{h}_j \\ \times c_u(t-\tau_l)dt, \end{aligned} \tag{3.67}$$

$J_{Mu}(l)$ represents the multi-user interference inflicted by the signals transmitted simultaneously by the other users, which can be expressed as:

$$\begin{aligned} J_{Mu}(l) = \sum_{k=2}^{K} \sum_{j=0}^{L_p-1} \sqrt{\frac{2P}{U^2}} \int_{\tau_l}^{UT_b+\tau_l} \mathbf{c}(t-\tau_j)^T \mathbf{B}_U(t-\tau_j)\mathbf{h}_j \\ \times c_u(t-\tau_l)dt, \end{aligned} \tag{3.68}$$

and finally $N_u(l)$ is due to the AWGN, formulated as:

$$N_u(l) = \int_{\tau_l}^{UT_b+\tau_l} n(t)c_u(t-\tau_l)dt, \tag{3.69}$$

which is a Gaussian distributed variable having a zero mean and a variance of $2UN_0T_b$.

Let $\mathbf{J}(l) = [J_1(l)\ J_2(l)\ \ldots\ J_U(l)]^T$. Then, the correlator's output variable vector $\mathbf{d}_l$ can be written as:

$$\mathbf{d}_l = \sqrt{2P}T_b\mathbf{B}_U\mathbf{h}_l + \mathbf{J}(l), \ l = 0, 1, \ldots, L_r, \tag{3.70}$$

where $\mathbf{B}_U$ is the reference user's $(U \times U)$-dimensional transmitted data matrix, which is given by Eq.(3.57), but ignoring the time dependence, while $\mathbf{h}_l$ is the channel's complex

impulse response between the base station and the reference user, as shown in Eq.(3.62) in the context of the reference user.

Attractive STS schemes have the property [25] of $\mathbf{B}_U\mathbf{h}_l = \mathbf{H}_U\mathbf{b}$, i.e. Equation (3.70) can be written as:

$$\mathbf{d}_l = \sqrt{2PT_b}\mathbf{H}_U\mathbf{b} + \mathbf{J}(l), \tag{3.71}$$

where $\mathbf{b} = [b_1\ b_2\ \ldots\ b_U]^T$ represents the U number of transmitted data bits, while $\mathbf{H}_U$ is a $(U \times U)$-dimensional matrix with elements from $\mathbf{h}_l$. Each element of $\mathbf{h}_l$ appears once and only once in a given row and also in a given column of the matrix $\mathbf{H}_U$ [25]. The matrix $\mathbf{H}_U$ can be expressed as:

$$\mathbf{H}_U(l) = \begin{pmatrix} \alpha_{11}(l) & \alpha_{12}(l) & \ldots & \alpha_{1U}(l) \\ \alpha_{21}(l) & \alpha_{22}(l) & \ldots & \alpha_{2U}(l) \\ \vdots & \vdots & \ddots & \vdots \\ \alpha_{U1}(l) & \alpha_{U2}(l) & \ldots & \alpha_{UU}(l) \end{pmatrix}, \tag{3.72}$$

where $\alpha_{ij}(l)$ takes the form of $d_{ij}h_l^m \exp(j\psi_l^m)$, and $d_{ij} \in \{+1, -1\}$ represents the sign of the (i,j)th element of $\mathbf{H}_U$, while $h_l^m \exp(j\psi_l^m)$ belongs to the mth element of $\mathbf{h}_l$. For $U = 2$ and 4, it can be shown with the aid of [25] that

$$\mathbf{H}_2(l) = \begin{pmatrix} h_l^1 \exp(j\psi_l^1) & h_l^2 \exp(j\psi_l^2) \\ -h_l^2 \exp(j\psi_l^2) & h_l^1 \exp(j\psi_l^1) \end{pmatrix}, \tag{3.73}$$

$$\mathbf{H}_4(l) = \begin{pmatrix} h_l^1 \exp(j\psi_l^1) & h_l^2 \exp(j\psi_l^2) & h_l^3 \exp(j\psi_l^3) & h_l^4 \exp(j\psi_l^4) \\ -h_l^2 \exp(j\psi_l^2) & h_l^1 \exp(j\psi_l^1) & -h_l^4 \exp(j\psi_l^4) & h_l^3 \exp(j\psi_l^3) \\ -h_l^3 \exp(j\psi_l^3) & h_l^4 \exp(j\psi_l^4) & h_l^1 \exp(j\psi_l^1) & -h_l^2 \exp(j\psi_l^2) \\ -h_l^4 \exp(j\psi_l^4) & -h_l^3 \exp(j\psi_l^3) & h_l^2 \exp(j\psi_l^2) & h_l^1 \exp(j\psi_l^1) \end{pmatrix}. \tag{3.74}$$

With the aid of the analysis provided in [25], it can be shown furthermore that the matrix $\mathbf{H}_U(l)$ has the property of $\mathrm{Re}\left\{\mathbf{H}_U^\dagger(l)\mathbf{H}_U(l)\right\} = \mathbf{h}_l^\dagger\mathbf{h}_l \cdot \mathbf{I}$, where $\dagger$ denotes the complex conjugate transpose and $\mathbf{I}$ represents a $(U \times U)$-dimensional unity matrix. Letting $\mathbf{h}_u(l)$ denote the uth column of $\mathbf{H}_U(l)$, the variable Z_{ul} in Eq.(3.63) can be formulated as [25]:

$$Z_{ul} = \mathrm{Re}\left\{\mathbf{h}_u^\dagger(l)\mathbf{d}_l\right\} = \sqrt{2PT_b}b_u \sum_{u=1}^{U} |h_l^u|^2 + \mathrm{Re}\left\{\mathbf{h}_u^\dagger(l)\mathbf{J}(l)\right\},\ u = 1, 2, \ldots, U. \tag{3.75}$$

Finally, according to Eq.(3.63) the decision variables associated with the U parallel transmitted data bits $\{b_1, b_2, \ldots, b_U\}$ of the reference user can be expressed as:

$$Z_u = \sqrt{2PT_b}b_u \sum_{l=0}^{L_r-1} \sum_{u=1}^{U} |h_l^u|^2 + \sum_{l=0}^{L_r-1} \mathrm{Re}\left\{\mathbf{h}_u^\dagger(l)\mathbf{J}(l)\right\},\ u = 1, 2, \ldots, U, \tag{3.76}$$

which shows that the receiver is capable of achieving a diversity order of UL_r, as indicated by the related sums of the first term.

Above we have analyzed the detection procedure applicable to W-CDMA signals generated using STS. Let us now derive the corresponding BER expression.

3.5.5 BER Analysis

In this section we derive the BER expression of the STS-assisted W-CDMA system by first analyzing the statistics of the variable Z_u, $u = 1, 2, \ldots, U$ with the aid of the Gaussian approximation [115]. According to Equation 3.76, for a given set of complex channel transfer factor estimates $\{h_l^u\}$, Z_u can be approximated as a Gaussian variable having a mean given by:

$$\mathrm{E}[Z_u] = \sqrt{2P}T_b b_u \sum_{l=0}^{L_r-1} \sum_{u=1}^{U} |h_l^u|^2. \tag{3.77}$$

Based on the assumption that the interferences imposed by the different users, the different paths as well as by the AWGN constitute independent random variables, the variance of Z_u may be expressed as:

$$\begin{aligned}
\mathrm{Var}[Z_u] &= \mathrm{E}\left[\left(\sum_{l=0}^{L_r-1} \mathrm{Re}\left\{\mathbf{h}_u^\dagger(l)\mathbf{J}(l)\right\}\right)^2\right] \\
&= \sum_{l=0}^{L_r-1} \mathrm{E}\left[\left(\mathrm{Re}\left\{\mathbf{h}_u^\dagger(l)\mathbf{J}(l)\right\}\right)^2\right] \\
&= \frac{1}{2}\sum_{l=0}^{L_r-1} \mathrm{E}\left[\left(\mathbf{h}_u^\dagger(l)\mathbf{J}(l)\right)^2\right].
\end{aligned} \tag{3.78}$$

Substituting $\mathbf{h}_u(l)$, which is the uth column of $\mathbf{H}_u(l)$ in Eq.(3.72), and $\mathbf{J}(l)$ having elements given by Eq.(3.66) into the above equation, it can be shown that for a given set of channel estimates $\{h_l^u\}$, Eq.(3.78) can be simplified as:

$$\begin{aligned}
\mathrm{Var}[Z_u] &= \frac{1}{2}\sum_{l=0}^{L_r-1}\sum_{u=1}^{U} |h_l^u|^2 \mathrm{E}\left[(J_u(l))^2\right] \\
&= \frac{1}{2}\sum_{l=0}^{L_r-1}\sum_{u=1}^{U} |h_l^u|^2 \mathrm{Var}[J_u(l)],
\end{aligned} \tag{3.79}$$

where $J_u(l)$ is given by Eq.(3.66). In deriving Eq.(3.79) we exploited the assumption of $\mathrm{Var}[J_1(l)] = \mathrm{Var}[J_2(l)] = \ldots = \mathrm{Var}[J_U(l)]$.

Scheme I – Walsh-Code Based STS Assisted CDMA

As shown in Equation 3.66, $J_u(l)$ consists of three terms, namely the first being the AWGN $N_u(l)$ having a variance of $2UN_0T_b$. The second term is $J_{Su}(l)$, which is the multipath-induced self-interference inflicted upon the lth path of the user-of-interest, while the

third one is $J_{Mu}(l)$ imposed by the $(K-1)$ interfering users. It can be shown by careful observation of Eq.(3.67) that $J_{Su}(l)$ consists of U^2 terms and each term takes the form

$$J_{su}(l) = \sum_{j=0, j\neq l}^{L_p-1} \sqrt{\frac{2P}{U^2}} \int_{\tau_l}^{UT_b+\tau_l} c_m(t-\tau_j) a_{mn} b_{mn}(t-\tau_j) h_j^n \exp(j\psi_j^n) \times c_m(t-\tau_l) dt. \quad (3.80)$$

Assuming that $\mathrm{E}[(h_j^n)^2] = \Omega_0 e^{-\eta j}$, i.e. that $\mathrm{E}[(h_j^n)^2]$ is independent of the index of the transmission antenna and we that have $\mathrm{E}[(h_j^n)^2] = \Omega_0 e^{-\eta j}$, as well as following the analysis of [102], it can be shown that the above term has a variance of $2\Omega_0 E_b T_b[q(L_p,\eta) - e^{-\eta j}]/(GU)$, where $q(L_p,\eta) = (1-e^{-L_p\eta})/(1-e^{-\eta})$, if $\eta \neq 0$ and $q(L_p,\eta) = L_p$, if $\eta = 0$. Consequently, we have $\mathrm{Var}[J_{Su}(l)] = U^2 \times 2\Omega_0 E_b T_b[q(L_p,\eta) - e^{-\eta l}]/(GU) = 2U\Omega_0 E_b T_b[q(L_p,\eta) - e^{-\eta l}]/G$. Hence, the multipath-induced variance of the STS scheme of [25] can be expressed as:

$$\mathrm{Var}[J_{Su}(l)]_{\mathrm{I}} = 2U\Omega_0 E_b T_b[q(L_p,\eta) - e^{-\eta l}]/G. \quad (3.81)$$

Similarly, the multi-user interference term $J_{Mu}(l)$ of Eq.(3.68) also consists of U^2 terms, and each term has the form of

$$J_{mu}(l) = \sum_{k=2}^{K} \sum_{j=0}^{L_p-1} \sqrt{\frac{2P}{U^2}} \int_{\tau_l}^{UT_b+\tau_l} c_m(t-\tau_j) a_{mn} b_{mn}(t-\tau_j) \times h_j^l \exp(j\psi_j^n) c_u(t-\tau_l) dt. \quad (3.82)$$

However, after the de-scrambling operation and exploiting that Walsh STS code is orthogonal at the zero code offset, no MAI is incurred when we have $\tau_j = \tau_l$, $J_{mu}(l)$ can be written as:

$$J_{mu}(l) = \sum_{k=2}^{K} \sum_{j=0, j\neq l}^{L_p-1} \sqrt{\frac{2P}{U^2}} \int_{\tau_l}^{UT_b+\tau_l} c_m(t-\tau_j) a_{mn} b_{mn}(t-\tau_j) \times h_j^l \exp(j\psi_j^n) c_u(t-\tau_l) dt. \quad (3.83)$$

Hence the variance of $J_{mu}(l)$ is $(K-1)2\Omega_0 E_b T_b[q(L_p,\eta) - e^{-\eta l}]/GU$, and $J_{Mu}(l)$ is constituted by U^2 number of $J_{mu}(l)$ terms. Consequently, the variance of $J_{Mu}(l)$ can be approximated as:

$$\mathrm{Var}[J_{Mu}(l)]_{\mathrm{I}} = (K-1)2U\Omega_0 E_b T_b[q(L,\eta) - e^{-\eta l}]/G \quad (3.84)$$

for the STS scheme of [25].

Scheme II – STS Assisted CDMA Using LS codes

Having characterized the various sources of interference, let us now demonstrate that with the advent of having an IFW, the LS codes are capable of suppressing both the MAI

and MPI. More specifically, only the paths which fall outside the IFW will impose MAI and MPI on the decision. We assume having $T_{\text{IFW}} = \iota T_c$, and the jth path will inflict interference upon the lth finger of the RAKE receiver only if we have:

$$|\tau_j - \tau_l| > \iota T_c, \tag{3.85}$$

which is corresponds to:

$$|j - l| > \iota. \tag{3.86}$$

Let us first consider the effect of MPI, Similarly to the benchmark of [25], for the proposed LS code based system, it can be shown that $J_{Su}(l)$ defined in Eq.(3.67) is also constituted by U^2 terms and each term takes the form of,

$$\begin{aligned} J_{su}(l) &= \sum_{\substack{j=0 \\ |j-l|>\iota}}^{L_p-1} \sqrt{\frac{2P}{U^2}} \int_{\tau_l}^{UT_b+\tau_l} c_m(t-\tau_j) a_{mn} b_{mn}(t-\tau_j) \times \\ &\qquad h_j^n \exp(j\psi_j^n) c_u(t-\tau_l) dt. \end{aligned} \tag{3.87}$$

If we define the partial auto-correlation coefficient as:

$$\rho_{mm}(j,l) = \frac{1}{UT_b} \int_0^{|\tau_j-\tau_l|} c_m(t) c_m(t - |\tau_j - \tau_l|) dt \tag{3.88}$$

$$\varrho_{mm}(j,l) = \frac{1}{UT_b} \int_{|\tau_j-\tau_l|}^{UT_b} c_m(t) c_m(t - |\tau_j - \tau_l|) dt, \tag{3.89}$$

then the integral in Eq.(3.87) can be expressed as:

$$\int_{\tau_l}^{UT_b+\tau_l} c_m(t-\tau_j) c_u(t-\tau_l) b_{mn}(t-\tau_j) dt = (\rho_{mm}(j,l) b[-1] + \varrho_{mm}(j,l) b[0]) UT_b. \tag{3.90}$$

Therefore, the corresponding MPI variance of $J_{su}(l)$, $u = 1, 2, \ldots, U$ can be expressed as:

$$\begin{aligned} \text{Var}[J_{su}(l)] &= \sum_{\substack{j=0 \\ |j-l|>\iota}}^{L_p-1} \left\{ 2\Omega_0 e^{-\eta j} [\rho_{mm}^2(j,l) + \varrho_{mm}^2(j,l)] \right\} \times 2E_b T_b \\ &= \sum_{\substack{j=1 \\ |j-l|>\iota}}^{L} \left\{ 2e^{-\eta j} [\rho_{mm}^2(j,l) + \varrho_{mm}^2(j,l)] \right\} \times 2\Omega_0 E_b T_b. \end{aligned} \tag{3.91}$$

For convenient formulation and comparison with the benchmarker STS scheme of [25], we define $\Upsilon_S(l) = GU \sum_{\substack{j=0 \\ |j-l|>\iota}}^{L_p-1} 2e^{-\eta j} [\rho_{mm}^2(j,l) + \varrho_{mm}^2(j,l)]$, which is the MPI reduction factor for the lth path, owing to the employment of LS codes. Then the MPI variance of $\text{Var}[J_{Su}(l)]$, which includes a total of U^2 number of terms of $\text{Var}[J_{su}(l)]$ terms, can be

approximated as:

$$\mathrm{Var}[J_{Su}(l)]_{\mathrm{II}} = \Upsilon_S(l) 2\Omega_0 E_b T_b U/G. \tag{3.92}$$

Having characterized the MPI, let us now focus our attention on the effects of MAI. Similarly to Eq.(3.88) and Eq.(3.89), we define the partial cross-correlation coefficients as:

$$\rho_{um}(j,l) = \frac{1}{UT_b}\int_0^{|\tau_j-\tau_l|} c_u(t)c_m(t-|\tau_j-\tau_l|)dt \tag{3.93}$$

$$\varrho_{um}(j,l) = \frac{1}{UT_b}\int_{|\tau_j-\tau_l|}^{UT_b} c_u(t)c_m(t-|\tau_j-\tau_l|)dt. \tag{3.94}$$

Hence the integral in Eq.(3.68) may be expressed as:

$$\int_{\tau_l}^{UT_b+\tau_l} c_m(t-\tau_j)c_u(t-\tau_l)b_{mn}(t-\tau_j)dt = (\rho_{um}(j,l)b_m[-1] + \varrho_{um}(j,l)b_m[0])UT_b. \tag{3.95}$$

Similar to the benchmarker of [25], in the LS code based STS scheme the MAI term, $J_{Mu}(l)$ defined in Eq.(3.68) also consists of U^2 terms, and each term takes the form of:

$$J_{mu}(l) = \sum_{k=2}^{K}\sum_{\substack{j=0\\|j-l|>\iota}}^{L_p-1}\sqrt{\frac{2P}{U^2}}\int_{\tau_l}^{UT_b+\tau_l} c_m(t-\tau_j)a_{mn}b_{mn}(t-\tau_j) \times h_j^l \exp(j\psi_j^n)c_u(t-\tau_l)dt, \tag{3.96}$$

while the variance of the MAI $J_{mu}(l)$ can be expressed as:

$$4\Omega_0 E_b T_b \sum_{\substack{m=1\\m\neq u}}^{K}\sum_{\substack{j=0\\|j-l|>\iota}}^{L_p-1} e^{-\eta j}[\rho_{um}^2 + \varrho_{um}^2]. \tag{3.97}$$

Similarly to the MPI reduction factor, we define the MAI reduction factor as: $\Upsilon_M(l) = \frac{GU}{K-1}\sum_{\substack{m=1\\m\neq u}}^{K}\sum_{\substack{j=0\\|j-l|>\iota}}^{L_p-1} 2e^{-\eta j}[\rho_{um}^2 + \varrho_{um}^2]$. Then for the proposed LS code based STS scheme, the MAI variance of $\mathrm{Var}[J_{Mu}(l)]$, which includes a total of U^2 terms of the form $\mathrm{Var}[J_{mu}(l)]$, can be approximated as::

$$\mathrm{Var}[J_{Mu}(l)]_{\mathrm{II}} = \Upsilon_M(l) \times 2(K-1)U\Omega_0 E_b T_b U/G. \tag{3.98}$$

Having characterized the MAI and MPI variance, let us now quantify the achievable BER performance the proposed system. Based on Eq.(3.66), the variance of $J_u(l)$ of the

traditional STS scheme can be written as:

$$\begin{aligned}\mathrm{Var}\left[J_u(l)\right]_{\mathrm{I}} &= 2N_0UT_b + \frac{2U\Omega_0E_bT_b[q(L_p,\eta) - e^{-\eta l}]}{G} \\ &\quad + \frac{(K-1)2U\Omega_0E_bT_b[q(L_p,e^{-\eta l}]}{G}, \\ &= 2N_0UT_b + \frac{2UK\Omega_0E_bT_b[q(L_p,e^{-\eta l}]}{G}. \end{aligned} \tag{3.99}$$

By contrast, the corresponding variance of $J_u(l)$ of the LS code based STS scheme can be expressed with the aid of Eq.(3.66) as:

$$\mathrm{Var}[J_u(l)]_{\mathrm{II}} = 2N_0UT_b + \frac{\Upsilon_S(l)2\Omega_0E_bT_bU}{G} + \frac{\Upsilon_M(l)(K-1)2\Omega_0E_bT_bU}{G}. \tag{3.100}$$

Let us now assume that the Rake receiver is capable of combining a maximum of L_r paths' energy owing to its complexity limitation. Then the variance of Z_u can expressed as:

$$\mathrm{Var}\left[Z_u\right] = \frac{1}{2}\sum_{l=0}^{L_r-1}\sum_{u=1}^{U}|h_l^u|^2 \times \mathrm{Var}[J_u(l)], \tag{3.101}$$

for a given set of channel estimates $\{h_l^u\}$ using Eq.(3.77). Hence the BER conditioned on h_l^u for $u = 1, 2, \ldots, U$ and $l = 0, 1, \ldots, L_r - 1$ can be written as:

$$P_b(E|\{h_l^u\}) = Q\left(\sqrt{\frac{\mathrm{E}^2\left[Z_u\right]}{\mathrm{Var}\left[Z_u\right]}}\right) = Q\left(\sqrt{\sum_{l=0}^{L_r-1}\sum_{u=1}^{U}2\gamma_{lu}}\right), \tag{3.102}$$

where $Q(x)$ represents the Gaussian Q-function, which can also be represented in its less conventional form as $Q(x) = \frac{1}{\pi}\int_0^{\pi/2}\exp\left(-\frac{x^2}{2\sin^2\theta}\right)d\theta$, where $x \geq 0$ [104, 106]. Furthermore, $2\gamma_{lu}$ in Eq.(3.102) represents the output Signal to Interference plus Noise Ratio (SINR) experienced at the lth finger of the RAKE receiver for the uth STS antenna.

In both the Walsh-code aided [25] and in the LS code based STS scheme, γ_{lu} of Eq.(3.102) is given by:

$$\gamma_{lu} = \frac{(\mathrm{E}[Z_{ul}])^2}{\mathrm{Var}[J_u(l)]} = \overline{\gamma}_{lc}\cdot\frac{(h_l^u)^2}{\Omega_0}. \tag{3.103}$$

However, in the Walsh-code based STS scheme of [25], $\overline{\gamma}_{lc}$ is given by:

$$\overline{\gamma}_{lc} = \frac{1}{U}\left[\frac{K[q(L,\eta) - e^{-\eta(l-1)}]}{G} + \left(\frac{\Omega_0E_b}{N_0}\right)^{-1}\right]^{-1}. \tag{3.104}$$

By contrast, in the LS code based STS scheme, $\overline{\gamma}_{lc}$ can be expressed as:

$$\overline{\gamma}_{lc} = \frac{1}{U}\left[\frac{\Upsilon_S(l)}{G} + \frac{(K-1)\Upsilon_M(l)}{G} + \left(\frac{\Omega_0E_b}{N_0}\right)^{-1}\right]^{-1}, \tag{3.105}$$

where the MPI and MAI reduction factors $\Upsilon_S(l)$, $\Upsilon_M(l)$, respectively, reflect how much interference is suppressed for the lth path with the advent of the IFW, which is mainly determined by the width of IFW and by the number of resolvable paths, *i.e*, by ι and L_p. As an illustrative example, Table 3.2 shows these two factors when communicating over an $L_p = 8$-path channel having a negative exponential decay factor of $\eta = 0.2$, Nakagami-m fading factor of $m = 1$, and when the width of the IFW is $\iota = 3$.

l	0	1	2	3	4	5	6	7
$q(L_p, \eta) - e^{-\eta l}$	3.40	3.58	3.73	3.85	3.95	4.03	4.10	4.16
$\Upsilon_S(l)$	0.12	0.04	0.01	0	0	0.03	0.15	0.40
$\Upsilon_M(l)$	3.56	2.89	2.34	1.91	7.74	6.37	5.34	4.5

Table 3.2: The interference suppression factors $\Upsilon_s(l)$ and $\Upsilon_M(l)$, when communicating over an $L = 8$-path channel having a negative exponential decay factor of $\eta = 0.2$, Nakagami-m fading factor of $m = 1$, and an IFW width of $\iota = 3$.

The average BER, $P_b(E)$ can be obtained by averaging the conditional BER expression of Eq.(3.102) over the joint PDF of the instantaneous SNR values corresponding to the L_r multipath components and to the U transmit antennas $\{\gamma_{lu} : l = 0, 1, \ldots, L_r - 1;\ u = 1, 2, \ldots, U\}$. Since the random variables $\{\gamma_{lu} : l = 0, 1, \ldots, L_r - 1;\ u = 1, 2, \ldots, U\}$ are assumed to be statistically independent, the average BER can be formulated as [107]:

$$P_b(E) = \frac{1}{\pi} \int_0^{\pi/2} \prod_{l=0}^{L_r-1} \prod_{u=1}^{U} I_{lu}\left(\overline{\gamma}_{lu}, \theta\right) d\theta, \tag{3.106}$$

where we have

$$I_{lu}\left(\overline{\gamma}_{lu}, \theta\right) = \int_0^{\infty} \exp\left(-\frac{\gamma_{lu}}{\sin^2\theta}\right) p_{\gamma_{lu}}(\gamma_{lu}) d\gamma_{lu}. \tag{3.107}$$

Since both $\gamma_{lu} = \overline{\gamma}_{lc} \cdot \frac{(h_l^u)^2}{\Omega_0}$ and h_l^u obey the Nakagami-m distribution characterized by Eq.(2.5), it can be shown that the PDF of γ_{lu} can be formulated as:

$$p_{\gamma_{lu}}(\gamma_{lu}) = \left(\frac{m_l}{\overline{\gamma}_{lu}}\right)^{m_l} \frac{\gamma^{m_l-1}}{\Gamma(m_l)} \exp\left(-\frac{m_l \gamma_{lu}}{\overline{\gamma}_{lu}}\right), \quad \gamma_{lu} \geq 0, \tag{3.108}$$

where $\overline{\gamma}_{lu} = \overline{\gamma}_{lc} e^{-\eta l}$ for $l = 0, 1, \ldots, L_p - 1$.

Upon substituting Eq.(3.108) into Eq.(3.107) it can be shown that [104]:

$$I_{lu}\left(\overline{\gamma}_{lu}, \theta\right) = \left(\frac{m_l^u \sin^2\theta}{\overline{\gamma}_{lu} + m_l^u \sin^2\theta}\right)^{m_l^u}. \tag{3.109}$$

Finally, upon substituting Eq.(3.109) into Eq.(3.106), the average BER of the STS-assisted W-CDMA system using U transmission antennas can be written as:

$$P_b(E) = \frac{1}{\pi} \int_0^{\pi/2} \prod_{l=0}^{L_r-1} \prod_{u=1}^{U} \left(\frac{m_l^u \sin^2\theta}{\overline{\gamma}_{lu} + m_l^u \sin^2\theta}\right)^{m_l^u} d\theta, \tag{3.110}$$

which shows that the diversity order achieved is $L_r U$, namely the product of the diversity due to STS and the diversity contributed by the RAKE receiver. Furthermore, if we assume that m_l is independent of u, i.e. that all of the parallel transmitted signals experience an identical Nakagami fading, then Eq.(3.110) can be expressed as:

$$P_b(E) = \frac{1}{\pi} \int_0^{\pi/2} \prod_{l=0}^{L_r-1} \left(\frac{m_l \sin^2\theta}{\overline{\gamma}_{lu} + m_l \sin^2\theta} \right)^{Um_l} d\theta. \tag{3.111}$$

3.5.6 Numerical Results

Having characterized the analytical performance of the system, let us now consider the achievable BER performance. Stańczak *et al.* [18] concluded that when using LS codes the width ι of the IFW and the number of users K has to obey:

$$(\iota - 1)K \leq G. \tag{3.112}$$

Furthermore, LS codes require W_0 number of zero-valued chips, which are inserted in the beginning and center of the code sequence for creating the IFW. In our scenario, the LS(N, P, W_0)=LS(4,32,4) codes having a length of $L_S = NP + 2W_0 = 136$ were invoked, and their effective spreading gain was $L_S = NP = 128$, since the zero-valued chips do not include the spreading gain. For the sake of maintaining the same chip rate and same spectral efficiency for both STS schemes, we set the spreading gain of the traditional STS assisted CDMA system to: $G' = NP + 2W_0 = 136$. Furthermore, for simplicity's sake we assume that all paths have the same Nakagami fading parameter, *i.e.* $m_l = m,\ l = 0, \ldots, L_r - 1$.

We assume that the chip rate is $1.2288M$chip/s, the channel's delay spread is negative exponentially distributed having a uniform distributed mean-delay in the range of $[0.3, 3]\mu s$ [114], and we assume that both the random and LAS-code based systems have a chip rate of $1.2288M$chips. The number of resolvable paths is $L_p = \lfloor \frac{\tau}{T_c} \rfloor + 1 = 4$, where we have $\tau = 3\mu s$. Both the traditional STS and the LS code based STS schemes supported $K = 32$ users, and the width of the IFW of the LS codes was $\iota = 3$. We can see from Figure 3.19 that the LS code based STS scheme exhibits a significantly better performance than the traditional Walsh-code based system having that the same diversity order of $L_r U$. The reason that the LS code based STS scheme outperforms the traditional STS scheme is that the MAI and MPI is reduced, as a benefit of using LAS codes, which was quantified by Eq.(3.111).

Figure 3.20 characterizes the achievable performance of these two schemes communicating over different fading channels associated with different Nakagami fading parameters[2]. More explicitly, when we have $m = 1$, we model a Rayleigh fading channel, $m = 2$ represents a Rician fading channel, while $m \to \infty$ corresponds to an AWGN channel. From this figure we can observe that the LS code based STS scheme exhibited a better

[2]In the figure, the random code represents the convolution of the Walsh spreading code and the Pseudo-Noise scrambling code, which was modelled as a random code.

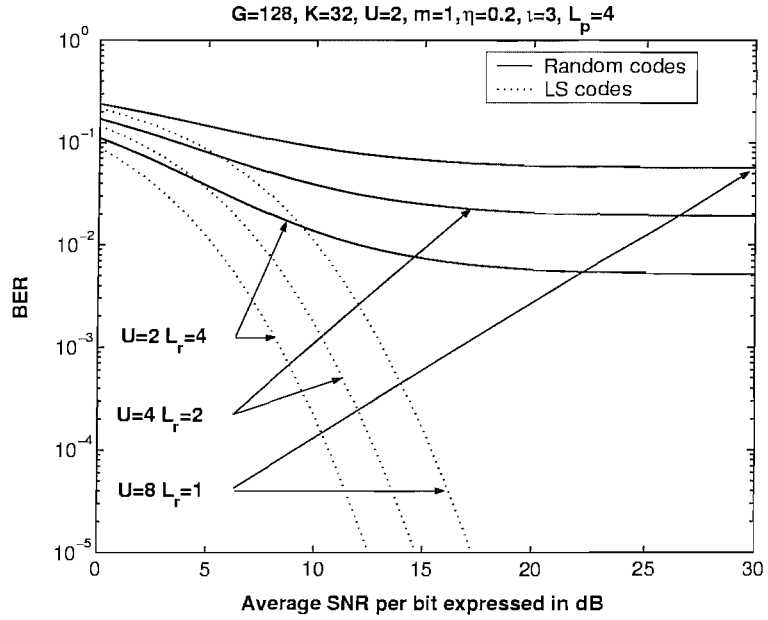

Figure 3.19: BER versus SNR per bit, E_b/N_0, performance comparison between the Walsh-code and LS-code based STS transmit diversity schemes having the same diversity order of $L_r \cdot U$, when communicating over a Nakagami-m ($m = 1$) fading multipath ($L_p = 4$) channel evaluated from Eq.(3.111) by assuming that the average power decay rate was $\eta = 0.2$. The remaining system parameters are listed at the top of the figure.

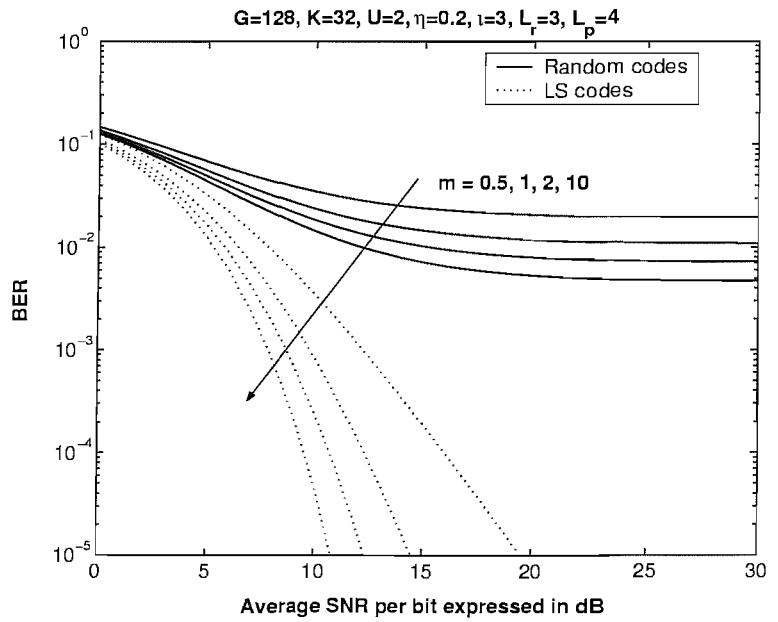

Figure 3.20: BER versus SNR per bit, E_b/N_0, performance comparison between the Walsh-code and LS-code based STS transmit diversity schemes, when communicating over various Nakagami-m fading multipath ($L_p = 4$) channels, where $L_r = 3$ out of the $L_p = 4$ available paths were combined by the Rake receiver. The remaining system parameters are listed at the top of the figure.

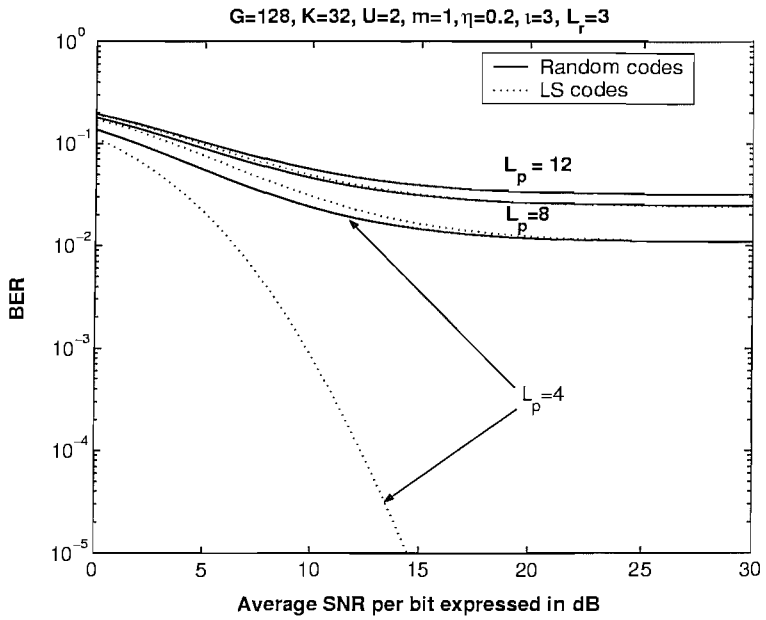

Figure 3.21: BER versus SNR per bit, E_b/N_0, performance comparison between the Walsh-code and LS-code based transmit diversity schemes and the conventional RAKE receiver arrangement, when communicating over different dispersive Nakagami-m channels having $L_p = 4, 8$ and 12 resolvable paths, but only combining $L_r = 3$ of them owing to the maximum complexity limitations.

performance than the traditional STS scheme, regardless of the value of m. More specifically, provided that we have $L_p = 4$, the LS code based STS scheme outperformed the traditional STS scheme, when communicating over different Nakagami multipath fading channels.

Figure 3.21 shows the performance of these two systems for transmission over different dispersive channels having $L = 4 \ldots 12$ resolvable multipath components, but assuming that only $L_r = 3$ of these components were combined by the RAKE receiver owing to its limited affordable complexity. From Figure 3.21, we may conclude that the LS codes are effective, when the number of resolvable paths is relatively low, for example when we have $L_p = 4$. When L_p is increased to 8, the LS code based STS scheme only has a slight gain over the traditional STS scheme, while when L_p is increased to 12, the LS code based STS scheme performs even worse than the traditional STS scheme. The reason for this performance erosion is that many of the paths will be located outside the IFW, when L_p is high and the auto-correlation as well as cross-correlation of the LS codes outside the IFW is higher than that of the random codes. Hence many of the multipath components arrive outside the IFW when L_p is high, which inevitably will increase both the MAI and the MPI.

From Figure 3.22, we can observe that if the system's user load is high, the LS code based STS scheme will have no advantage over the traditional Walsh-code based STS scheme of [25], which is caused by two factors. First, the number of LS codes having an IFW of $\iota = 3$ is limited. For example, when we consider $G = 128$, only 32 LS codes have an IFW of $\iota = 3$, and when the number of users K exceeds 32, the width of the IFW will be

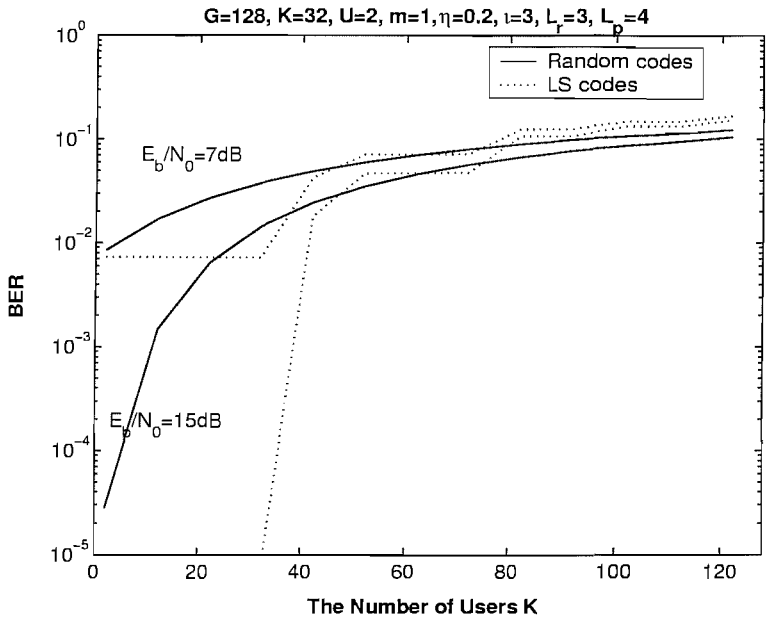

Figure 3.22: BER versus SNR per bit, E_b/N_0, performance comparison between the Walsh-code and LS-code based STS transmit diversity schemes as a function of the number of users K. The remaining system parameters are listed at the top of the figure.

reduced to zero, since even the codes having $\iota = 0$ will be required for supporting $K \geq 32$ users. In this scenario, the LS code based STS scheme becomes incapable of effectively suppressing the MAI and MPI. Second, it may be shown that the cross-correlation of LS codes outside the IFW is higher than that of the random codes, hence LS codes may impose increased interferences, when the number of users K increased. Therefore, the LS code base STS scheme is more effective in low-user-load scenarios, *i.e* when we have $K \leq G/3$.

3.6 Chapter Conclusions

In conclusion, LAS-CDMA was investigated, which exhibited a significantly better performance than the traditional random code based DS-CDMA system in a relatively low chip-rate scenario, provided that all users operate in a quasi-synchronous manner. As the chip-rate increases, the number of resolvable paths also increases, which will impose a performance degradation. Hence, LAS-CDMA may be expected to have a moderate performance gain over the traditional DS-CDMA system, when L_p is in excess of 12. Furthermore, the limited number of available LAS codes having a certain IFW width suggests that the employment of LAS-CDMA is beneficial in a low-user load scenario.

The MC LAS DS-CDMA exhibited a significantly better performance than traditional MC DS-CDMA, provided that all users operate in a quasi-synchronous manner. The number of subcarriers U was optimized for the sake of attaining the best performance trade-off between the achievable multipath diversity and MAI as well as MPI suppression. For a 20 $Mchips/s$ system, $U = 32$ was found to be the best design option. Furthermore, the MC LAS DS-CDMA systems require accurate adaptive timing advance control [108].

As a benefit, they are capable of outperforming the family of the traditional random codes and can dispense with the employment of multiuser detectors.

Furthermore, the proposed LS code based STS scheme exhibited a significantly better performance than that of the traditional Walsh-code based STS scheme [25]. As the number of resolvable paths L of the channel increases, the LS code based STS scheme only has a slight gain over the traditional STS scheme [25], owing the fact that many of the paths arrive outside the IFW, when L is high and also because the auto-correlation as well as cross-correlation of LS codes outside the IFW is higher than that of the random codes. Furthermore, when communicating in a high-user-load scenario, for example when we have $K = G$, the LS code based STS scheme may exhibit a worse performance than the traditional STS scheme of [25].

Number of Subcarrier U	**Bit Error Ratio** P_b	**Width of the IFW** μs
$U = 1$	8.0×10^{-2}	$0.77\mu s$
$U = 4$	2.0×10^{-3}	$3.09\mu s$
$U = 8$	6.0×10^{-5}	$6.18\mu s$
$U = 16$	2.0×10^{-3}	$12.36\mu s$

Table 3.3: BER performance in conjunction with different number of subcarriers for LAS CDMA when we had $E_b/N_0 = 20$dB and $K = 32$ users were supported. The channel's delay spread was $\tau_{ch} = 3\mu s$ and the maximum delay difference was $\tau_{max} = 5\mu s$

Finally, in Table 3.3 we summarized the width of the IFW and the achievable BER performance of LAS CDMA in conjunction with different number of subcarriers U, when we considered a system having a chip rate of 3.84Mchips/s. The channel's delay spread was $\tau_{ch} = 3\mu$ and the maximum delay difference of users was $\tau_{max} = 5\mu s$.

CHAPTER 4

Iterative Multiuser Detection for DS-CDMA

4.1 Introduction

Following the philosophy of iterative decoding of turbo codes [116] in recent years, iterative multiuser detection captured growing interest in the wireless communications community. In reference [60] an iterative decoding scheme designed for synchronous Code Division Multiple Access (CDMA) systems has been characterised. The algorithm proposed in [60] has a computational complexity proportional to the order of $O(2^{Kv})$, where K is the number of users supported, and v is the channel codec's memory length. This iterative multiuser detector exhibits near single-user performance. However, its excessive complexity renders its real-time implementations unrealistic, except when the number of users supported is low.

In reference [79] [80] several schemes have been proposed for reducing the implementational complexity imposed. In the set of these schemes, Interference Cancellation (IC) based iterative multiuser detection exhibits the lowest complexity, rendering the complexity proportional to the order of $O(K \cdot 2^v)$.

In reference [117] an IC based iterative Multiuser Detector (MUD) was developed, which exhibits a further reduced implementational complexity. The iterative receiver advocated in this chapter obeys a similar structure to that proposed in [117], except for employing different channel coding schemes and modulation schemes. In [79] [80] the proposed iterative multiuser detectors invoked soft estimation of the real-valued BPSK modulated signal. In our approach, we develop a method which is capable of generating soft estimates of the complex transmitted symbol by exploiting the channel coded

bits' A Posteriori Probabilities (APP). We also propose a novel symbol probability based iterative multiuser detection assisted receiver for employment in a Trellis Coded Modulation (TCM) and Turbo Trellis Coded Modulation (TTCM) aided system. Symbol-based *Maximum aposteriori* (MAP) algorithms [78] are employed for both the TCM decoder and the TTCM decoder, which are capable of feeding back the symbol probabilities to the soft-symbol estimation and interference cancellation stages. More specifically, this algorithm relies on utilizing the probabilities of the channel-coded information symbols for symbol estimation, rather than on employing the individual APP of the coded bits.

This chapter is organized as follows: In Section 4.2 we introduce the basic philosophy of the TCM and TTCM schemes as well as that of the symbol-based MAP algorithm. In Section 4.3 we continue our discourse by describing the IC based iterative multiuser detector scheme. Section 4.4 discusses the performance of the convolutional coding assisted iterative multiuser detector, while Section 4.5 characterises the performance of the TCM based iterative multiuser detector. These evaluations are followed in Section 4.6 by the performance study of the TTCM aided iterative multiuser detector. Similar studies are conducted in Section 4.7 and 4.8 in the context of turbo decoded and LDPC decoded systems. Finally, in Section 4.9 we offer our conclusions and outline the topics of our future research.

4.2 Coded Modulation Schemes

TCM [118] was originally proposed for communicating over Gaussian channels and it was later further developed for applications in mobile communications [119]. Turbo Trellis Coded Modulation (TTCM) [120] is a more recent joint coding and modulation scheme that has a structure similar to that of the family of power-efficient binary turbo codes [116], but employs TCM schemes as component codes. Both TCM and TTCM use symbol–based interleavers and Set–Partitioning (SP) based signal labelling [78].

4.2.1 TCM Assisted Turbo Decoder

The TCM aided turbo MUD operates similarly to the corresponding module of a trained convolutional coding based turbo equaliser [77]. The sole difference is the replacement of the convolutional decoder by a TCM decoder. Hence, a bit–to–symbol converter is placed before the TCM decoder for converting the Log Likelihood Ratio (LLR) values to symbol probabilities, which are necessary for facilitating TCM decoding. Similarly, a symbol–to–bit converter is employed at the output of the TCM decoder for feeding the users' bits to the MUD's input. The calculation of the symbol probabilities from the probabilities of the input bits is based on the following relationship [78]:

$$\begin{aligned} Prob(Symbol = A_i) &= \prod_j Prob(Bit_j(Symbol) = Bit_j(A_i)), \\ & i = 0, \cdots, Q, \;\; j = 0, \cdots, K, \end{aligned} \tag{4.1}$$

where Q is the number of symbols in the modulation constellation used, K is the number of bits per symbol, A_i represents the symbols of the modem's constellation and the function $Bit_j(A_i)$ returns the value of the j–th bit of symbol A_i. The assumption implicitly stipulated here is that the bits of a TCM symbol are independent of each other. This, however, is not a valid assumption, since channel coding has deliberately imposed a certain amount of correlation or interdependence on the bits, in order to be able to exploit this redundancy for correcting transmission errors. Hence the symbol probability calculation is somewhat inaccurate. Fortunately the effects of this inaccuracy are gradually mitigated by the iterative detection process. Similarly to the bit–to–symbol conversion of Equation 4.1, the symbol–to–bit conversion procedure is based on the following relationship:

$$Prob(Bit_j = Bit) = \sum_i Prob[Symbol_i; Bit_j(Symbol_i) = Bit] \quad i = 0, \cdots, Q, \;\; j = 0, \cdots, K. \tag{4.2}$$

This formula is accurate in the sense that it does not require any assumptions concerning the correlation of the input symbols.

The LLR [78] is defined as the logarithm of the ratio of the two possible bit probabilities [78], i.e. as:

$$LLR(Bit) = ln\left[\frac{Prob(Bit = 1)}{Prob(Bit = 0)}\right]. \tag{4.3}$$

Given the LLR value, namely $LLR(Bit)$ of a binary bit, we can calculate the probability of $Bit = +1$ or $Bit = -1$ as follows. Remembering that $Prob(Bit = -1) = 1 - Prob(Bit = +1)$, and taking the exponent of both sides in Equation 4.3 we can write:

$$e^{LLR(Bit)} = \frac{Prob(Bit = +1)}{1 - Prob(Bit = +1)}. \tag{4.4}$$

Hence we have:

$$Prob(Bit = 1) = \frac{e^{LLR(Bit)}}{1 + e^{LLR(Bit)}}, \tag{4.5}$$

and

$$Prob(Bit = -1) = \frac{1}{1 + e^{LLR(Bit)}}. \tag{4.6}$$

Then, assuming that the bits of a symbol are independent of each other, the probability of a *symbol*, which is represented by the bits $Bit^1, \ldots, Bit^n$, can be calculated as in Equation 4.1, where we have $symbol \in (0, \ldots, 2^n - 1)$ for the 2^n-ary modulation scheme used. The probability of the trellis transition from states s' to state s, commonly defined as $\gamma(s', s)$, in the context of the non–binary MAP decoder [116], can be calculated as:

$$\gamma(s', s) = \eta_{Symbol} \cdot \prod_{i=1}^{i=n} Prob(Bit^i), \tag{4.7}$$

where $Symbol$ is the trellis transition branch label associated with state s' to state s, and η_{Symbol} is the "a priori" information of the $Symbol$. Then the α and β values of the

forward and backward recursion involved in the MAP algorithm can be obtained from:

$$\alpha_k(s) = \sum_{s'} \gamma_k(s', s) \cdot \alpha_{k-1}(s') \tag{4.8}$$

$$\beta_{k-1}(s') = \sum_{s} \gamma_k(s', s) \cdot \beta_k(s). \tag{4.9}$$

The number of transitions emerging from a specific trellis state is equal to 2^k, where k is the number of information bits per n–bit modulation symbol. The coding rate used is $R = \frac{k}{n}$, where $k = n-1$. Therefore the log–MAP decoder used is non–binary, when $k > 1$. By contrast, if $k = 1$, then the number of transitions emerging from a trellis state is equal to $2^1 = 2$, i.e. a binary MAP decoder is used. The a–posteriori probability (APP) of the information symbol u_t, $u_t \in (0, \ldots, 2^k - 1)$ at time instant t can be computed as [116]:

$$APP(u_t) = \sum_{s' \to s, u_t} \alpha_{k-1}(s') \cdot \gamma_k(s', s) \cdot \beta_k(s). \tag{4.10}$$

The final decoded information symbol at instant t is the hard decision based symbol generated from these APP values. However, we have to feed back the LLR values of all the n number of coded bits of a symbol to the IC scheme after improving their reliability by the channel decoder, rather than just the LLRs of the k information bits. The APP of the coded symbol x_t, $x_t \in (0, \ldots, 2^n - 1)$ at time instant t can be computed from:

$$APP(x_t) = \sum_{s' \to s, x_t} \alpha_{k-1}(s') \cdot \gamma_k(s', s) \cdot \beta_k(s), \tag{4.11}$$

while Equation (4.10) formulated the APP of the original encoded information symbol. The probability of bit i assuming a value of binary 1 in a coded symbol x is calculated from:

$$Prob(Bit^i = 1) = \sum_{x=0}^{x=2^n-1} APP(x^i = 1), \tag{4.12}$$

where x^i denotes the binary value at bit position i of the symbol x, $x^i \in (0, 1)$ and in verbal terms the probability of $Bit^i = 1$ is given by the sum of the probabilities of all symbols from the set of $2^n - 1$ number of phasors, which host a binary 1 at bit position i. A similar procedure is invoked for determining $Prob(Bit^i = 0)$ and finally the LLR of the bits can be computed from Equation 4.3.

4.2.2 TTCM Assisted Turbo Decoder

An extension of the turbo–PSP equaliser employing Turbo Trellis–Coded Modulation (TTCM) has also been considered. TTCM was proposed in [120], where the information bits are transmitted only once, while the parity bits are provided alternatively by the two constituent TCM encoders [78]. The schematic of the TTCM encoder [116] [78] is shown in Figure 4.1, which comprises two identical TCM encoders linked by the symbol interleaver Π [116].

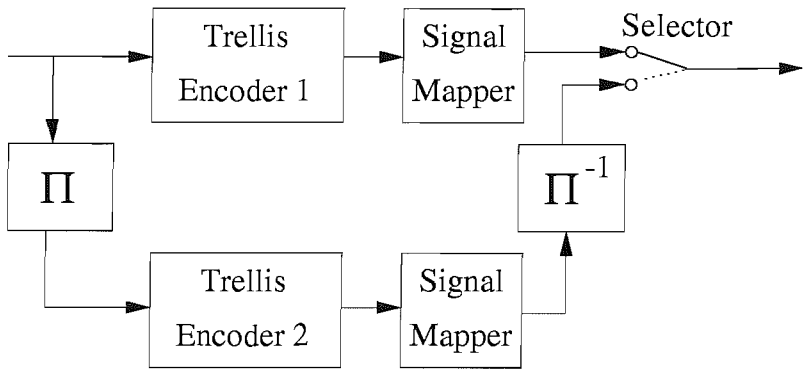

Figure 4.1: Turbo trellis-coded modulation encoder.

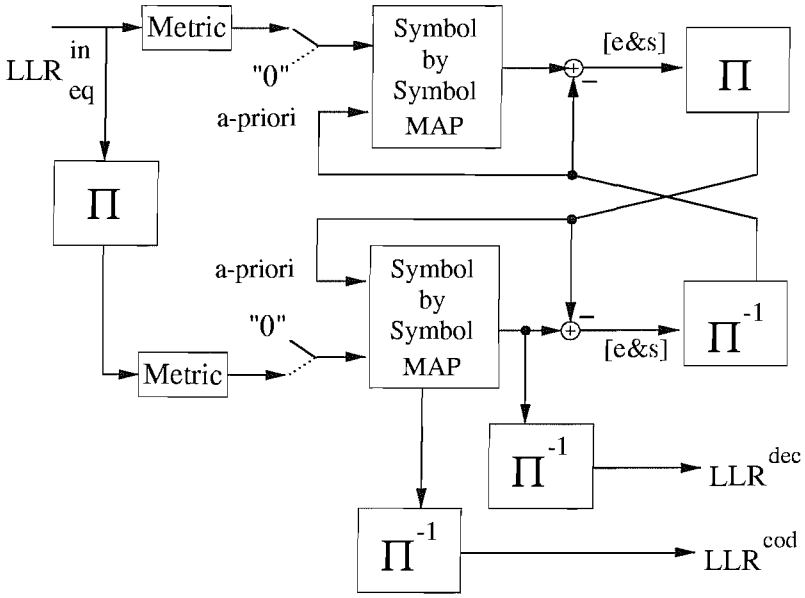

Figure 4.2: TTCM decoder schematic.

The TTCM decoder structure shown in Figure 4.2 is similar to that of binary turbo codes, except for the difference in the nature of the information passed from one decoder to the other. Each decoder alternately processes its corresponding encoder's channel impaired output symbol, and then the other encoder's channel impaired output symbol. The information bits, i.e. the systematic bits, are constituted by the corresponding systematic TCM encoder's output bits received over the channel in both cases. The systematic information and the parity information are transmitted together in the same symbol. Hence, the systematic information component cannot be separated from the extrinsic information, since the noise that affects the parity component of a TTCM symbol also affects the systematic information component. The output of each symbol-based MAP decoder of Figure 4.2 can be split into two components [116]:

1. the *a priori* component, and
2. the amalgamated i.e. inseparable (extrinsic and systematic) $[e\&s]$ component.

Each decoder of Figure 4.2 has to pass only the $[e\&s]$ component to the other decoder, which is written in parentheses in order to emphasize the inseparability of the extrinsic and systematic components. The reason the a-priori information component is subtracted from the output of the symbol-based MAP decoder of Figure 4.2 is that this information

component was generated by the other constituent decoder and hence it must not be fed back to it. Otherwise the probability estimates of the two decoders become dependent on each other, and this lack of independent estimates prevents them from enhancing the decoder's decision reliability. The LLR_{eq}^{in} output of the equaliser is forwarded to the "metric" calculation block of Figure 4.2, in order to generate a set of 2^n number of symbol reliabilities. The selectors at the input of the symbol-by-symbol MAP decoder of Figure 4.2 select the current symbol's reliabilities from the "metric" calculation block, if the current received symbol corresponds to the specific component decoder concerned. Otherwise depuncturing will be applied, where the reliabilities of the symbols are set to "0" corresponding to the absence of a–priori information. The "metric" calculation block provides the decoder with the parity and systematic [$p\&s$] information, and the second input to the symbol by symbol MAP decoder of Figure 4.2 is the *a priori* information acquired from the other component decoder. The MAP decoder then provides the *a posteriori* information constituted by the (*a priori* + [$e\&s$]) components as the output. Then the *a priori* information is subtracted from the *a posteriori* information, again, for the sake of ensuring that information is not used more than once in the other decoder. The resultant [$e\&s$] information is appropriately interleaved (or de–interleaved) in order to create the *a priori* input of the other constituent decoder. This decoding process will continue iteratively, in order to generate an improved version of the set of symbol reliabilities for the other component decoder. One iteration comprises the decoding of the received symbols by both of the component decoders. Then, the *a posteriori* information of the lower component decoder of Figure 4.2 will be de–interleaved, in order to extract $(n-1)$ decoded information bits per symbol. On the other hand, the *a posteriori* information of the n coded bits is de–interleaved, in order to convert the LLR^{cod} to symbol probabilities with the aid of equation 4.2 and 4.4. Finally, the symbol probabilities will be fed back to the input of the MUD as shown in Figure 4.4.

4.3 The Parallel Interference Cancellation Based Iterative Multiuser Detection Receiver

4.3.1 The Concept of Interference Cancellation

Interference Cancellation (IC) techniques may be divided into two categories, namely successive interference cancellation (SIC) [121] and parallel interference cancellation (PIC) [122]. Both techniques rely on the philosophy that if all users' decision bits have been detected without decision errors, then the multiple access interference (MAI) can be readily recreated by remodulating the detected bits and subtracting them from the received MAI-contaminated signal, provided that we have perfect knowledge of the channel parameters. In comparison to the family of joint detectors (JD) [22], the interference cancellation algorithms exhibit a lower complexity, which increases linearly as a function of the number of users. In this chapter we focus our attention on a powerful PIC scheme. Interference cancellation techniques typically employ "hard" decisions concerning the transmitted bits or symbols. However, hard decision techniques are prone to error propagation effects.

Hence, in order to improve the achievable performance, we rely on the soft estimation of the transmitted bits or symbols during the process of interference cancellation.

Fig 4.3 shows the structure of a parallel interference cancellation scheme, where the soft estimates of the transmitted symbols, namely $\hat{b}_k$, which are output by the channel decoder, are utilized for reconstructing the transmitted signal. Then, for the sake of decontaminating the received signal of each user, the reconstructed signals of all the other users are subtracted from the composite multiuser signal, and the resultant signal is processed by a matched filer or RAKE receiver as seen in Figure 4.3, then generate the signal $\hat{y_k}$ for channel decoding procedure. These steps of modulated signal reconstruction, interference cancellation and desired signal re-estimation stage are repeated as many times, as the number of affordable iterations employed in the multiuser detector.

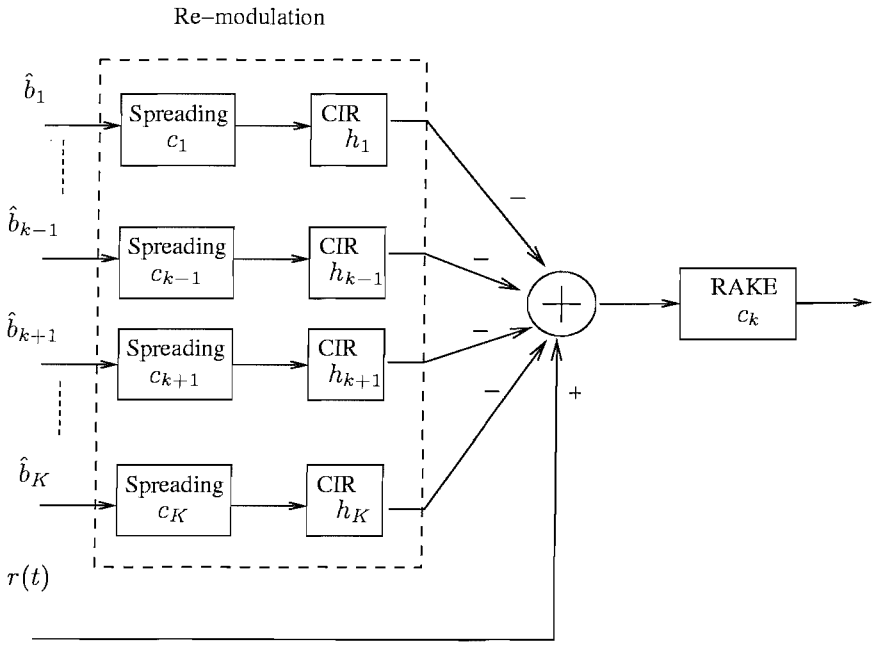

Figure 4.3: Schematic of a single PIC stage.

4.3.2 Estimation of the M-ary Coded Symbol

Let us assume that an M-QAM modulation scheme [30] is employed. Then the M-ary TCM or TTCM based symbols [78] can be written as: $s_i = u_i + jv_i$, $i = 1, ...M$. For the TTCM and TCM schemes the kth user's channel decoder will output all the M-ary soft symbol probabilities $\mathbf{Pr}\{b_k = s_i\}$, $k = 1, ..., K$, $i = 1, ..., M$ of the K users supported. Hence, the estimated symbol $\hat{b}_k$ may be obtained as:

$$\hat{b}_k = \sum_{i=1}^{M} \mathbf{Pr}\{b_k = s_i\} \cdot s_i, \tag{4.13}$$

where s_i is a TCM or TTCM symbol. By contrast, if a convolutional code is employed in this system, the kth user's channel decoder will output the soft APP of the channel coded bits. Hence a transformation between the APP of the channel coded bits and

the symbol probabilities is needed. Firstly, we may generate the symbol probabilities $Prob(symbol)$ according to Equation 4.1, again, bearing in mind that this equation assumes the independence of the bits of a symbol, and this inaccuracy is compensated by the iterative detection process. Once we acquired the symbol probabilities, we can estimate the symbols according to Equation 4.13.

4.3.3 Iterative Multiuser Detection

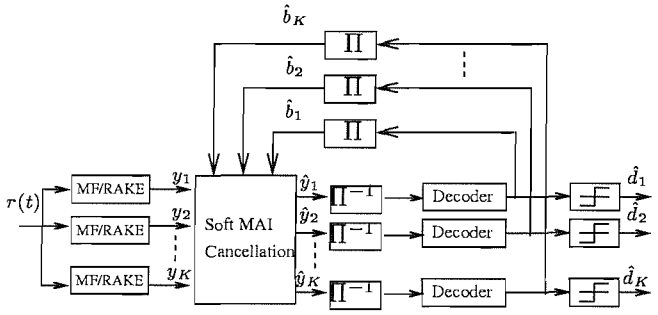

Figure 4.4: Schematic of the iterative multiuser detector

Fig 4.4 shows the schematic of the PIC assisted iterative multiuser detector, where the Matched Filter's (MF) output is given by: $\mathbf{y} = [y_1, ..., y_K]^T$. The vector $\hat{\mathbf{b}}$ contains the estimated symbols of all the K users, which are represented by the symbol probabilities or by the soft APP of the channel coded bits output by the channel decoder, which can be represented for the K users as: $\hat{\mathbf{b}} = [\hat{b}_1, ..., \hat{b}_K]^T$. Once we acquired a soft-estimate of a symbol, soft MAI cancellation is performed. The soft output signal vector $\hat{\mathbf{y}}$ generated by the interference cancellation precess of Figure 4.4 is expressed as: $\hat{\mathbf{y}} = [\hat{y}_1, ..., \hat{y}_K]^T$. The Π and Π^{-1} denote the channel interleaver and deinterleaver, respectively.

Iterative MUD for Synchronous DS-CDMA

Let us now consider a special case, when the synchronous DS-CDMA system communicates over a non-dispersive Additive White Gaussian Noise (AWGN) channel. According to [22], we can express the received signal vector $\mathbf{y} = [y_1, ..., y_K]^T$ containing the output of the MF related to each of the K users seen in Figure 4.3 as:

$$\mathbf{y} = \mathbf{RAb} + \mathbf{n}, \tag{4.14}$$

where $\mathbf{R}$ is the normalized $K \times K$ dimensional cross-correlation matrix of the user's spreading code. The element in the ith row and jth column of the matrix is denoted as ρ_{ij}, and we have $\rho_{ij} = \rho_{ji}$. Furthermore, the vector $\mathbf{b}$ containing each transmitted symbol of the K users is expressed as $\mathbf{b} = [b_1, ..., b_K]^T$, and $\mathbf{n} = [n_1, ..., n_K]^T$ is the $K \times 1$ dimensional vector of noise samples at the output of the MF, while $\mathbf{A} = \text{diag}\{A_1, ..., A_K\}$ is a diagonal matrix, which contains the amplitude of each user's signal.

Let us define $\hat{\mathbf{b}}_k$ as a vector which equals $\hat{\mathbf{b}}$ except that its kth element is zero. Then the signal vector $\hat{\mathbf{y}}_k$ containing the desired signal of user k in its kth position, which was

decontaminated from the effects of MAI, can be written as:

$$\hat{\mathbf{y}}_k = \mathbf{R} \cdot \mathbf{A} \cdot (\mathbf{b} - \hat{\mathbf{b}}_k) + \mathbf{n}, \quad k = 1, ..., K. \tag{4.15}$$

Explicitly, once a sufficiently reliable soft estimate $\hat{\mathbf{b}}$ becomes available, the signal vector components hosted by $\hat{\mathbf{y}}$ become free from MAI, which are now contaminated only by the channel noise.

Iterative MUD for Asynchronous DS-CDMA

According to [22], in an asynchronous DS-CDMA scenario the K-dimensional received signal vector $\mathbf{y}$ containing the signal components of the K users can also be expressed as:

$$\mathbf{y}[i] = \mathbf{R}^T[1] \cdot \mathbf{A} \cdot \mathbf{b}[i+1] + \mathbf{R}[0] \cdot \mathbf{A} \cdot \mathbf{b}[i] + \mathbf{R}[1] \cdot \mathbf{A} \cdot \mathbf{b}[i-1] + \mathbf{n}[i], \tag{4.16}$$

where i is the time instant index and the zero-mean Gaussian process $\mathbf{n}[i]$ has the cross-correlation matrix of [22]:

$$E[\mathbf{n}[i]\mathbf{n}^T[j]] = \begin{cases} \sigma^2\mathbf{R}^T[1], & \text{if } j = i+1; \\ \sigma^2\mathbf{R}[0], & \text{if } j = i; \\ \sigma^2\mathbf{R}[1], & \text{if } j = i-1; \\ \mathbf{0}, & otherwise. \end{cases} \tag{4.17}$$

Furthermore, the matrix $\mathbf{R}[1]$ and $\mathbf{R}[0]$ are defined by:

$$\mathbf{R}_{jk}[0] = \begin{cases} 1, & \text{if j = k;} \\ \rho_{jk}, & \text{if } j < k; \\ \rho_{kj}, & \text{if } j > k, \end{cases} \tag{4.18}$$

$$\mathbf{R}_{jk}[1] = \begin{cases} 0, & \text{if } j \geq k; \\ \rho_{kj}, & \text{if } j < k. \end{cases} \tag{4.19}$$

Let us define the vectors $\hat{\mathbf{b}}_k[i+1], \hat{\mathbf{b}}_k[i], \hat{\mathbf{b}}_k[i-1]$ $k = 1, \ldots, K$ which contain the estimates of the transmitted signal at the time index of $i+1, i$ and $i-1$, where the component corresponding to user k is zero. Therefore, after the soft MAI cancellation process obeying Equation 4.15 is invoked, the signal vector $\hat{\mathbf{y}}_k[i]$, $k = 1, \ldots, K$ containing in its kth position the signal of the kth user, which was decontaminated from the MAI can be represented as:

$$\begin{aligned} \hat{\mathbf{y}}_k[i] = \quad & \mathbf{R}^T[1] \cdot \mathbf{A} \cdot (\mathbf{b}[i+1] - \hat{\mathbf{b}}_k[i+1]) + \mathbf{R}[0] \cdot \mathbf{A} \cdot (\mathbf{b}[i] - \hat{\mathbf{b}}_k[i]) \\ & + \mathbf{R}[1] \cdot \mathbf{A} \cdot (\mathbf{b}[i-1] - \hat{\mathbf{b}}_k[i-1]) + \mathbf{n}[i]. \end{aligned} \tag{4.20}$$

According to Equation 4.20, we can observe that the signal vector $\hat{\mathbf{y}}_k[i]$ contains components, which are free from multiple access interference, provided that the estimated symbols $\hat{\mathbf{b}}_k[i+1], \hat{\mathbf{b}}_k[i], \hat{\mathbf{b}}_k[i-1]$ are reliable. In comparison to the synchronous scenario

of Equation 4.15, we can see that this iterative multiuser receiver operating in an asynchronous environment is more prone to error propagation, because its reliable operation requires three consecutive correctly estimated K-dimensional symbol vectors. Even if only one of these three vectors contains errors, this will lead to the incorrectly cancelled interference and to inevitable error propagation between the various user decisions. Hence, as expected, it is more difficult to ensure that the PIC-based iterative multiuser receiver converges in an asynchronous scenario, than in a synchronous system.

When communicating over a dispersive multipath channel, this PIC-assisted multiuser receiver maintains the same structure and requires the same operations as in a non-dispersive channel, except for the remodulation process and for the soft MAI cancellation stage, since all the K users have different Channel Impulsive Responses (CIR), as seen in Figure 4.3

Having described the operation of the PIC assisted multiuser detector, let us now consider its performance under the condition that all these coded schemes had a similar complexity. More explicitly, when it was possible, we fixed the total number trellis states of all the trellis-based decoders to be 64. Hence we chose the non-iterative coded schemes' (CC, TCM) memory length to be $m = 6$, yielding a total of 64 trellis states. By contrast, the iterative TC and TTCM schemes had a memory length of $m = 3$ and the number of inner TC and TTCM iterations was set to 2. At the final outer iteration stages the number of inner TC and TTCM iterations was set to 4 and since there are two TTCM decoders, the total number of trellis states was again 64. Finally, the corresponding number of inner iterations for the LDPC schemes was set to 8 and 16 for the intermediate and final outer iterations, respectively, which was deemed to result in a similar complexity. All these parameters are listed in the Table 4.1. In our system, a random channel interleaver length of $L = 1920$ bits was adopted and an $N = 15$-chip m-sequence spreading code was employed. Since the PIC exhibited a slower converge in the asynchronous scenario than in the synchronous environment, especially when the number of users supported exceeded a certain threshold, the PIC became incapable of converging and therefore exhibited a significant performance degradation. Hence in the synchronous AWGN environment $K = 15$ users were supported, while in the asynchronous AWGN channel $K = 7$ users were accommodated. Finally, in the 2-path equal-weight Rayleigh fading channel, $K = 10$ users were supported.

Coded Scheme	memory length m	inner iterations
CC	6	
TCM	6	
TTCM	3	2/4
TC	3	2/4
LDPC		8/16

Table 4.1: The basic simulation parameters for the employed coded schemes of the iterative MUD.

4.4 Performance of the PIC Based Iterative Multiuser Detector Assisted by Convolutional Decoding

We adopted the LOG-MAP technique [123] [78] as the convolutional channel decoding algorithms, which required a slight modification. Specifically, the procedure outlined in [123] only provides the *a posteriori* probabilities of the information bits, but not those of the parity bits. However, in turbo detection algorithms all the bits have to be fed back to the detector's input and hence we additionally need the *a posteriori* probabilities of the parity bits for both soft estimation and for interference cancellation. These can be obtained in the same manner as highlighted in [60] [117]. Apart from this modification, the Log-MAP algorithm invoked here is the same as that described in [78] [123].

In this section, we study the performance of a convolutional coded DS/CDMA system supporting $K = 15$ users with the aid of an m-sequence based spreading code having $N = 15$ chips and QPSK modulation. The low-complexity half rate convolutional code employed in this system has a low memory length of $m = 3$, which is sufficient for employment in an iterative receiver. We investigate the achievable performance for transmission over two types of channels, an asynchronous two-path uncorrelated Rayleigh fading environment and a synchronous non-dispersive AWGN environment. Figure 4.5 shows the achievable BER performance, when communicating over a synchronous non-dispersive AWGN environment. From Figures 4.5, 4.6 we observe that the receiver assisted by the low-complexity convolutional decoder is capable of approaching the optimum single-user bound after two iterations, when communicating over the synchronous and asynchronous non-dispersive AWGN channel. However, Figure 4.7 exhibited that the proposed iterative multiuser detector may require four iteration to approach the near-single user performance, when when communicating over a two-path uncorrelated Rayleigh fading channel having an equal-weight, chip-spaced CIR.

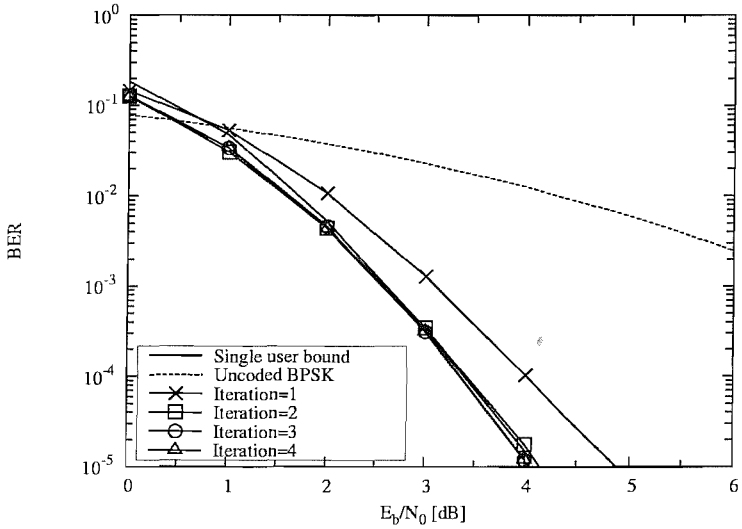

Figure 4.5: The PIC based iterative multiuser detector's **BER** versus E_b/N_0 performance, when communicating over a **synchronous non-dispersive AWGN** channel, while supporting $K = 15$ users, each encoded with the aid of a $\frac{1}{2}$ rate, $m = 6$ convolutional code. **QPSK** modulation is employed.

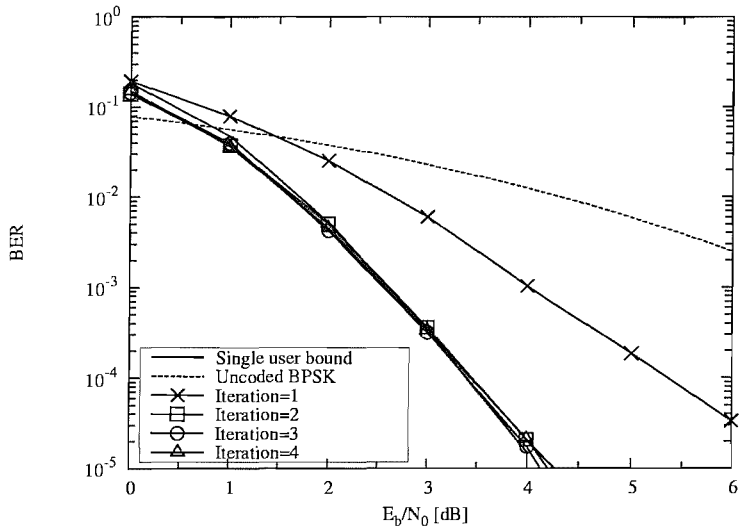

Figure 4.6: The PIC based iterative multiuser detector's **BER** versus E_b/N_0 performance, when communicating over an **asynchronous non-dispersive AWGN** channel, while supporting $K = 7$ users, each encoded with the aid of a $\frac{1}{2}$ rate, $m = 6$ convolutional code. **QPSK** modulation is employed.

4.5 Performance of the PIC Based Iterative Multiuser Detector Assisted by TCM Decoding

In this section we will investigate the performance of the TCM based iterative multiuser detector in the context of **QPSK**, **8PSK** and **16QAM** schemes. The corresponding schemes have a coding rate of $R = \frac{1}{2}, \frac{2}{3}$ and $\frac{3}{4}$, and a corresponding effective throughput of 1, 2 and 3 Bits Per Symbol (BPS). The system employs m-sequences as spreading codes, each having a length of $N = 15$ chips. When a $\frac{1}{2}$ rate **QPSK** based TCM scheme is invoked as seen in Figures 4.8, 4.9 and 4.10, we may observe that the receiver is capable of achieving the single-user bound after 2 iterations over a AWGN channel, while the receiver required 4 iterations to approach the promising performance when communicating over a two-path Rayleigh channels, as seen in Figure 4.10.

Similarly, from Figures 4.11 we observe that the receiver is also capable of approaching the single-user bound after two iterations, when communicating over a synchronous non-dispersive AWGN channel using the $\frac{2}{3}$ rate **8PSK TCM** scheme, while the receiver using **8PSK TCM** scheme required three iterations to approach the single-user performance when communicating over a asynchronous non-dispersive AWGN channel, as seen in Figures 4.12. Finally, from Figures 4.13 and 4.14, we may conclude that when a $\frac{3}{4}$ rate **16QAM TCM** scheme is invoked, the receiver required three iterations for approaching the single-user bound, when transmitting over a synchronous AWGN channel, while necessitating four iterations to achieve the single-user performance, when communicating over an asynchronous AWGN channel.

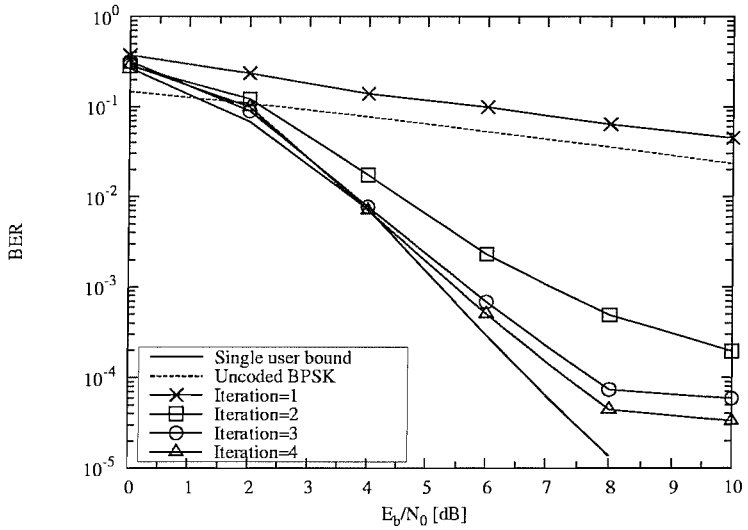

Figure 4.7: The PIC based iterative multiuser detector's **BER** versus E_b/N_0 performance, when communicating over an **asynchronous two-path uncorrelated Rayleigh** channel having a chip-spaced equal-weight CIR, while supporting $K = 10$ users, each encoded with the aid of a $\frac{1}{2}$ rate, $m = 6$ convolutional code. **QPSK** modulation is employed.

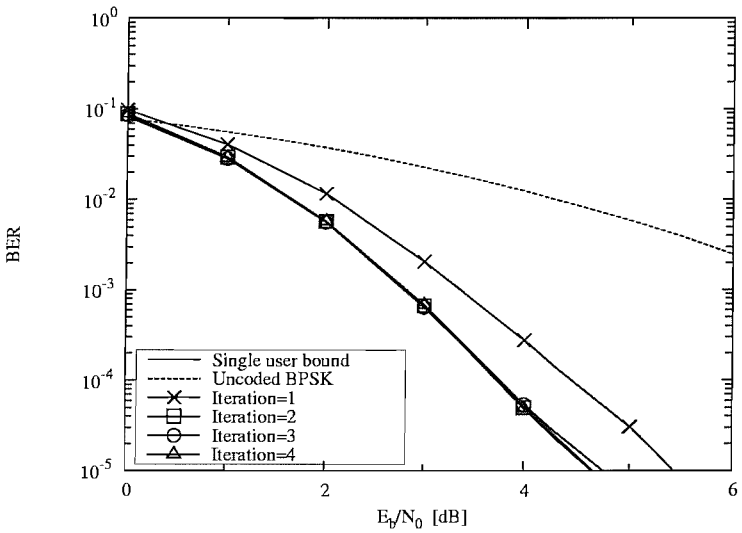

Figure 4.8: The PIC based iterative multiuser detector's **BER** versus E_b/N_0 performance, when communicating over a **synchronous non-dispersive AWGN** channel, while supporting $K = 15$ users. A $\frac{1}{2}$ rate **QPSK TCM** scheme having an effective throughput of 1 BPS was invoked.

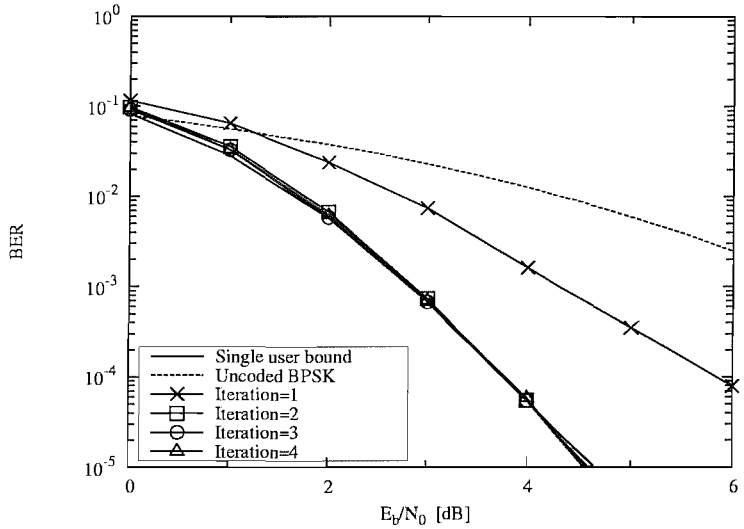

Figure 4.9: The PIC based iterative multiuser detector's **BER** versus E_b/N_0 performance, when communicating over an **asynchronous non-dispersive AWGN** channel, while supporting $K = 7$ users. A $\frac{1}{2}$ rate **QPSK TCM** scheme having an effective throughput of 1 BPS was invoked.

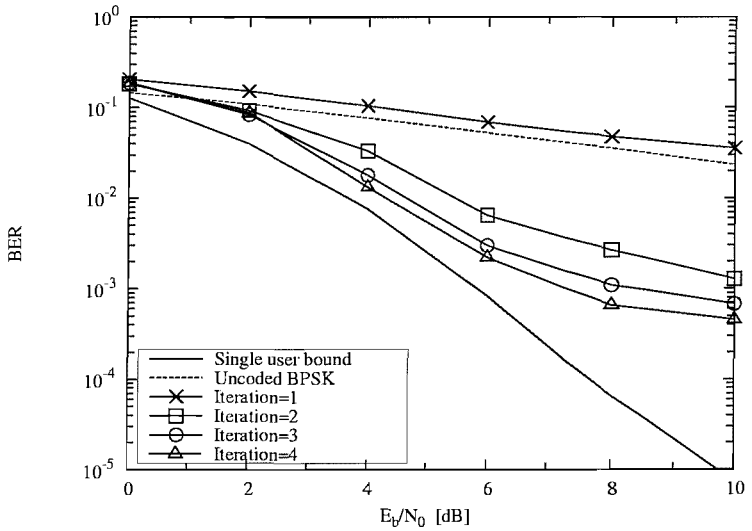

Figure 4.10: The PIC based iterative multiuser detector's **BER** versus E_b/N_0 performance, when communicating over an **asynchronous two-path equal-weight uncorrelated Rayleigh** channel, while supporting $K = 10$ users. A $\frac{1}{2}$ rate **QPSK TCM** scheme having an effective throughput of 1 BPS was invoked.

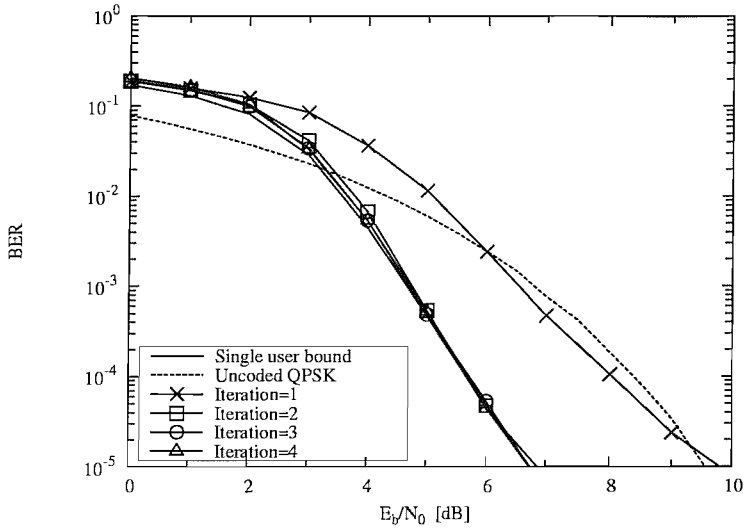

Figure 4.11: The PIC based iterative multiuser detector's **BER** versus E_b/N_0 performance, when communicating over a **synchronous non-dispersive AWGN** channel, while supporting $K = 7$ users. A $\frac{2}{3}$ rate **8PSK TCM** scheme having an effective throughput of 2 BPS was invoked.

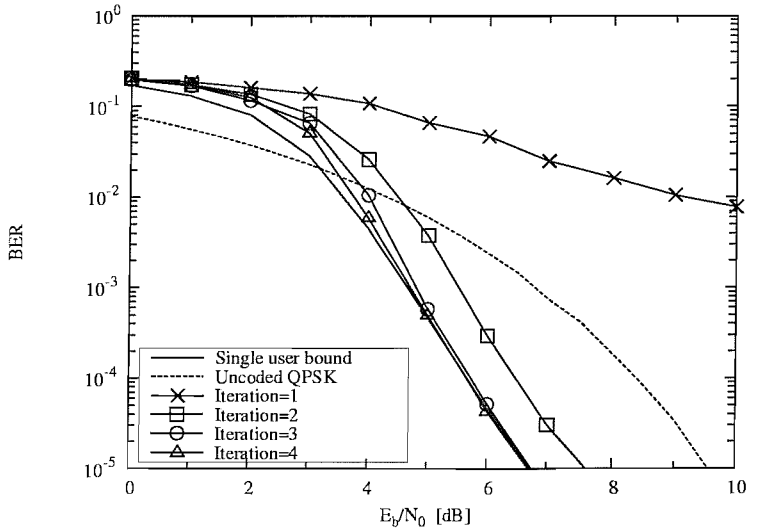

Figure 4.12: The PIC based iterative multiuser detector's **BER** versus E_b/N_0 performance, when communicating over an **asynchronous non-dispersive AWGN** channel, while supporting $K = 7$ users. A $\frac{2}{3}$ rate **8PSK TCM** scheme having an effective throughput of 2 BPS was invoked.

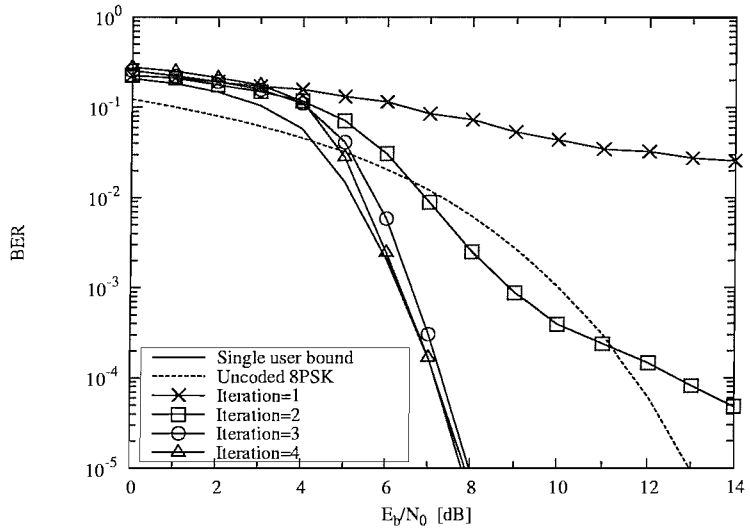

Figure 4.13: The PIC based iterative multiuser detector's **BER** versus E_b/N_0 performance, when communicating over a **synchronous non-dispersive AWGN** channel, while supporting $K = 7$ users. A $\frac{3}{4}$ rate **16QAM TCM** scheme having an effective throughput of 3 BPS was invoked.

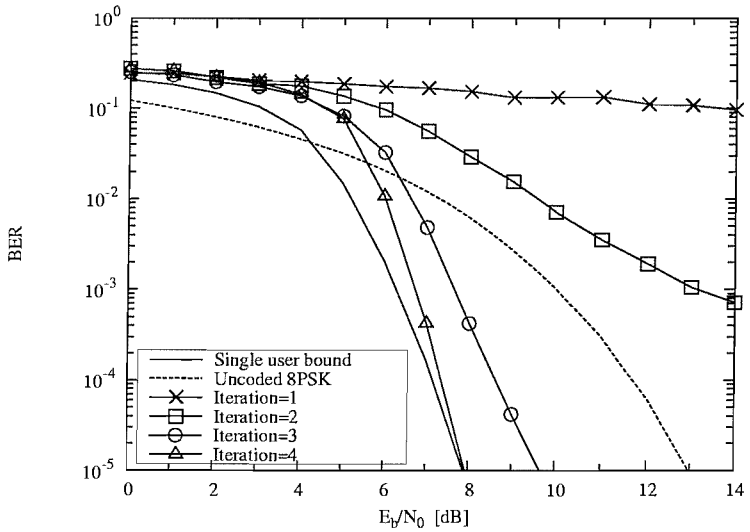

Figure 4.14: The PIC based iterative multiuser detector's **BER** versus E_b/N_0 performance, when communicating over an **asynchronous non-dispersive AWGN** channel, while supporting $K = 7$ users. A $\frac{3}{4}$ rate **16QAM TCM** scheme having an effective throughput of 3 BPS was invoked.

4.6 Performance of PIC Based Iterative Multiuser Detector Assisted by TTCM Decoding

Similarly, in this section we will investigate the achievable performance of the TTCM based iterative multiuser detector in the context of QPSK, 8PSK and 16QAM modulation schemes, which have a corresponding coding rate of $\mathbf{R} = \frac{1}{2}, \frac{2}{3}$ and $\frac{3}{4}$, as well as effective throughputs of 1, 2 and 3 BPS, respectively. When a $\frac{1}{2}$ rate **QPSK** based TTCM scheme is invoked as seen in Figures 4.15, 4.16 and 4.17, we may infer that the receiver is capable of achieving the single-user bound after 2 iterations over a AWGN channel as seen in Figures 4.15 and 4.16, while the receiver required 4 iterations to approach the promising performance when communicating over a two-path Rayleigh channels, as seen in Figure 4.17. Furthermore, when the $\frac{2}{3}$-rate **8PSK** based TTCM scheme is invoked as seen in Figures 4.18 and 4.19, we observe that the receiver is capable of approaching the single-user bound after two iterations as shown in Figure 4.18 when communicating over a synchronous non-dispersive AWGN channel, while it requires three iterations to attaining the single-user performance as shown in Figure 4.19, when communicating over an asynchronous non-dispersive AWGN channel. Finally, when the $\frac{3}{4}$-rate **16QAM** based TTCM scheme is employed as seen in Figures 4.20 and 4.21, we may conclude that the receiver also requires three iterations for maintaining a near single-user bound, when transmitted over a synchronous AWGN channel as shown in Figure 4.20, however, as shown in Figure 4.21 the number of required iterations becomes four for approaching a near single-user performance, when communicating over an asynchronous AWGN channel.

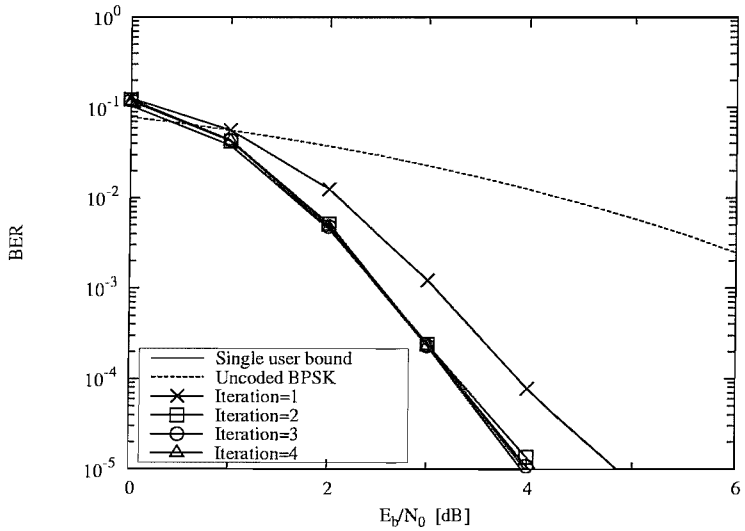

Figure 4.15: The PIC based iterative multiuser detector's **BER** versus E_b/N_0 performance, when communicating over a **synchronous non-dispersive AWGN** channel, while supporting $K = 15$ users. A $\frac{1}{2}$ rate **QPSK TTCM** scheme having an effective throughput of 1 BPS was invoked.

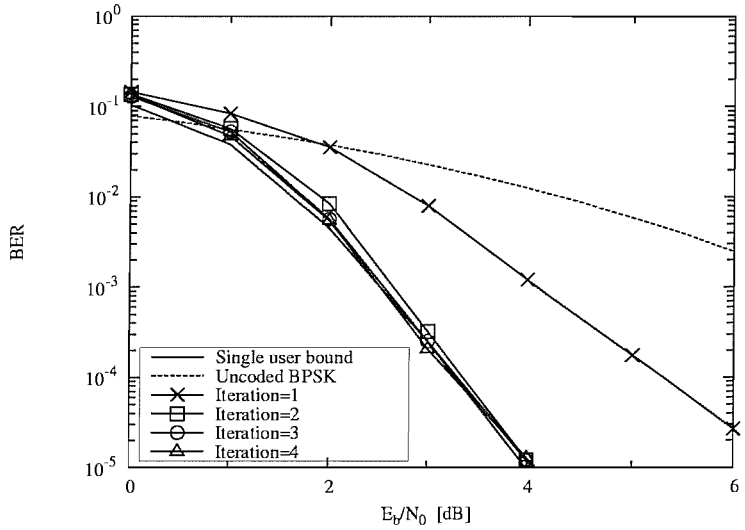

Figure 4.16: The PIC based iterative multiuser detector's **BER** versus E_b/N_0 performance, when communicating over an **asynchronous non-dispersive AWGN** channel, while supporting $K = 7$ users. A $\frac{1}{2}$ rate **QPSK TTCM** scheme having an effective throughput of 1 BPS was invoked.

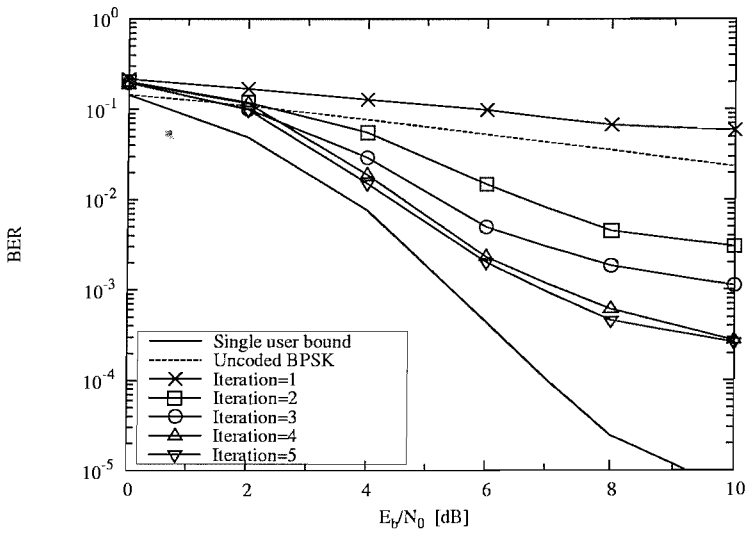

Figure 4.17: The PIC based iterative multiuser detector's **BER** versus E_b/N_0 performance, when communicating over an **asynchronous two-path equal-weight uncorrelated Rayleigh** channel, while supporting $K = 10$ users. A $\frac{1}{2}$ rate **QPSK TTCM** scheme having an effective throughput of 1 BPS was invoked.

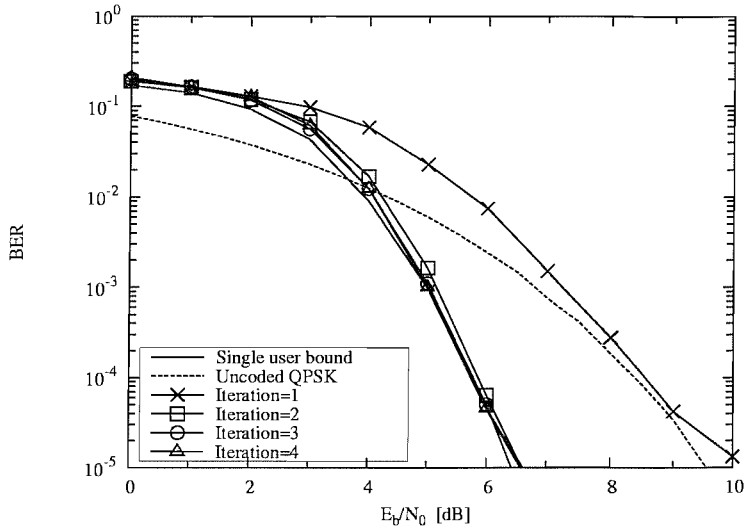

Figure 4.18: The PIC based iterative multiuser detector's **BER** versus E_b/N_0 performance, when communicating over a **synchronous non-dispersive AWGN** channel, while supporting $K = 7$ users. A $\frac{2}{3}$ rate **8PSK TTCM** scheme having an effective throughput of 2 BPS was invoked.

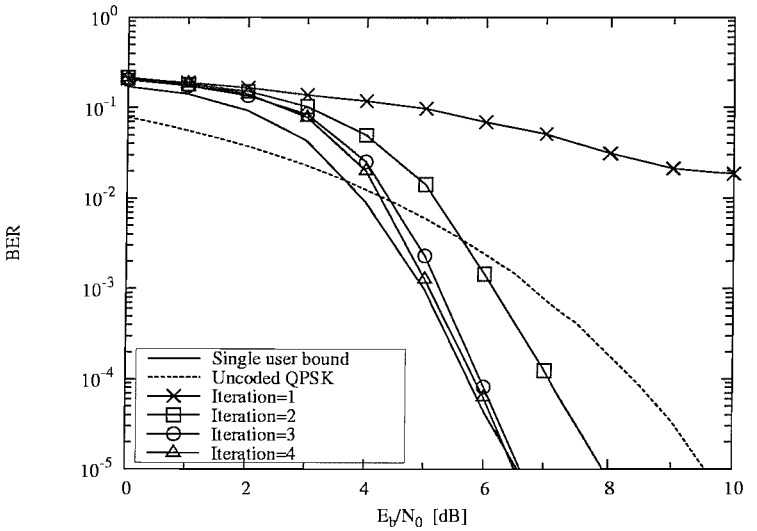

Figure 4.19: The PIC based iterative multiuser detector's **BER** versus E_b/N_0 performance, when communicating over an **asynchronous non-dispersive AWGN** channel, while supporting $K = 7$ users. A $\frac{2}{3}$ rate **8PSK TTCM** scheme having an effective throughput of 2 BPS was invoked.

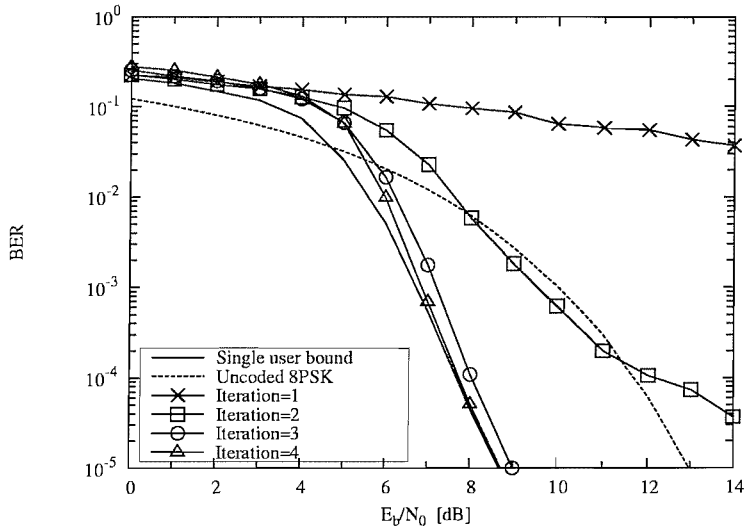

Figure 4.20: The PIC based iterative multiuser detector's **BER** versus E_b/N_0 performance, when communicating over a **synchronous non-dispersive AWGN** channel, while supporting $K = 7$ users. A $\frac{3}{4}$ rate **16QAM TTCM** scheme having an effective throughput of 3 BPS was invoked.

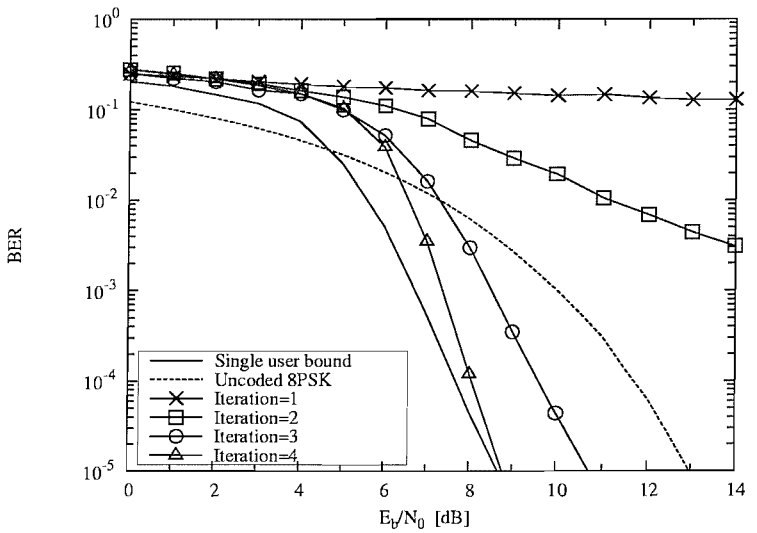

Figure 4.21: The PIC based iterative multiuser detector's **BER** versus E_b/N_0 performance, when communicating over an **asynchronous non-dispersive AWGN** channel, while supporting $K = 7$ users. A $\frac{3}{4}$ rate **16QAM TTCM** scheme having an effective throughput of 3 BPS was invoked.

4.7 Performance of the PIC Based Iterative Multiuser Detector Assisted by Turbo Decoding

Turbo coding [116] was proposed in 1993 by Berrou, Glavieux and Thitimajashima, who reported excellent coding gain results, approaching Shannon's channel capability predictions [124]. Specifically, the information sequence is encoded twice by the turbo encoder, with an interleaver between the two encoders invoked for ensuring that the two encoded data sequences become approximately statistically independent of each other. Often half-rate Recursive Systematic Convolutional (RSC) encoders are used, with each RSC encoder producing a systematically encoded output bit stream containing both the original information bits sequence, as well as a stream of parity bits. The two parity sequences can then be punctured before being transmitted along with the original information sequence to the decoder. The puncturing of the parity information allows a wide range of coding rates to be realised. In our system, half rate turbo codes are employed. The Log-MAP turbo decoder [78] was employed with the same slight modifications, which was invoked for the convolutional code in Section 4.4, for the sake of producing the APP also for the parity bits, rather than only for the information bits, as in case of conventional turbo decoding. The RSC code's memory length was $m = 3$ and a random channel interleaver length of 1920 bits was employed in our system. The turbo interleaver was a 10×10 dimensional block interleaver. Figure 4.22 shows the achievable BER performance, when communicating over a synchronous non-dispersive AWGN channel. From Figure 4.22 we can observe that the PIC based MUD exhibits an approximately 0.5dB E_b/N_0 loss in comparison to the single-user performance at a BER of 10^{-5}.

Figures 4.23 characterises the PIC based MUD's BER performance, when communicating over an asynchronous non-dispersive AWGN channel. From Figures 4.23 we can observe that the PIC based MUD suffers an approximately 0.9dB E_b/N_0 loss in comparison to the single-user performance, when communicating in an asynchronous AWGN environment.

Figures 4.24 characterises the PIC based MUD's BER performance, when communicating over an asynchronous two-path uncorrelated Rayleigh fading channel. From Figures 4.24 we can observe that the PIC based MUD requires more than 4 iterations to approach the near single-user performance when communicating over a dispersive fading channel.

4.8 Performance of the PIC Based Iterative Multiuser Detector Assisted by LDPC Decoding

In 1963, Gallager [125] [126] devised the family of Low Density Parity Check (LDPC) codes during his Ph.D study at MIT. In 1981, Tanner [127] suggested a recursive approach for the construction of LDPC codes. In 1995, MacKay and Neal [128] [129] have shown that LDPC codes are capable of achieving a comparable performance to that of the family of turbo codes. Hence in this section we employed the family of LDPC codes in our system.

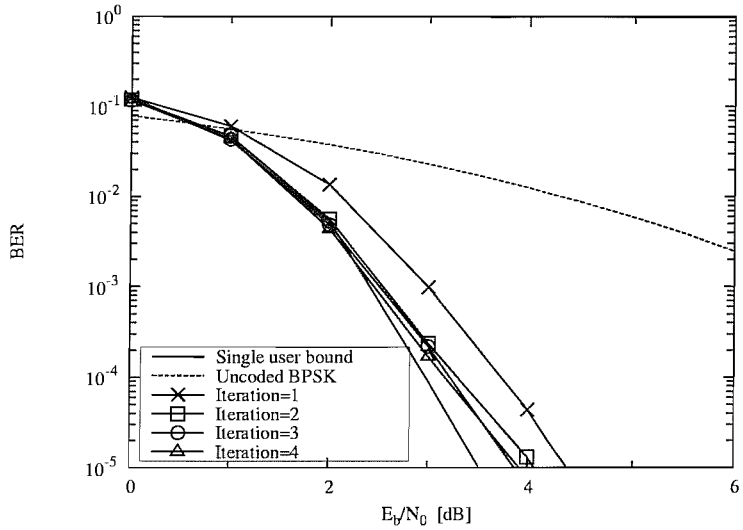

Figure 4.22: The PIC based iterative multiuser detector's **BER** performance, when communicating over a **synchronous non-dispersive AWGN** channel, while supporting $K = 15$ users, each encoded with the aid of a $\frac{1}{2}$-rate, $m = 3$ **turbo code. QPSK** modulation was employed.

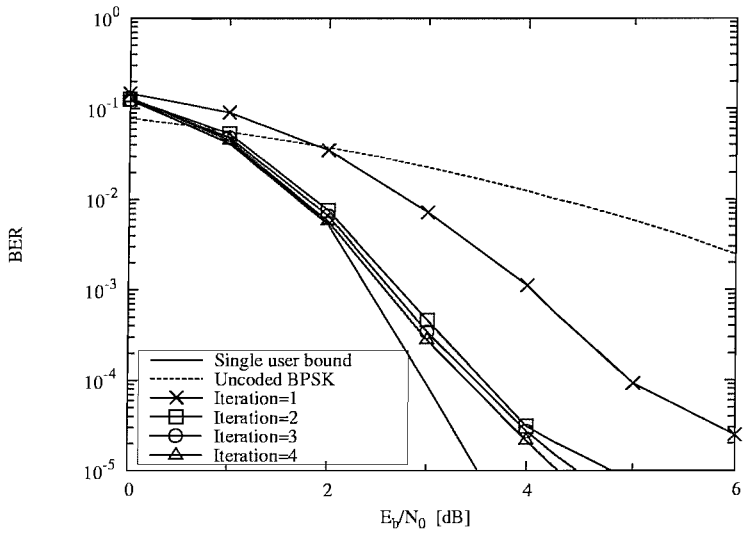

Figure 4.23: The PIC based iterative multiuser detector's **BER** performance, when communicating over an **asynchronous non-dispersive AWGN** channel, while supporting $K = 7$ users, each encoded with the aid of a $\frac{1}{2}$-rate, $m = 3$ **turbo code. QPSK** modulation was employed.

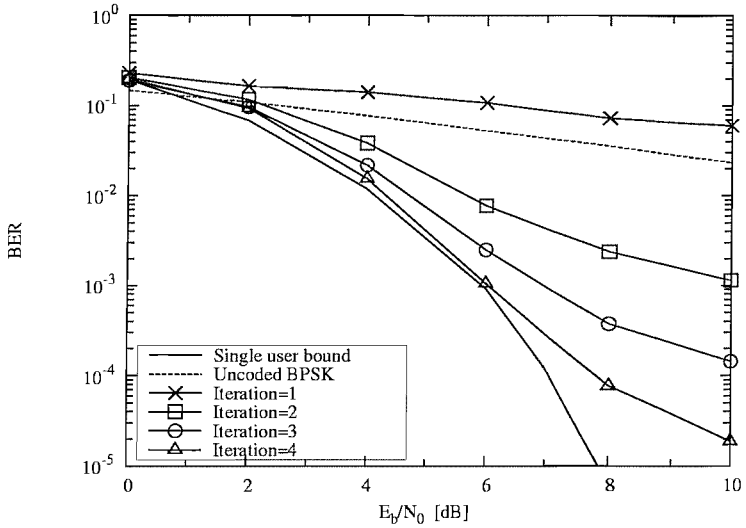

Figure 4.24: The PIC based iterative multiuser detector's **BER** performance, when communicating over an **asynchronous two-path uncorrelated Rayleigh fading** channel, while supporting $K = 7$ users, each encoded with the aid of a $\frac{1}{2}$-rate, $m = 3$ **turbo code. QPSK** modulation was employed.

When we consider the achievable performance of this system in a non-dispersive AWGN channel, we can infer from Figures 4.25 and 4.26 that the system achieves a slightly further gain when the number of outer iterations is higher than 2. Furthermore, Figure 4.27 characterizes the PIC based MUD's BER performance, when communicating over an asynchronous two-path uncorrelated Rayleigh fading channel. From Figures 4.27 we can observe that the PIC based MUD requires more than 4 iterations to approach the near single-user performance when communicating over a dispersive fading channel.

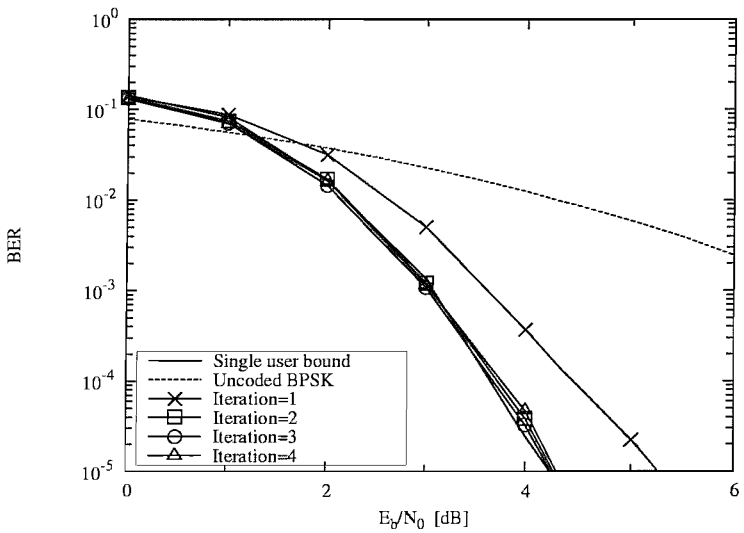

Figure 4.25: The PIC based iterative multiuser detector's **BER** performance, when communicating over a **synchronous non-dispersive AWGN** channel, while supporting $K = 15$ users. A $\frac{1}{2}$-rate **LDPC** was invoked as well as **QPSK** modulation was employed.

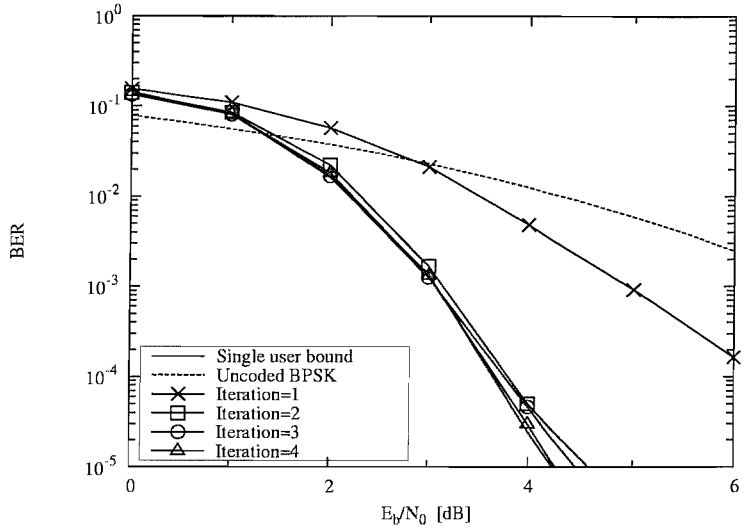

Figure 4.26: The PIC based iterative multiuser detector's **BER** performance, when communicating over a **asynchronous non-dispersive AWGN** channel, while supporting $K = 7$ users. A $\frac{1}{2}$-rate **LDPC** was invoked as well as **QPSK** modulation was employed.

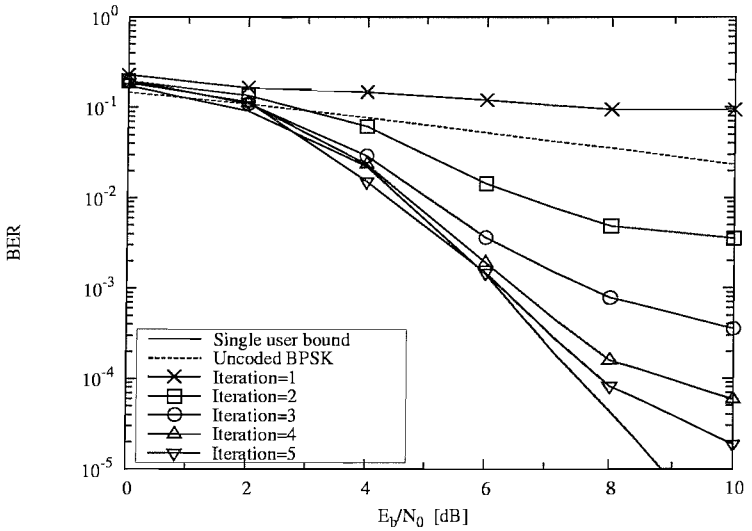

Figure 4.27: The PIC based iterative multiuser detector's **BER** performance, when communicating over a **asynchronous two-path uncorrelated Rayleigh fading** channel, while supporting $K = 7$ users. A $\frac{1}{2}$-rate **LDPC** was invoked as well as **QPSK** modulation was employed.

4.9 Chapter Conclusions

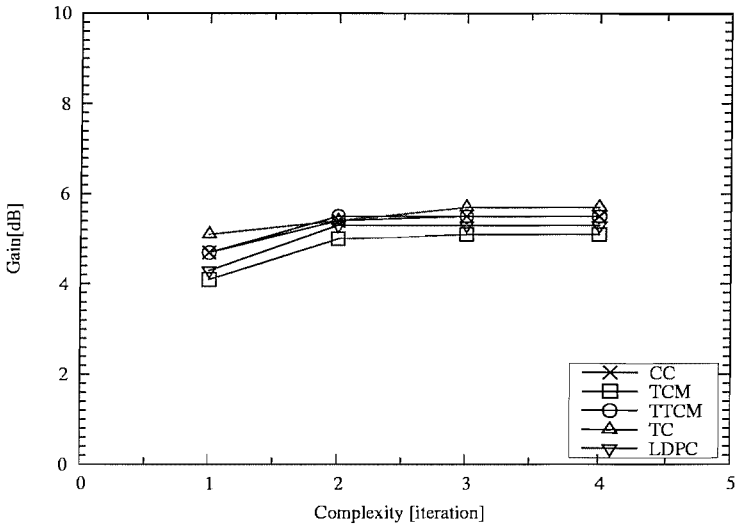

Figure 4.28: The PIC based iterative multiuser detector's coding gain versus the complexity of all these coding schemes at a BER of 10^{-5}, when communicating over a **synchronous AWGN** channel, while supporting $K = 15$ users, and **QPSK** modulation was employed.

For the sake of fair comparison, initially all the systems studied were configured for maintaining the same complexity. Specifically, a code memory of $v = 6$ was invoked by the TCM scheme [78]. To ensure that the TTCM scheme exhibited a similar decoding complexity in comparison to the TCM scheme of memory $v = 6$ expressed in terms of the number of decoding trellis states [78], two components of TCM code memory of $v = 3$ was used in the TTCM scheme, and the number of decoding iterations was set to 4 for TTCM. Hence there were 2 decoders, again, yielding a total of $2^3 \times 2 \times 4 = 2^6 = 64$ trellis states. All the iterative multiuser detector invoked 4 outer iterations. These similar configuration was employed for the convolutional codes and turbo codes for maintaining the same complexity. Furthermore, for maintaining the same complexity, the number of decoding iterations for the LDPC was set to 16 [78].

Figures 4.28 and 4.29 show the coding gain versus complexity of all these coded schemes when QPSK modulation scheme was invoked, and when communicating over an AWGN channel, where no dramatic performance differences are observed. This suggests that the system's overall performance is predetermined by the outer PIC scheme and that a low number of iterations is sufficient for approaching the maximum achievable gain. Figure 4.30 shows the coding gain versus complexity of all these schemes when communicating over a two-path uncorrelated Rayleigh fading channel, from this figure we can observe that the performance of iterative MUD converges slower when communicating over a Rayleigh fading channel than over AWGN channel, again, turbo code and convolutional code exhibited a better performance than that of the other schemes. Figures 4.31 and 4.32 show the coding gain versus complexity of TCM and TTCM when **8PSK** and **16QAM** are employed. From these figures we observe that the iterative MUD converges

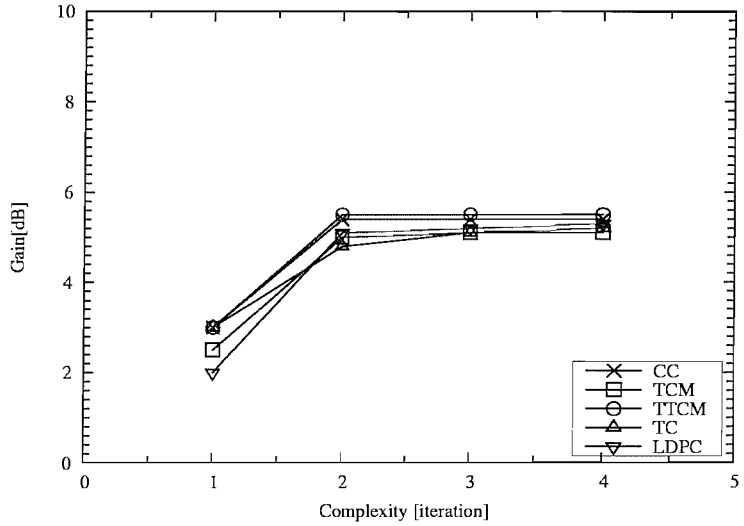

Figure 4.29: The PIC based iterative multiuser detector's coding gain versus the complexity of different coding schemes at a BER of 10^{-5}, when communicating over a **asynchronous AWGN** channel, while supporting $K = 7$ users, and **QPSK** modulation was employed.

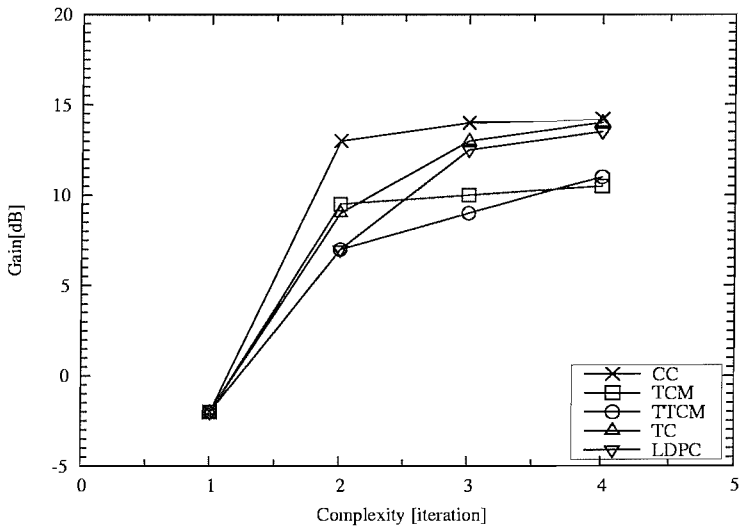

Figure 4.30: The PIC based iterative multiuser detector's coding gain versus the complexity of different coding schemes when communicating over a **two pathes equal weigth uncorrelated Rayleigh fading** channel at a BER of 10^{-3}, while supporting $K = 10$ users, and **QPSK** modulation was employed.

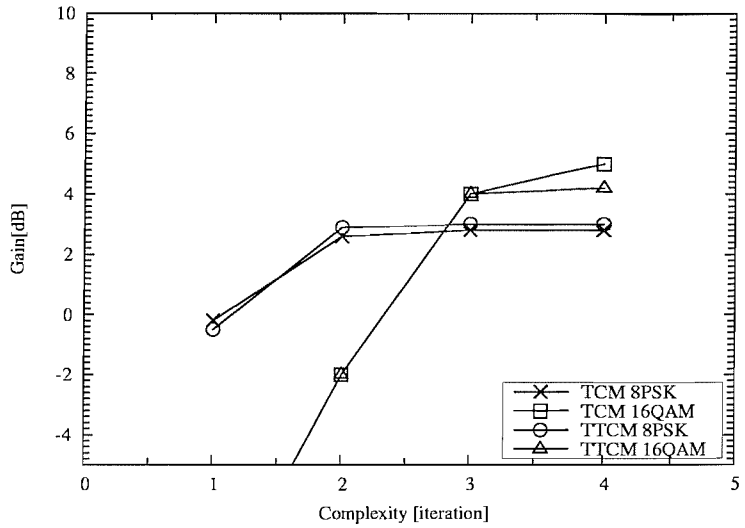

Figure 4.31: The PIC based iterative multiuser detector's coding gain versus the complexity of coded modulation schemes when communicating over a **synchronous** channel at a BER of 10^{-5}, while supporting $K = 15$ users, and **8PSK** and **16QAM** modulation were employed.

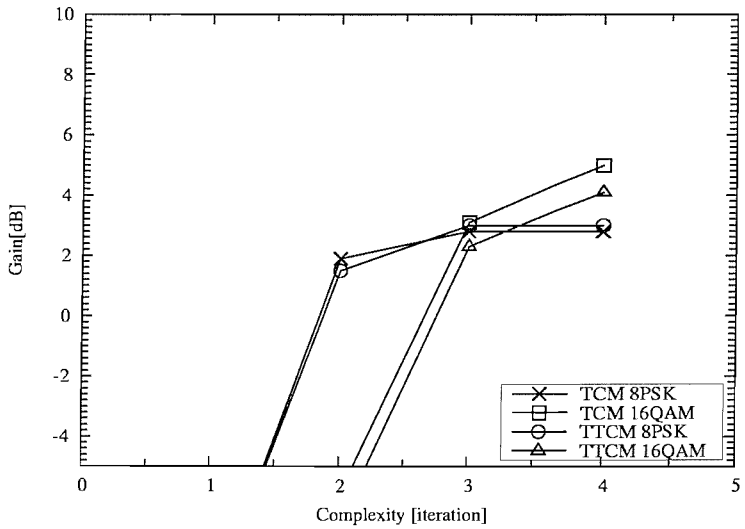

Figure 4.32: The PIC based iterative multiuser detector's coding gain versus the complexity of coded modulation schemes when communicating over a **asynchronous** channel at a BER of 10^{-5}, while supporting $K = 7$ users, and **8PSK** and **16QAM** modulation were employed.

slower in the asynchronous environments than in the synchronous environments, and it requires more outer iterations to achieve a better coding gain.

CHAPTER 5

Blind Multiuser Detection for MC-CDMA

5.1 Introduction

Over the past decade the topic of adaptive multiuser detection has captured a growing interest in the wireless communications community. For example, Woodward [130] investigated a range of adaptive multiuser detectors such as the adaptive decorrelating detector, the zero-forcing detector, the linear MMSE detector and the Minimum Mean Square Error Block Decision Feedback (MMSE-BDF) detector. However, all these adaptive detectors considered require training sequences, which significantly reduces the achievable effective throughput and the resultant spectrum efficiency. To circumvent this problem, Honig [58] proposed the minimum-output-energy (MOE) based blind adaptive detector, which only requires the prior knowledge of the signature waveform and the timing of the reference user, where the timing information is the corresponding delay information of the reference user, but does not invoke any training sequence. However, the performance of the MOE based blind detector is not ideal in the high-SNR region.

Subspace based blind multiuser detectors were first proposed by Wang and Poor [62] for single-carrier DS-CDMA systems communicating over synchronous AWGN channels, which exhibited a significantly better performance than that of the MOE based blind multiuser detector. Wang and Poor [90] later extended their work to dispersive asynchronous CDMA environments, where a subspace based channel estimation approach was proposed. In [63, 91], Wang and Host-Madsen proposed group-blind multiuser detectors for uplink single-carrier DS-CDMA, which exploited the prior knowledge of all known signature waveforms, rather than only that of the reference user. With the advent of

this extra information their group-blind multiuser detector exhibited a substantial performance improvement over that of a blind multiuser detector.

In this chapter, we first introduce the concept and architecture of the subspace based multiuser detector in Section 5.2 and investigate several subspace tracking algorithms [131, 132]. Then in Section 5.3 we investigate the family of space-time blind multiuser detectors in conjunction with antenna arrays. We continue in Section 5.4 by studying the application of subspace-based semi-blind and group-blind multiuser detectors designed for the MC-CDMA uplink, where a short cyclic prefix, rather than differential encoding is used for removing the phase ambiguity encountered. Furthermore, the Akaike information theoretic criterion (AIC) [26] is invoked for the estimation of the rank of the signal space, *i.e.* for estimating the number of users supported. As alternative design options, a blind MMSE multiuser detector [62] and a form-II group-blind multiuser detector [63] are studied in conjunction with Zadoff-Chu spreading codes [27], Gold codes [28] and Walsh codes [28].

5.2 Blind and Group-Blind MUD for DS-CDMA Communicating over AWGN Channels

5.2.1 The Philosophy of Subspace-Based Blind Linear Multiuser Detection

A synchronous baseband DS-CDMA system's received signal can be expressed as

$$\mathbf{r} = \sum_{k=1}^{K} A_k b_k \mathbf{c}_k + \sigma \mathbf{n}, \tag{5.1}$$

where $\mathbf{c}_k$ is the normalized signature waveform given by $\mathbf{c}_k = \frac{1}{\sqrt{N}}[c_1, c_2, \ldots, c_N]^T$, b_k is the transmitted bit of user k, A_k is the amplitude of user k and $\mathbf{n}$ is a white Gaussian noise vector having a mean of 0 and covariance matrix of $\mathbf{I}_N$, where $\mathbf{I}_N$ denotes the $N \times N$-dimensional identity matrix and N is the spreading factor.

Let us define the matrices $\mathbf{C} \triangleq [\mathbf{c}_1, \mathbf{c}_2, \ldots, \mathbf{c}_N]$ and $\mathbf{A} \triangleq \text{diag}[A_1^2, A_2^2, \ldots, A_K^2]$. Then the autocorrelation matrix $\mathbf{R}$ of the N-dimensional received sample vector $\mathbf{r}$, which is the output of the chip-matched filter, can be expressed theoretically as:

$$\mathbf{R} \triangleq E\{\mathbf{r}\mathbf{r}^H\} \triangleq \sum_{k=1}^{K} A_k^2 \mathbf{c}_k \mathbf{c}_k^T + \sigma^2 \mathbf{I}_N \triangleq \mathbf{C}\mathbf{A}\mathbf{C}^T + \sigma^2 \mathbf{I}_N. \tag{5.2}$$

Let us consider the eigenanalysis [62] of the received sample correlation matrix $\mathbf{R}$, assuming that the unique, user-specific spreading waveforms $\{\mathbf{c}_k\}_{k=1}^K$ of the K users are linearly independent. Then the matrix $\mathbf{R}$ has a rank of K, more specifically, $\mathbf{R}$ has K eigenvalues that are theoretically strictly larger than the noise power σ^2 and $(N - K)$ eigenvalues that are equal to σ^2 [62]. The eigen-decomposition of the received samples' correlation

matrix $\mathbf{R}$ can be expressed as [62]:

$$\mathbf{R} = \mathbf{U}\mathbf{\Lambda}\mathbf{U}^H = [\mathbf{U}_s \ \ \mathbf{U}_n] \begin{bmatrix} \mathbf{\Lambda}_s & 0 \\ 0 & \mathbf{\Lambda}_n \end{bmatrix} \begin{bmatrix} \mathbf{U}_s^H \\ \mathbf{U}_n^H \end{bmatrix}, \tag{5.3}$$

where we have $\mathbf{U} = [\mathbf{U}_s \ \ \mathbf{U}_n]$, and $\mathbf{\Lambda} = \text{diag}(\mathbf{\Lambda}_s, \mathbf{\Lambda}_n)$, and $\mathbf{\Lambda}_s = \text{diag}\{\lambda_1, \ldots, \lambda_K\}$ contains the largest K eigenvalues of the received samples' correlation matrix $\mathbf{R}$, while $\mathbf{U}_s = [\mathbf{u}_1, \ldots, \mathbf{u}_K]$ are the eigenvectors corresponding to the largest K eigenvalues. Finally, the matrix $\mathbf{U}_n = [\mathbf{u}_{K+1}, \ldots, \mathbf{u}_N]$ contains the $(N-K)$ orthogonal eigenvectors corresponding theoretically to the smallest eigenvalues that are equal to σ^2 in $\mathbf{\Lambda}_n$. The column space of $\mathbf{U}_s$ is referred to as the *signal space*, while the *noise space* is spanned by the columns of $\mathbf{U}_n$ [62]. This concept may be further interpreted with the aid of the following numerical example.

A linear multiuser detector designed for demodulating the kth user's data bit can be expressed in the form [62]:

$$\hat{b}_k = \text{sgn}(\mathbf{w}_k^H \mathbf{r}), \tag{5.4}$$

where $\mathbf{w}_k$ represents the MUD's weight vector optimized for detecting user k.

Blind Decorrelating and MMSE multiuser detector

Wang and Poor [62] first proved that the decorrelating detector's weight vector $\mathbf{w}_d$ and the MMSE detector's weight vector $\mathbf{w}_m$ can be generated from the signal subspace parameters. More explicitly, the decorrelating detector's weight vector $\mathbf{w}_d$ can be explicitly described in terms of the signal subspace parameters $\mathbf{U}_s$, $\mathbf{\Lambda}_s$ and σ as follows [62]:

$$\mathbf{w}_d = \frac{1}{\mathbf{c}_k^H \mathbf{U}_s (\mathbf{\Lambda}_s - \sigma^2 \mathbf{I}_K)^{-1} \mathbf{U}_s^H \mathbf{c}_k} \mathbf{U}_s (\mathbf{\Lambda}_s - \sigma^2 \mathbf{I}_K)^{-1} \mathbf{U}_s^H \mathbf{c}_k. \tag{5.5}$$

Furthermore, the linear MMSE detector's weight vector $\mathbf{w}_m$ can be expressed using the parameters of the signal space $(\mathbf{U}_s, \mathbf{\Lambda}_s)$ [62]:

$$\mathbf{w}_m = \frac{1}{\mathbf{c}_k^H \mathbf{U}_s \mathbf{\Lambda}_s^{-1} \mathbf{U}_s^H \mathbf{c}_k} \mathbf{U}_s \mathbf{\Lambda}_s^{-1} \mathbf{U}_s^H \mathbf{c}_k, \tag{5.6}$$

since the received signal's autocorrelation matrix $\mathbf{R}$ and the parameters of its eigendecomposition $\mathbf{U}_s, \mathbf{\Lambda}_s, \sigma$ can be estimated from the received sample vector $\mathbf{r}$. More explicitly, in the context of Eq.(5.5) and Eq.(5.6) we observed that both the decorrelating detector's weight vector $\mathbf{w}_d$ and the linear MMSE's weight vector $\mathbf{w}_m$ can be estimated from the received samples $\mathbf{r}$ relying on the prior knowledge of only the signature waveform and timing of the user of interest, but without requiring a reductant training or pilot sequence. Therefore, the weight vectors $\mathbf{w}_d, \mathbf{w}_m$ can be constructed blindly. In Section 5.2.3, we will consider how to derive the parameters $\mathbf{U}_s, \mathbf{\Lambda}_s, \sigma$ of the eigendecomposition.

5.2.2 Group-Blind Multiuser Detection

In contrast to the totally blind multiuser detection philosophy, where no knowledge of other users' spreading code is available, the group-blind multiuser detector exploits the knowledge of a group of $\tilde{K}$ out of the total of K users' signature waveforms. In our investigations we only consider the hybrid group-blind multiuser detection schemes of [63, 91], because this form of group-blind MUD requires only a slight modification of the blind MUD of [62]. More specifically, let us define the set $\tilde{\mathbf{G}}$ such that $\tilde{\mathbf{G}} = [\mathbf{c}_1 \dots \mathbf{c}_{\tilde{K}}]$ is an $(N \times \tilde{K})$-dimensional matrix, which includes the signature waveforms of the group of $\tilde{K}$ users communicating within the cell of the reference user. The linear hybrid group-blind detector of user k, $k = 1, \dots, \tilde{K}$, is given by the solution of the following constrained optimization problem [63]:

$$\begin{aligned} \mathbf{w}_k = \quad & \arg \min_{\mathbf{w}_k \in range(\mathbf{G})} E\{\| b_k - \mathbf{w}_k^H \mathbf{r} \|^2\} \\ & \text{subject to} \quad \tilde{\mathbf{G}}^H \mathbf{w}_k = \mathbf{1}_k^T, \quad k = 1, \dots, \tilde{K}, \end{aligned} \tag{5.7}$$

where $\mathbf{1}_k$ is the vector having a length of $\tilde{K}$ and having zero-valued elements only, except for the kth element, which is 1. More explicitly, Eq.(5.7) implies that finding that the specific MUD wight vector $\mathbf{w}_k$, which minimizes the expected value of the Eucledian norm $\| b_k - \mathbf{w}_k^H \mathbf{r} \|$. This corresponds to processing the composite received signal vector of the K users with the aid the kth user's weight vector $\mathbf{w}_k$ and deciding on the binary value of the bit b_k on the basis of having the lowest Eucledian distance from $\mathbf{w}_k^H \mathbf{r}$. Generally speaking, this detector invokes zero-forcing of the interference caused by the group of $\tilde{K}$ users communicating in the reference cell, whose signature sequences are known, and suppresses the interference imposed by the other-cell users whose signature sequences are unknown with the aid of the MMSE criterion. The so-called form-II MUD weight solution of [63] and the corresponding bit estimate of user k may be written as [63]:

$$\mathbf{w}_k = \mathbf{U}_s \mathbf{\Lambda}_s^{-1} \mathbf{U}_s^H \tilde{\mathbf{G}} [\tilde{\mathbf{G}}^H \mathbf{U}_s \mathbf{\Lambda}_s^{-1} \mathbf{U}_s^H \tilde{\mathbf{G}}]^{-1} \mathbf{1}_k \tag{5.8}$$

$$\hat{b}_k = \text{sgn}\{\text{Re}(\mathbf{w}_k^H \mathbf{r})\}, \quad k = 1, \dots, \tilde{K}. \tag{5.9}$$

Hence, we require the knowledge of the signature waveforms of the group of $\tilde{K}$ users supported within the reference cell, in order to construct $\tilde{\mathbf{G}}$.

5.2.3 Subspace Tracking Algorithms

Eigenvalue Decomposition and Singular Value Decomposition

Assuming that we received M number of samples $\mathbf{r}_i, i = 1, \dots M$, the corresponding auto-correlation matrix $\mathbf{R}$ can be expressed as:

$$\mathbf{R} = \frac{1}{M} \sum_{i=1}^{M} \mathbf{r}_i \mathbf{r}_i^H, \tag{5.10}$$

As it was outlined in Eq.(5.3), the eigendecomposition of the auto-correlation matrix can be expressed as $\text{EVD}(\mathbf{R}) = \mathbf{U}\mathbf{\Lambda}\mathbf{U}^H$, where the matrix $\mathbf{U}$ is constituted by the eigenvectors and the diagonal matrix $\mathbf{\Lambda}$ contains the corresponding eigenvalues, while the largest K number of eigenvalues and eigenvectors describe the corresponding *signal subspace*. For example, let us consider a system having the parameters of $N = 4$, $K = 2$, $A_1 = A_2 = 1$, and $\mathbf{c}_1 = [1/2, 1/2, 1/2, 1/2]^T$, $\mathbf{c}_2 = [-1/2, 1/2, 1/2, 1/2]^T$. In order to exemplify these quantities, we ran simulations at $E_b/N_0 = 20dB$, and recorded the corresponding autocorrelation matrix $\mathbf{R}$ after we received $M = 200$ number of multiuser received signal samples, which is given by:

$$\mathbf{R} = [\mathbf{c}_1, \mathbf{c}_2] \begin{bmatrix} \mathbf{c}_1^H \\ \mathbf{c}_2^H \end{bmatrix} + \sigma^2 \mathbf{I}_4 = \begin{bmatrix} 0.51 & 0 & 0 & 0 \\ 0 & 0.51 & 0.50 & 0.50 \\ 0 & 0.50 & 0.51 & 0.50 \\ 0 & 0.50 & 0.50 & 0.51 \end{bmatrix}. \tag{5.11}$$

The corresponding eigendecomposition can be expressed as:

$$\mathbf{R} = \mathbf{U}\mathbf{\Lambda}\mathbf{U}^H = \left[\begin{array}{cc|cc} 0 & 1.00 & 0 & 0 \\ 0.58 & 0 & -0.51 & 0.64 \\ 0.58 & 0 & 0.81 & 0.12 \\ 0.58 & 0 & -0.30 & -0.76 \end{array}\right] \times \left[\begin{array}{cc|cc} 1.51 & 0 & 0 & 0 \\ 0 & 0.51 & 0 & 0 \\ 0 & 0 & 0.01 & 0 \\ 0 & 0 & 0 & 0.01 \end{array}\right] \times \left[\begin{array}{cc|cc} 0 & 1.00 & 0 & 0 \\ 0.58 & 0 & -0.51 & 0.64 \\ 0.58 & 0 & 0.81 & 0.12 \\ 0.58 & 0 & -0.30 & -0.76 \end{array}\right].$$

The first two columns of $\mathbf{U}$ constitute the *signal subspace*, while the 3rd and 4th columns of $\mathbf{U}$ are referred to as the *noise subspace*, which correspond to the smallest eigenvalues of $\sigma^2 = 0.01$.

Singular Value Decomposition (SVD) is another technique designed for decomposing the received signal matrix $\mathbf{X} = [\mathbf{r}_1, \ldots, \mathbf{r}_M]$ constituted by the M number of multiuser received signal samples $\mathbf{r}_i, i = 1, \ldots M$, which can be expressed as $\text{SVD}(\mathbf{X}) = \mathbf{V}\mathbf{\Lambda}\mathbf{U}^H$, where again, $\mathbf{U}$ is constituted by the eigenvectors and $\mathbf{\Lambda}$ contains the corresponding eigenvalues.

However, carrying out both the EVD and the SVD is computationally expensive, because the number of operations to be carried out is on the order of $O(N^3)$. Hence in the forthcoming section we will introduce low-complexity algorithms that may be used for directly tracking the components of the EVD, rather than having to carry out the EVD for each block of the received signal samples.

Subspace Tracking Algorithm [62, 131, 132]

The classic approach to subspace estimation is based on the EVD of the multiuser received samples' autocorrelation matrix, or on the SVD of the received signal sample matrix.

However, both of these are computationally expensive for applications, where they have to be carried out in an on-line fashion on a regular basis. Modern subspace tracking algorithms are recursive in their nature, updating the subspace parameters on a received sample-by-sample fashion. The so-called Projection Approximation Subspace Tracking deflation algorithm of [62, 131] (PASTd) will be invoked for adaptive blind multiuser detection in Section 5.2.1. The advantages of this algorithm [62,131] include fairly reliable global convergence to the required eigenvectors and eigenvalues as well as having a low computational complexity, which is on the order of $O(N \cdot K)$. The philosophy of the PASTd algorithm [62,131] designed for tracking the eigenvalues and eigenvectors of the signal subspace is based on the following principle. At the nth time instant we update the most dominant eigenvector and eigenvalue and determine the projection of the current data vector $\mathbf{r}(n)$ to the most dominant eigenvector. Then we remove this projection from $\mathbf{r}(n)$ itself. Now the second most dominant eigenvector becomes the most dominant one in the updated data vector, which can be extracted similarly. We then continue by repeatedly applying this procedure until all the K eigenvectors have been sequentially estimated. For the detailed operation of the PASTd algorithm, the interested readers might like to refer to [62,131].

As a further design alterative, Reynolds and Wang [132] proposed a low-complexity, high-performance Fast Subspace Tracking (FST) algorithm, which also exhibited a low complexity that was on the order of $O(N \cdot K)$. The FST algorithm employs the well-known symmetric Jacobian SVD algorithm [133] for the diagonalization of the autocorrelation matrix $\mathbf{R}$. More explicitly, the FST algorithm invokes a series of Givens rotations [132, 133] for diagonalizing the matrix $\mathbf{R}$. After a number of Givens rotation operations, the autocorrelation matrix $\mathbf{R}$ becomes a "near" diagonal matrix $\mathbf{R}_a$, whose diagonal elements may be viewed as the corresponding eigenvalues, while the result of a series of Givens rotations may be viewed as the corresponding eigenvectors. The readers interested in implementing the FST algorithm might like to consult [132] for further detail.

5.2.4 Performance of Both Blind and Group-Blind Multiuser Detectors Over AWGN Channels

Host-Madison and Wang [91] investigated the performance of both blind and group-blind MUDs, when communicating over AWGN channels. Following an arduous mathematical analysis, the output Signal to Interference plus Noise Ratio (SINR) of the blind multiuser detector communicating over AWGN channels can be expressed as [91]:

$$\begin{aligned}\mathrm{SINR}_{out} = A_1^2(\mathbf{w}_1^T\mathbf{c}_1)^2/\{\sum_{k=2}^{K} A_k^2(\mathbf{w}_1^T\mathbf{c}_k)^2 + \sigma^2 \parallel \mathbf{w}_1 \parallel^2 + \\ + \frac{1}{M}[(K+1)\mathbf{w}_1^T\mathbf{c}_1) - 2\sum_{k=1}^{K} A_k^4(\mathbf{w}_1^T\mathbf{c}_k)^2(\mathbf{w}_k^T\mathbf{c}_k) + (N-K)\hat{\sigma}^2]\}, \qquad (5.12)\end{aligned}$$

where we have [91]:

$$\mathbf{w}_l^T \mathbf{c}_k = \frac{1}{A_l^2}[\mathbf{R}(\mathbf{R}+\sigma^2\mathbf{A}^{-2})^{-1}]_{k,l}, \quad k,l = 1,\ldots,K \tag{5.13}$$

$$\| \mathbf{w}_1 \|^2 = \frac{1}{A_l^4}[(\mathbf{R}+\sigma^2\mathbf{A}^{-2})^{-1}\mathbf{R}(\mathbf{R}+\sigma^2\mathbf{A}^{-2})^{-1}]_{1,1}, \tag{5.14}$$

$$\hat{\sigma}^2 = \frac{\sigma^2}{A_l^4}[(\mathbf{R}+\sigma^2\mathbf{A}^{-2})^{-1}\mathbf{A}^{-2}\mathbf{R}^{-1}]_{1,1}. \tag{5.15}$$

The output SINR of the group-blind hybrid detector is given by:

$$\text{SINR}_{out} = \frac{A_1^2}{\sum_{k=1}^{K-\tilde{K}} A_{k+\tilde{K}}^2(\mathbf{w}_1^T\mathbf{c}_{k+\tilde{K}})^2 + \sigma^2 \| \mathbf{w}_1 \|^2 + \hat{\sigma}^2}, \tag{5.16}$$

where we have:

$$\mathbf{w}_1^T \mathbf{c}_{k+\tilde{k}} = [\Psi_{12}^T\Psi_{11}^{-1}]_{k,1} \tag{5.17}$$

$$\| \mathbf{w}_1 \|^2 = [\Psi_{11}^{-1}\Pi\Psi_{11}^{-1}]_{1,1}, \tag{5.18}$$

$$\begin{aligned}\hat{\sigma}^2 = \frac{1}{M}\{&(K-\tilde{K})[\Psi_{11}^{-1}]_{1,1} \\ &-2\sum_{k=1}^{K-\tilde{K}} A_{K+\tilde{K}}^4 \cdot [\Psi_{12}^T\Psi_{11}^{-1}]_{k,1}^2[\Psi_{22}-\Psi_{12}^T\Psi_{11}^{-1}\Psi_{12}]_{k,k} \\ &+(N-K)\sigma^4[\Psi_{11}^{-1}\Xi\Psi_{11}^{-1}]_{1,1}\}.\end{aligned} \tag{5.19}$$

The $(\tilde{K}\times\tilde{K})$-dimensional matrix Ψ_{11}, the $[\tilde{K}\times(K-\tilde{K})]$-dimensional matrix Ψ_{12}, the $[(K-\tilde{K})\times\tilde{K}]$-dimensional matrix Ψ_{21} and $[(K-\tilde{K})\times(K-\tilde{K})]$ are defined as:

$$\mathbf{R}(\mathbf{R}+\sigma^2\mathbf{A}^{-2})^{-1}\mathbf{A}^{-2} = \begin{bmatrix} \Psi_{11} & \Psi_{12} \\ \Psi_{12}^T & \Psi_{22} \end{bmatrix}. \tag{5.20}$$

The $(\tilde{K}\times\tilde{K})$-dimensional matrices Π and Ξ are defined as

$$\Pi = [\mathbf{A}^{-2}(\mathbf{R}+\sigma^2\mathbf{A}^{-2})^{-1}\mathbf{R}(\mathbf{R}+\sigma^2\mathbf{A}^{-2})^{-1}\mathbf{A}^{-2}]_{1:\tilde{K},1:\tilde{K}} \tag{5.21}$$

$$\Xi = [\mathbf{A}^{-2}(\mathbf{R}+\sigma^2\mathbf{A}^{-2})^{-1}\mathbf{A}^{-2}\mathbf{R}^{-1}\mathbf{A}^{-2}]_{1:\tilde{K},1:\tilde{K}}. \tag{5.22}$$

Figure 5.1 exhibits the achievable performance of the blind and group-blind multiuser detectors of Section 5.2.1 when the PASTd tracking algorithm was invoked for transmission over an AWGN channel. We may observe in this figure that these adaptive blind multiuser detectors will converge reasonably accurately after receiving about 500 symbols. Furthermore, the group-blind multiuser detector significantly outperforms the blind multiuser detector. For example, when we supported $K = 8$ users and the signature sequences of $\tilde{K} = 7$ users were known, the group-blind multiuser detector had a 5dB higher output SINR than that of the blind multiuser detector.

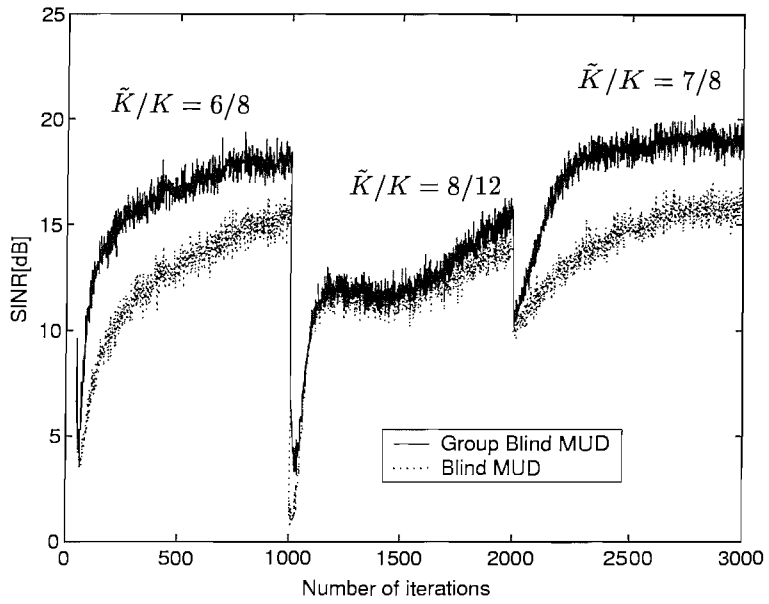

Figure 5.1: Performance of both the blind and group-blind multiuser detectors of Section 5.2 using the PASTd subspace tracking algorithm for communicating in an AWGN channel. The E_b/N_0 ratio of each user was 20dB, and m-sequences having a spreading factor of $N = 15$ were invoked. At $t = 0$, $K = 8$ users are activated and we have $\tilde{K} = 6$. At $t = 1000$ four more users engage in communications, hence we have $K = 12$ and $\tilde{K} = 8$. Finally, at $t = 2000$, four users exit the system and hence we have $K = 8$ as well as $\tilde{K} = 7$.

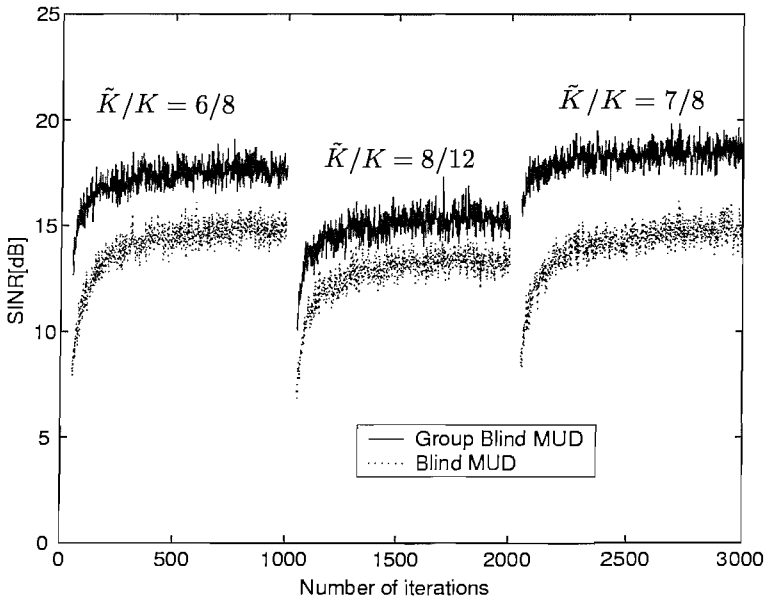

Figure 5.2: Performance of both the blind and group-blind multiuser detectors of Section 5.2 using the FST algorithm for communicating in an AWGN channel. The E_b/N_0 ratio of each user was 20dB, and m-sequences having a spreading factor of $N = 15$ were invoked. At $t = 0$, $K = 8$ users are activated and we have $\tilde{K} = 6$. At $t = 1000$ four more users engage in communications and we have $K = 12$ and $\tilde{K} = 8$. Finally, at $t = 2000$, four users exit the system and we have $K = 8$ and $\tilde{K} = 7$.

Figure 5.2 characterizes the achievable performance of the blind and group-blind multiuser detectors of section 5.2.1 when the FST algorithm was employed for transmission over an AWGN channel. Comparing Figure 5.2 to Figure 5.1, we may conclude that the FST tracking algorithm exhibited a faster convergence performance than that of the PASTd tracking algorithm characterized in Figure 5.1. More explicitly, we can observe in Figure 5.2 that the FST algorithm converged after receiving approximately 100 symbols.

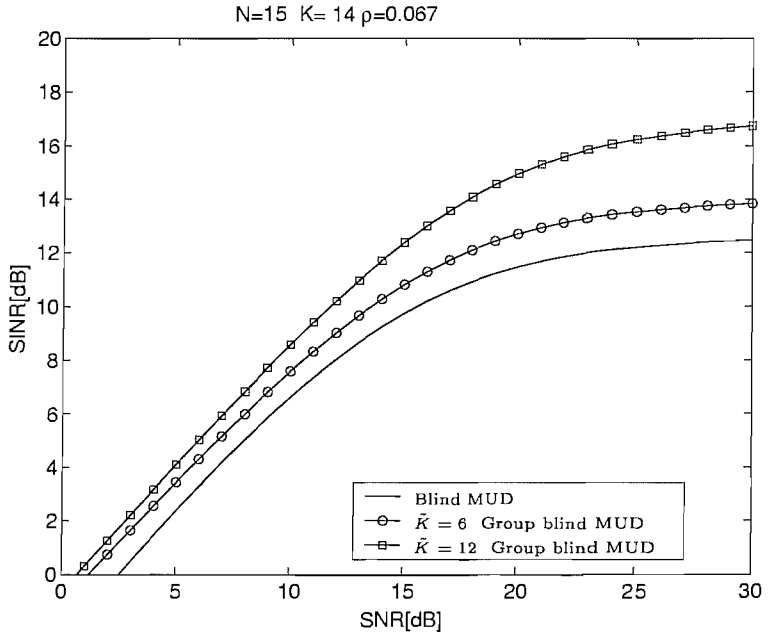

Figure 5.3: SINR versus E_b/N_0 performance of the blind and group-blind multiuser detectors, when m-sequence based spreading codes were invoked for transmission over AWGN channels. A total of $K = 14$ users were supported and the spreading codes of $\tilde{K}$=6 and 12 users were known to the group-blind MUD.

Figure 5.3 portrays the output SINR performance of the blind and group-blind multiuser detectors of section 5.2 as a function of E_b/N_0, when the total number of users supported is $K = 14$ and m-sequences having a length of $N = 15$ chips were invoked. Furthermore, group-blind multiuser detectors benefitting from the explicit knowledge of a group of $\tilde{K} = 6$ and $\tilde{K} = 12$ spreading codes were investigated. We can observe in Figure 5.3 that the more users' signature waveforms are known, the better the group-blind multiuser detector's achievable performance. To elaborate a little further, Figure 5.4 shows the attainable performance of both blind and group-blind multiuser detectors, when different cross-correlation coefficients ρ were recorded between the different spreading codes. We observe from this figure that when the codes' cross-correlation coefficient ρ increased, the performance of blind and group-blind multiuser detectors significantly degraded. In Figure 5.5 the near-far performance of the blind and group-blind multiuser detectors is studied. We may conclude that the blind detectors were resistant to the near-far phenomenon. Figure 5.6 illustrates the SINR performance of the blind and group-blind multiuser detectors, when different number of received samples were utilized for tracking the *signal subspace*. As a result, when the number of received samples M increases, the blind detectors are capable of generating more accurate subspace parameters $\mathbf{U}_s$ and $\mathbf{\Lambda}_s$,

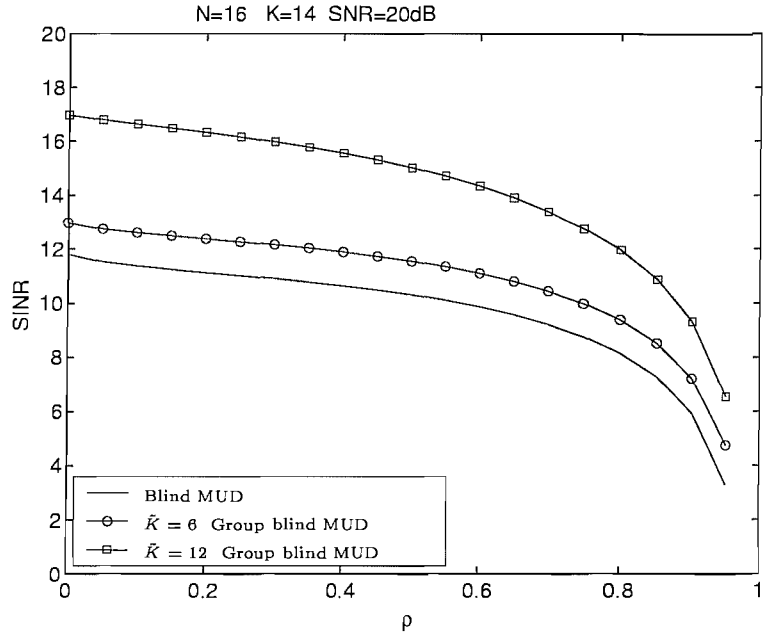

Figure 5.4: SINR versus m-sequence cross-correlation, ρ, performance of both the blind and group-blind multiuser detectors. The spreading factor was $N = 16$ and a total of $K = 14$ users were supported. The spreading codes of $\tilde{K} = 6$ and 12 users were known to the group-blind MUD.

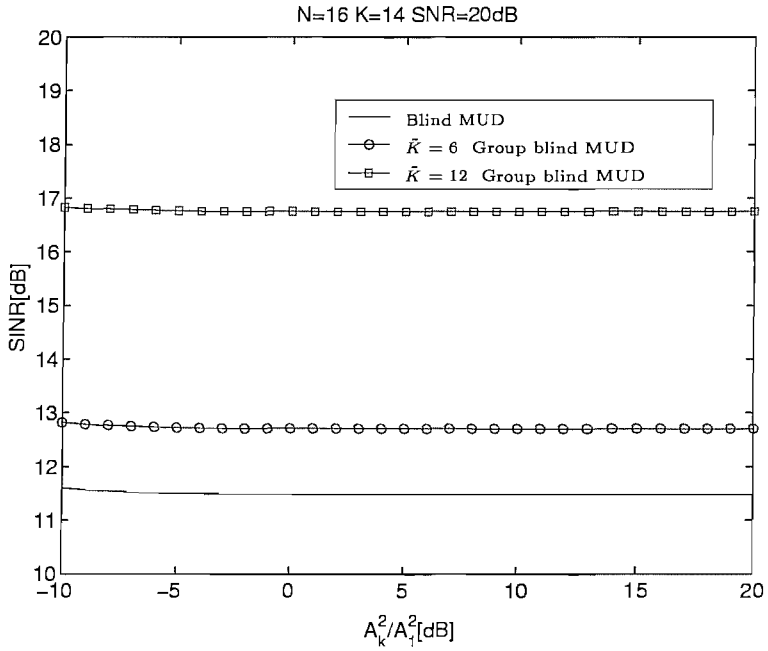

Figure 5.5: Near-far performance of both the blind and group-blind multiuser detectors supporting a total of $K = 14$ users, when employing m-sequences having and communicating over AWGN channels having an SNR of 20dB. The group-blind MUDs benefitted from the knowledge of $\tilde{K} = 6$ or 12 spreading codes.

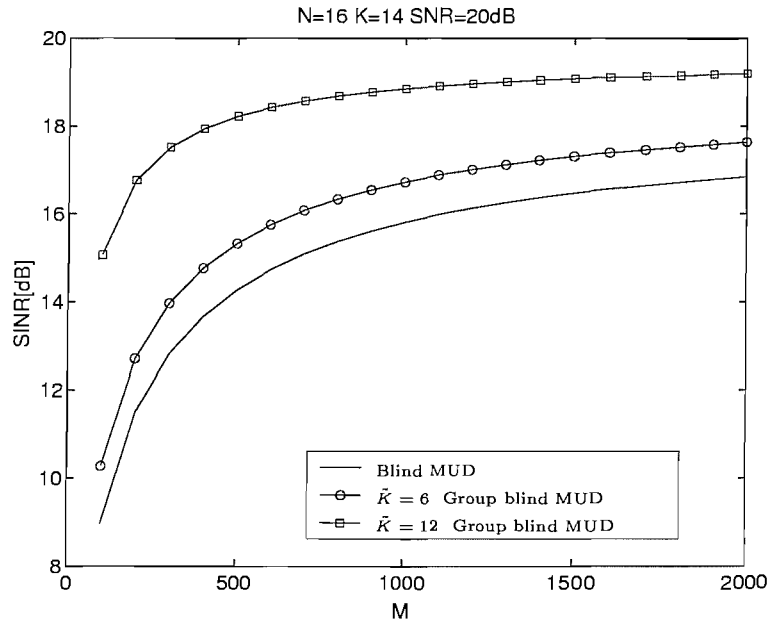

Figure 5.6: The SINR versus the number of samples M used for subspace tracking by both the blind and group-blind multiuser detectors employing a spreading factor of $N = 16$ for supporting $K = 14$ users over an AWGN channel at SNR=20dB. The group-blind MUDs benefitted from the knowledge of $\tilde{K}$=6 or 12 spreading codes.

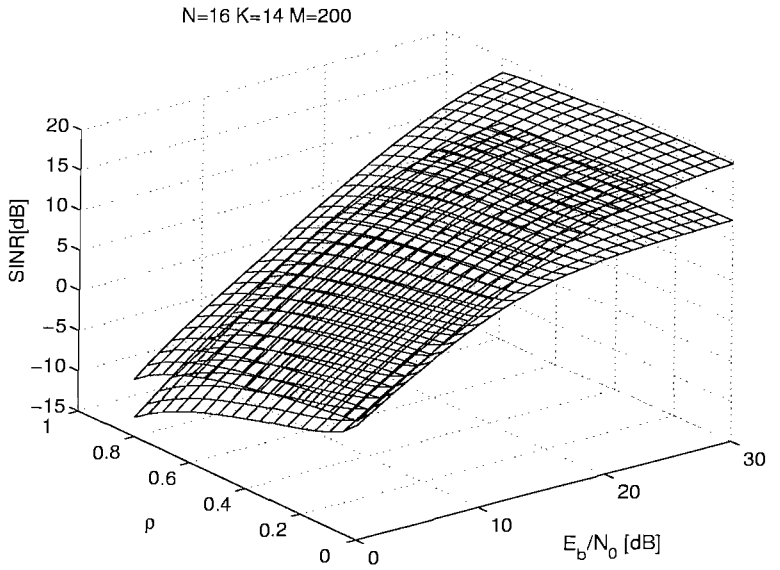

Figure 5.7: SINR versus SNR and m-sequence correlation, ρ, for the blind and group-blind multiuser detectors having a spreading factor of $N = 16$ and supporting $K = 14$ users after $M = 200$ subspace tracking training samples, when communicating over an AWGN channel. The upper curve represents the group-blind MUDs which exploited the knowledge of $\tilde{K} = 12$ spreading codes.

hence achieving a higher output SINR. Finally, Figure 5.7 shows the SINR versus E_b/N_0 performance of both blind and group-blind multiuser detectors as a function of the m-sequences' cross-correlation ρ and that of the E_b/N_0 ratio. As expected, the upper curve characterized the group-blind multiuser detector associated with $K = 14$ and $\tilde{K} = 12$. Having introduced the concepts of blind and group-blind MUDs, let us now extend these concepts to space-time MUDs.

5.3 Blind and Group-Blind Space-Time Multiuser Detection

5.3.1 System Model

Let us consider a synchronous CDMA system benefitting from perfect power control and a diversity reception antenna array. We consider L number of antenna elements, and at the lth antenna, the output of the chip-matched receiver filter can be expressed as:

$$\mathbf{r}_l = \sum_{k=1}^{K} A_k b_k h_k^l \mathbf{c}_k + \sigma \mathbf{n}_l, \tag{5.23}$$

where N is the spreading gain, $\mathbf{c}_k$ represents the normalized signature waveforms, $\mathbf{c}_k = \frac{1}{\sqrt{N}}[c_1, c_2, \ldots, c_N]^T$ and $\mathbf{n}_l$ is a white noise Gaussian noise vector having a mean of 0 and a covariance matrix of $\mathbf{I}_N$, where $\mathbf{I}_N$ denotes the $(N \times N)$-dimensional identity matrix. Furthermore, A_k is the received signal energy of user k and h_k^l is the complex-valued channel phase and gain at the lth antenna, where the array elements are sufficiently far apart to ensure that they experience independent fading. Combining all the antenna elements' signal, we denote the vector of the phases and gains of the kth user's by $\mathbf{h}_k = [h_k^1, h_k^2, \ldots, h_k^L]^T$. Then the output of the L-element antenna array can be expressed as:

$$\mathbf{r} = \begin{bmatrix} \mathbf{r}_1 \\ \vdots \\ \mathbf{r}_L \end{bmatrix} = \sum_{k=1}^{K} A_k b_k \tilde{\mathbf{c}}_k + \sigma \mathbf{n}, \tag{5.24}$$

where $\tilde{\mathbf{c}}_k$ is the spatio-temporal signature waveform, which can be expressed as $\tilde{\mathbf{c}}_k = \mathbf{h}_k \otimes \mathbf{c}_k$, where $\otimes$ denotes the Kronecker product of two matrices, and $\mathbf{r} = [\mathbf{r}_1^T, \ldots \mathbf{r}_L^T]^T$, $\mathbf{n} = [\mathbf{n}_1^T, \ldots \mathbf{n}_L^T]^T$, and $E[\mathbf{n}\mathbf{n}^H] = \sigma^2 \mathbf{I}_{LN}$. Hence the rank of the autocorrelation matrix $\mathbf{R} = E[\mathbf{r}\mathbf{r}^H]$ of the received samples is K.

We denote the spatio-temporal signatures of the K users by $\tilde{\mathbf{C}} = [\tilde{\mathbf{c}}_1, \ldots, \tilde{\mathbf{c}}_K]^T$, while the associated autocorrelation of the received samples $\mathbf{r}$ can be expressed as:

$$\mathbf{R} = E[\mathbf{r}\mathbf{r}^H] = \sum_{1}^{K} A_k^2 \tilde{\mathbf{c}}_k \tilde{\mathbf{c}}_k^H + \sigma^2 \mathbf{I}_{LN} \triangleq \tilde{\mathbf{C}} \mathbf{A} \tilde{\mathbf{C}}^H + \sigma^2 \mathbf{I}_{LN}. \tag{5.25}$$

Similar to the blind temporal multiuser detector of Section 5.2, the EVD of the space-time autocorrelation matrix $\mathbf{R}$ may be expressed in a form identical to Eq.(5.3), which is

repeated here for convenience:

$$\mathbf{R} = \mathbf{U}\mathbf{\Lambda}\mathbf{U}^H = [\mathbf{U}_s \ \ \mathbf{U}_n] \begin{bmatrix} \mathbf{\Lambda}_s & 0 \\ 0 & \mathbf{\Lambda}_n \end{bmatrix} \begin{bmatrix} \mathbf{U}_s^H \\ \mathbf{U}_n^H \end{bmatrix}. \tag{5.26}$$

Again, similar to Eq.(5.5) of Section 5.2.1, the weight vector $\mathbf{w}_d$ of the space-time decorrelating detector (ST-DD) formulated for the kth user can be expressed in terms of the signal space parameters ($\mathbf{U}_s, \mathbf{\Lambda}_s$ and σ) as [62]:

$$\mathbf{w}_d = \frac{1}{\tilde{\mathbf{c}}_k^H \mathbf{U}_s (\mathbf{\Lambda}_s - \sigma^2 \mathbf{I}_K)^{-1} \mathbf{U}_s^H \tilde{\mathbf{c}}_k} \mathbf{U}_s (\mathbf{\Lambda}_s - \sigma^2 \mathbf{I}_K)^{-1} \mathbf{U}_s^H \tilde{\mathbf{c}}_k. \tag{5.27}$$

As expected, the weight vector $\mathbf{w}_m$ of the space-time MMSE detector (ST-MMSE) determined for the kth user can be expressed in terms of the signal space parameters ($\mathbf{U}_s, \mathbf{\Lambda}_s$) as [62]:

$$\mathbf{w}_m = \frac{1}{\tilde{\mathbf{c}}_k^H \mathbf{U}_s \mathbf{\Lambda}_s^{-1} \mathbf{U}_s^H \tilde{\mathbf{c}}_k} \mathbf{U}_s \mathbf{\Lambda}_s^{-1} \mathbf{U}_s^H \tilde{\mathbf{c}}_k. \tag{5.28}$$

Furthermore, assuming that we know $\tilde{K}$ out of the set of K number of spatio-temporal signature waveforms, we can form the spatio-temporal matrix $\tilde{\mathbf{G}} = [\tilde{\mathbf{c}}_1, \tilde{\mathbf{c}}_2, \ldots \tilde{\mathbf{c}}_{\tilde{K}}]$, and the corresponding weight vector $\mathbf{w}_k$ of the space-time group-blind multiuser detector for the kth user can be expressed as [63]:

$$\mathbf{w}_k = \mathbf{U}_s \mathbf{\Lambda}_s^{-1} \mathbf{U}_s^H \tilde{\mathbf{G}} [\tilde{\mathbf{G}}^H \mathbf{U}_s \mathbf{\Lambda}_s^{-1} \mathbf{U}_s^H \tilde{\mathbf{G}}]^{-1} \mathbf{1}_k. \tag{5.29}$$

5.3.2 Blind Spatio-Temporal Channel Estimation [134]

In all these space-time blind and group-blind detectors we have to obtain the spatio-temporal signature waveform $\tilde{\mathbf{c}}_k$, which is unknown to the receiver, because we only have the *prior* knowledge of $\mathbf{c}_k$, rather than that of the spatio-temporal waveform $\tilde{\mathbf{c}}_k$. Therefore, we have to estimate the CIR $\mathbf{h}_k$ based on the *signal subspace*, *noise subspace* and on the explicit knowledge of $\mathbf{c}_k$. For the sake of obtaining the spatio-temporal waveform $\tilde{\mathbf{c}}_k$, we exploit the orthogonality between the *noise* and the *signal* subspaces when estimating the CIR $\mathbf{h}_k$. More specifically, the *noise subspace* vectors contained by the matrix $\mathbf{U}_n$ are orthogonal to $\tilde{\mathbf{c}}_k$, hence we can estimate the CIR $\mathbf{h}_k$ by minimizing the noise-related Eucledian norm $\| \mathbf{U}_n^H (\mathbf{h}_k \otimes \mathbf{c}_k) \|^2$, which in fact should be zero owing to the above-mentioned orthogonality. However, in conjunction with the antenna array, the rank of the noise subspace $\mathbf{U}_n$ is significantly higher than that of the signal space $\mathbf{U}_s$. Hence, for the sake of reducing the associated complexity of the MUD, we estimate the CIR $\mathbf{h}_k$ by maximizing $\| \mathbf{U}_s^H (\mathbf{h}_k \otimes \mathbf{c}_k) \|^2$, which is equivalent to minimizing $\| \mathbf{U}_n^H (\mathbf{h}_k \otimes \mathbf{c}_k) \|^2$. Hence, we can express $\| \mathbf{U}_n^H (\mathbf{h}_k \otimes \mathbf{c}_k) \|^2$ as [134]:

$$\| \mathbf{U}_s^H (\mathbf{h}_k \otimes \mathbf{c}_k) \|^2 = \mathbf{h}_k^H (\mathbf{I}_L \otimes \mathbf{c}_k^H) \mathbf{U}_s \mathbf{U}_s^H (\mathbf{I}_L \otimes \mathbf{c}_k) \mathbf{h}_k. \tag{5.30}$$

Therefore, the CIR $\mathbf{h}_k$ can be estimated as the principal unit-norm eigenvector of the matrix $(\mathbf{I}_L \otimes \mathbf{c}_k^H)\mathbf{U}_s\mathbf{U}_s^H(\mathbf{I}_L \otimes \mathbf{c}_k)$, which is the eigenvector corresponding to the maximum eigenvalue of the matrix $(\mathbf{I}_L \otimes \mathbf{c}_k^H)\mathbf{U}_s\mathbf{U}_s^H(\mathbf{I}_L \otimes \mathbf{c}_k)$.

Finally, the operation of the blind and group-blind space-time MUD can be summarized as seen in Table 5.1.

Operation of the blind and group blind space-time MUD $\mathbf{X} = [\mathbf{r}_1, \mathbf{r}_2, \ldots, \mathbf{r}_M]$
1. Compute the spatio-temporal received samples' autocorrelation matrix $\mathbf{R} = \frac{1}{M}\mathbf{r}\mathbf{r}^H$;
2. Compute the EVD of the matrix $\mathbf{R}$, yielding: $\mathbf{R} = \mathbf{U}_s\mathbf{\Lambda}_s\mathbf{U}_s^H + \sigma^2\mathbf{U}_n\tilde{\mathbf{U}}_n^H$;
3. Blind channel estimation $\mathbf{h}_k = \text{max-eigenvector}\{(\mathbf{I}_L \otimes \mathbf{c}_k^H)\mathbf{U}_s\mathbf{U}_s^H(\mathbf{I}_L \otimes \mathbf{c}_k)\}$; $\tilde{\mathbf{c}}_k = \mathbf{h}_k \otimes \mathbf{c}_k, \quad k = 1 \ldots \tilde{K}$;
4. Construct the matrix $\tilde{\mathbf{G}}$ using $(\tilde{\mathbf{c}}_1, \ldots, \tilde{\mathbf{c}}_{\tilde{K}})$;
5. Form the weight vectors of the blind and group-blind MUDs according to Eq.(5.27), Eq.(5.28), and Eq.(5.29).

Table 5.1: The operation of the blind and group-blind space-time multiuser detector.

5.3.3 Performance of Blind and Group-Blind Spatio-Temporal DS-CDMA Multiuser Detection

In this section we investigate the attainable performance of a DS-CDMA system invoking diversity reception antenna array in conjunction with blind and group-blind space-time multiuser detectors. The antenna array has three elements, *i.e.* we have $L = 3$, and the spatio-temporal CIR of the 3-element system, namely $\mathbf{h}_k = [h_{k1}, h_{k2}, h_{k3}]$ obeys the non-dispersive Rayleigh fading channel model [7]. Furthermore, the antenna elements' fading coefficients h_{ki}, $i = 1, 2, 3$ are also statistically independent of each other, which implies that the array elements are sufficiently far apart. The system supported $K = 10$ users and employed m-sequence based spreading codes having a length of $N = 15$ chips. Figure 5.8 shows the attainable BER performance. We can observe in this figure that the group-blind multiuser detector benefitting from the prior knowledge of the $\tilde{K} = 7$ users' signature waveforms has a 2dB SNR gain over the blind multiuser detector at a BER of 10^{-4}. Furthermore, the blind and group-blind space-time MUDs equipped with the subspace based CIR estimator perform only slightly worse than the estimator exploiting the perfect knowledge of the CIR. More specifically, the associated performance degradation imposed by the channel estimator error is negligible. Finally, Figure 5.9 portrays the Mean Square Error (MSE) performance of the subspace based spatio-temporal estimator when we carry out the EVD operations after receiving $M = 200$ spatio-temporal samples, which demonstrates that the subspace based CIR estimator is capable of accurately tracking the channel.

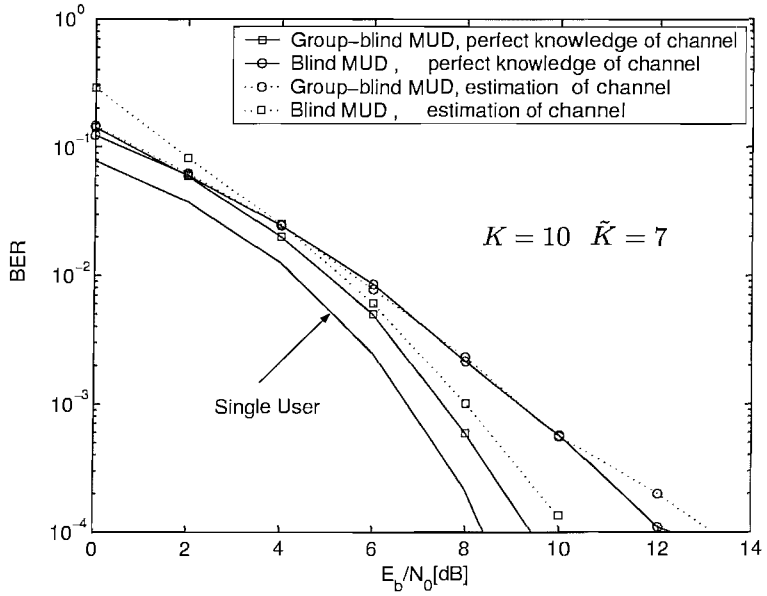

Figure 5.8: BER versus E_b/N_0 performance of the blind and group-blind space-time DS-CDMA MUDs using both perfect and subspace-estimated CIRs. The spreading factor of the temporal m-sequence was $N = 15$. A total of $K = 10$ users were supported and the group-blind spatio-temporal MUD benefitted from the knowledge of $\tilde{K} = 7$ spreading codes.

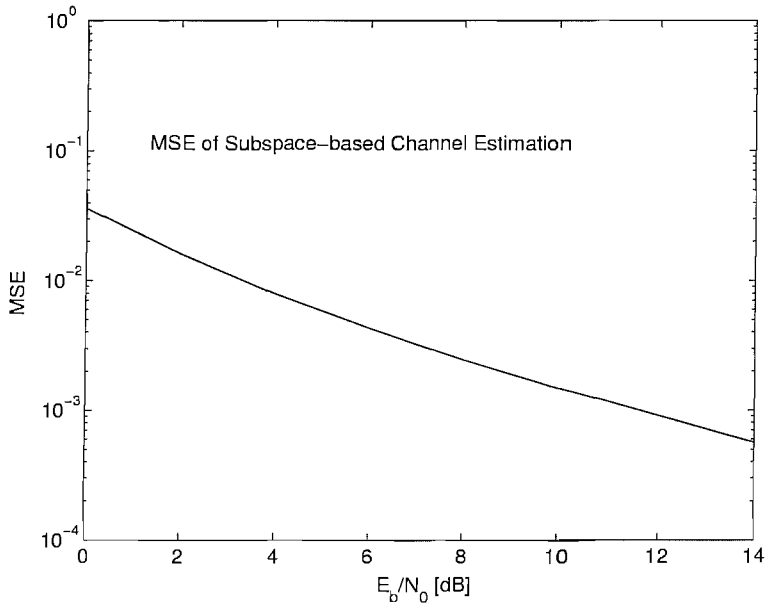

Figure 5.9: MSE performance of the subspace-based CIR estimator of the 3-element diversity receiver array aided DS-CDMA system using $K = 10, \tilde{K} = 7, N = 15$.

5.4 Semi-Blind and Group-Blind Multiuser Detection for the MC-CDMA Uplink

5.4.1 System Model

Having considered single-carrier DS-CDMA in Section 5.2, let us now consider the employment of a K-user MC-CDMA system in the uplink. We assume that a total of K users are supported and that $\tilde{K}$ of them are roaming in the reference cell, where their signature sequence are known to the Base Station (BS). We assume furthermore that the signature waveforms of the $\bar{K} = K - \tilde{K}$ other-cell users are unknown. BPSK modulation was invoked. The modulating symbols of $b_k \in \{-1, +1\}$ having a duration of T_b are first spread using a user-specific spreading sequence $\mathbf{c}_k = [c_{k,1}, c_{k,2}, \ldots, c_{k,N}]$ of length N, where we have $\mathbf{c}_k \cdot \mathbf{c}_k^H = 1$. For simplicity, in our investigations we assume that frequency-domain spreading aided OFDM using N subcarriers was invoked [4], where N consecutive chips of the MC-CDMA spreading sequences were mapped to N different subcarriers during an OFDM symbol and hence the OFDM symbol duration was $T_s = T_b$. The frequency-domain (FD) spread OFDM bit-vector of N subcarriers can be expressed as $\mathbf{s}_k = \mathbf{c}_k b_k = [s_1, s_2, ...s_N]$. Then the Inverse Fast Fourier Transform (IFFT) is invoked for modulating the N subcarriers by the spread information bits $\mathbf{s}_k$ [4]. This signal is transmitted through a multipath fading channel, which is assumed to have L paths, hence the CIR can be expressed as:

$$h_k(t) = \sum_{\ell=0}^{L-1} h_{k,\ell} \cdot \delta(t - mT_c), \tag{5.31}$$

where $h_{k,\ell}$ is the complex-valued channel tap magnitude experienced by the signal of the kth user in the ℓth path, which obeys Rayleigh fading, while $T_c = T_b/N$ is the chip-duration. We assume that a sufficiently long cyclic prefix is incorporated in the OFDM symbol prior to transmission for the sake of compensating for both the asynchronous delay differences of the different users as well as for the delay-spread-induced inter-OFDM-symbol interference imposed by the dispersive channel [4]. At the receiver, the samples of the received signal corresponding to the cyclic prefix are first removed and N-point FFT is invoked for demodulating the remaining N samples [4]. Hence the received signal can be expressed in vectorial form as $\mathbf{r} = [r_1, r_2, \ldots, r_N]^T$,

$$\mathbf{r} = \sum_{k=1}^{K} \mathbf{S}_k \cdot \mathbf{H}_k + \mathbf{n} = \mathbf{G} \cdot \mathbf{b} + \mathbf{n}, \tag{5.32}$$

where $\mathbf{H}_k = [H_{k,0}, H_{k,1}, \ldots, H_{k,N}]^T$ denotes the frequency domain channel transfer function and $\mathbf{S}_k$ is a diagonal matrix given by $\mathbf{S}_k = diag\{\mathbf{s}_k\}$. Again, since we assume that a sufficiently long cyclic prefix was inserted, no OFDM intersymbol interference (ISI) is incurred. Hence $\mathbf{H}_k$ can be expressed as the N-point DFT of $\mathbf{h}_k = [h_{k,0}, \ldots, h_{L-1}]^T$, where the operator $[\ ]^T$ denotes the matrix transpose. More explicitly, we have $\mathbf{H}_k = \mathbf{F}_L \cdot \mathbf{h}_k$, where $\mathbf{F}_L$ is an $(N \times L)$-dimensional matrix, which is given by the first L columns of the

DFT matrix $\mathbf{F}$ formulated as [135]:

$$\mathbf{F} = \begin{pmatrix} 1 & 1 & \dots & 1 \\ 1 & e^{-j2\pi/N} & \dots & e^{-j2\pi(N-1)/N} \\ \vdots & \vdots & \ddots & \vdots \\ 1 & e^{-j2\pi(N-1)/N} & \dots & e^{-j2\pi(N-1)(N-1)/N} \end{pmatrix}. \tag{5.33}$$

Hence the effective signature waveform of the kth user, which is constituted by the convolution of the spreading codes and the CIR, can be expressed as: $\mathbf{g}_k = \mathbf{C}_k\mathbf{H}_k$, where $\mathbf{C}_k = diag\{\mathbf{c}_k\}$. The matrix $\mathbf{G}$ in Eq.(5.32) is an $(N \times K)$-dimensional matrix comprising the channel's complex fading factors and the spreading signatures of all the K users, hence we have $\mathbf{G} = [\mathbf{g}_1, \mathbf{g}_2, \dots, \mathbf{g}_K]$. The vector $\mathbf{b} = [b_1, b_2, \dots, b_N]^T$ is the data vector and $\mathbf{n}$ is the white Gaussian noise vector associated with the covariance matrix of $\sigma^2\mathbf{I}_N$, where $\mathbf{I}_N$ denotes the $(N \times N)$-dimensional identity matrix.

5.4.2 Blind Channel Estimation for MC-CDMA

In this section we will consider subspace based blind channel estimation, as well as semi-blind and group-blind linear multiuser detection invoking rank estimation. Let us first consider the underlying blind channel estimation philosophy. When the background noise is white, we may invoke the EVD of the autocorrelation matrix of the received MC-CDMA signal vector $\mathbf{r}$. Upon extending the single-carrier DS-CDMA philosophy of Section 5.2 [62, 130] to our MC-CDMA scenario, the corresponding eigendecomposition is given by:

$$\begin{aligned} \mathbf{R} &= E\{\mathbf{r}\mathbf{r}^H\} = \mathbf{G}\mathbf{G}^H + \sigma^2\mathbf{I}_N \\ &= \mathbf{U}_s\mathbf{\Lambda}_s\mathbf{U}_s^H + \sigma^2\mathbf{U}_n\mathbf{U}_n^H, \end{aligned} \tag{5.34}$$

where the superscript $(\ )^H$ denotes the conjugate transpose of a matrix. Since the matrix $\mathbf{G}$ has a full column rank of $r = K$, the matrix $\mathbf{G}\mathbf{G}^H$ in Eq.(5.34) has a rank of r. Therefore, in Eq.(5.34) $\mathbf{\Lambda}_s = diag(\lambda_1, \lambda_2, \dots, \lambda_r)$ contains the r largest eigenvalues of $\mathbf{R}$ in descending order (*i.e.* we have $\lambda_1 \geq \lambda_2 \geq \dots \geq \lambda_r > \sigma^2$), $\mathbf{U}_s = [\mathbf{u}_1 \dots \mathbf{u}_r]$ contains the corresponding orthonormal eigenvectors, while $\mathbf{U}_n = [\mathbf{u}_{r+1} \dots \mathbf{u}_N]$ contains the $(N - r)$ number of orthonormal eigenvectors that correspond to the eigenvalue σ^2. The channel response $\mathbf{h}_k$ can be estimated by exploiting the orthogonality between the signal space and the noise space. Specifically, since $\mathbf{U}_n$ is orthogonal to the column space of $\mathbf{G}$, while $\mathbf{g}_k$ is in the column space of $\mathbf{G}$, we have:

$$\mathbf{U}_n^H\mathbf{g}_k = \mathbf{U}_n^H\mathbf{C}_k\mathbf{F}_L\mathbf{h}_k = 0. \tag{5.35}$$

Hence, an estimate of the CIR $\mathbf{h}_k$ can be obtained by computing the minimum eigenvector of the matrix $(\mathbf{F}_L^H\mathbf{C}_k^H\mathbf{U}_n\mathbf{U}_n^H\mathbf{C}_k\mathbf{F}_L)$, which constitutes a necessary condition for such a channel estimate to be unique, when we have $L \leq N - K$. Furthermore, note that there is an arbitrary phase ambiguity in the estimate of the CIR, but we can remove this specific phase ambiguity with the aid of a short cyclic prefix using the technique proposed in [136].

5.4.3 Rank Estimation for MC-CDMA

Based on the estimated eigenvalues $\mathbf{\Lambda} = [\lambda_1, \lambda_2, \ldots, \lambda_N]$, using the Akaike information theoretic criterion (AIC) [26,62], the rank of the signal space (*i.e.* the number of active users in the system), can be estimated [26,62]. The quantities invoked in the AIC are defined as follows:

$$\mathrm{AIC}(k) = (N-k) \cdot M \cdot \ln\alpha(k) + k \cdot (2N-k), \tag{5.36}$$

where M is the number of data bits used for the estimation of the total number of users supported, namely K, and M is conveniently chosen to be the transmission burst length. Furthermore, $\alpha(k)$ can be expressed as [26]:

$$\alpha(k) = \frac{(\sum_{i=k+1}^{N} \lambda_i)/(N-k)}{(\Pi_{i=k+1}^{N} \lambda_i)^{1/(N-k)}}. \tag{5.37}$$

The estimate $\hat{K}$ of the rank K of the signal space is given by that particular value of k which minimizes Eq.(5.36) [26]. Hence we have

$$\hat{K} = \arg \min_{0 \le k \le N-1} \{\mathrm{AIC}(k)\}. \tag{5.38}$$

5.4.4 Semi-Blind and Group-Blind MUD for MC-CDMA

Again, similar to Eq.(5.6) of Section 5.2, the linear blind MMSE multiuser detector, which assumes only the knowledge of the reference user's signature waveform plus knowledge of timing and CIR (via $\mathbf{g}$) but not of the other users is given by [62]:

$$\mathbf{w}_k = \frac{1}{\mathbf{g}_k^T \mathbf{U}_s \mathbf{\Lambda}_s^{-1} \mathbf{U}_s^H \mathbf{g}_k} \mathbf{U}_s \mathbf{\Lambda}_s^{-1} \mathbf{U}_s^H \mathbf{g}_k. \tag{5.39}$$

Furthermore, the so-called form-II MUD weight solution [63] can be expressed in the form of Eq.(5.8) given in Section 5.2.2. The corresponding bit estimate of user k may be written as [63]:

$$\mathbf{w}_k = \mathbf{U}_s \mathbf{\Lambda}_s^{-1} \mathbf{U}_s^H \tilde{\mathbf{G}} [\tilde{\mathbf{G}}^H \mathbf{U}_s \mathbf{\Lambda}_s^{-1} \mathbf{U}_s^H \tilde{\mathbf{G}}]^{-1} \mathbf{1}_k \tag{5.40}$$

$$\hat{b}_k = \mathrm{sgn}\{\mathrm{Re}(\mathbf{w}_k^H \mathbf{r})\}, \quad k = 1, \ldots, \tilde{K}. \tag{5.41}$$

Hence, we require the knowledge of the signature waveforms of the group of $\tilde{K}$ users supported within the reference cell, in order to construct $\tilde{\mathbf{G}}$. Finally, the operation of this receiver is summarized in Table 5.2.

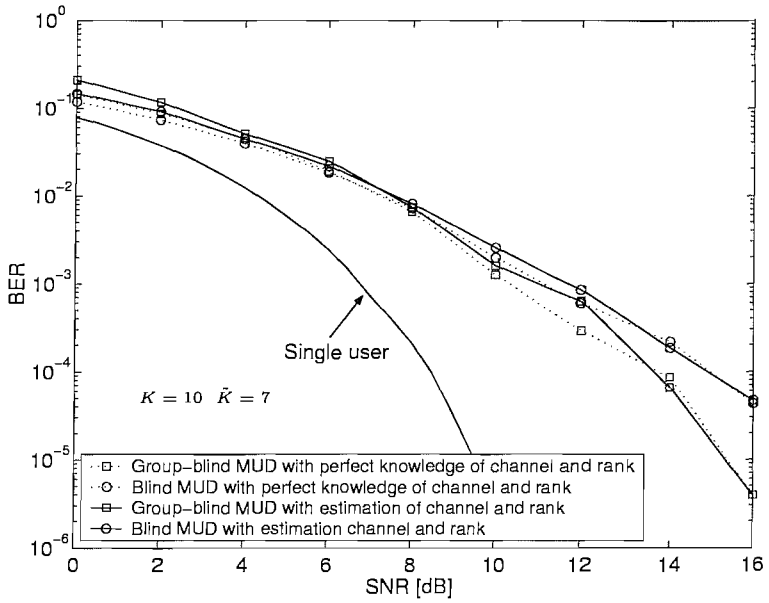

Figure 5.10: BER performance of the various MC-CDMA MUDs considered. Both the scenario of having the perfect knowledge of the complex-valued CIR coefficients and the rank as well as their estimation was characterized. Walsh codes having a spreading factor of $N = 16$ were employed and $K = 10$, $\tilde{K} = 7$ users were supported. BPSK transmission and an $L = 3$-path chip-spaced independent Rayleigh fading channel were used. All system parameters are summarized in Table 5.3.

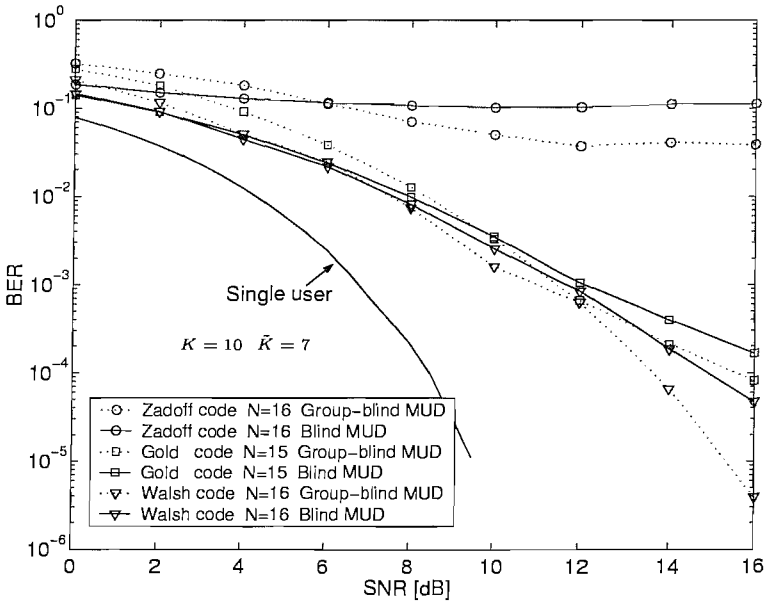

Figure 5.11: BER performance comparison of blind and group-blind multiuser detectors MC-CDMA MUDs, when Walsh, Gold and Zadoff-Chu codes were invoked and $K = 10$, $\tilde{K} = 7$ users were supported. BPSK transmission and an $L = 3$-path chip-spaced independent Rayleigh fading channel were used. All system parameters are summarized in Table 5.3.

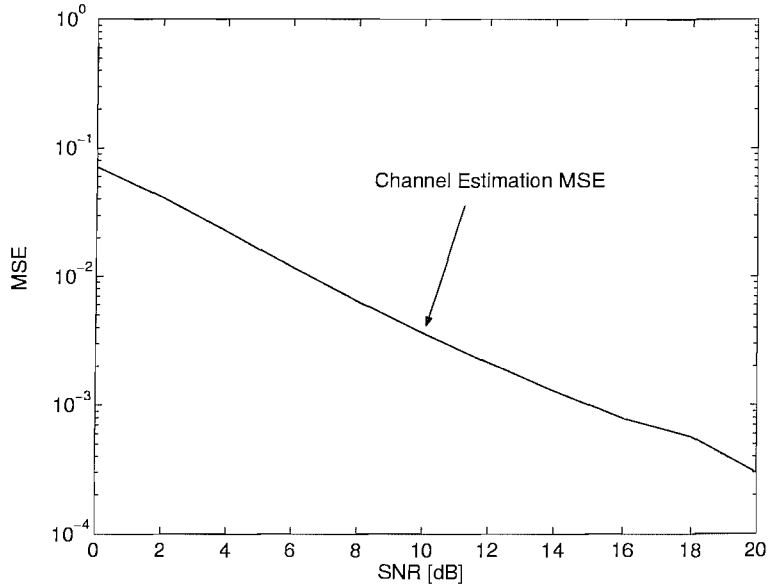

Figure 5.12: MSE performance of the blind CIR estimator in the context of MC-CDMA, when Walsh codes having a spreading factor of $N = 16$ were employed and $K = 10$ users were supported. BPSK transmission and an $L = 3$-path chip-spaced independent Rayleigh fading channel were used. All system parameters are summarized in Table 5.3.

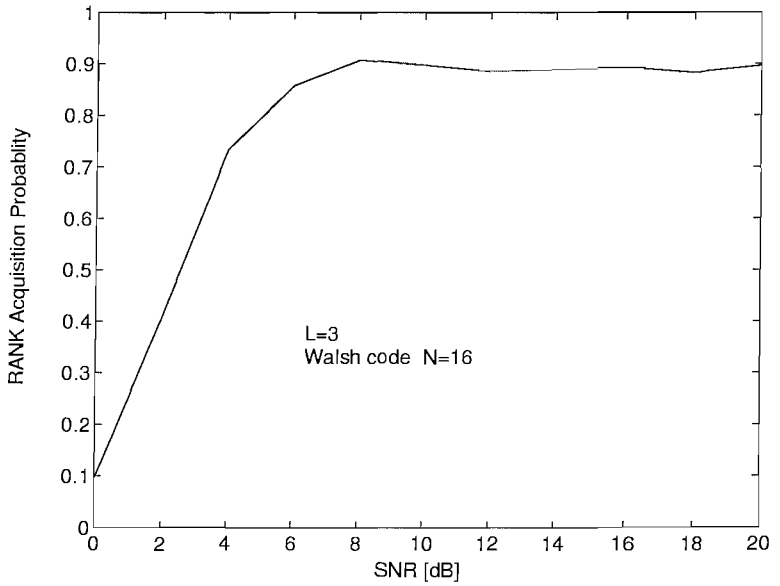

Figure 5.13: Correct rank acquisition probability in the context of MC-CDMA, when Walsh codes having a spreading factor of $N = 16$ were employed and $K = 10$ users were supported. BPSK transmission and an $L = 3$-path Rayleigh fading channel were used. All system parameters are summarized in Table 5.3.

Operation of the MUD in white noise based on the received signal samples $\mathbf{X} = [\mathbf{r}_1, \mathbf{r}_2, \ldots, \mathbf{r}_M]$
1. Compute the received samples' autocorrelation $\mathbf{R} = \frac{1}{M}\mathbf{X}\mathbf{X}^H$;
2. Compute the eigen-decomposition of $\mathbf{R} = \mathbf{U}_s\mathbf{\Lambda}_s\mathbf{U}_s^H + \sigma^2\mathbf{U}_n\mathbf{U}_H$;
3. Rank estimation $\hat{K} = \arg \min_{0 \le k \le N-1} \{\text{AIC}(k)\}$;
4. Blind channel estimation $\mathbf{h}_k = \text{min-eigenvector}(\mathbf{F}_L^H\mathbf{C}_k^H\mathbf{U}_n\mathbf{U}_n^H\mathbf{C}_k\mathbf{F}_L)$ $\tilde{\mathbf{g}}_k = \mathbf{C}_k\mathbf{F}_L\mathbf{h}_k, \quad k = 1 \ldots \tilde{K}$ form $\tilde{\mathbf{G}}$ using $(\mathbf{g}_1, \ldots, \mathbf{g}_{\tilde{K}})$;
5. Form the detector according to Eq.(5.39) and Eq.(5.40);

Table 5.2: Operation of the blind and group-blind MC-CDMA multiuser detector communicating over a dispersive channel.

Parameters	**Value**
Chips-spaced CIR length L	3
Normalized Dopper frequency	0.01
Short cyclic prefix	2 chips
Burst length M	256
Number of subcarriers N	16
Spreading gain	16

Table 5.3: Basic simulation parameters for the semi-blind and group-blind MC-CDMA MUDs.

5.4.5 Performance of the Semi-Blind and Group-Blind MC-CDMA Multiuser Detector

In this section we provide computer simulation results for characterizing the performance of the proposed blind and group-blind multiuser detectors, when communicating over a multipath Rayleigh fading channel having $L = 3$ paths. More specifically, the fading factors of each complex-valued path are generated according to the Rayleigh distribution, where the paths are normalized so that each user's signal arrives at the receiver with an equal power, *i.e.* we have $\| \mathbf{h}_k \|^2 = 1$. The complex-valued fading coefficients are assumed to be static during a block of $M = 256$ MC-CDMA bits, which is the transmission burst length, and the number of subcarriers as well as the spreading gain are $N = 16$.

In Fig. 5.10 we observe that both the semi-blind and group-blind multiuser detectors are capable of achieving a performance, which is close to that associated with a perfect knowledge of both the channel coefficients and the number of users K. More specifically, the BER performance degradation incurred by the imperfect CIR estimation technique of Section 5.4.2 and rank estimation algorithm of Section 5.4.3 was found negligible.

Fig. 5.11 characterizes the BER performance of the semi-blind and group-blind multiuser detectors considered in conjunction with different spreading codes. Observe that

the performance of the Zadoff-Chu codes [4] is the worst, while Walsh codes achieved the best performance.

Finally, Fig. 5.12 portrays the Mean Square Error (MSE) performance of the subspace-based CIR estimator of Section 5.4.2, while Fig. 5.13 characterizes the achievable correct rank acquisition probability based on the AIC algorithm of Section 5.4.3.

5.5 Chapter Conclusions

When considering a DS-CDMA system communicating over an AWGN channel, the family of blind and group-blind multiuser detectors is capable of suppressing the MAI and hence it is robust against the near-far effect. As seen in Figure 5.3, the group-blind multiuser detector exhibited a better performance, when more signature waveforms were known to the receiver. When considering a DS-CDMA communication system benefitting from the diversity gain of an antenna array having sufficiently widely spaced elements, the space-time blind and group-blind multiuser detectors of Section 5.3 are capable of achieving a similar performance to that attained with the aid of perfect knowledge of the CIR coefficients. Furthermore, we investigated the attainable performance of both semi-blind and group-blind multiuser detector schemes in the context of the MC-CDMA uplink using a short cyclic prefix, which assisted us in removing the effects of ISI and in resolving the phase ambiguity associated with the blind channel estimation process. In our study, both the blind and group-blind multiuser detectors of Section 5.4 were shown to be capable of achieving a similar performance to that attained with the aid of perfect knowledge of the CIR coefficients, spreading codes and the rank information, *i.e.* the number of users supported. Furthermore, the Walsh spreading code based MC-CDMA scheme outperformed the corresponding Gold and Zadoff-Chu code based systems.

CHAPTER 6

GA-RBF Assisted Multiuser Detection for DS-CDMA

6.1 Introduction

Direct Sequence Code Division Multiple Access (DS-CDMA) [10] is the access technology of all the third generation (3G) systems. However, there are a number of problems associated with transmitting at high bit rates, such as $2Mb/s$, since a high grade of channel-induced dispersion is experienced, which results in Inter Symbol Interference (ISI) and Inter Chip Interference (ICI). Therefore, in order to jointly mitigate the effects of the ISI, ICI and Multiuser Interference (MUI), the employment of multiuser equalization or detection (MUD) techniques has been proposed in [22].

The GA-based MUD was first proposed by Juntti *et al.* [82] for a synchronous CDMA system communicating over an Additive White Gaussian Noise (AWGN) channel. Yen *et al.* [84,86] further improved the performance of the GA-based MUD, demonstrating that the performance of the GA-aided MUD approaches the single-user performance bound at a significantly lower computational complexity, than that of Verdu's optimum MUD [22].

The tree-search M-algorithm based MUD was described in [59]. In reference [59], the M-Algorithm (MA) and T-Algorithm (TA) assisted MUD employed at the output of receiver's Matched Filter were analyzed. These suboptimal detectors exhibit a low complexity in comparison to the full tree-search assisted Viterbi Algorithm (VA) based MUD [22].

In this chapter we first comparatively study the GA assisted MUD and the MA assisted MUD in the context of a synchronous DS-CDMA system, when transmitting over non-dispersive AWGN channels. We will evaluate their complexity and their achievable

performances. Furthermore, we will compare their near-far resistance in the case of imperfect power control.

After invoking the MA assisted MUD, we will consider GA-RBF assisted multiuser detection. It is important to note that as far as the receiver is concerned, its actions required for removing the effects of interference and noise, regardless whether the interference was caused by K number of simultaneous users, for example, or by K distinct propagation paths. Hence a whole host of well-documented solutions are available from the literature of conventional channel equalization, which can be invoked for MUD. In this chapter we focus our attention on a specific class of multiuser equalizers, namely on the family of Radial Basis Function (RBF) assisted equalizers [137]. The RBF equalizer was proposed by Chen *et al.* [138] [139], which has the potential of approaching the performance of the optimum Bayesian *maximum a posteriori* (MAP) equalizer [138]. The justification for favoring this particular class of equalizers is that they exhibit a range of advantages in comparison to conventional channel equalizers. Specifically, a conventional equalizer attempts to mimic the inverse of the channel's dispersive effects and then filter the received signal appropriately for the sake of removing the effects of ISI. By contrast, the actions of the RBF equalizer [137] are reminiscent of a 'classification' task. More explicitly, the transmitted phasors are dispersed by the channel. A simple example of this is, when BPSK modulated binary phasors are transmitted over a channel having a symbol-spaced, equal-weight two-tap Channel Impulse Response (CIR). In this case the received phasors may assume four different values, since the received signal is now constituted by the convolution of the transmitted bits with the two-tap CIR. When using the RBF assisted equalizer, instead of conventional filtering-based equalization, the equalizer attempts to classify fading and noise-contaminated received phasors into one of these legitimate channel output states for the sake of removing the effects the channel-induced dispersion. One of the most attractive properties of the RBF equalizer is that even if the above-mentioned four channel-output states cannot be separated by a single line into distinct classes corresponding to the two binary values of logical '1' and '0', their classification-based decision may be ensured without decision errors [137]. By contrast, a conventional receiver using a linear decision boundary would be prone to erroneous decisions. The implementation of RBF based MUDs has been originally proposed by the Edinburgh research team [29], [140], [141] and was further investigated in [142]. However, until recently its high complexity has hindered its wide-spread implementation. For the sake of reducing its complexity, in this chapter we propose the employment of a Genetic Algorithm (GA) as well as RBF assisted MUD and investigate its performance. We invoke the GA for selecting a specific subset of the RBF centers, which have the highest contribution to the GA-RBF based MUD's performance, while discard the RBF centers, which have a low contribution. Therefore we can reduce the number of RBF centers from 2^K to P, where P is the population size of the GA. Our goal is to minimize the associated MUD performance degradation, while maintaining an affordable complexity. Hence, again we invoke the GA for selecting a subset of the RBF centers, which have the highest contribution to the GA-RBF based MUD's output formulated in Equation 6.27.

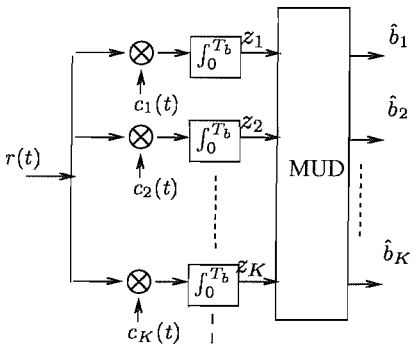

Figure 6.1: Schematic of the DS-CDMA MUD invoked at the output of the K users'matched filter

During the GA assisted RBF center selection process, the specific centers, which have a low contribution to the output of the GA-RBF MUD formulated in Equation 6.27 are discarded. Therefore we can reduce the number of RBF centers from 2^K to P, where P is the population size of the GA. Our goal is to minimize the associated MUD performance degradation, while maintaining an affordable complexity.

In this chapter, Section 6.2 describes the GA assisted MUD and MA assisted MUD, and comparatively studies their associated performances. Section 6.3 investigated the performance of GA and RBF assisted MUD. Finally, Section 6.4 offers our conclusions.

6.2 GA versus M-algorithm Assisted Multiuser Detection

6.2.1 System Model

Consider a synchronous system supporting K users. The output vector $\mathbf{Z}$ of the bank of matched filters portrayed in Figure 6.1 can be formulated similarly to Equation 1.3 as [22]:

$$\begin{aligned} \mathbf{Z} &= [z_1, \ldots, z_K]^T \\ &= \mathbf{RAb} + \mathbf{n}, \end{aligned} \tag{6.1}$$

where we have

$$\begin{aligned} \mathbf{A} &= \text{diag}[\sqrt{E_{b1}}, \ldots, \sqrt{E_{bK}}] \\ \mathbf{b} &= [b_1, \ldots, b_K]^T \\ \mathbf{n} &= [n_1, \ldots, n_K]^T \end{aligned} \tag{6.2}$$

$$\mathbf{R} = \begin{bmatrix} 1 & \rho_{12} & \cdots & \rho_{1K} \\ \rho_{21} & 1 & \cdots & \rho_{2K} \\ \vdots & \vdots & \vdots & \vdots \\ \rho_{K1} & \rho_{K2} & \cdots & 1 \end{bmatrix} \tag{6.3}$$

and E_{bk} is the energy-per-bit, the superscript T denotes the matrix transpose and the elements ρ_{jk} of the matrix $\mathbf{R}$ are the cross-correlation coefficients of the spreading codes between the ith user's signature waveform $c_i(t)$ and jth user's signature waveform $c_j(t)$,

which can be expressed as:

$$\rho_{jk} = \int_0^{T_b} c_j(t)c_k(t)dt. \tag{6.4}$$

According to [22], the optimum multiuser detector will maximize the following function:

$$\Omega(\mathbf{b}) = 2\mathbf{Z}^T\mathbf{Ab} - \mathbf{b}^T\mathbf{ARAb}, \tag{6.5}$$

where we define $\mathbf{H} = \mathbf{A}^T\mathbf{RA}$. Hence Equation 6.5 can be written as:

$$\Omega(\mathbf{b}) = 2\mathbf{Z}^T\mathbf{Ab} - \mathbf{b}^T\mathbf{Hb}. \tag{6.6}$$

Verdu's optimal multiuser detector [22] selects K-dimensional user vector $\hat{\mathbf{b}}$, which maximizes the objective function of

$$\hat{\mathbf{b}} = \arg\left\{\max_{\mathbf{b}}[2\mathbf{Z}^T\mathbf{Ab} - \mathbf{b}^T\mathbf{Hb}]\right\}, \mathbf{b} \in \{\mathbf{b}_j, j = 1, \ldots, 2^K\} \tag{6.7}$$

using an exhaustive search of the 2^K-dimensional search-space of a binary modulation scheme.

Equation 6.7 can be also expressed as:

$$\hat{\mathbf{b}} = \arg\left\{\max_{\mathbf{b}}\sum_{k=1}^{K} -m_k\right\}, \mathbf{b} \in \{\mathbf{b}_j, j = 1, \ldots, 2^K\} \tag{6.8}$$

where we have

$$m_k = -b_k[2r_k\sqrt{E_{bk}} - b_k\sqrt{E_{bk}} - 2\sum_{j=1}^{k-1} b_j H_{jk}. \tag{6.9}$$

Verdu's optimal detector will test the probability of all the 2^K number of legitimate hypotheses based on Equation 6.5 and select the maximum likelihood hypothesis as the decision vector. Again, we have a total of 2^K hypotheses in conjunction with Binary Phase Shift Keying (BPSK) modulation. The optimal tree-search based detector can be implemented by an exhaustive search based on Equation 6.8 can be performed by the Viterbi Algorithm (VA) [22, 59]. As shown in Figure 6.2, the VA computes all the accumulated path metric of search-tree corresponding to the K-dimensional user vector for each hypothesis based on Equation Equation 6.8 and selects the one, which has the maximum path-metric as the maximum-likelihood hypothesis. As expected, this full tree-search based algorithm is capable of achieving the optimum performance. However, its complexity is on the order of 2^K in conjunction with BPSK modulation, which is excessive when the number of users K is high. In order to reduce the complexity of the optimum MUD, let us now consider both the GA and MA assisted MUDs in following sections.

6.2.2 M-Algorithm

The GA algorithms have been described in Section 1.4.6, we will focus on the process of M-algorithm in this section. The philosophy of the that of the M-Algorithm is similar to

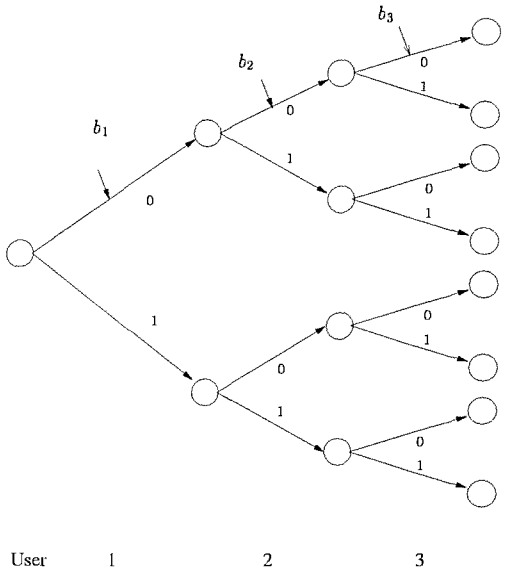

Figure 6.2: The full tree-search based Viterbi Algorithm for $K = 3$ users.

that of the VA characterised in Figure 6.2. In the VA all surviving paths are extended by adding the branch metrics to the path metrics during the full search of the tree, hence the VA based MUD has to evaluate 2^K number of hypotheses. By contrast, in the context of the MA, only the best $M < 2^K$ number of paths are retained during the tree search. All the other paths are dropped for the sake of reducing the complexity, which will lead to a performance degradation. Furthermore, for the case of $M = 2^{K-1}$, the MA based MUD becomes equivalent to the optimum VA based MUD, which is capable of finding the optimum K-bit user vector. When we have $M \ll 2^{K-1}$, the MA based MUD exhibits a low complexity, because the number of retained paths is reduced. Since only a subset of all the paths are retained, the MA based MUD cannot guarantee finding the specific optimum path, which has the maximum metric during the process of tree-search. This will inevitably lead to a performance degradation in comparison to that of the VA based MUD.

6.2.3 Simulation Results

The DS-CDMA system studied employed a random spreading code having a length of $N_c = 31$ in the context of BPSK modulation. For the sake of fair comparison, initially all the systems concerned were configured for maintaining the same complexity. Specifically, both GA and MA aided MUD will evaluate objective functions of Equations 7.11 and 6.8 the same number of times, respectively. Based on Section 1.4.6, we may conclude that the GA based MUD requires $(P \cdot Y)$ number of objective function evaluations. By contrast we argued in Section 6.2.2 that the MA based MUD requires $(K \cdot M)$ number of objective function evaluation.

From Figure 6.3 we can see that when we have $M = P \geq 16$, the GA based MUD outperforms the MA based MUD, although they have the same complexity, when supporting $K = 10$ users. However, in case of $M = P = 4$, the performance of the MA based

Parameters	Value
Modulation scheme	BPSK
Spreading code	Random Sequence
Spreading Gain N_c	31
GA's selection method	Fitness-proportionate
GA's mutation method	Standard binary mutation
GA's crossover method	Uniform crossover
GA's mutation probability p_m	0.1
GA's crossover probability p_c	1
Mating pool size T	5
Elitism	Yes
Incest Prevention	Yes

Table 6.1: The basic simulation parameters used by the GA assisted MUD aided DS-CDMA system

MUD is better than that of the GA aided MUD.

From Figures 6.4 and 6.5 we observe that the GA based MUD outperforms the MA based MUD also at a complexity of $M = P \geq 64$. Moreover, as seen in Figure 6.6, the MA based MUD has the edge over the GA based MUD when supporting $K = 40$ users. From Figures 6.3, 6.4 and 6.5 we can see that the performance of the GA based MUD degraded significantly, when the number of users K increases, because the GA's performance depends on the number of K-dimensional vectors in the search space, which hosts 2^K elements in a synchronous DS-CDMA system. When K increases, the search space becomes excessive, which results in a reduced-accuracy convergence for the GA assisted MUD, and leads an inevitable performance degradation of the GA assisted MUD, unless the affordable detection complexity is increased, resulting in an increased search space.

From Figure 6.7 we can observe that the GA assisted MUD exhibits a higher near-far resistance in comparison to the MA assisted MUD. When we had $\frac{E_{b1}}{E_{bk}} = -10dB$, the performance of the MA assisted MUD was degraded significantly. By contrast, the GA assisted MUD remained capable of maintaining the same performance.

6.3 GA-RBF Assisted Multiuser Detection

6.3.1 Radial Basis Function Networks

In this section, we will introduce the concept of the so-called *Radial Basis Function* RBF networks and highlight their architecture [137]. The RBF network [143] consists of three different layers, as shown in Figure 6.8. The input layer is constituted by p source nodes. A set of M nonlinear activation functions $\varphi_i, i = 1, \ldots, M$, constitutes the hidden second layer. The output of the network is provided by the third layer [137], which is comprised of output nodes. Figure 6.8 shows only one output node, in order to simplify our discussion. This construction is based on the basic neural network design. As suggested by the

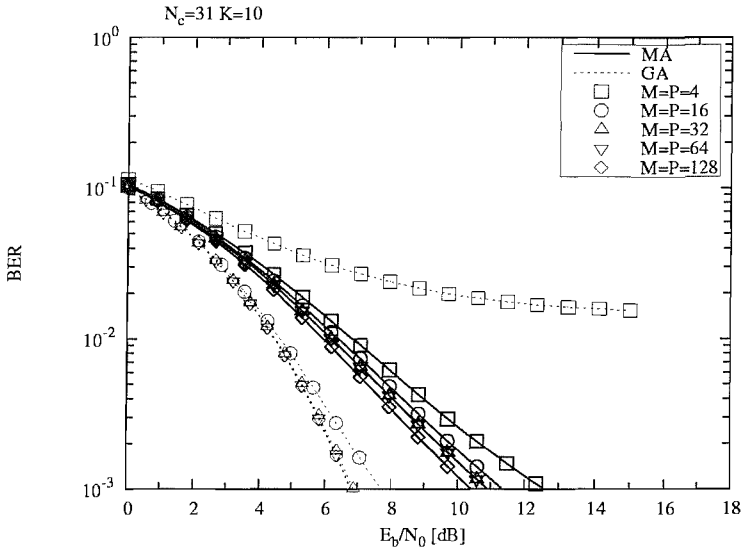

Figure 6.3: BER performance of the GA and MA assisted MUDs for transmission over AWGN channel in conjunction with different detection-complexity configurations, when supporting $K = 10$ users. All the other parameters are described in Table 6.1.

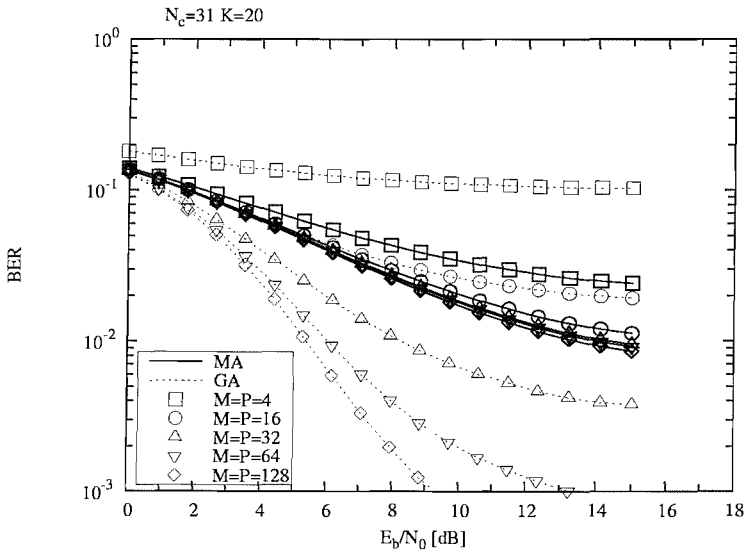

Figure 6.4: BER performance of the GA and MA assisted MUDs for transmission over AWGN channel in conjunction with different detection-complexity configurations, when supporting $K = 20$ users. All the other parameters are described in Table 6.1.

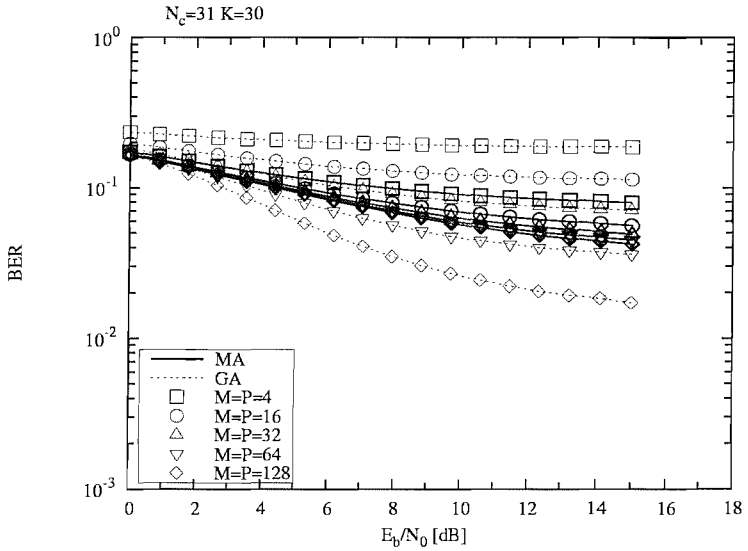

Figure 6.5: BER performance of the GA and MA assisted MUDs for transmission over AWGN channel in conjunction with different detection-complexity configurations, when supporting $K = 30$ users. All the other parameters are described in Table 6.1.

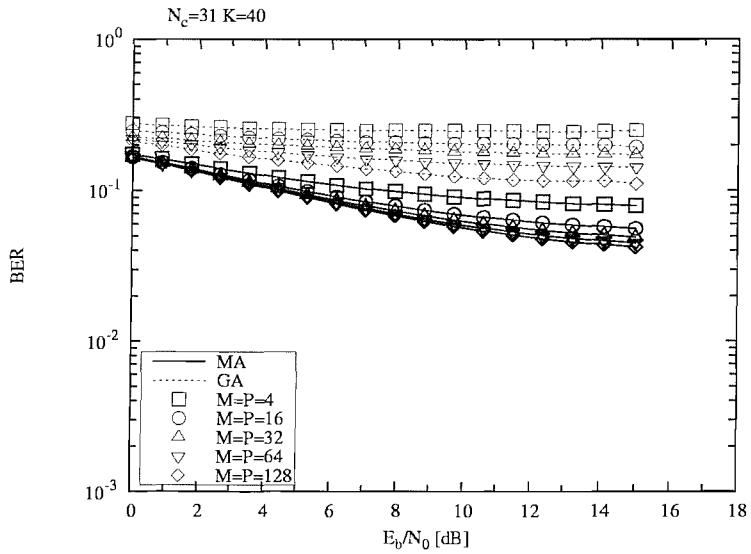

Figure 6.6: BER performance of the GA and MA assisted MUDs for transmission over AWGN channel in conjunction with different detection-complexity configurations, when supporting $K = 40$ users. All the other parameters are described in Table 6.1.

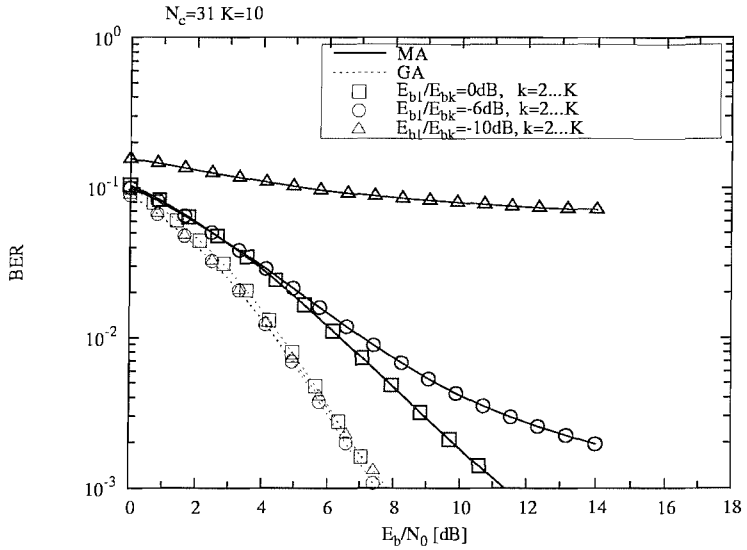

Figure 6.7: BER performance of the GA and MA assisted MUDs for transmission over AWGN channel in conjunction with different detection-complexity configurations, when supporting $K = 10$ users. These scenarios were studied namely when the desired user's signal power was the same as that of others, as well as -6dB and -10dB lower and the desired user was user 1. All the other parameters are described in Table 6.1.

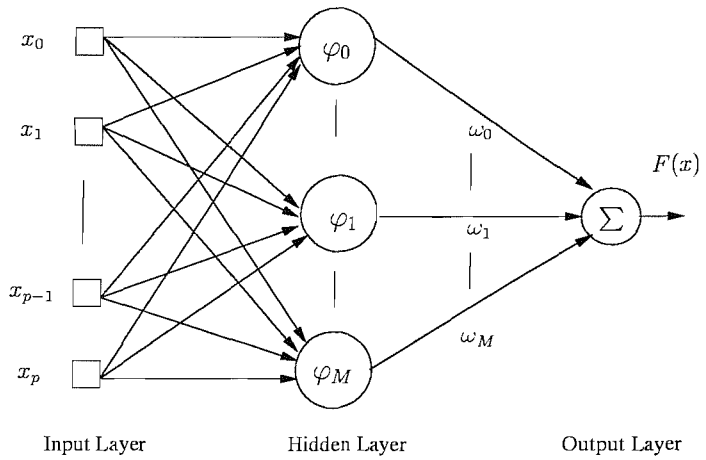

Figure 6.8: Architecture of a radial basis function network.

terminology, the activation functions in the hidden layer take the form of radial basis functions [143].

Radial functions are characterized by their responses that decrease or increase monotonically with distance from a central point, $\mathbf{c}$, i. e. as the Euclidean norm $\|\mathbf{x} - \mathbf{c}\|$ is increased, where $\mathbf{x} = [x_1\ x_2\ \ldots\ x_p]^T$ is the input vector of the RBF network. The central points in the vector $\mathbf{c}$ are often referred to as the RBF centers. Therefore, the radial basis functions take the form

$$\varphi_i(\mathbf{x}) = \varphi(\|\mathbf{x} - \mathbf{c}_i\|), \qquad i = 0, \ldots, M, \tag{6.10}$$

where M is the number of independent basis functions in the RBF network. This justifies the 'radial' terminology. A typical radial function is the Gaussian function which assumes

the form:

$$\varphi_i(\mathbf{x}) = exp\left(-\frac{\|\mathbf{x}-\mathbf{c}_i\|^2}{2\sigma_i^2}\right), \qquad i = 0, \ldots, M, \tag{6.11}$$

where $2\sigma_i^2$ is representative of the 'spread' of the Gaussian function that controls the radius of influence of each basis function. Figure 6.9 illustrates a Gaussian RBF, in the case of a scalar input, having a scalar centre of $c = 0$ and a spread or width of $2\sigma_i^2 = 1$.

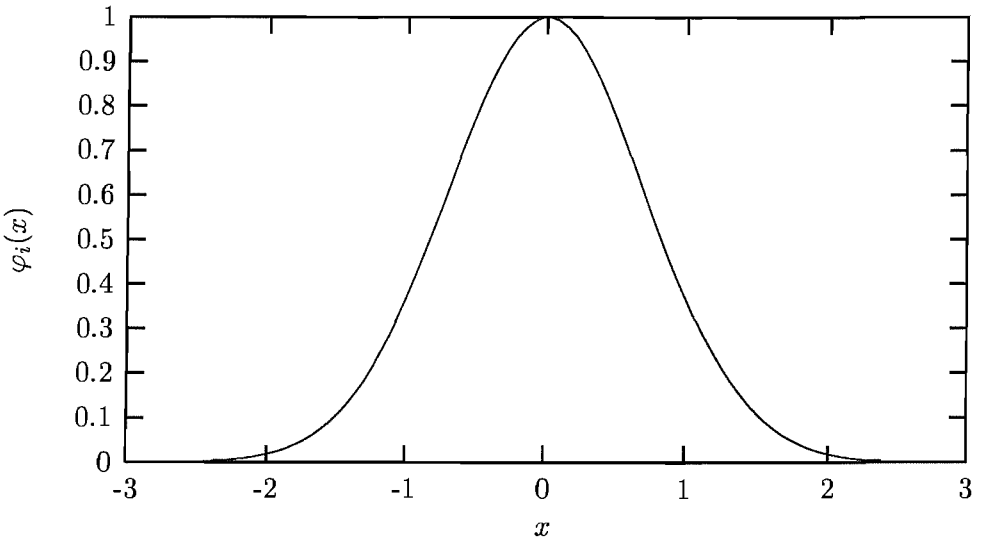

Figure 6.9: Gaussian radial basis function described by Equation 6.11 with centre $c_i = 0$ and spread of $2\sigma_i^2 = 1$.

Gaussian-like RBFs are localized, i. e. they give a significant response only in the vicinity of the centre and $\varphi(x) \to 0$ as $x \to \infty$. As well as being localized, Gaussian basis functions have a number of useful analytical properties, which will be highlighted in our following discourse.

Referring to Figure 6.8, the RBF network can be represented mathematically as follows:

$$F(\mathbf{x}) = \sum_{i=0}^{M} w_i \varphi_i(\mathbf{x}). \tag{6.12}$$

The bias b in Figure 6.8 is absorbed into the summation as w_0 by including an extra basis function φ_0, whose activation function is set to 1. Bishop [144] gave an insight into the role of the bias w_0 when the network is trained by minimizing the sum-of-squared error between the RBF network output vector and the desired output vector. The bias is found to compensate for the difference between the mean of the RBF network output vector and the corresponding mean of the target data evaluated over the training data set. The w_i is the so called RBF network weights.

Having described briefly the RBF network architecture, the next sections will present its design in context of multiuser detection.

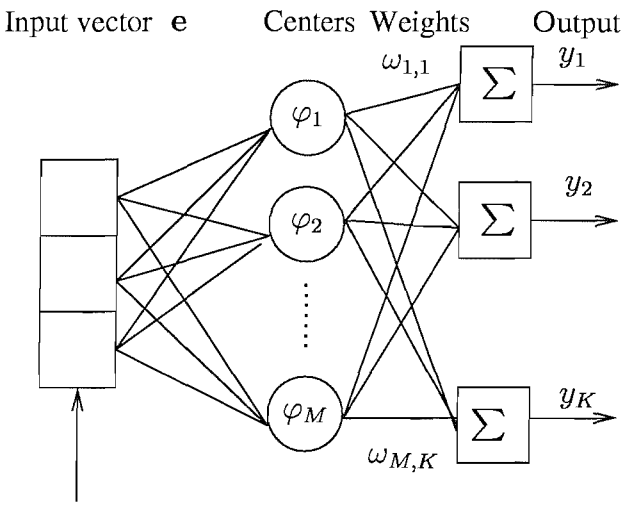

Figure 6.10: The architecture of RBF based MUD.

6.3.2 RBF based Multiuser Detection

In this section, we will extend the RBF network to RBF based MUD in context of a DS-CDMA system. The architecture of the RBF based MUD is shown in Fig 6.10. By comparing Figure 6.8 and 6.10, it become clear that the difference between the RBF based MUD and the RBF network is that the latter has multiple outputs rather a single output of RBF network. However, each output of the RBF based MUD is still constituted by an independent RBF network. Therefore, the each output of RBF based MUD can also be represented as follows:

$$y_k = \sum_{i=1}^{M} w_{i,k}\varphi_i(\mathbf{e}) \quad k = 1, 2, ...K \tag{6.13}$$

where $w_{i,k}$ denotes the weights of the RBF based MUD, and $\varphi_i(\mathbf{x})$ is the radial basis function in case of having a vector $\mathbf{e}$ as input, as well as a vector center v_i, where the $\varphi_i(e)$ is given by:

$$\varphi_i(\mathbf{e}) = exp(-\frac{\| \mathbf{e} - \mathbf{v}_i \|^2}{2\sigma_i^2}). \tag{6.14}$$

Each of the K outputs of Fig 6.10 corresponds to the output signal of one of the K users, where the $w_{i,k}$ provide the appropriate weighting for producing a high-confidence K-dimensional received bit vector. Having introduced briefly the RBF based MUD, we can observe that the RBF based MUD actually is a particular RBF network as we will highlight it later in the next section.

6.3.3 GA and RBF Assisted Multiuser Detection for Synchronous DS-CDMA

In this section, we will describe the philosophy of the proposed reduced-complexity GA-RBF assisted MUD scheme applied in the context of MUD and characterize its performance, when communicating over an Additive White Gaussian Noise (AWGN) channel in case of bit-synchronous DS-CDMA. First, we will introduce the discrete-time bit-synchronous DS-CDMA system model.

Discrete-Time Synchronous CDMA System Model

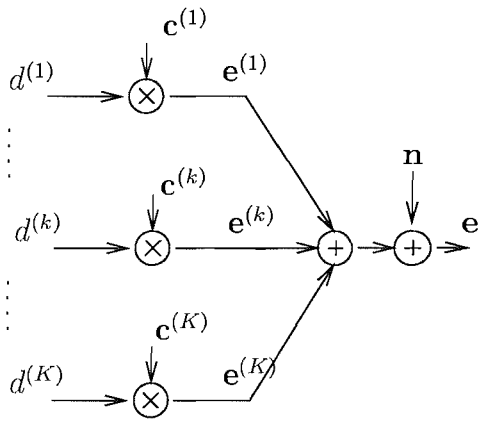

Figure 6.11: The basic DS-CDMA model

Let us consider a basic DS-CDMA system using a spreading code length of N and supporting K users, which is shown in Figure 6.11, assuming that the kth user's spreading code at symbol instant j is given by: $\mathbf{c}_j^{(k)} = [c_{j,T_c=1}^{(k)}, ..., c_{j,T_c=N}^{(k)}]^T$, where the term $[.]^T$ indicates the transpose operator. After spreading an input data bit d_j^k at the time instant j, the signal of the kth user becomes:

$$\mathbf{e}_j^{(k)} = \mathbf{c}_j^{(k)} \cdot d_j^{(k)}, \tag{6.15}$$

where $\mathbf{e}_j^{(k)} = [e_{j,T_c=1}^{(k)}, ..., e_{j,T_c=N}^{(k)}]^T$ and $d_j^{(k)} \in \{+1, -1\}$. We have used a vector notation for representing a single user's signal during the symbol interval j, and we will introduce a matrix notation for representing the spread signal during the time interval of T_u data bits. Therefore we can formulate the spread signal of a single user during the bit intervals $j = 1, 2, ..., T_u$ as:

$$\mathbf{e}^{(k)} = \mathbf{A}^{(k)} \cdot \mathbf{d}^{(k)}, \tag{6.16}$$

where we have $\mathbf{e}^{(k)} = [e^{(1)}_{j=1,T_c=1}, ...e^{(N)}_{j=1,T_c=N}, e^{(1)}_{j=2,T_c=1}, ..., e^{(N)}_{j=T_u,T_c=N}]^T$, $\mathbf{d}^{(k)} = [d^{(k)}_{j=1}, ..., d^{(k)}_{j=T_u}]^T$ and the matrix $\mathbf{A}^{(k)}$ can be written as:

$$\mathbf{A}^{(k)} = \begin{bmatrix} c^{(k)}_{1,1} & 0 & 0 & 0 \\ c^{(k)}_{1,2} & 0 & 0 & 0 \\ \vdots & 0 & 0 & 0 \\ c^{(k)}_{1,N} & 0 & 0 & 0 \\ 0 & c^{(k)}_{2,1} & 0 & 0 \\ 0 & c^{(k)}_{2,2} & 0 & 0 \\ 0 & \vdots & 0 & 0 \\ 0 & c^{(k)}_{2,N} & 0 & 0 \\ 0 & 0 & \ddots & 0 \\ 0 & 0 & 0 & c^{(k)}_{T_u,1} \\ 0 & 0 & 0 & c^{(k)}_{T_u,2} \\ 0 & 0 & 0 & \vdots \\ 0 & 0 & 0 & c^{(k)}_{T_u,N} \end{bmatrix}. \tag{6.17}$$

where $c^{(k)}_{j,T_c}$ represents the T_c-th chip of the spreading code of the kth user at the time interval j. In a multi-user scenario, this linear algebraic model can also be used for representing the spread composite signal of multiple users of a data bit for synchronous system as:

$$\mathbf{e} = \mathbf{A} \cdot \mathbf{d}, \tag{6.18}$$

where the data vector $\mathbf{d}$ contains the multiplexed T_u number of bits from each of user, in other words we have:
$\mathbf{d} = [d^{(1)}_{j=1}, \ldots, d^{(K)}_{j=1}, d^{(1)}_{j=2}, \ldots, d^{(K)}_{j=2}, \ldots, d^{(1)}_{j=T_u}, \ldots, d^{(K)}_{j=T_u}]^T$.
The multiuser system matrix $\mathbf{A}$ can be constructed from the matrix $\mathbf{A}^{(k)}$ as :

$$\mathbf{A} = \begin{bmatrix} c^{(1)}_{1,1} & \ldots & c^{(K)}_{1,1} & 0 & 0 & 0 & 0 & 0 & 0 & 0 \\ c^{(2)}_{1,2} & \ldots & c^{(K)}_{1,2} & 0 & 0 & 0 & 0 & 0 & 0 & 0 \\ \vdots & \ldots & \vdots & 0 & 0 & 0 & 0 & 0 & 0 & 0 \\ c^{(2)}_{1,N} & \ldots & c^{(K)}_{1,N} & 0 & 0 & 0 & 0 & 0 & 0 & 0 \\ 0 & 0 & 0 & c^{(1)}_{2,1} & \ldots & c^{(K)}_{2,1} & 0 & 0 & 0 & 0 \\ 0 & 0 & 0 & c^{(2)}_{2,2} & \ldots & c^{(K)}_{2,2} & 0 & 0 & 0 & 0 \\ 0 & 0 & 0 & \vdots & \ldots & \vdots & 0 & 0 & 0 & 0 \\ 0 & 0 & 0 & c^{(2)}_{2,N} & \ldots & c^{(K)}_{2,N} & 0 & 0 & 0 & 0 \\ 0 & 0 & 0 & 0 & 0 & 0 & \ddots & 0 & 0 & 0 \\ 0 & 0 & 0 & 0 & 0 & 0 & 0 & c^{(1)}_{T_u,1} & \ldots & c^{(K)}_{T_u,1} \\ 0 & 0 & 0 & 0 & 0 & 0 & 0 & c^{(2)}_{T_u,2} & \ldots & c^{(K)}_{T_u,2} \\ 0 & 0 & 0 & 0 & 0 & 0 & 0 & \vdots & \ldots & \vdots \\ 0 & 0 & 0 & 0 & 0 & 0 & 0 & c^{(2)}_{T_u,N} & \ldots & c^{(K)}_{T_u,N} \end{bmatrix} \tag{6.19}$$

Correspondingly, the spread composite signal vector $\mathbf{e}$ constituted by the T_u bits of the K users equals:

$$\mathbf{e} = \mathbf{A} \cdot \mathbf{d}. \tag{6.20}$$

The additive noise component of this system model can be readily incorporated, which is a vector $\mathbf{n}$ having $T_u N$ number of elements. The elements of the vector $\mathbf{n}$ are independent and identically distributed (i.i.d) variables obeying the Gaussian distribution. The expectation of this vector is given by $E[\mathbf{n}\mathbf{n}^T] = \mathbf{I}\sigma_n^2$, where the noise variance is $\sigma_n^2 = N_0/2$, and $N_0/2$ is the double-sided noise power spectral density encountered across the signal's bandwidth. With aid of these definitions, we can now write the composite multiuser channel output of a bit-synchronous system as:

$$\mathbf{e} = \mathbf{A} \cdot \mathbf{d} + \mathbf{n}. \tag{6.21}$$

We can also extend this discrete-time transmission model for incorporating the effects

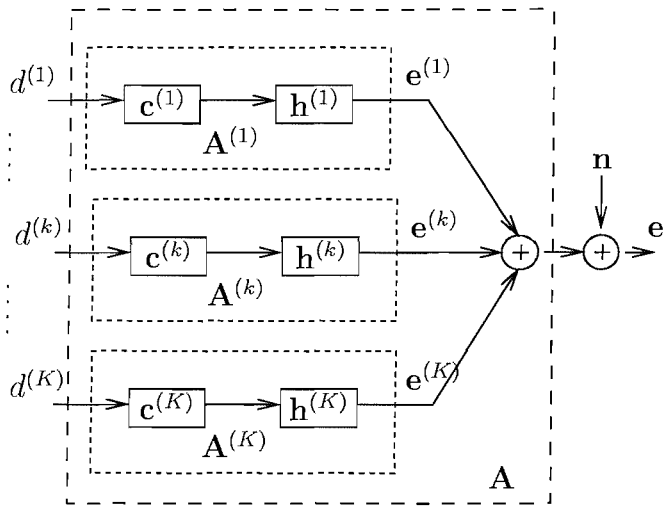

Figure 6.12: The DS-CDMA model for multipath channel

of the multipath channel. Figure 6.12 depicts this multipath scenario in context of a DS-CDMA system, where we observe that the individual user's spreading codes are effectively convolved individually with their CIR. Assuming that the Channel Impulse Response (CIR) has a length of L chips spaced taps, the CIR tap vector $\mathbf{h}^{(k)}$ consists of the L multipath components, given by :
$\mathbf{h}^{(k)} = [h_1^{(k)}, h_2^{(k)}, ..., h_L^{(k)}]^T$,
In order to describe the effects of dispersive channels, the system matrix $\mathbf{A}^{(k)}$ can be extended as follows:

$$\mathbf{A}^{(k)} = \mathbf{C}^{(k)} \cdot \mathbf{h}^{(k)}, \tag{6.22}$$

where k users matrix $\mathbf{C}^{(k)}$ is constituted from its spreading sequence as follows:

$$\mathbf{C}^{(k)} = \begin{bmatrix} c_1^{(k)} & 0 & \dots & 0 \\ c_2^{(k)} & c_1^{(k)} & \ddots & 0 \\ c_3^{(k)} & c_2^{(k)} & \ddots & c_1^{(k)} \\ \vdots & \vdots & \ddots & c_2^{(k)} \\ c_N^{(k)} & c_{N-1}^{(k)} & \dots & \dots \\ \vdots & \vdots & \ddots & \vdots \\ 0 & 0 & 0 & c_N^{(k)} \end{bmatrix}.$$

According to Equation 6.21, in the multi-user case the composite multiuser received vector $\mathbf{e}$, which incorporated the effects of the additive noise is still given by:

$$\mathbf{e} = \mathbf{A} \cdot \mathbf{d} + \mathbf{n}, \tag{6.23}$$

where the system matrix $\mathbf{A}$ now obeys Equation 6.22, and the noise vector the $\mathbf{n}$ has $T_u N + L - 1$ elements, and $E[\mathbf{n}\mathbf{n}^T] = \mathbf{I}\sigma_n^2$, where the noise variance is $\sigma_n^2 = N_0/2$.

6.3.4 GA and RBF Assisted Multiuser Detection in AWGN Channels

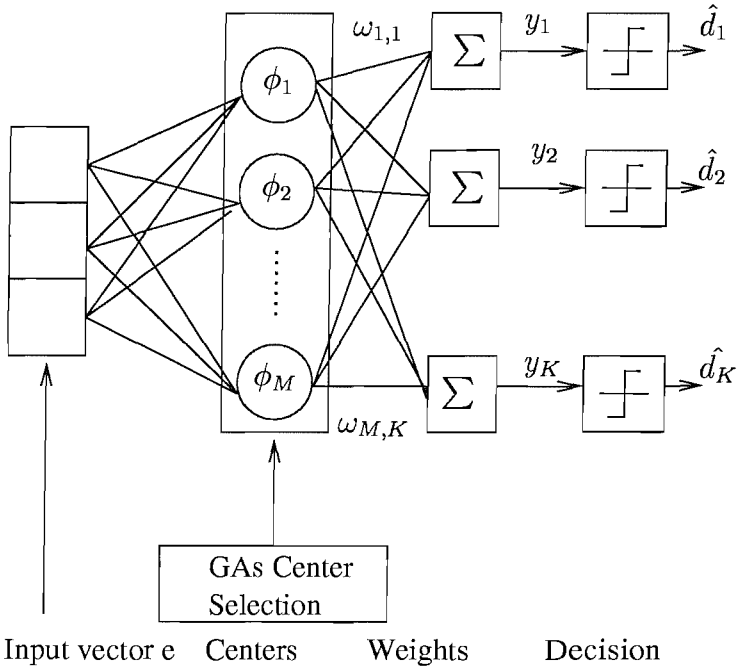

Figure 6.13: Structure of GA-RBF assisted MUD

The structure of the GA-RBF assisted MUD can be seen Figure 6.13, where the input vector $\mathbf{e}$ of the RBF network is the composite multiuser received signal vector at the output of AWGN channel, this vector is still an N dimensional vector since no dispersion is induced, when communicating over the memoryless AWGN channel ($T_u = 1$). As discussed in our introduction to RBF based MUD in section 6.3.2, the GA-RBF assisted

MUD has a number of reference RBF centers, denoted as $v_i, i = 1, 2, ...M$, and In Fig 6.13 the output of this RBF network can be represented by the vector $\mathbf{y}$:
$\mathbf{y} = [y_1, \cdots, y_K]^T$.
The M number of RBF centers are weighted by the RBF weights $\omega_{i,k}$, where we have $i = 1, 2, ..., M$ and $k = 1, 2, ..., K$, and all weighted RBF center outputs are summed up, resulting in the output vector $\mathbf{y}$, where y_k is given by Equation 6.24 and 6.25:

$$y_k = \sum_{i=1}^{M} w_{i,k}\varphi_i(\mathbf{e}). \tag{6.24}$$

$$\varphi_i(\mathbf{e}) = exp(-\frac{\| \mathbf{e} - \mathbf{v}_i \|^2}{2\sigma_i^2}). \tag{6.25}$$

In a no-dispersive AWGN channel, we only have to consider the effects of a single bit during the MUD process. According to Section 6.19, the system matrix $\mathbf{A}$ is generated only for $T_u = 1$, When supporting K users, there are 2^K possible combinations of the bits contained by the channel output vector corresponding to the combinations of the K users' transmitted data. All of these channel output vectors can be adopted as RBF center vectors, which are denoted by the vector $\mathbf{v}_i$. Therefore the RBF center vector $\mathbf{v}_i$ can be represented as :

$$\mathbf{v}_i = \mathbf{A} \cdot \mathbf{d}_i \qquad i = 1, 2, ..., M, \tag{6.26}$$

where $\mathbf{v}_i = [v_i^{(1)}, ..., v_i^{(N)}]^T$, $\mathbf{d}_i = [d_i^{(1)}, ..., d_i^{(K)}]^T$, and $\mathbf{v}_i$ is the noiseless channel output corresponding to the transmitted K-bit data $\mathbf{d}_i$ vector. According to [145], the RBF weight parameter $w_{i,k}$ may assume a limited set of two value, namely ± 1. More explicitly, we can extend this in our scenario as:
$w_{i,k} = 1 \qquad if\ d_i^{(k)} = 1,$
$w_{i,k} = -1 \qquad if\ d_i^{(k)} = -1.$
Therefore, the output vector $\mathbf{y}$ of the GA-RBF assisted MUD seen in Figure 6.13 can be represented as follows:

$$\mathbf{y} = \mathbf{W} \cdot \mathbf{\Psi}, \tag{6.27}$$

where $\mathbf{\Psi} = [\varphi_1(\mathbf{e}), ..., \varphi_M(\mathbf{e})]^T$, and the $\mathbf{W}$ is :

$$\mathbf{W} = \begin{bmatrix} w_{1,1} & w_{2,1} & \cdots & w_{M,1} \\ w_{1,2} & w_{2,2} & \cdots & w_{M,2} \\ \vdots & \vdots & \vdots & \vdots \\ w_{1,K} & w_{2,K} & \cdots & w_{M,K} \end{bmatrix}.$$

When no complexity reduction techniques are employed, the total number M of channel output states seen in Fig 6.13 is 2^K, which may become excessive, if the number of users K is relatively high. In order to circumvent this problem, we involve the GA for selecting a subset of the RBF centers, which have the highest constitution to the GA-RBF based MUD's output formulated in Equation 6.27. During the GA assisted RBF center selection process, the specific centers, which have a low contribution to output of

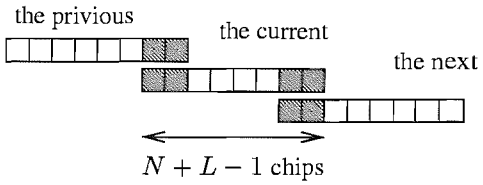

Figure 6.14: ISI-contaminated multiuser scenario in DS-CDMA system

the GA-RBF MUD formulated in Equation 6.27 are discarded. Therefore we can reduce the number of RBF centers from 2^K to P, where P is the population size of the GA. Our goal is to minimize the associated MUD performance degradation while maintaining an affordable complexity, These performance versus complexity issues will be discussed in Section 6.3.6. In order to select the most influential RBF centers having the highest constitution to Equation 6.27, we employ the RBF formula of Equation 6.25 as the GA's objective function. Based on Equation 6.25, this process will assist us in identifying the specific set of RBF centers $\mathbf{v}_i$, which are the closest ones to the components of the channel's output vector $\mathbf{e}$, hence have the highest impact on to the performance of the GA-RBF assisted MUD. For more information on RBF-assisted receivers, the interesting reading is referred in [137].

6.3.5 GA and RBF assisted Multiuser Detection in Dispersive Channels

In the previous section we have highlighted the philosophy of GA-RBF assisted MUD communicating over the non-dispersive AWGN channel. The structure of the GA-RBF assisted MUD communicating over the multipath channels is the same as that designed for transmission over the AWGN channel, which was shown in Figure 6.13. However, due to the channel-induced ISI, which is shown in Figure 6.14 in a stylized format, the effects of the current symbol will spill over to the adjacent symbols. Hence, we have taken into account the previous and the next symbol when detecting the current symbol. In other words, the multipath-induced ISI requires us to increase the number of RBF centers quite considerably. For example, in conjunction with BPSK transmission and a 1-bit duration dispersion induced pre- and post-cursor we have to consider 2^{3K} RBF centers, which are obtained by convolving all the 2^{3K} possible number of combinations of transmitted data bits with the Channel Impulse Response (CIR). According to Section 6.3.3, the system matrix $\mathbf{A}$ has to be generated for $T_u = 3$, while the received channel output signal vector is given by:

$$\mathbf{e_{T_u=3}} = [e_1, e_2, ...e_{3N}]^T,$$

because the transmitted symbol after convolution with the CIR will spread to a duration of $N + L - 1$ chips, where L is the CIR duration. In practice, as it is seen in Figure 6.14 we can curtail the duration of the MUD's input vector $\mathbf{e}$ from $3N$ to $N + L - 1$, the vector $\mathbf{e}$ can be expressed as:

$$\mathbf{e} = [e_{T_u=3,N}, e_{T_u=3,N+1}, ..., e_{T_u=3,N+L-1}]^T.$$

Therefore, the MUD's input vector $\mathbf{e}$ has an increased duration of $N + L - 1$ chips, in comparison to N, which was sufficient when communicating over non-dispersive the

AWGN channels. The RBF centre vector $\mathbf{v}_i$ can also be expressed as :

$$\mathbf{v}_i = \mathbf{A} \cdot \mathbf{d_i}, \quad i = 1, 2, ..., M \tag{6.28}$$

where $\mathbf{A}$ is the system matrix associated with $T_u = 3$, and $\mathbf{d}$ is the transmitted data vector of the K users containing 3 bits of each user. As argued in the context of Figure 6.14, we can also shorten the length of the RBF centre vector $\mathbf{v}_i$ from $3N$ to $N + L - 1$, as we have seen for the MUD's input vector $\mathbf{e}$.

6.3.6 Experimental Result

In Section 1.4.6, the GA's performance depends on numerous factors, such as the population size P, the number of generations Y, on the choice of the specific method used for selecting the parents used for creating the next generation, on the crossover probability and method, on the mutation probability, as well as on the GA's termination criterion used. In this section, we will highlight how these parameters affect the GA's performance and investigate which configurations attain the best performance in the context of our specific optimization problem.

The computational complexity of the GA is essentially governed by the number of generations Y and by the population size P, required for achieving the target performance of the system, hence we indicate the dependence of the complexity P and Y as $O(P.Y)$. The convergence accuracy is mainly dominated by the population size P. Hence, our aim is the selection of the appropriate compromise in terms of P and Y required for an attractive balance between the achievable BER and an acceptable computational complexity. We will also investigate the effects of the crossover probability and the mutation probability.

We will assume that perfect power control is invoked by all users. Therefore, the transmitted signal of all the users will reach the Base Station (BS) at the same power. Furthermore, perfect synchronization and code acquisition are assumed. We support burst-by-burst based rather than continuous transmission. Specifically, the transmission burst length is 200 bits. At the different channel SNRs, a different number of frames is transmitted in order to guarantee that at least 1000 symbol errors are encountered for the sake of maintaining a high confidence in the result recorded. The basic simulation parameters are listed Table 6.2, there parameters are used throughout our simulations, unless otherwise stated.

Modulation scheme	BPSK
Spreading code	WALSH
Spreading gain	32
GA's selection method	Fitness-proportionate
GA's mutation method	Standard binary mutation
GA's crossover method	Single-point crossover
GA's mutation probability p_m	0. 1
GA's crossover probability p_c	0. 5
GA's maximum number of generations	6

Table 6.2: The basic simulation parameters used for the GA and RBF assisted MUD

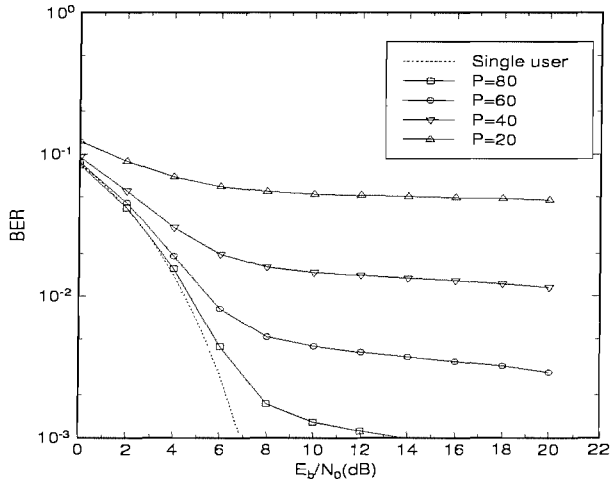

Figure 6.15: Effects of the population size: BER versus E_b/N_0 performance of the GA-RBF assisted MUD, when communicating over non-dispersive AWGN channels, while supporting K=20 users. The population size was $P = 20, 40, 60, 80$, respectively. The system parameters are enumerated in Table 6.2

Effects of the Population Size

In Section 2, we argued that amongst other factors, the GA's convergence accuracy is dramatically influenced by the population size P. Hence, in this section we will quantify the effects of the population size P on the convergence accuracy of the proposed RBF-GA assisted MUD shhemes. The simulation parameter employed are listed in Table 6.2.

As expected, it is seen in Figure 6.15 that the convergence accuracy of the detector increases, as the population size is expanded, and vice versa.

Effects of the Mutation Probability

Maintaining the diversity of the individual vectors in the GA's population is an important design issue of the family of GAs. Hence the appropriate choice of the mutation probability is essential for ensuring the efficient operation of the GAs. In this section, we will investigate how the mutation probability affects the performance of GA-RBF assisted MUD. The simulation parameter configuration is listed in Table 6.2 and the number of users K was 10.

According to Figure 6.16 we can observe that from the set of the mutation probabilities considered, $p_m = 0.1$ offer the best performance, although the conventionally recommended value of p_m typically found in the literature [146] is continued to the range of $0.001 - 0.01$. The associated effects are explained as follows. If the mutation probability is too low, the diversity of the individuals in the population will be insufficient for exploring the entire 2^K-element transmitted data space. This phenomenon hence will lead to premature convergence associated with a local optimum due to the associated lack of population diversity. However, if the mutation probability is excessive, it will

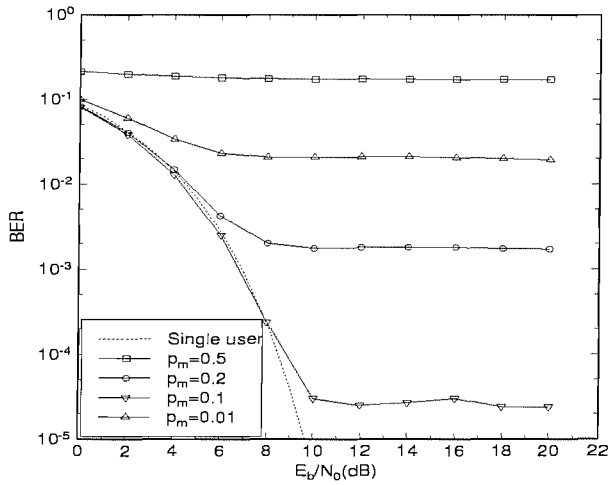

Figure 6.16: Effects of the mutation probability: BER versus E_b/N_0 performance of the GA-RBF assisted MUD over non-dispersive AWGN channels, while supporting K=10 users. The mutation probability was set to 0. 01, 0. 1, 0. 2 and 0. 5, respectively. The other parameters are summarised in Table 6.2

lead to a poor final solution due to the birth of an excessive number of low-fitness individuals. Therefore, there is a trade-off between achieving sufficient diversity and a high convergence rate. In our specific MUD problem, the choice of $p_m = 0.1$ provided the best trade-off. In the next section, we will consider how the choice of the crossover probability affects the performance of the GA-RBF assisted MUD.

Effects of the Crossover Probability

In this section we will investigate the appropriate choice of the crossover probability required for obtaining the best performance. Hence a variety of different crossover probabilities are selected for the sake of quantifying the effects of the crossover probability. The GA configuration parameters use in this section are listed in Table 6.2, except for the variable crossover probability p_c.

Figure 6.17 shows that the crossover probability has only a moderate effect on the BER performance of the GA-RBF MUD. This may be a consequence of the fact that the crossover operation of GA does not give birth to numerous many new high-fitness individuals. Hence this may can not lead to a considerable BER performance improvement. However, since the crossover probability of $p_c = 1.0$ has the highest convergence rate, we adopted $p_c = 1.0$ for all our subsequent simulations. From Figure 6.16 and Figure 6.17 we observe that the birth of the high-fitness individuals is promoted as a beneficial effect of the mutation operation, rather than as a consequence of the crossover operation. Nonetheless, it is important for us to further investigate the effects of the choice of the crossover method used. Hence in the next section we will discuss the benefits of employing a single-point crossover method as well as a uniform crossover method.

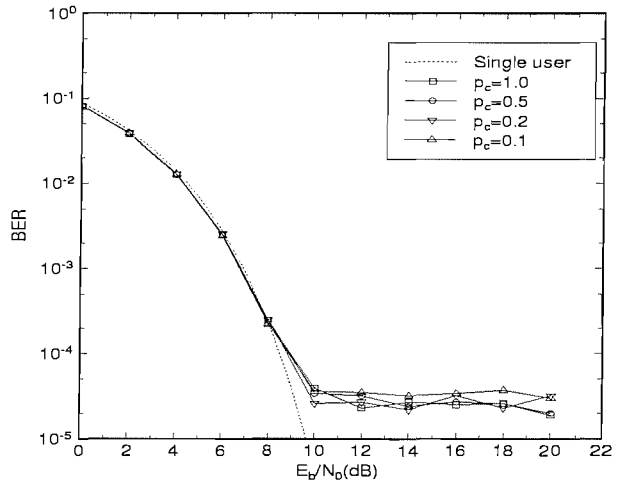

Figure 6.17: Effects of the crossover probability: BER versus E_b/N_0 performance of the GA-RBF assisted MUD over non-dispersive AWGN channels, while supporting $K = 10$ users in conjunction with the crossover probability set of 0. 1, 0. 2, 0. 5 and 1. 0, respectively. The other system parameters are listed in Table 6.2

Effects of the Crossover Method

In this section we will investigate the impact of different crossover methods on the achievable performance. Both a single point crossover [146] and a uniform crossover [146] is studied in this section. The GA's other configuration parameters are listed in Table 6.2, except that a variety of different crossover methods was employed and the number of users was $K = 20$.

In Figure 6.18 we observe that the uniform crossover method achieves a slightly better performance, than the single-point crossover technique, which may be a consequence of the fact that in context of the uniform crossover operation every bit of the K-bit individual has an equal probability of being exchanged. By contrast in case of the single-point crossover where the leftmost and the rightmost bits have a lower probability of being exchanged. Therefore, the uniform crossover method is the preferred choice in our future investigations. Let us now in the next section study the achievable performance, when investing an increased computational complexity.

Effects of the Computational Complexity

As we mentioned before, the computational complexity of the GA and RBF assisted MUD is mainly dependent on the number of generations Y and on the population size P. In this section we investigate the relationship between the achievable performance and the required computational complexity. The simulation parameters are listed in Table 6.2 except that we employ different number of generations Y and different population size P while supporting $K = 10$ users.

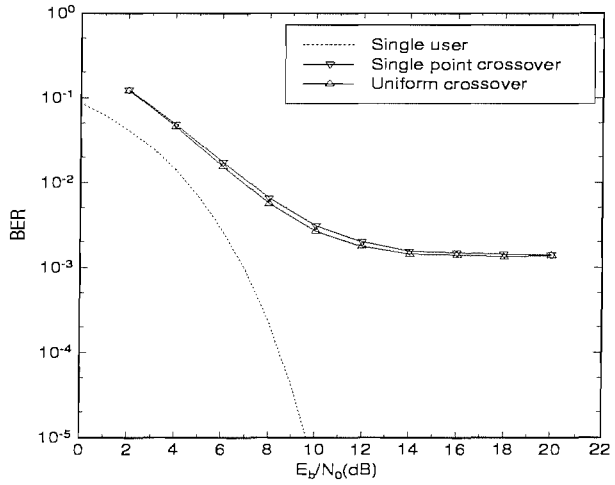

Figure 6.18: Effects of the choice of crossover method: BER versus E_b/N_0 performance of GA-RBF assisted MUD, when communicating over non-dispersive AWGN channels while supporting $K = 20$ users. The population size P was 40, both the uniform crossover and single point crossover were employed in the GA's center selection. The other parameters are listed in Table 6.2

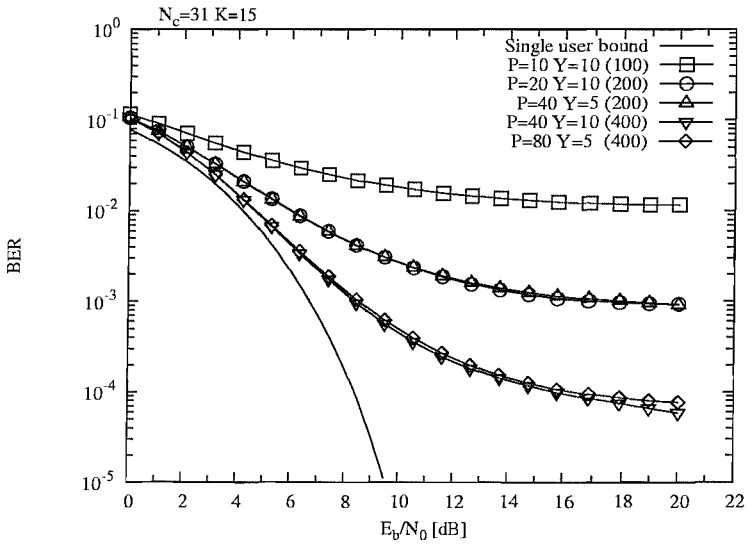

Figure 6.19: BER versus E_b/N_0 performance of the GA-RBF assisted MUD, when communicating over the non-dispersive AWGN channel while the system supports $K = 15$ users employing m-sequence spreading code. The different configurations have the same complexity, but different configuration of population sizes P and number of generations Y

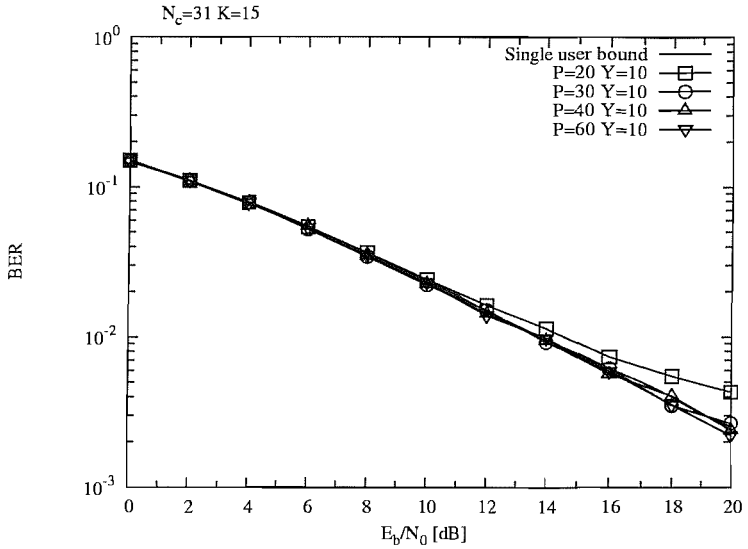

Figure 6.20: BER versus E_b/N_0 performance of the GA-RBF assisted MUD, when communicating over the non-dispersive Rayleigh channel while the system supports $K = 15$ users employing m-sequence spreading code. The different configurations have the same complexity, but different configuration of population sizes P and number of generations Y

In Figure 6.19 and Figure 6.20 we can observe that the achievable BER performance is similar for the different configurations having the same computational complexity related to $O(P.Y)$, regardless of the specific choice of P and Y, and the performance of GA-RBF assisted MUD is determined by the affordable complexity $O(P.Y)$.

6.3.7 GA-RBF assisted MUD in Multipath Channels

In this section the GA and RBF assisted MUD's performance is investigated, when communicating over a channel exhibiting the channel profile of $H(z) = 0.3482 + 0.8704z^{-1} + 0.3482z^{-2}$, where each of the paths obeys the Rayleigh distribution. Figure 6.21 shows the achievable performance.

In Figure 6.21 we can observe that the GA and RBF assisted MUD is capable of jointly suppressing the effects of the MUI, ISI and ICI, attaining a considerably better performance than the classic Rake receiver [10]. As seen in Figure 6.21, the GA-RBF assisted MUD is capable of approaching the single user performance, when the GA-RBF assisted MUD's complexity is sufficiently high for exploring the 2^{3K}-element of K-user search space. Yet, its complexity is substantially lower than that of the conventional optimum Verdu's MUD.

6.4 Chapter Conclusions

In this chapter we investigated a range of GA-RBF assisted MUDs in terms of their computational complexity and BER performance, when communicating over both non-dispersive AWGN channels and dispersive Rayleigh-fading channels, we demonstrated

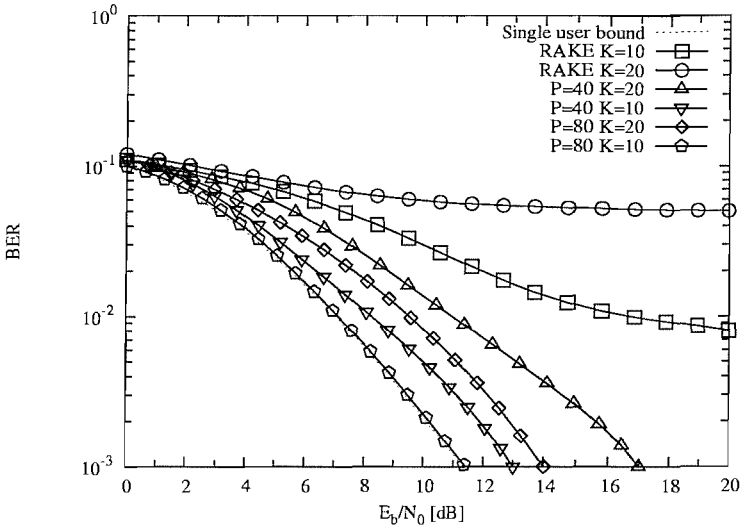

Figure 6.21: The BER versus E_b/N_0 performance of GA-RBF assisted MUD when communicating over a dispersive three-path Rayleigh-fading channel in conjunction with different population size Y while supporting $K = 10$ and $K = 20$ users. The other system parameters are listed in Table 6.2

that the GA-RBF assisted MUD exhibits a significantly lower complexity than the traditional RBF based MUD, although this complexity reduction is achieved at the cost of a slight performance degradation. The proposed technique is capable of approaching the optimum performance of the full-complexity RBF based MUD at the cost of increasing the population size, also approaching the single user the performance. Furthermore, Table 6.3 summarized the BER versus complexity for the GA-RBF MUD when we have $K = 10$ and $N = 31$ at $E_b/N_0 = 10$dB for transmission over a 3-path independent Rayleigh fading channel.

Complexity $O(P \cdot Y)$	**Bit Error Ratio** P_b
P=20 Y =10	3.0×10^{-2}
P=40 Y =10	6.0×10^{-3}
P=80 Y =10	1.2×10^{-3}

Table 6.3: BER versus complexity for the GA-RBF MUD when we have $K = 10$ and $N = 31$ at $E_b/N_0 = 10$dB for transmission over a 3-path independent Rayleigh fading channel.

In our future work, we will also study the performance of GA-RBF assisted MUD in asynchronous scenarios and in context of iterative Soft-In and Soft Out (SISO) Multiuser Detection.

CHAPTER 7

GA Assisted Multiuser Detection for MC-CDMA

7.1 Introduction

Multicarrier CDMA (MC-CDMA) [8] [147] [3] is a novel transmission technique, which combines DS-CDMA and Orthogonal Frequency Division Multiplexing (OFDM) [4, 30, 148, 149]. In MC-CDMA systems, instead of applying spreading sequences in the time domain for spreading each bit, we employ spreading sequences in the frequency domain. Hence, we are capable of achieving frequency diversity gain at the cost of a reduced spreading gain. Numerous Multiuser Detection (MUD) schemes have been proposed in the literature [93,95,150]. For example, the Minimum Mean Square Error (MMSE) MUD has been described for example in [3,93], while an Interference Cancellation (IC) based MUD has been proposed in [3,95].

In [92], the Maximum Likehood (ML) MUD designed for MC-CDMA had been considered. In this specific MUD, the receiver constructs all the possible combinations of the transmitted signal and employs the estimated channel transfer function for generating all the possible received signals, in order to find the one, which has the smallest Euclidean distance from the received signal. Hence, the ML detection based MUD designed for MC-CDMA is capable of achieving the optimum performance. However, it requires the calculation of 2^K number of possible received signal combinations in conjunction with Binary Phase Shift Keying (BPSK) modulation. In other words, the ML detection based MUD's complexity will increase exponentially with the number of users K. Hence the complexity imposed will become excessive, when the number of users K is high. Therefore, in this chapter we will invoke Genetic Algorithms (GA) [151, 152] for reducing the

complexity of the ML detection based MUD employed in MC-CDMA systems. In this chapter we will employ a GA assisted MUD scheme as a suboptimal MUD technique applicable to both bit-synchronous and asynchronous MC-CDMA systems communicating over broadband frequency selective fading channels. We assume that each subcarrier obeys independent Rayleigh fading. More explicitly, we will investigate the performance of this specific GA-assisted MUD as a function of the affordable detection complexity.

This chapter is organized as follows. Sections 7.2 and 7.5 describe the operation of the GA assisted MUD in the context of both synchronous MC-CDMA and asynchronous MC-CDMA, respectively. Sections 7.3 and 7.6 characterise the achievable performance of the GA assisted MUD, when no channel coding techniques are employed. By contrast, Sections 7.4 and 7.7 characterise the performance of this MUD when turbo codes are invoked for enhancing the achievable performance. Finally, Section 7.8 offers our conclusions and outlines our future work.

7.2 GA Assisted MUD for Synchronous MC-CDMA systems

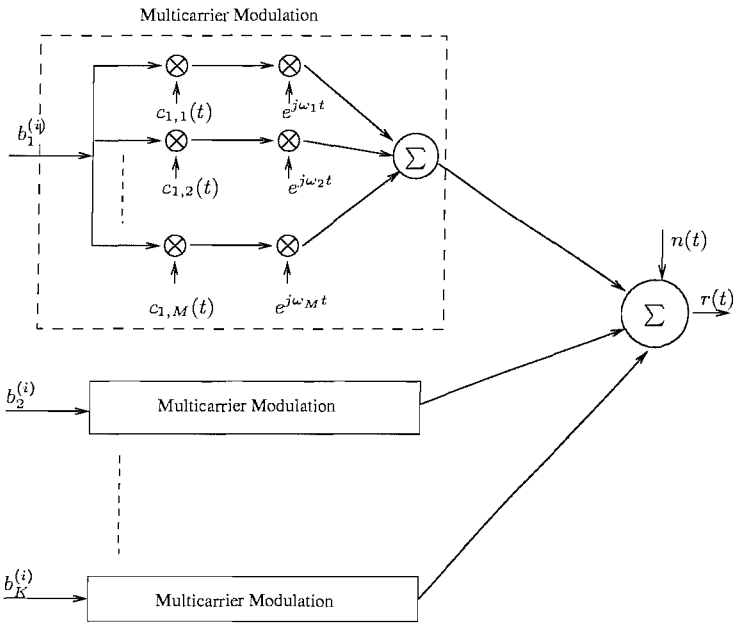

Figure 7.1: The transmitter of a MC-CDMA system

Initially we consider the bit-synchronous MC-CDMA system illustrated in Figure 7.1. Observe in Figure 7.1 that the ith bit $b_k^{(i)}$ of the kth user is spread to M parallel subcarriers, each conveying one of the M number of N-chip spreading signature sequences $c_{k,m}(t)$, $m = 1, \ldots, M$, each of which spans $(0, T_b)$ and we have $T_b/T_c = N$, where T_b and T_c are the bit duration and chip duration, respectively. Each of the M spreading signatures is mapped to a different subcarrier. In other words, a single-carrier system occupying the same bandwidth as the multicarrier system considered would use a spreading signature having NM chips/bit, and both of these systems have a processing gain of

NM. Hence, the transmitted signal of the kth user associated with the mth subcarrier can be expressed in an equivalent lowpass representation as:

$$s_{k,m}(t) = \sqrt{\frac{2P_k}{M}} c_{k,m}(t) b_k^{(i)} e^{jw_m t}, \tag{7.1}$$

where P_k is the kth user's signal energy per bit, $b_k^{(i)} \in (1, -1)$, $k = 1, \ldots, K$ denotes the ith transmitted bit of the kth user, while the kth user's signature waveform is $c_{k,m}(t)$, $k = 1, \ldots, K$, $m = 1, \ldots, M$ on the mth subcarrier, which again has a length of N chips, and can be written as:

$$c_{k,m}(t) = \sum_{n=0}^{N-1} c_{k,m}^{(n)} p(t - nT_c), \quad m = 1, \ldots, M, \quad k = 1, \ldots, K, \tag{7.2}$$

where T_c is the chip duration, N is the number of chips per bit associated with each subcarrier and we have $T_b/T_c = N$. Again, the total processing gain is NM, while $p(t)$ is the rectangular chip waveform employed, which can be expressed as:

$$p(t) = \begin{cases} 1 & 0 \leq t < T_c \\ 0 & otherwise. \end{cases} \tag{7.3}$$

Without loss of generality, we assume that the signature waveform $c_{k,m}(t)$ used for spreading the bits to a total of M subcarriers for all the K users has unity energy, which can be written as:

$$\int_0^{T_b} c_{k,m}^2(t) dt = 1 \quad k = 1, \ldots, K, \quad m = 1, \ldots, M. \tag{7.4}$$

Each user's signal $s_{k,m}(t)$ transmitted on the mth subcarrier is assumed to propagate over an independent non-dispersive single-path Rayleigh fading channel and the fading envelope of each path is statistically independent for all the users. Hence, the single-tap narrowband Channel Impulse Response (CIR) of the kth user on the m subcarrier can be expressed as: $\gamma_{k,m} e^{j\phi_{k,m}}$, where the amplitude $\gamma_{k,m}$ is a Rayleigh distributed random variable, while the phase $\phi_{k,m}$ is uniformly distributed between $[0, 2\pi)$.

Having described the transmitter and the channel, the received signal on the mth subcarrier can be expressed as:

$$r_m(t) = \sum_{i=-\infty}^{\infty} \sum_{k=1}^{K} \sqrt{\frac{2P_k}{M}} c_{k,m}(t - iT_b) \gamma_{k,m} b_k^{(i)} e^{(jw_m t + \phi_{k,m})} + n(t), \tag{7.5}$$

where K is the number of users supported and $n(t)$ is the Gaussian noise process with a variance of $N_0/2$.

Figure 7.2 shows the schematic of the GA-assisted MUD employed in a synchronous MC-CDMA system. The first step of the receiver's operation is the demodulation of all the subcarrier signals. This is followed by Matched Filtering (MF) for each of the K users and the outputs of the K users' matched filters are input to the GA-based MUD. It is more convenient to express the associated signals in matrix and vectorial formats, when

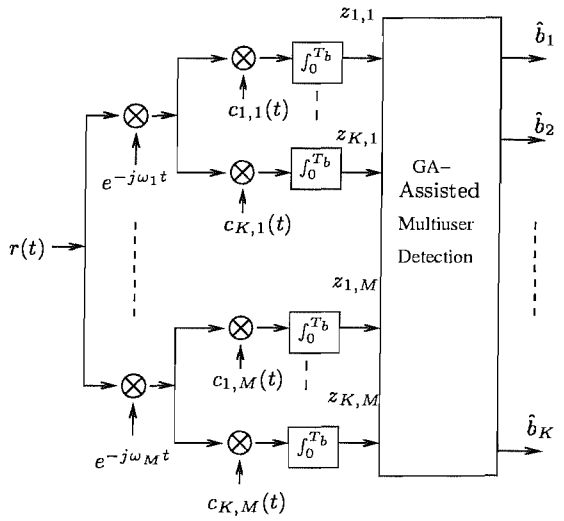

Figure 7.2: Schematic of the GA assisted MUD aided MC-CDMA base station receiver

the sum of the transmitted signals of all users can be expressed in vectorial notation as :

$$r_m = \mathbf{C}_m \mathbf{W}_m \mathbf{A} \mathbf{b} + \mathbf{n}, \tag{7.6}$$

where we have

$$\begin{aligned} \mathbf{C_m} &= [c_{1,m}, \ldots, c_{K,m}] \\ \mathbf{W}_m &= \text{diag}[\gamma_{1,m} e^{j\phi 1,m}, \ldots, \gamma_{K,m} e^{j\phi K,m}] \\ \mathbf{A} &= \text{diag}[\sqrt{\tfrac{2P_1}{M}}, \ldots, \sqrt{\tfrac{2P_K}{M}}] \\ \mathbf{b} &= [b_1, \ldots, b_K]^T \\ \mathbf{n} &= [n_1, \ldots, n_K]^T. \end{aligned} \tag{7.7}$$

Based on Equation 7.6, the output vector $\mathbf{Z}_m$ of the bank of matched filters portrayed in Figure 7.2 can be formulated as [22]:

$$\begin{aligned} \mathbf{Z}_m &= [z_{1,m}, \ldots, z_{K,m}]^T \\ &= \mathbf{R}_m \mathbf{W}_m \mathbf{A} \mathbf{b} + \mathbf{n} \end{aligned} \tag{7.8}$$

where we have

$$\mathbf{R}_m = \begin{bmatrix} \rho_{11}^{(m)} & \rho_{12}^{(m)} & \cdots & \rho_{1K}^{(m)} \\ \rho_{21}^{(m)} & \rho_{22}^{(m)} & \cdots & \rho_{2K}^{(m)} \\ \vdots & \vdots & \vdots & \vdots \\ \rho_{K1}^{(m)} & \rho_{K2}^{(m)} & \cdots & \rho_{KK}^{(m)} \end{bmatrix}. \tag{7.9}$$

and the elements $\rho_{jk}^{(m)}$ of the matrix $\mathbf{R}_m$ are the auto- and cross-correlation of the spreading code, which can be expressed as:

$$\rho_{jk}^{(m)} = \int_0^{T_b} c_{j,m}(t) c_{k,m}(t) dt. \tag{7.10}$$

According to [86] [22], the optimum multiuser detector of the mth subcarrier will maximize the following objective function:

$$\Omega_m(\mathbf{b}) = 2\mathrm{Re}[\mathbf{b}^T\mathbf{A}\mathbf{W}_m^*\mathbf{Z}_m] - \mathbf{b}^T\mathbf{A}\mathbf{W}_m\mathbf{R}_m\mathbf{W}_m^*\mathbf{A}\mathbf{b}, \tag{7.11}$$

where the superscript $*$ indicates the conjugate complex version of a matrix. Therefore, combining the contributions of a total of M parallel subcarriers, the objective function to be maximized in the context of an optimum multiuser detected MC-CDMA system can be expressed as:

$$\begin{aligned} \Omega(\mathbf{b}) &= \sum_{m=1}^{M} \Omega_m(\mathbf{b}) \\ &= \sum_{m=1}^{M} \{2\mathrm{Re}[\mathbf{b}^T\mathbf{A}\mathbf{W}_m^*\mathbf{Z}_m] - \mathbf{b}^T\mathbf{A}\mathbf{W}_m\mathbf{R}_m\mathbf{W}_m^*\mathbf{A}\mathbf{b}\}. \end{aligned} \tag{7.12}$$

Hence the decision rule for Verdu's optimum CDMA multiuser detection scheme based on the maximum likelihood criterion is to choose the specific K-user bit combination $\mathbf{b}$, which maximizes the metric of Equation 7.12. Hence, we have to find:

$$\hat{\mathbf{b}} = \arg\left\{\max_{\mathbf{b}}[\Omega(\mathbf{b})]\right\}. \tag{7.13}$$

The maximization of Equation 7.12 is a combinatorial optimisation problem, which requires an exhaustive search for each of the $J = 2^K$ combinations of $\mathbf{b}$, in order to find the one that maximizes the metric of Equation 7.12. Explicitly, since in case of binary transmissions there are $J = 2^K$ possible combinations of $\mathbf{b}$, the optimum multiuser detector has a complexity that increases exponentially with the number of users K.

Hence, we invoked GA for finding a solution near to the maximum of the objective function defined by the metric of Equation 7.12 without an exhaustive search. Again, the legitimate solutions are the $J = 2^K$ possible combinations of the K-bit vector $\mathbf{b}$. During the GA's operation, each individual of the GA [86] will take the form of a K-bit vector corresponding to the K users' transmitted bits during a single bit interval, which can be denoted for the pth individual of the GA as $\tilde{\mathbf{b}}_p(y) = [\tilde{b}_{p,1}(y), \ldots, \tilde{b}_{p,K}(y)]^T$, where y, $y = 1, \ldots, Y$ denotes the yth generation, and p, $p = 1, \ldots, P$ denotes the pth individual in the mating pool.

We create the initial biased population with the aid of the Maximum Ratio Combining (MRC) based matched filter outputs, which are subjected to hard decision, rather than randomly generating the initial population at the commencement of a GA-assisted search. Explicitly, according to [8], the MRC-combined output vector $\hat{\mathbf{b}}_{MRC}$ of the matched filter output can be expressed as: $\hat{\mathbf{b}}_{MRC} = [\hat{b}_{1,MRC}, \ldots, \hat{b}_{K,MRC}]$, where we have:

$$\hat{b}_{k,MRC} = \sum_{m=1}^{M} z_{k,m}\gamma_{k,m}e^{-j\phi_{k,m}}. \tag{7.14}$$

Having generated $\hat{\mathbf{b}}_{MRC}$, we adopt a 'mutated' version of the hard decision vector $\hat{\mathbf{b}}_{MRC}$ for creating each individual in the initial population, where each bits of the vector $\hat{\mathbf{b}}_{MRC}$ is toggled according to the mutation probability used. Hence, the first individual of the population, namely $\tilde{\mathbf{b}}_p(0)$ can be written as:

$$\tilde{\mathbf{b}}_p(0) = \text{MUTATION}[\hat{\mathbf{b}}_{MRC}]. \tag{7.15}$$

To elaborate a little further, Figure 7.3 shows the flowchart of the GA assisted MUD, which follows the philosophy of [3, 84]. We will characterise the performance of the GA-assisted MUD in the following section.

7.3 Performance of GA Assisted MUD aided Synchronous MC-CDMA

Parameters	Value
Modulation scheme	BPSK
Spreading code	WALSH
Number of subcarriers M	4
length of subcarrier spreading signature N	8
Total spreading gain MN	32
GA's selection method	Fitness-proportionate
GA's mutation method	Standard binary mutation
GA's crossover method	Uniform crossover
GA's mutation probability p_m	0. 1
GA's crossover probability p_c	1
Mating pool size T	5
Elitism	Yes
Incest Prevention	Yes

Table 7.1: The basic simulation parameters used by the GA assisted MUD aided MC-CDMA system

The basic parameters of the GA used in our simulations are listed in Table 7.1. From Figures 7.4 and 7.5 we observe that the GA-assisted MUD's performance improves, when the population size P increases. For example, for E_b/N_0 values below 14dB a near-single-user performance can be achieved for $K = 10$ users, when evaluating the objective function of Equation 7.12, which imposes a complexity on the order of $O(P \cdot Y) = O(40 \cdot 10) = O(400)$, as seen in Fig 7.4. Furthermore, when the number of users K is increased to 20, the GA assisted MUD has a complexity of $O(P \cdot Y) = O(160 \cdot 10) = O(1600)$, as seen in Fig 7.5. We can see in Figure 7.6 that the GA-assisted MUD is also near-far resistant, provided that we perfectly know the channel parameters. More explicitly, the GA assisted MUD exhibits a high robustness against power control errors. Figure 7.7 shows the BER performance as a function of the number of users K. We can infer from Figure 7.7 that the GA-assisted MUD required a population population size P in excess of 80 for achieving a near-single-user performance, when the number of users K is higher

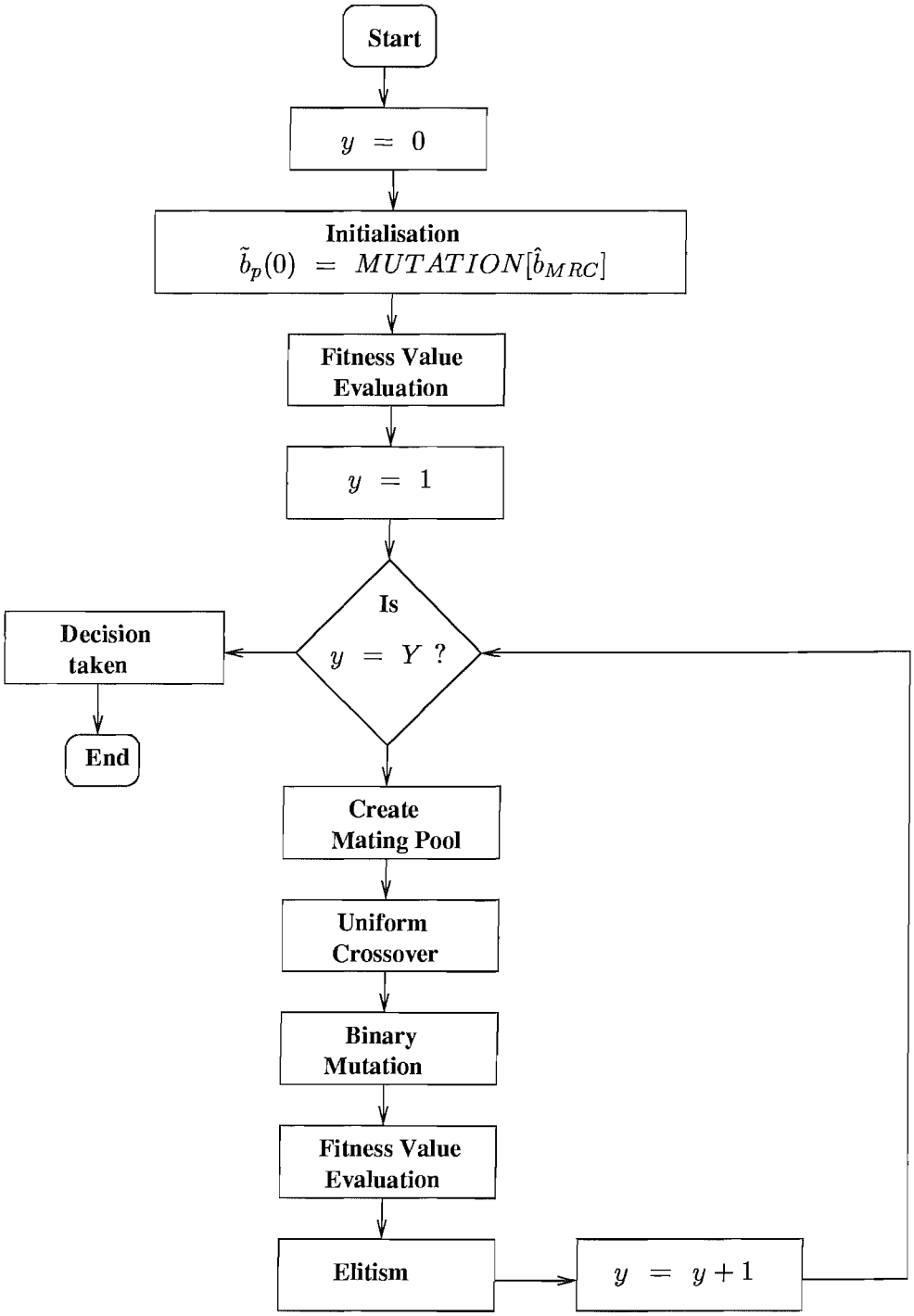

Figure 7.3: A flowchart depicting the structure of a genetic algorithm assisted MUD in the context of the synchronous MC-CDMA base station receiver

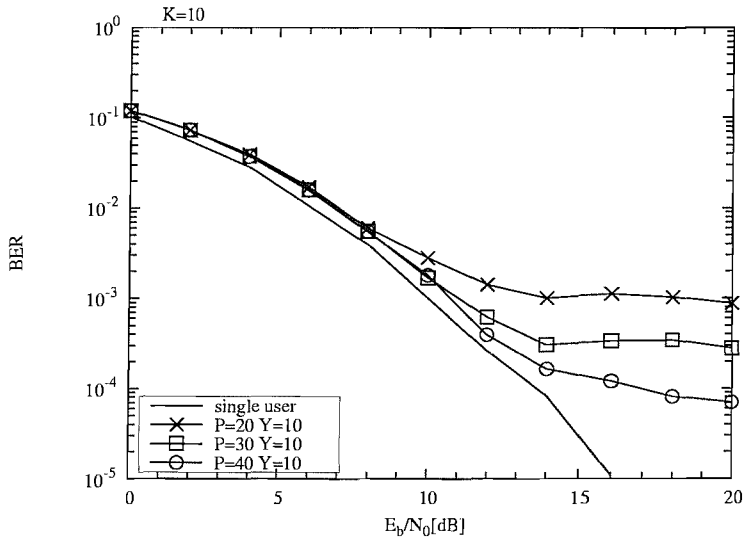

Figure 7.4: BER performance of the GA assisted MUD designed for a bit-synchronous MC-CDMA system, using a 32-chip Walsh code. The number of users supported was $K = 10$. The number of generations was $Y = 10$ and the population size was $P = 20$, 30 and 40. The number of subcarriers was $M = 4$ and each subcarrier experienced uncorrelated narrowband Rayleigh fading.

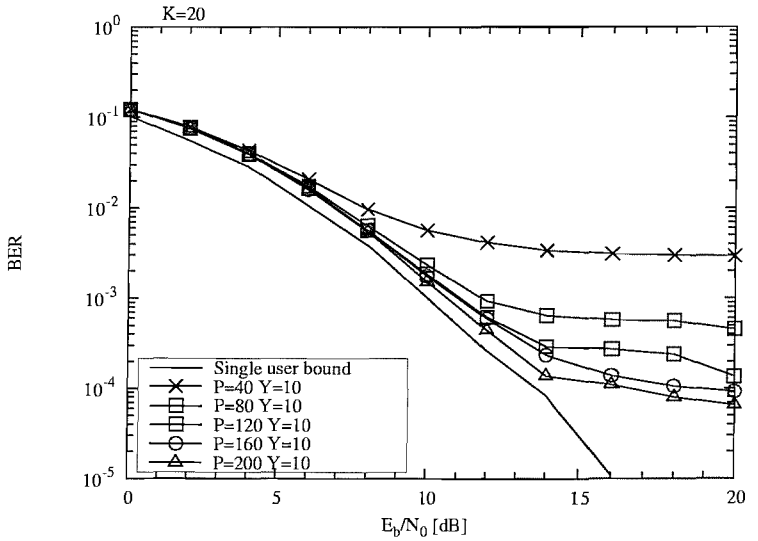

Figure 7.5: BER performance of the GA assisted MUD designed for a bit-synchronous MC-CDMA system, using a 32-chip Walsh code. The number of users supported was $K = 20$. The number of generations was $Y = 10$ and the population size was $P = 40$, 80, 120, 160 and 200. The number of subcarriers was $M = 4$ and each subcarrier experienced uncorrelated narrowband Rayleigh fading.

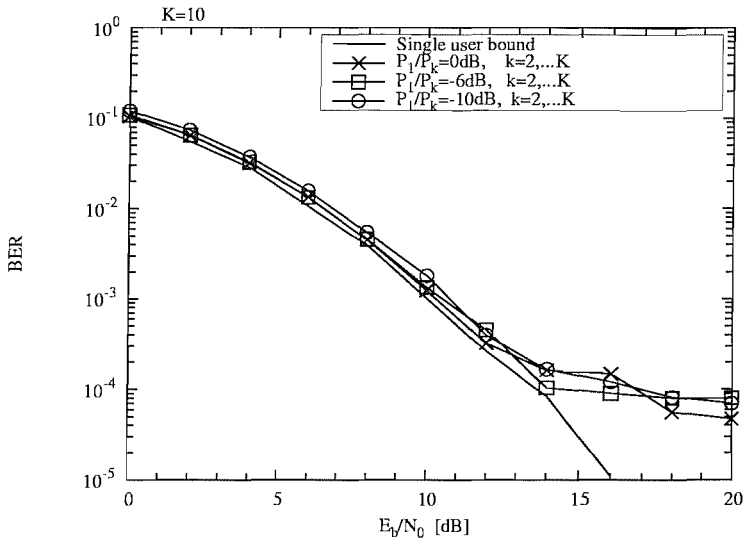

Figure 7.6: BER performance of the GA assisted MUD designed for a bit-synchronous MC-CDMA system when the power of the interfering users was varied. The number of users supported was $K = 10$. The number of generations was $Y = 10$ and the population size was $P = 40$. The ratio of the reference user to interfering user power was $\frac{P_1}{P_k} = 0, -6, -10\text{dB}$, $k = 2, \ldots, K$, respectively.

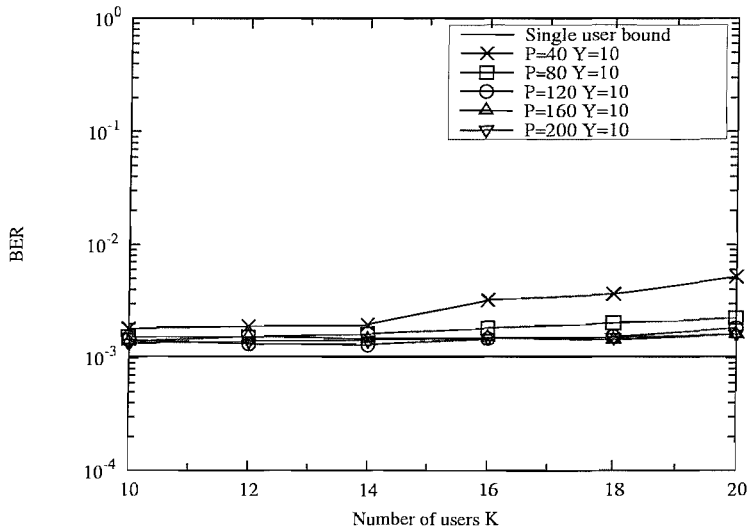

Figure 7.7: BER performance of the GA assisted MUD as a function of the number of users K for the population sizes of $P = 40$, 80, 120, 160, 200, and for $Y = 10$ generations. We had $E_b/N_0 = 10\text{dB}$.

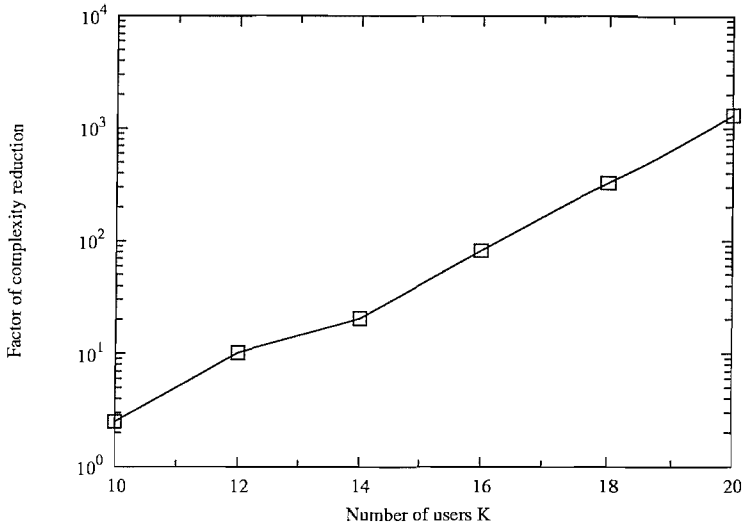

Figure 7.8: The complexity reduction factor of $\frac{2^K}{P \times Y}$ was defined as the ratio of the number of objective function computations required for approaching the single-user bound at a BER of 10^{-3}, when communicating over a **synchronous** environment, where P is the population size, and Y is the number of generations, while K is the number of users supported.

than 14. We can observe in Figure 7.8 that GA-assisted MUD is capable of significantly reducing the complexity of Verdu's optimum MUD. For example, the complexity was reduced by a factor of 1300, when the number of users was $K = 20$. Let us in the next section consider the performance benefits of employing turbo coding.

7.4 Performance of GA Assisted MUD aided Synchronous MC-CDMA using Turbo Coding

Figure 7.9 shows the schematic of the GA assisted MUD aided MC-CDMA receiver employing turbo decoding. In our system a half-rate turbo encoder with a constraint length of $v = 3$ was adopted and the turbo decoder employed four iterations in the process of decoding. The transmission burst length was $L = 100$ and a 10×10 dimensional block turbo interleaver was employed. Furthermore, a random channel interleaver having a memory of $100 \times 2 \times 4 = 800$ bits was employed in our system. As seen in Figures 7.10 and 7.11, when channel coding was used, the GA-assisted MUD was capable of further reducing the complexity required for attaining a BER of 10^{-5}. When the number of users was $K = 10$, the MUD required only $P = 20$ and $Y = 10$ for approaching the single-user bound, resulting in a total complexity of $O(200)$. By contrast, recall from Figure 7.4, where no turbo coding was used that the GA-assisted MUD required a complexity investment of $O(400)$ for approaching the single-user bound, while attaining a BER of 10^{-3}. When the number of users supported was increased to $K = 20$, the MUD required $P = 80$ and $Y = 10$ for approaching the single-user bound, which corresponded to a complexity of $O(800)$. For the sake of comparison recall from Figure 7.5, where no turbo coding was used that the GA-assisted MUD required a complexity of $O(1600)$ for approaching the

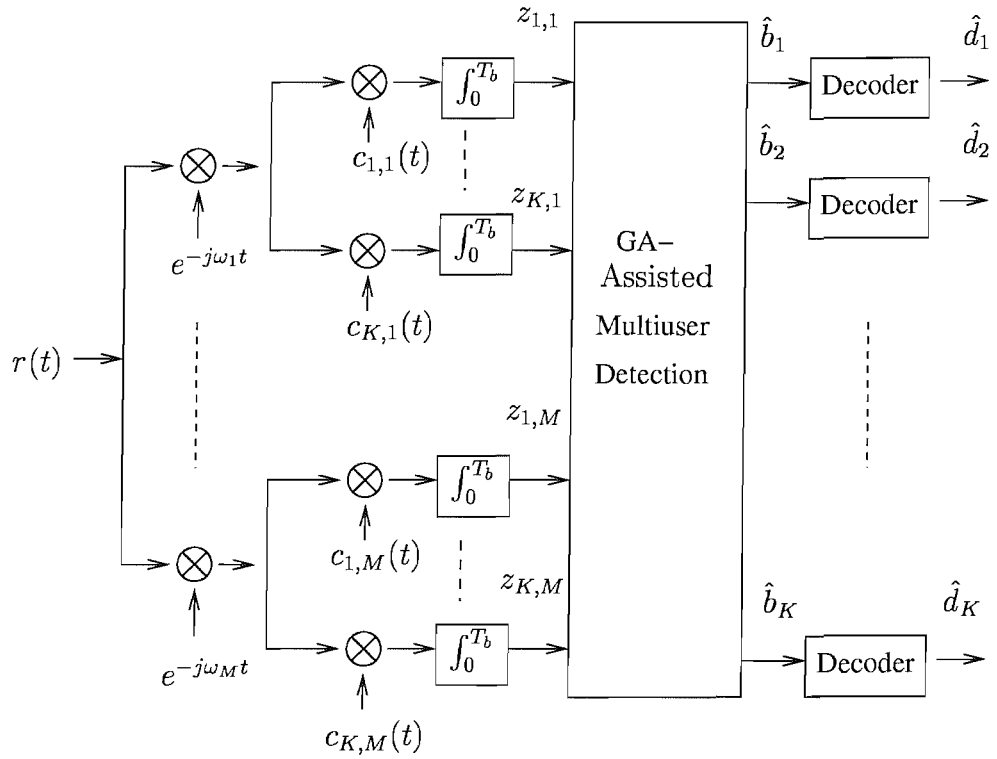

Figure 7.9: Schematic of the GA assisted MUD aided MC-CDMA base station receiver employing turbo decoding.

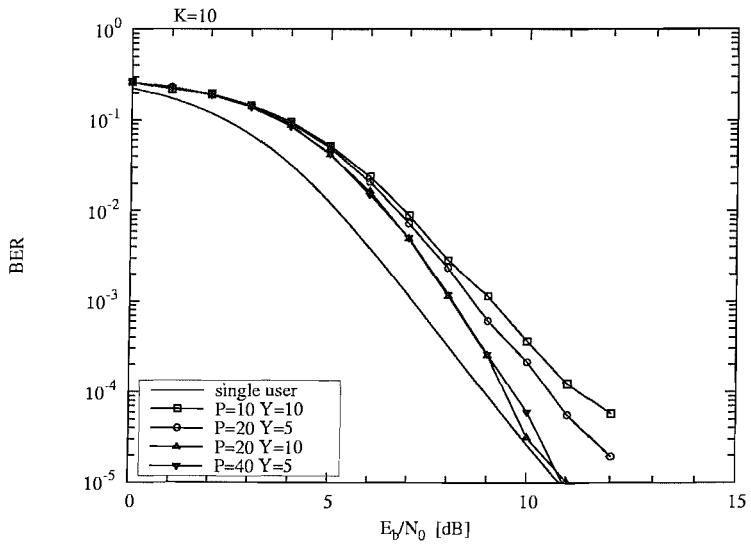

Figure 7.10: BER performance of the GA-assisted MUD designed for synchronous MC-CDMA assisted by $R = \frac{1}{2}$ rate, constraint length $m = 3$ turbo coding using four iterations, when the number of users supported was $K = 10$. The number of generations was $Y = 5$ or 10 and the population size was $P = 10$, 20 and 40. The number of subcarriers was $M = 4$ and each subcarrier obeyed uncorrelated narrowband Rayleigh fading.

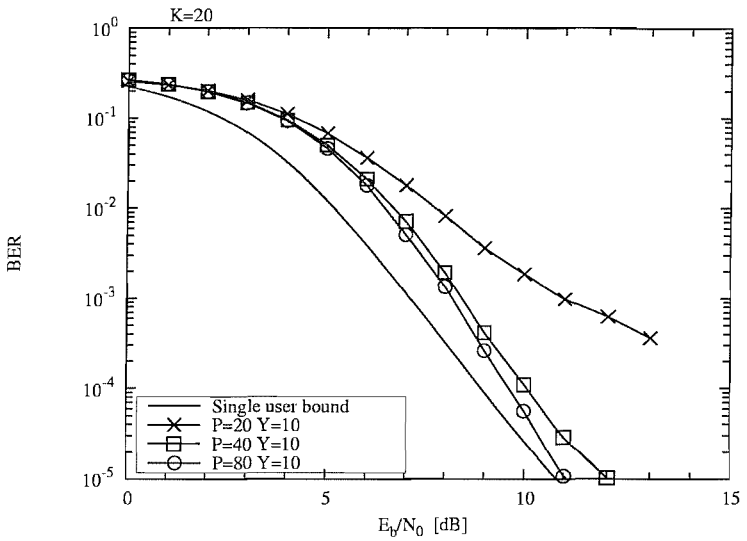

Figure 7.11: BER performance of the GA-assisted MUD designed for synchronous MC-CDMA assisted by $R = \frac{1}{2}$ rate, constraint length $m = 3$ turbo coding using four iterations, when the number of users supported was $K = 20$. The number of generations was $Y = 5$ or 10 and the population size was $P = 10$, 20 and 40. The number of subcarriers was $M = 4$ and each subcarrier obeyed uncorrelated narrowband Rayleigh fading.

single-user bound, while aiming for a BER of 10^{-3}. Having studied the less realistic scenario of synchronous GA assisted MUD aided MC-CDMA, let us now focus our attention on the more realistic asynchronous uplink scenario.

7.5 GA Assisted MUD aided Asynchronous MC-CDMA System

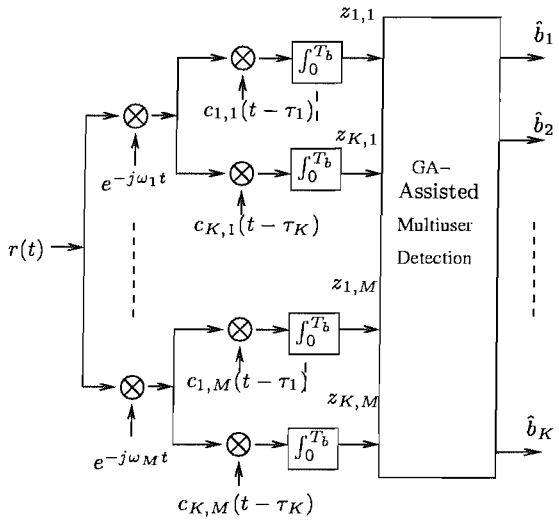

Figure 7.12: Schematic of the GA assisted MUD aided asynchronous MC-CDMA base station receiver.

Figure 7.12 shows the schematic of the GA assisted MUD aided asynchronous MC-CDMA base station receiver, which retains the same structure as the synchronous MC-CDMA BS's receiver. However, the each user's matched filter must be synchronized according to the user's individual delay τ_k. A similar formalism to that of the synchronous MC-CDMA system can be adopted. Therefore, when communicating over asynchronous environments, the received signal can also be expressed similarly to Equation 7.16, namely as:

$$r_m(t) = \sum_{i=-\infty}^{\infty} \sum_{k=1}^{K} \sqrt{\frac{2P_k}{M}} c_{k,m}(t - iT_b - \tau_k)\gamma_{k,m} b_k^{(i)} e^{(jw_m t + \phi_{k,m})} + n(t), \tag{7.16}$$

where τ_k is the kth user's delay. Without loss of generality, we assume that we have $0 \leq \tau_1 < \tau_2 \cdots < \tau_K < T_b$.

The output of the kth user's matched filter corresponding to the mth subcarrier sampled at the end of the ith symbol interval is given as:

$$\mathbf{z}_{k,m}^{(i)} = \int_{-\infty}^{\infty} r(t) c_{k,m}(t - iT_b - \tau_k) dt. \tag{7.17}$$

According to [22], the received signal vector $\mathbf{Z}_m$ recorded at the output of the bank of matched filters on the mth subcarrier can be expressed as [22]:

$$\begin{aligned} \mathbf{Z}_m^{(i)} &= [z_{1,m}, \ldots, z_{K,m}]^T \\ &= \mathbf{R}_m[1]\mathbf{W}_m\mathbf{A}\mathbf{b}^{(i-1)} + \mathbf{R}_m[0]\mathbf{W}_m\mathbf{A}\mathbf{b}^{(i)} + \mathbf{R}_m^T[1]\mathbf{W}_m\mathbf{A}\mathbf{b}^{(i+1)} + \mathbf{n_m}, \end{aligned} \tag{7.18}$$

where i is the time instant index and the zero-mean Gaussian noise vector $\mathbf{n_m}$ has the crosscorrelation matrix of:

$$E[\mathbf{n}[i]\mathbf{n}^T[j]] = \begin{cases} \sigma^2\mathbf{R}^T[1], & \text{if } j = i+1; \\ \sigma^2\mathbf{R}[0], & \text{if } j = i; \\ \sigma^2\mathbf{R}[1], & \text{if } j = i-1; \\ \mathbf{0}, & otherwise. \end{cases} \tag{7.19}$$

The partial crosscorrelation matrix $\mathbf{R}_m[1]$ and the crosscorrelation matrix $\mathbf{R}_m[0]$ of the spreading codes, when communicating over an asynchronous channel, are defined as [22]:

$$\mathbf{R}_{jk}^{(m)}[0] = \begin{cases} 1, & \text{if } j = k; \\ \rho_{jk}^{(m)}, & \text{if } j < k; \\ \rho_{kj}^{(m)}, & \text{if } j > k, \end{cases} \tag{7.20}$$

$$\mathbf{R}_{jk}^{(m)}[1] = \begin{cases} 0, & \text{if } j \geq k; \\ \rho_{kj}^{(m)}, & \text{if } j < k. \end{cases} \tag{7.21}$$

where the coefficients $\rho_{kj}^{(m)}$ and $\rho_{kj}^{(m)}$ on the mth subcarrier are the pair of crosscorrelations of the spreading codes recorded in the asynchronous CDMA environment, which can be

written as [22]:

$$\rho_{jk}^{(m)} = \int_{\tau}^{T_b} c_{j,m}(t)c_{k,m}(t-\tau)dt \tag{7.22}$$

$$\rho_{kj}^{(m)} = \int_{0}^{\tau} c_{j,m}(t)c_{k,m}(t-\tau+T_b)dt, \tag{7.23}$$

according to Equation 7.18, the noise sampling vector $\mathbf{n_m}$ can also be expressed as :

$$\begin{aligned} \mathbf{n_m} &= \mathbf{Z}_m^{(i)} - \mathbf{R}_m[1]\mathbf{W}_m\mathbf{A}\mathbf{b}^{(i-1)} \\ &\quad -\mathbf{R}_m[0]\mathbf{W}_m\mathbf{A}\mathbf{b}^{(i)} - \mathbf{R}_m^T[1]\mathbf{W}_m\mathbf{A}\mathbf{b}^{(i+1)}. \end{aligned} \tag{7.24}$$

Hence, the objective function of the optimum ML detector on the mth subcarrier can be expressed as:

$$\mathbf{\Omega}_m(\mathbf{b}^{(i)}) = \arg\{\min_{\mathbf{b}^{(i-1)},\mathbf{b}^{(i)},\mathbf{b}^{(i+1)}} E[\mathbf{n_m}\cdot\mathbf{n_m}^T]\}. \tag{7.25}$$

Hence, according to Equation 7.25, the GA's objective metric for the mth subcarrier, which have to maximize, can expressed as:

$$\begin{aligned} \mathbf{\Omega}_m(\mathbf{b}^{(i)}) &= \exp\{-\parallel \mathbf{Z}_m^{(i)} - \mathbf{R}_m[1]\mathbf{W}_m\mathbf{A}\mathbf{b}^{(i-1)} \\ &\quad - \mathbf{R}_m[0]\mathbf{W}_m\mathbf{A}\mathbf{b}^{(i)} - \mathbf{R}_m^T[1]\mathbf{W}_m\mathbf{A}\mathbf{b}^{(i+1)} \parallel^2\}, \end{aligned} \tag{7.26}$$

where $\parallel\cdot\parallel$ denotes the Eucledian norm of a complex quantity expressed for the arbitrary variable $v = a + jb$ as $\parallel v \parallel = \sqrt{a^2+b^2}$.

Therefore, when combining the signals of the M subcarriers, the modified objective function becomes:

$$\begin{aligned} \mathbf{\Omega}(\mathbf{b}^{(i)}) &= \exp\{-\sum_{m=1}^{M} \parallel \mathbf{Z}_m^{(i)} - \mathbf{R}_m[1]\mathbf{W}_m\mathbf{A}\mathbf{b}^{(i-1)} \\ &\quad -\mathbf{R}_m[0]\mathbf{W}_m\mathbf{A}\mathbf{b}^{(i)} - \mathbf{R}_m^T[1]\mathbf{W}_m\mathbf{A}\mathbf{b}^{(i+1)} \parallel^2\} \end{aligned} \tag{7.27}$$

Therefore, for achieving the optimum performance, we have to maximize the metric $\mathbf{\Omega}$ of Equation 7.27. More explicitly, the optimum decision concerning the K-dimensional Current Estimated Bit (CEB) vector $\mathbf{b}^{(i)}$ will maximize the crosscorrelation metric in Equation 7.27, provided that the K-dimensional Start Estimated Bit (SEB) vector $\mathbf{b}^{(i-1)}$ and the K-dimensional End Estimated Bit (EEB) vector $\mathbf{b}^{(i+1)}$ are perfectly known to the receiver. However, in practice the receiver is oblivious of the K-dimensional EEB vectors $\mathbf{b}^{(i+1)}$ during the detection of $\mathbf{b}^{(i)}$, unless these are estimate based on pilot bits or training bits. Furthermore, the K-dimensional SEB vector $\mathbf{b}^{(i-1)}$ is never perfectly known by the receiver as a consequence of channel errors. Hence we have to invoke appropriate strategies for finding reasonable choices of $(\mathbf{b}^{(i-1)}, \mathbf{b}^{(i)}, \mathbf{b}^{(i+1)})$ for the maximization of Equation 7.27. In the next subsection, we will describe four strategies in detail.

7.5.1 Edge-bit Generation

In the context of all these four edge-bit selection strategies we will employ the hard decision bit vector $\hat{\mathbf{b}}^{(i-1)}$ as the bit vector $\mathbf{b}^{(i-1)}$ in order to reduce the search space of

the GA, although this is a suboptimum strategy. Nevertheless, in a low-BER scenario we may assume that the vector $\hat{\mathbf{b}}^{(i-1)}$ is close to a perfect estimate. Let us now describe the four different edge-bit selection strategies in detail.

According to the **first strategy (S1)**, the SEB vector $\mathbf{b}^{(i-1)}$ will be set to the hard decision vector $\hat{\mathbf{b}}^{(i-1)}$. Hence, in Equation 7.27 $\hat{\mathbf{b}}^{(i-1)}$ will replace the vector $\mathbf{b}^{(i-1)}$ and hence we will maximize the following function:

$$\begin{aligned}\Omega(\mathbf{b}^{(i)}, \hat{\mathbf{b}}^{(i+1)}) = \exp\{-\sum_{m=1}^{M} \| \mathbf{Z}_m^{(i)} - \mathbf{R}_m[1]\mathbf{W}_m\mathbf{A}\hat{\mathbf{b}}^{(i-1)} \\ -\mathbf{R}_m[0]\mathbf{W}_m\mathbf{A}\mathbf{b}^{(i)} - \mathbf{R}_m^T[1]\mathbf{W}_m\mathbf{A}\mathbf{b}^{(i+1)} \|^2\},\end{aligned} \tag{7.28}$$

and the initial population is given by:

$$\mathbf{b}_p^{(i)}(0) = \text{MUTATION}[\hat{\mathbf{b}}_{MRC}^{(i)}], \tag{7.29}$$

$$\mathbf{b}_p^{(i+1)}(0) = \text{MUTATION}[\hat{\mathbf{b}}_{MRC}^{(i+1)}] \quad p = 1, \ldots, P; \tag{7.30}$$

where the subscript p indicates the individuals' index in the population of the GA, and (0) refers to the initial generation of the GA.

According to the **second strategy S2**, we also employ Equation 7.28 as the function to be maximized. However, in order to obtain a higher grade of diversity for the individuals of the GA invoked for finding the most likely K-dimensional vector $\mathbf{b}^{(i)}$, we randomly initialized the K-dimensional vector $\mathbf{b}^{(i)}$ and hence the initial population associated with the 0th generation can be expressed as:

$$\mathbf{b}_p^{(i)}(0) = \hat{\mathbf{b}}_{GA}^{(i)}, \tag{7.31}$$

$$\mathbf{b}_p^{(i+1)}(0) = \text{MUTATION}[\hat{\mathbf{b}}_{MRC}^{(i+1)}]. \tag{7.32}$$

The philosophical difference between Equations 7.29, 7.30 and Equations 7.31, 7.32 is that the MRC output $\mathbf{b}_{MRC}^{i}$ used in Equation 7.29 for initialization has been replaced by $\mathbf{b}_{GA}^{i}$, which is a randomly initalised K-bit vector, subjected to no mutation.

From Equation 7.28 we can observe that it requires a GA assisted search for the best individual in a space of 2^{2K} elements, which requires a larger population size P and a higher number of generation Y, than that necessitated by the search space of 2^K elements required by the synchronous system. According to the **third strategy (S3)**, we will reduce the size of the search space having 2^{2K} elements to a search space of 2^K elements. This is achieved by invoking a hard decision both for the vector $\mathbf{b}^{(i+1)}$ and for the vector $\mathbf{b}^{(i-1)}$. Explicitly, according to strategy S3, the vectors $\mathbf{b}^{(i+1)}$ and $\mathbf{b}^{(i-1)}$ are given by:

$$\mathbf{b}^{(i-1)} = \hat{\mathbf{b}}^{(i-1)}, \tag{7.33}$$

$$\mathbf{b}^{(i+1)} = \hat{\mathbf{b}}_{MRC}^{(i+1)}. \tag{7.34}$$

Furthermore, we randomly initialize the population $\mathbf{b}_p^{(i)}(0)$ using no mutation, which can be expressed as:

$$\mathbf{b}_p^{(i)}(0) = \mathbf{b}_{GA}^{(i)}. \tag{7.35}$$

Finally, according to **fourth strategy S4**, the vectors $\mathbf{b}^{(i+1)}$ and $\mathbf{b}^{(i-1)}$ are set to the same value as in the context of strategy S3 expressed in Equation 7.33 and 7.34. However, as in the context of the synchronous MC-CDMA system, we adopted biased initialization for creating the individuals of the initial population, where each bit of the MRC's output vector is toggled according to the mutation probability used. Hence, the initial generation for the vector $\mathbf{b}_p^{(i)}(0)$ can be created according to:

$$\mathbf{b}_p^{(i)}(0) = \text{MUTATION}[\mathbf{b}_{MRC}^{(i)}]. \tag{7.36}$$

Therefore, the objective function to be maximized for the strategies S3 and S4 can be expressed as:

$$\begin{aligned}\Omega(\mathbf{b}^{(i)}) = \exp\{-\sum_{m=1}^{M} \| \mathbf{Z}_m^{(i)} - \mathbf{R}_m[1]\mathbf{W}_m\mathbf{A}\hat{\mathbf{b}}^{(i-1)} \\ -\mathbf{R}_m[0]\mathbf{W}_m\mathbf{A}\mathbf{b}^{(i)} - \mathbf{R}_m^T[1]\mathbf{W}_m\mathbf{A}\hat{\mathbf{b}}_{MRC}^{(i+1)} \|^2\}.\end{aligned} \tag{7.37}$$

	$\mathbf{b}^{(i-1)}$	$\mathbf{b}^{(i)}$	$\mathbf{b}^{(i+1)}$	$\tilde{\mathbf{b}}_p^{(i)}(0)$	$\tilde{\mathbf{b}}_p^{(i+1)}(0)$
S1	$\hat{\mathbf{b}}^{(i-1)}$	$\tilde{\mathbf{b}}_p^{(i)}(y)$	$\tilde{\mathbf{b}}_p^{(i+1)}(y)$	biased initialization	biased initialization
S2	$\hat{\mathbf{b}}^{(i-1)}$	$\tilde{\mathbf{b}}_p^{(i)}(y)$	$\tilde{\mathbf{b}}_p^{(i+1)}(y)$	random initialization	biased initialization
S3	$\hat{\mathbf{b}}^{(i-1)}$	$\tilde{\mathbf{b}}_p^{(i)}(y)$	$\hat{\mathbf{b}}_{MRC}^{(i+1)}$	random initialization	
S4	$\hat{\mathbf{b}}^{(i-1)}$	$\tilde{\mathbf{b}}_p^{(i)}(y)$	$\hat{\mathbf{b}}_{MRC}^{(i+1)}$	biased initialization	

Table 7.2: Summary of the four different edge-bit generation strategies characterising the CEB vector $\mathbf{b}^{(i)}$, SEB vector $\mathbf{b}^{(i-1)}$, EEB vector $\mathbf{b}^{(i+1)}$ generation and the initialization method.

Finally, the four different edge-bit generation strategies are summarized in Table 7.2, showing the differences and similarities of these strategies at a glance. The entire process of the GA aided MUD's operation is depicted in Figure 7.13 for the asynchronous MC-CDMA system considered.

Having described the four different edge-bit generation strategies, let us now investigate their performance in the next section.

7.6 Performance of GA Assisted MUD aided Asynchronous MC-CDMA

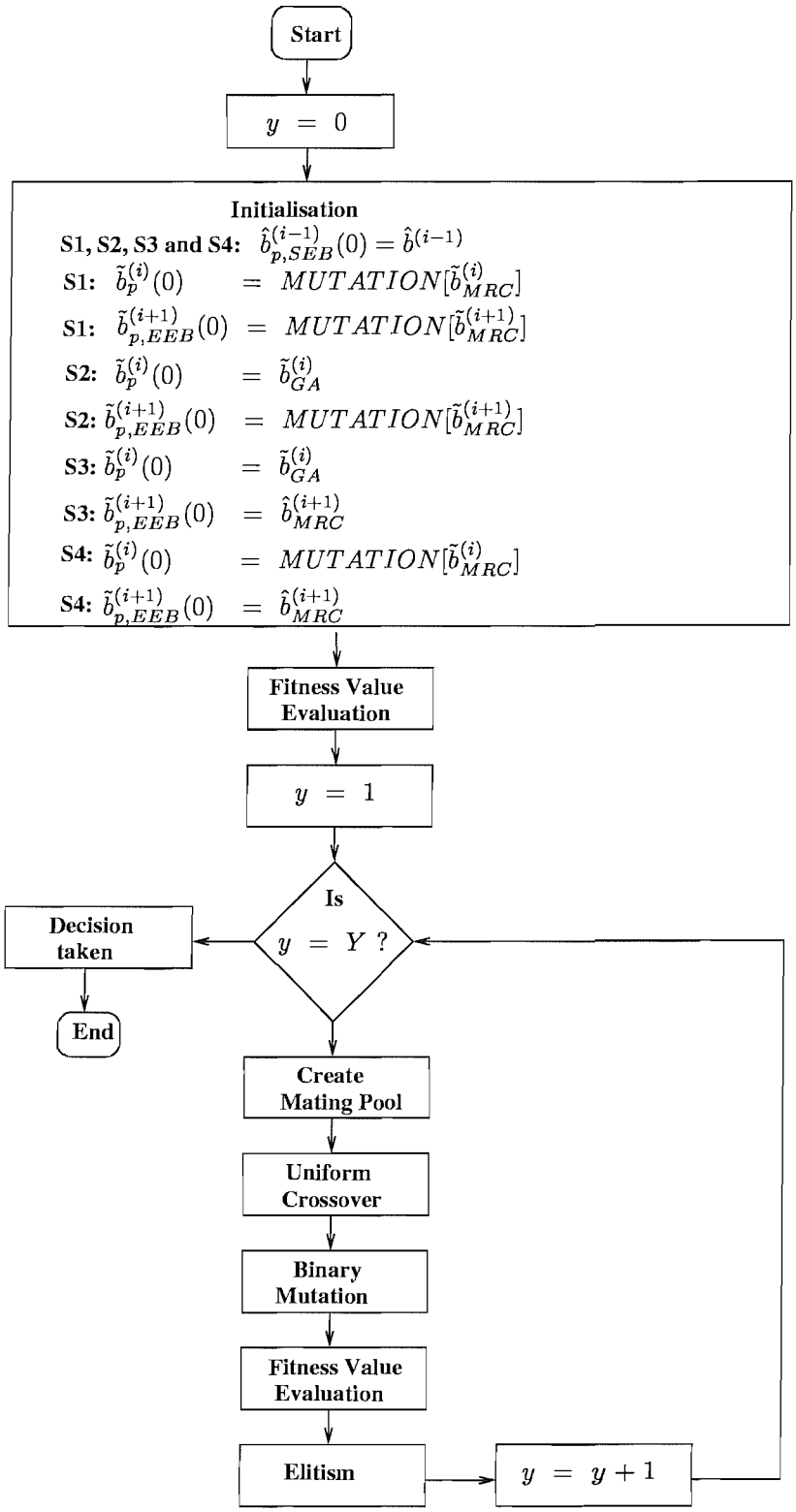

Figure 7.13: A flowchart depicting the structure of a genetic algorithm assisted MUD aided MC-CDMA base station receiver.

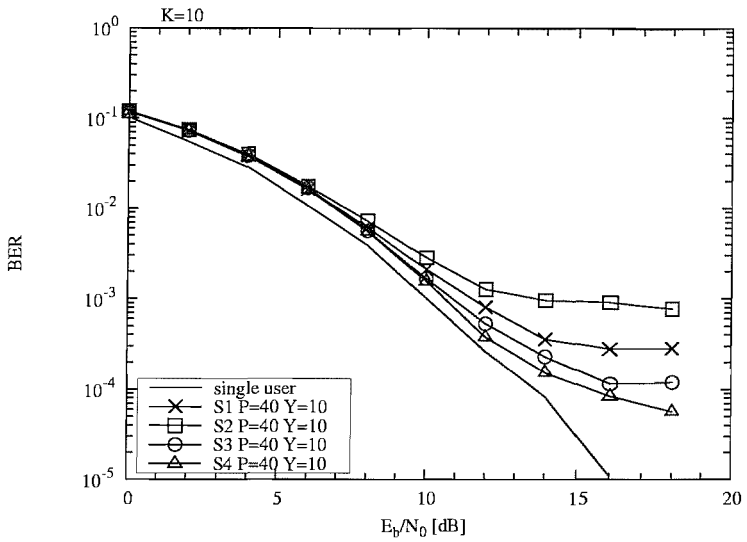

Figure 7.14: The GA assisted MC-CDMA MUD's BER performance, when communicating over asynchronous environments. The four different GA strategies listed in Table 7.2 were adopted for approaching the optimum MUD's performance and the number of users supported was $\mathbf{K = 10}$. The population size was $\mathbf{P = 40}$ and the number of generations was $Y = 10$. Furthermore, the number of subcarriers was $M = 4$ and each subcarrier experienced uncorrelated narrowband Rayleigh fading.

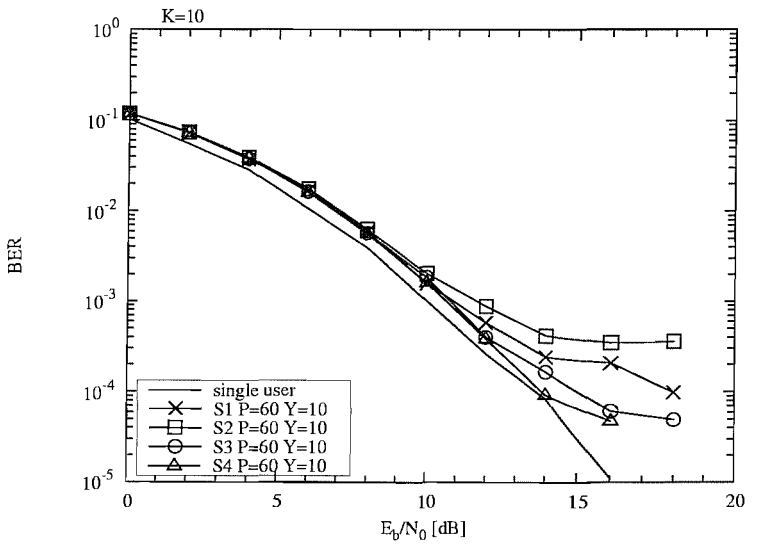

Figure 7.15: The GA assisted MC-CDMA MUD's BER performance, when communicating over asynchronous environments. The four different GA strategies listed in Table 7.2 were adopted for approaching the optimum MUD's performance and the number of users supported was $\mathbf{K = 10}$. The population size was $\mathbf{P = 60}$ and the number of generations was $Y = 10$. Furthermore, the number of subcarriers was $M = 4$ and each subcarrier experienced uncorrelated narrowband Rayleigh fading.

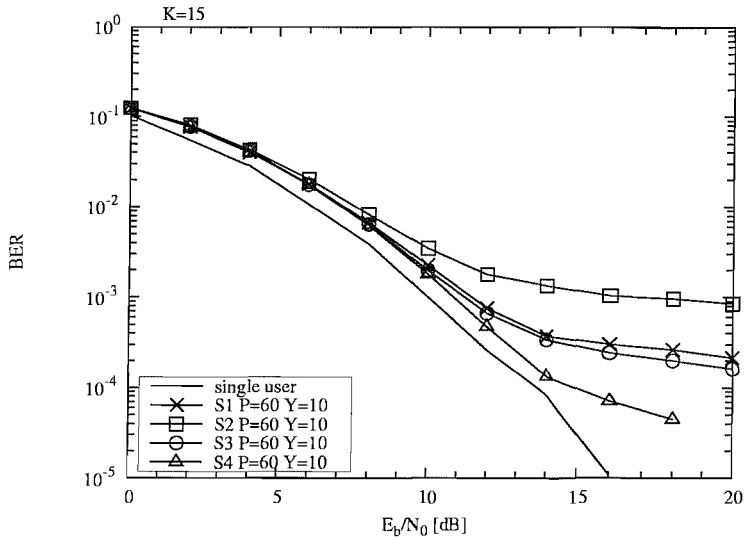

Figure 7.16: The GA assisted MC-CDMA MUD's BER performance, when communicating over asynchronous environments. The four different GA strategies listed in Table 7.2 were adopted for approaching the optimum MUD's performance and the number of users supported was $\mathbf{K = 15}$. The population size was $\mathbf{P = 60}$ and the number of generations was $Y = 10$. Furthermore, the number of subcarriers was $M = 4$ and each subcarrier experienced uncorrelated narrowband Rayleigh fading.

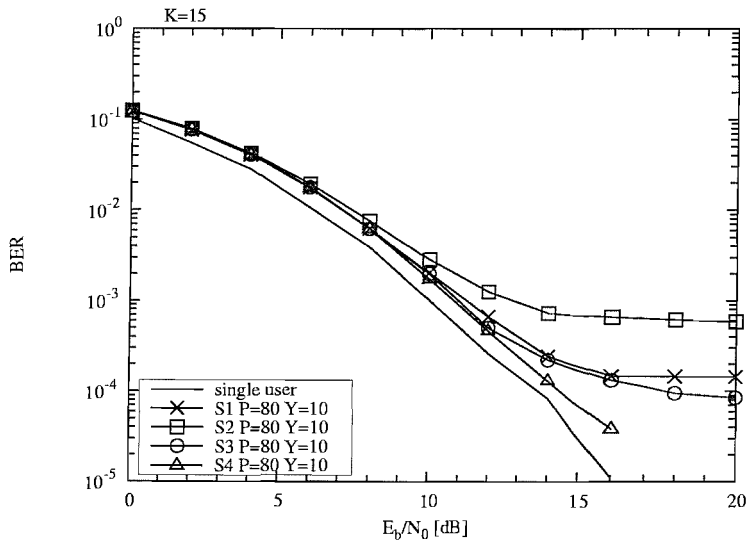

Figure 7.17: The GA assisted MC-CDMA MUD's BER performance, when communicating over asynchronous environments. The four different GA strategies listed in Table 7.2 were adopted for approaching the optimum MUD's performance and the number of users supported was $\mathbf{K = 15}$. The population size was $\mathbf{P = 80}$ and the number of generations was $Y = 10$. Furthermore, the number of subcarriers was $M = 4$ and each subcarrier experienced uncorrelated narrowband Rayleigh fading.

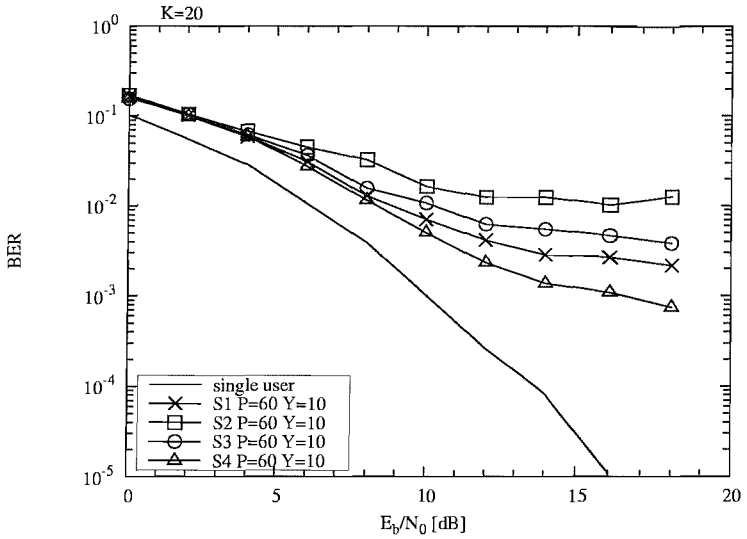

Figure 7.18: The GA assisted MC-CDMA MUD's BER performance, when communicating over asynchronous environments. The four different GA strategies listed in Table 7.2 were adopted for approaching the optimum MUD's performance and the number of users supported was $\mathbf{K = 20}$. The population size was $\mathbf{P = 60}$ and the number of generations was $Y = 10$. Furthermore, the number of subcarriers was $M = 4$ and each subcarrier experienced uncorrelated narrowband Rayleigh fading.

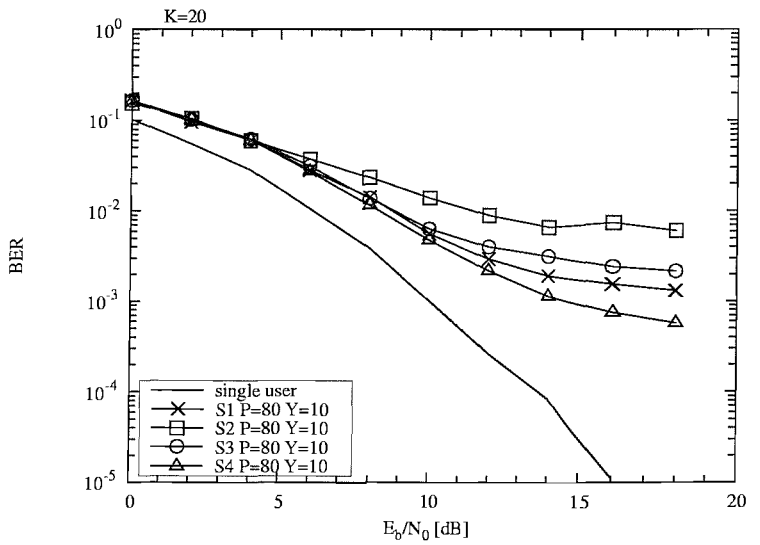

Figure 7.19: The GA assisted MC-CDMA MUD's BER performance, when communicating over asynchronous environments. The four different GA strategies listed in Table 7.2 were adopted for approaching the optimum MUD's performance and the number of users supported was $\mathbf{K = 20}$. The population size was $\mathbf{P = 80}$ and the number of generations was $Y = 10$. Furthermore, the number of subcarriers was $M = 4$ and each subcarrier experienced uncorrelated narrowband Rayleigh fading.

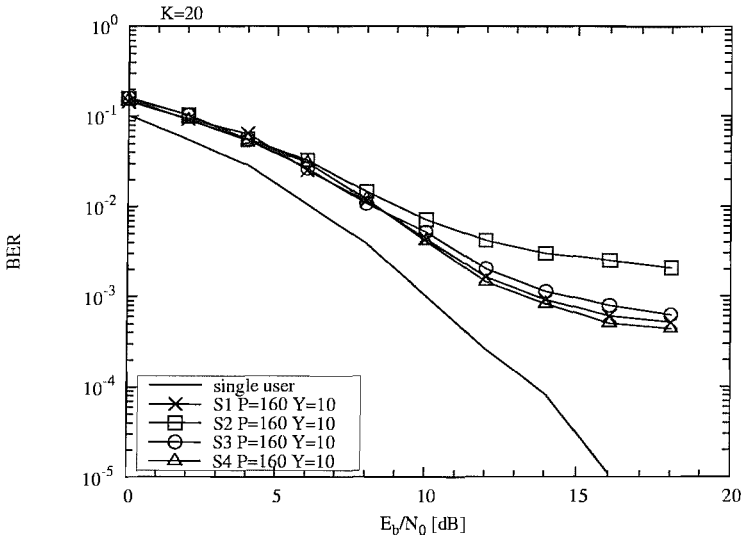

Figure 7.20: The GA assisted MC-CDMA MUD's BER performance, when communicating over asynchronous environments. The four different GA strategies listed in Table 7.2 were adopted for approaching the optimum MUD's performance and the number of users supported was $\mathbf{K = 20}$. The population size was $P = 160$ and the number of generations was $\mathbf{Y = 10}$. Furthermore, the number of subcarriers was $M = 4$ and each subcarrier experienced uncorrelated narrowband Rayleigh fading.

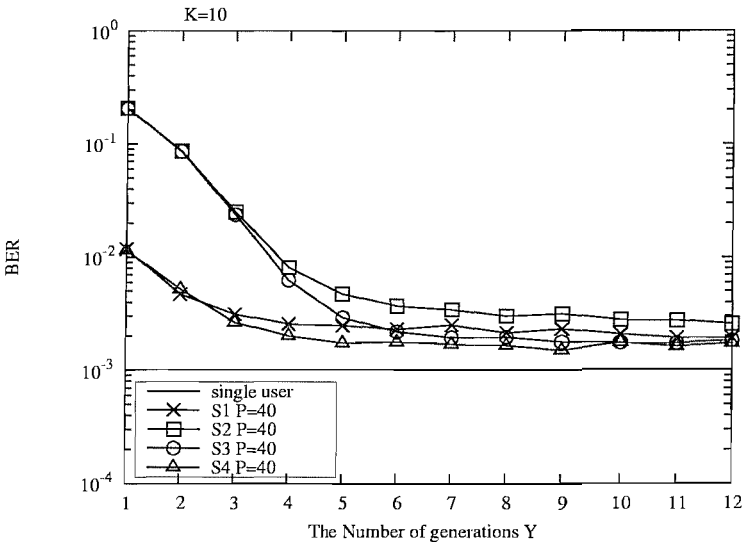

Figure 7.21: The GA assisted MC-CDMA MUD's BER performance as a function of the number of generations Y, when communicating over asynchronous environments. The four different GA strategies listed in Table 7.2 were adopted for approaching the optimum MUD's performance and the number of users supported was $\mathbf{K = 10}$. The population size was $\mathbf{P = 40}$, the number of subcarriers was $M = 4$ and each subcarrier experienced uncorrelated narrowband Rayleigh fading.

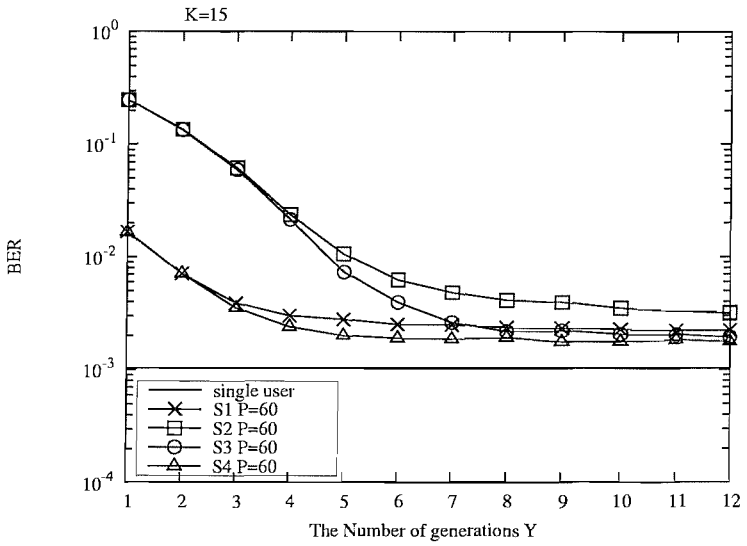

Figure 7.22: The GA assisted MC-CDMA MUD's BER performance as a function of the number of generations Y, when communicating over asynchronous environments. The four different GA strategies listed in Table 7.2 were adopted for approaching the optimum MUD's performance and the number of users supported was $\mathbf{K = 15}$. The population size was $\mathbf{P = 40}$, the number of subcarriers was $M = 4$ and each subcarrier experienced uncorrelated narrowband Rayleigh fading.

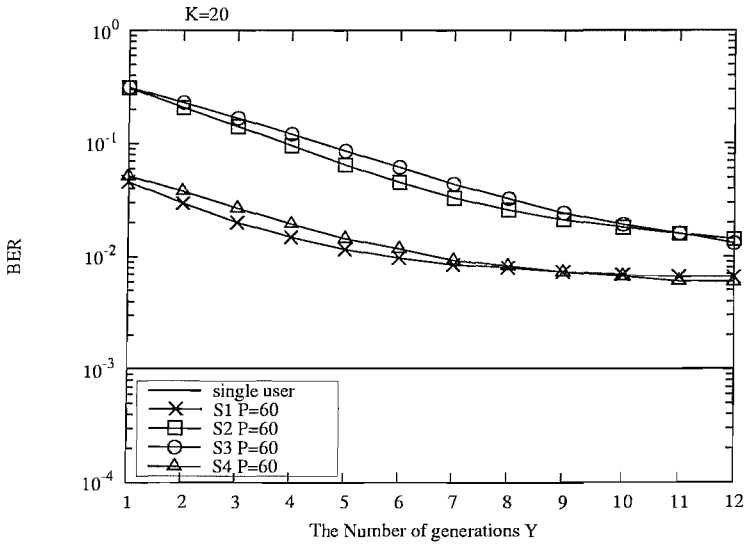

Figure 7.23: The GA assisted MC-CDMA MUD's BER performance as a function of the number of generations Y, when communicating over asynchronous environments. The four different GA strategies listed in Table 7.2 were adopted for approaching the optimum MUD's performance and the number of users supported was $\mathbf{K = 20}$. The population size was $\mathbf{P = 60}$, the number of subcarriers was $M = 4$ and each subcarrier experienced uncorrelated narrowband Rayleigh fading.

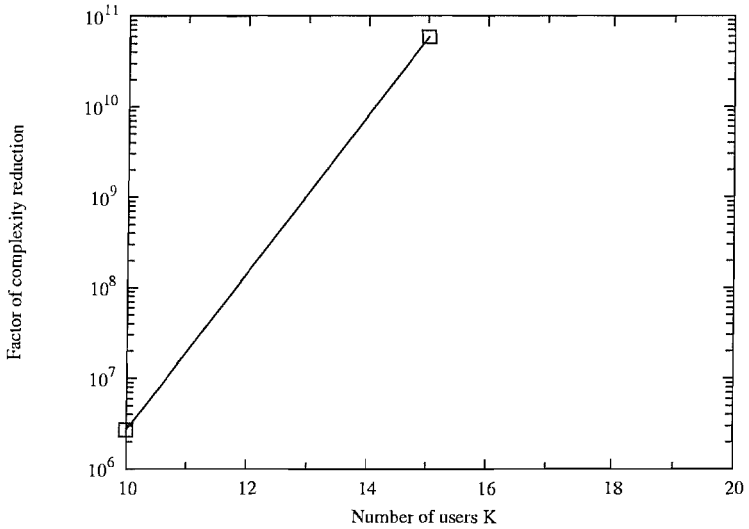

Figure 7.24: The complexity reduction factor of $\frac{2^{3K}}{P \times Y}$ was defined as the ratio of the number of objective function computations required for approaching the single-user bound at a BER of 10^{-3}, in comparison to Verdu's optimum MUD when communicating over an **asynchronous** environment, where P is the population size, and Y is the number of generations, while K is the number of users supported.

From Figures 7.14 and 7.16 we can observe that strategy S4 is capable of achieving a better performance than the other strategies. By studying Figures 7.14, 7.15, 7.16 and 7.17, we can infer that the biased initialization strategies, namely S1 and S4 outperformed the random initialization strategies of S2 and S3.

Furthermore, the strategy S4 is capable of approaching the near-single-user performance, despite its low complexity, when the number of users K is not higher than 15. However, from Figures 7.18, 7.19 and 7.20, we can observe that for $K = 20$ the GA assisted MUD becomes incapable of approaching the single-user performance, because the search space has 2^{60} elements and hence its complexity would become excessive.

Figures 7.21, 7.22 and 7.23 show the performance of the GA assisted MUD as a function of the number of generations Y. From Figures 7.21, 7.22 and 7.23 we may conclude that the biased initialization strategies tend to approach the single-user performance faster than the random initialization strategies.

From Figures 7.4 and 7.14 we can see that the GA assisted MUD imposes a similar complexity, when approaching the single-user performance in case of supporting $K = 10$ users communicating either over synchronous or asynchronous environments. However, from Figures 7.5 and 7.20 we can see that the performance of the GA assisted MUD communicating over the synchronous environment is superior in comparison to that over the asynchronous channel, when the number of users K is increased to 20. This is because the search space hosts 2^{60} elements when communicating in an asynchronous scenario, which imposes an excessive complexity. In this excessive search space the GA assisted MUD cannot approach the single-user performance and hence an inferior performance is achieved. By contrast, when communicating over the synchronous channel, the search space has 2^{20} elements and hence the GA assisted MUD is capable of approaching the single-user performance.

From Figure 7.24 we can observe that the GA assisted MUD is capable of reducing the complexity imposed by a factor of 6×10^{10} in comparison to that of Verdu's optimum MUD, when the number of users K is 15, suggesting that the GA assisted MUD has the potential of significantly reducing the complexity of the optimum MUD.

7.7 Performance of GA Assisted MUD aided Asynchronous MC-CDMA using Turbo Coding

In this section, we briefly investigate the performance of the GA assisted MUD aided asynchronous MC-CDMA scheme employing turbo decoding. From Figures 7.25 and 7.26 we can observe that in asynchronous environments the GA assisted MUD employing turbo decoding has a 1.5dB E_b/N_0 loss at a BER of 10^{-4} in comparison to the single-user performance. The GA assisted MUD's implementation complexity is significantly lower than that of Verdu's optimum MUD [22]. For example, when supporting $K = 10$ users, the complexity expressed in terms of the number of objective function evaluations was $O(200)$, while for $K = 15$ the complexity was $O(300)$.

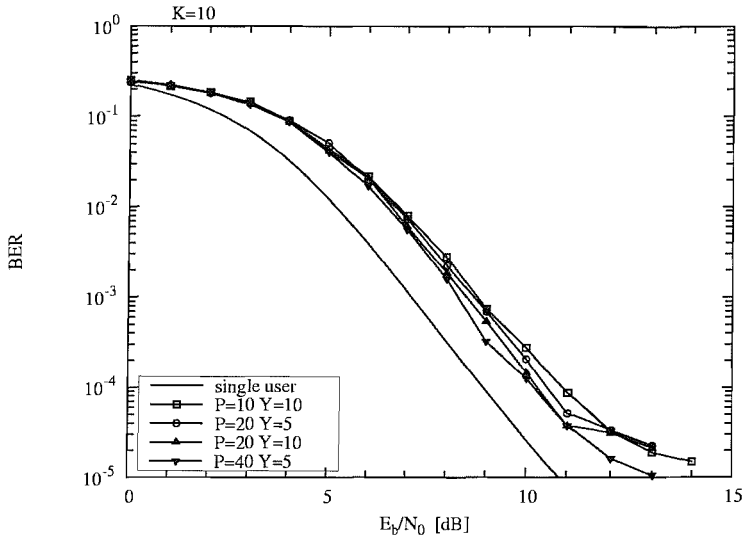

Figure 7.25: BER performance of the GA-assisted MUD designed for asynchronous MC-CDMA assisted by $R = \frac{1}{2}$ rate, constraint length $m = 3$ turbo coding using four iterations, when the number of users supported was $K = 10$. The number of generations was $Y = 5$ or 10 and the population size was $P = 10$, 20 and 40. Furthermore, the number of subcarriers was $M = 4$ and each subcarrier obeyed uncorrelated narrowband Rayleigh fading.

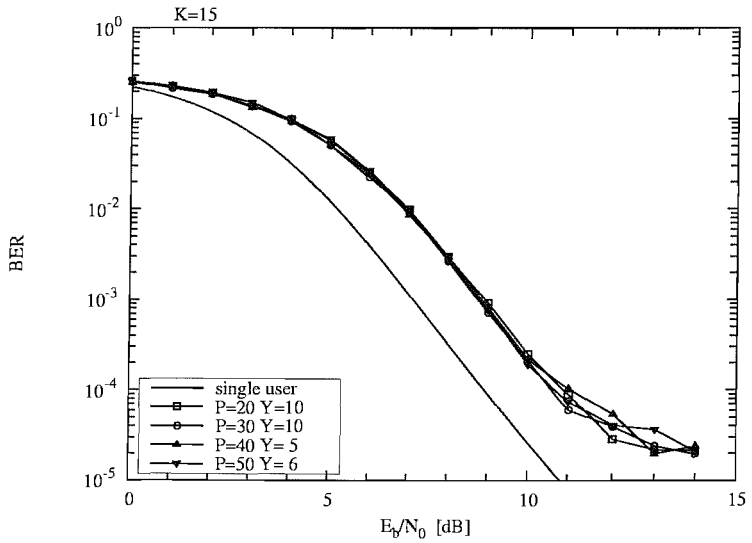

Figure 7.26: BER performance of the GA-assisted MUD designed for asynchronous MC-CDMA assisted by $R = \frac{1}{2}$ rate, constraint length $m = 3$ turbo coding using 4 iterations, when the number of users supported was $K = 15$. The number of generations was $Y = 5$, 6 or 10 and the population size was $P = 20$, 30, 40 and 50. Furthermore, the number of subcarriers was $M = 4$ and each subcarrier obeyed uncorrelated narrowband Rayleigh fading.

7.8 Chapter Conclusions

In conclusion, the GA assisted MUD is capable of significantly reducing the detection complexity in comparison to Verdu's optimum MUD, especially when the number of users supported is higher than $K = 15$. When channel coding techniques are employed, the GA-assisted MUD has the potential of further reducing the complexity imposed. Table 7.3 summarizes the complexity reduction factor of the GA assisted MUD for both synchronous and asynchronous MC-CDMA in comparison to Verdu's optimum MUD.

System	Complexity reduction factor
Synchronous MC-CDMA $K = 10$	2.5×10^0
Synchronous MC-CDMA $K = 15$	3.0×10^2
Asynchronous MC-CDMA $K = 10$	2.6×10^6
Asynchronous MC-CDMA $K = 15$	5.1×10^{10}

Table 7.3: Complexity reduction factor of the GA assisted MUD for both synchronous and asynchronous MC-CDMA in comparison to Verdu's optimum MUD.

Another important area of further study is the employment of multilevel modulation schemes both with and without various trellis coded error protection schemes.

CHAPTER 8

Time-Domain and Frequency-Domain Spreading Assisted MC DS-CDMA

8.1 Introduction

In context of code-division multiple-access (CDMA) communication, there are two fundamental types of spread-spectrum schemes. The first scheme spreads the original data stream in the time (T)-domain [10, 28], while the second in the frequency (F)-domain, resulting in a scheme known as MC-CDMA [4, 8, 147]. In [153], an amalgam of above spreading schemes has been developed. Explicitly, the original data stream is spread not only in the T-Domain, but also in the F-domain. Hence each user is assigned two spreading sequences for this operation, namely a T-domain and a F-domain sequence. This system exhibits a high flexibility as well as a reduced Multiuser Detection (MUD) complexity. In [153], several TF-domain spreading assisted MC DS-CDMA MUD schemes have been considered. However, the complexity imposed may become excessive, when the number of users supported is high. In this chapter, we will consider the employment of two specific families of spreading codes as the T-domain spreading code, which are known as generalized orthogonal codes [53] and Loosely Synchronized (LS) codes [18] [19]. These codes exhibit a so-called Interference Free Window (IFW). Over the duration of the IFW both the cross-correlation and the auto-correlation of the spreading codes is zero. The benefit of employing these specific codes as the T-domain code is that we are capable of reducing the complexity of the MUD, while achieving a frequency diversity gain. Specifically, the MUD's complexity is reduced because only a small fraction of the total number of users has to be separated and detected by the MUD, which belong to a given MUD group. By contrast, the set of users which are differentiated with the aid of unique user-specific

spreading codes having an IFW do not interfere with each other, as a benefit of the IFW provided by the T-Domain codes used. Another advantage of the proposed scheme is that we can significantly extend the width of the IFW in comparison with a single-carrier DS-CDMA system, because as a benefit of distributing the bits to serval subcarriers MC DS-CDMA has the potential of significantly reducing the chip rate, thereby extending the duration T_c of the chips. This also allows us to extend the width of the IFW, which renders the system more insensitive to timing imperfections, since larger timing errors can be accumulated without imposing interference.

This chapter is organized as follows. Sections 8.2 will briefly describe the family of generalized orthogonal codes. Section 8.3 characterises the philosophy of TF-domain spreading in the context of MC DS-CDMA signals. Section 8.4 considers two different correlation based detection schemes, while in Section 8.5 we discuss the beneficial features of this specific system. Finally, in Section 8.6 we provide simulation results for characterising different generalized orthogonal codes and LS codes, while in Section 8.7 we present our conclusions.

8.2 Generalized Orthogonal Codes

Since the basic properties of generalized orthogonal codes have been characterized in [53], we will concentrate our attention on procedures used for creating generalized orthogonal codes. Firstly, we define a sequence set $\mathbf{c}_1, \ldots, \mathbf{c}_N$, where $\mathbf{c}_n = [c_{n,0}, \ldots, c_{n,L-1}]$ is a spreading sequence having a length of L. The spreading codes result in an IFW width of τ_{IFW}, if the auto- and cross-correlation of the spreading codes satisfies:

$$R_{jk}(\tau) = \sum_{l=0}^{L-1} c_{j,l} c_{k,(l+\tau) \bmod L} = \begin{cases} L, & for \ \tau = 0, j = k \\ 0, & for \ \tau = 0, j \neq k \\ 0, & for \ 0 < \mid \tau \mid \leq \tau_{\text{IFW}}. \end{cases} \tag{8.1}$$

The family of generalized orthogonal binary codes is generated from a pair of so-called complementary sequences also referred to as mates [110, 112], which can be recursively generated as follows:

$$[X_0, Y_0] = [1, 1]. \tag{8.2}$$

$$[X_m, Y_m] = [X_{m-1} Y_{m-1}, (-X_{m-1}) Y_{m-1}]. \tag{8.3}$$

Hence, the length of X_m, Y_m is $L_m = 2^m$, and for a given complementary sequence pair $[X_m, Y_m]$, we can construct the 0th order generalized orthogonal code's mother matrix $F^{(0)}$, which can be expressed as [53]:

$$F^{(0)} = \begin{bmatrix} -X_m & Y_m \\ -\tilde{Y}_m & -\tilde{X}_m \end{bmatrix}, \tag{8.4}$$

where $\tilde{Y}_m$ is generated by reversing the order of the sequence Y_m, while $-X_m$ is the negated version of X_m. Each row of the mother matrix $F^{(0)}$ constitutes a spreading sequence, hence two spreading sequences are hosted by the matrix $F^{(0)}$. Once we obtained

the mother matrix $F^{(0)}$, the so-called $(n+1)$th-order generalized orthogonal code's matrix can be recursively generated according to:

$$F^{(n+1)} = \begin{bmatrix} F^{(n)} \otimes F^{(n)} & (-F^{(n)}) \otimes F^{(n)} \\ (-F^{(n)}) \otimes F^{(n)} & F^{(n)} \otimes F^{(n)} \end{bmatrix}, \tag{8.5}$$

where $\otimes$ denotes an operation referred to as interleaving, and the interleaving interval is 2^{m+n-1}. For the example of two vectors, namely for $A = [a_1, a_2, a_3, a_4, \ldots]$, $B = [b_1, b_2, b_3, b_4, \ldots]$ and for the interleaving interval of 2 we have:

$$A \otimes B = [a_1, a_2, b_1, b_2, a_3, a_4, b_3, b_4, \ldots]. \tag{8.6}$$

For simplicity, we denote the nth-order generalized orthogonal codes as $F(L, M, Z)$, where L is the length of generalized orthogonal code, M is the number of the codes generated and Z is the width of the IFW. Explicitly, we have $L = 2^{2n+m+1}$, $M = 2^{n+1}$, $Z = 2^{n+m-1}$. As an example, we consider $m = 2$ complementary pairs, which can be obtained with the aid of Equation 8.2 and 8.3 as follows:

$X_m = \{- - + - - - -+\}$

$Y_m = \{- + + + - + - -\}$.

Once we obtained the complementary pair X_m, Y_m, we can construct the 0th-order mother matrix $F^{(0)}$ according to Equation 8.4, and the matrix $F(32, 4, 4)$ of the codes can be constructed according to Equation 8.5, while the interleaving interval is $2^{m+n-1} = 2^{2+1-1} = 4$. Therefore, following the interleaving operation, the spreading code $F(32, 4, 4)$ can be constructed as:

$\{- - + - - - + - - - - + - - - + + + - + - - + - + + + - - - -+\}$

$\{- + + + - + + + - + - - - + - - + - - - - + + + + - + + - + - -\}$

$\{+ + - + - - + - + + + - - - - + - - + - - - + - - - - + - - -+\}$

$\{+ - - - - + + + + - + + - + - - - + + + - + + + - + - - - + - -\}$

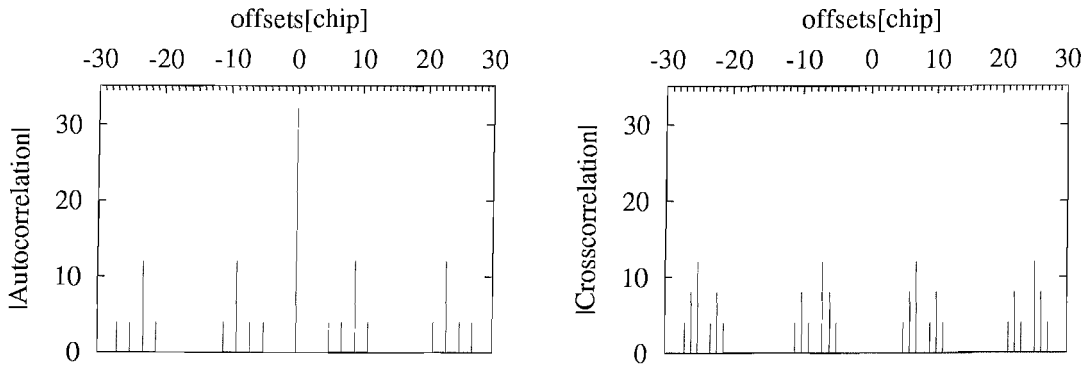

(a) Autocorrelation (b) Crosscorrelations

Figure 8.1: The auto- and cross-correlation magnitudes of the $F(32, 4, 4)$ codes. (a) All four codes of the family exhibit the same autocorrelation magnitude. (b) The crosscorrelation magnitudes of the four codes are also identical.

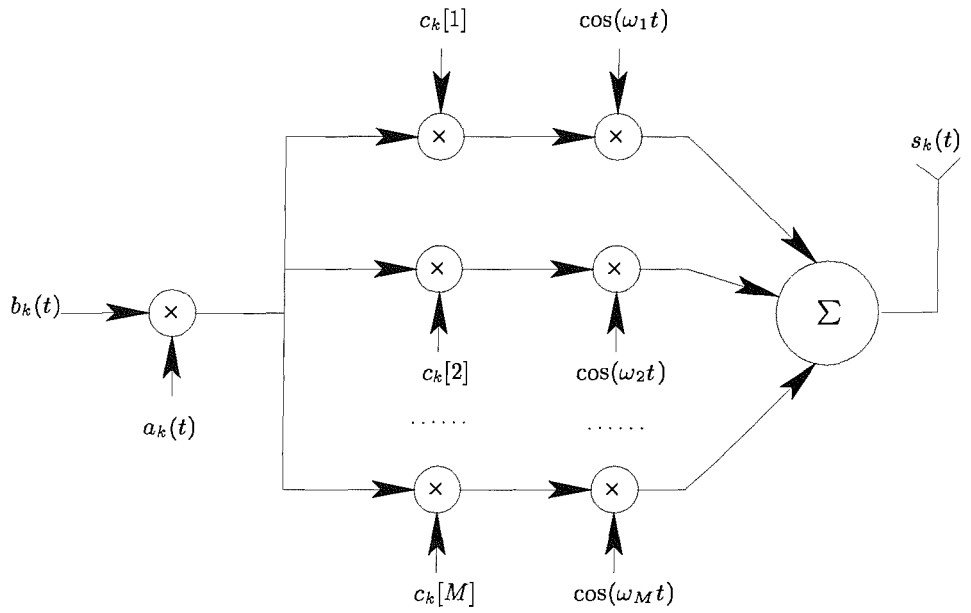

Figure 8.2: Transmitter model of MC DS-CDMA using both time-domain and frequency-domain spreading. T-domain spreading is achieved using the code $a_k(t)$ and each chip of $a_k(t)$ is spread in the frequency-domain by mapping it to M subcarriers, each carrying one of the M F-domain chips c_k.

All four different codes of the $F(32,4,4)$ family exhibited the same autocorrelation magnitudes, namely that seen in Figure 8.1(a). It can be observed in Figure 8.1(a) that the off-peak autocorrelation $R_p[\tau]$ $p = 1,\ldots,4$ becomes zero for $|\tau| \leq 4$. The crosscorrelation magnitudes $|R_{j,k}(\tau)|$ depicted in Figure 8.1(b) are also zero for $|\tau| \leq 4$. From the observations made as regards to the aperiodic correlations we may conclude that the $F(32,4,4)$ codes exhibit an IFW within an offset duration of ± 4 chip intervals.

Furthermore, we can shorten the generalized orthogonal code set $F(L,M,Z)$ for creating a new generalized orthogonal code set $F'(L',M,Z')$, where we have $L' = 2^{2n+m+1-t}, M = 2^{n+1}, Z' = 2^{n+m-1-t}$, provided that we have $t < min\{m,n\}$. This shortening operation will reduce the code length L, however, it also reduces the width τ_{IFW} of the interference free window. Our general objective is to maximize the relative duration of the IFW in comparison to the code length, while generating the highest possible number of codes. Broadly spreading this allows us to support the highest possible number of users without imposing multiuser interference. Having described the process of creating generalized orthogonal codes, in the next section we will consider another family of codes, which also exhibits an IFW, namely the family of LS codes.

8.3 System Model

The transmitter schematic of the MC DS-CDMA scheme using both T-domain and F-domain, i.e. TF-domain spreading is shown in Fig.8.2 in the context of the kth user. At the transmitter side, the binary data stream $b_k(t)$ is first direct-sequence (DS) spread using the T-domain signature sequence $a_k(t)$. Following T-domain spreading,

the T-domain DS spread signal is divided into M parallel branches, where each branch-signal is multiplied by a corresponding chip value of the F-domain spreading sequence $\mathbf{c}_k = [c_k[1], c_k[2], \ldots, c_k[M]]^T$ of length M. Following F-domain spreading each of the M branch signals modulates a subcarrier frequency using binary phase shift keying (BPSK). Then, the M number of subcarrier-modulated substreams are added in order to form the transmitted signal. Hence, the transmitted signal of user k can be expressed as

$$s_k(t) = \sqrt{\frac{2P}{M}} \sum_{m=1}^{M} b_k(t) a_k(t) c_k[m] \cos(\omega_m t), \quad k = 1, 2, \ldots, K, \tag{8.7}$$

where P represents the transmitted power of each user and $\{\omega_m\}$, $m = 1, \ldots, M$ represents the subcarrier frequency set. The binary data stream's waveform $b_k(t) = \sum_{i=0}^{\infty} b_k P_{T_b}(t - iT_b)$, $k = 1, \ldots, K$ consists of a sequence of mutually independent rectangular pulses P_{T_b} of duration T_b and of amplitude +1 or -1 with equal probability. The spreading sequence $a_k(t) = \sum_{j=0}^{\infty} a_{kj} P_{T_c}(t - jT_c)$, $k = 1, \ldots, K$ denotes the T-domain spreading sequence waveform of the kth user, where $P_{T_c}(t)$ is the rectangular chip waveform, which is defined over the interval $[0, T_c)$. We assume that the T-domain spreading factor is $N = T_b/T_c$, which represents the number of chips per bit-duration. Furthermore, we assume that the subcarrier signals are orthogonal and the spectral main-lobes of the subcarrier signals are not overlapping with each other.

We assume that K quasi-synchronous[1] TF-domain spread MC DS-CDMA signals obeying the form of (8.7) are transmitted over the uplink frequency selective channel, but each subcarrier of each user experiences statistically independent single-path flat Rayleigh fading. Hence, the mth subcarrier's Channel Impulse Response (CIR) can be written as $\gamma_{m,k} e^{j\phi_{m,k}}$, $m = 1, \ldots, M$, $k = 1, \ldots, K$, where the amplitude $\gamma_{m,k}$ is a Rayleigh distributed random variable and the phase $\phi_{m,k}$ is uniformly distributed between $[0, 2\pi)$. We also assume furthermore that each user experienced a different delay of τ_k, which obeys $\tau_k \leq \tau_{\text{IFW}}$. This can be achieved by invoking a Global Positioning System (GPS) assisted synchronization protocol. Then the received signal may be expressed as:

$$r(t) = \sum_{k=1}^{K} \sqrt{\frac{2P}{M}} \sum_{m=1}^{M} b_k(t) a_k(t - \tau_k) c_k[m] \gamma_{m,k} \cos(\omega_m t + \phi_{m,k}) + n(t), \tag{8.8}$$

where $n(t)$ represents the AWGN having zero mean and double-sided power spectral density of $N_0/2$.

Moreover, let $\{a_1(t), a_2(t), \ldots, a_N(t)\}$ and $\{\mathbf{c}_1, \mathbf{c}_2, \ldots, \mathbf{c}_M\}$ be the N number of T-domain spreading sequences and M number of F-domain spreading sequences, respectively, where $\mathbf{c}_u = [c_u[1]\ c_u[2]\ \ldots\ c_u[M]]^T$, $u = 1, \ldots, M$ represents a F-domain spreading code. Furthermore, we assume that the number of active users is K. We also introduce a new variable of $\mathcal{K} = \lfloor K/N \rfloor$, where $\lfloor x \rfloor$ represents the smallest integer not less than

[1] Quasi-synchronous in this context implies that the delay-differences of the individual users are within the IFW.

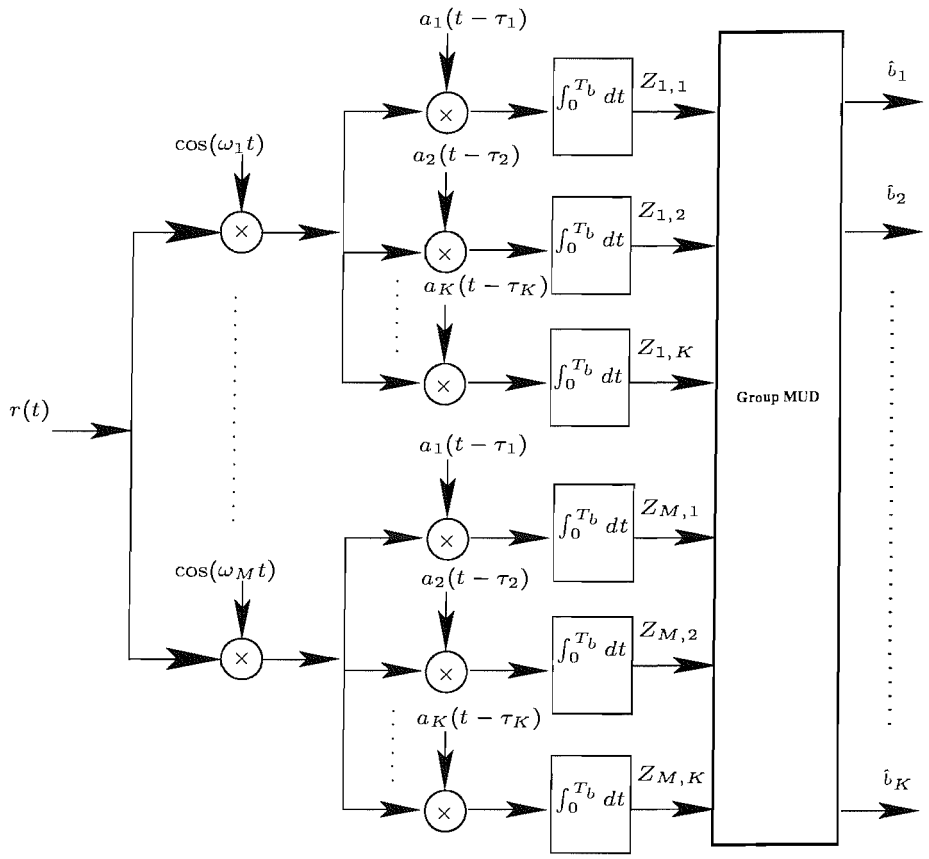

Figure 8.3: Receiver model of MC DS-CDMA using both time-domain and frequency-domain spreading.

x, for denoting the number users associated with a specific T-domain code, which are differentiated by unique F-domain code. Then, we have $1 \leq \mathcal{K} \leq M$, since the total number of users is less than the product of the T-domain and F-domain spreading factor, *i.e.* we have $K \leq NM$ and $\mathcal{K} \leq M$. Based on the above assumptions, the K number of users supported can be grouped into N user groups, with each group supporting at most $\mathcal{K}$ users. Consequently, it can be readily shown that each of the N user groups can be distinguished by assigning one of the N number of T-domain spreading sequences.

As shown in Fig.8.2 and Equation (8.7), each TF-domain spread MC DS-CDMA signal is identified with the aid of two spreading sequences, one applied in the context of the T-domain and one in the F-domain. In the following sections we will analyze the detection of TF-domain spread MC DS-CDMA signals by invoking two different detection schemes. Specifically, in Section 8.4 we used both Maximum Ratio Combining (MRC) as well as a low-complexity Maximum Likelihood (ML) decision based MUD.

8.4 Detection Schemes

In this section we will discuss the receiver model of the MC DS-CDMA schemes employed, which is shown in Fig 8.3. We consider a correlation-based receiver, which essentially carries out the inverse operation seen in Fig 8.2. In Fig 8.3 the output variable $Z_{m,k}$

corresponding to the mth subcarrier of the kth user can be expressed as:

$$Z_{m,k} = \int_0^{T_b} r(t)a_k(t-\tau_k)\cos(\omega_m t)dt, \ k = 1,\ldots,K, \ m = 1,\ldots,M. \tag{8.9}$$

According to [22], the received signal vector $\mathbf{Z}_m$ at the output of the bank of matched filters related to the mth subcarrier can be expressed as:

$$\begin{aligned} \mathbf{Z}_m^{(i)} &= [z_{m,1},\ldots,z_{m,K}]^T \\ &= \mathbf{R}[1]\mathbf{W}_m\mathbf{C}_m\mathbf{b}^{(i-1)} + \mathbf{R}[0]\mathbf{W}_m\mathbf{C}_m\mathbf{b}^{(i)} + \mathbf{R}^T[1]\mathbf{W}_m\mathbf{C}_m\mathbf{b}^{(i+1)} + \mathbf{n_m}, \end{aligned} \tag{8.10}$$

where we have:

$$\begin{aligned} \mathbf{C}_m &= \text{diag}[c_1[m],\ldots,c_K[m]] \\ \mathbf{W}_m &= \text{diag}[\gamma_{m,1}e^{j\phi_{m,1}},\ldots,\gamma_{m,K}e^{j\phi_{m,K}}] \\ \mathbf{b} &= [b_1,\ldots,b_K]^T \\ \mathbf{n} &= [n_1,\ldots,n_K]^T \\ i &\text{ is the time index,} \end{aligned} \tag{8.11}$$

and the zero-mean Gaussian noise vector $\mathbf{n_m}$ has the same crosscorrelation matrix as described in Equations 7.19 - 7.21 of Section 7.5.

However, in our system the time-domain spreading codes are either LS codes or generalized orthogonal codes, which exhibit an IFW. Therefore, the partial cross-correlation matrix $\mathbf{R}[1]$ is an all-zero matrix, provided that the delay differences obey $\tau_k \leq \tau_{\text{IFW}}$, $k = 1,\ldots,K$. Hence, Equation 8.10 can be simplified to:

$$\mathbf{Z}_m^{(i)} = \mathbf{R}[0]\mathbf{W}_m\mathbf{C}_m\mathbf{b}^{(i)} + \mathbf{n}_m. \tag{8.12}$$

In Equation 8.12 we can ignore the time index (i) in the superscripts. Hence, Equation 8.12 can be written as:

$$\mathbf{Z}_m = \mathbf{R}[0]\mathbf{W}_m\mathbf{C}_m\mathbf{b} + \mathbf{n}_m. \tag{8.13}$$

8.4.1 Maximum Ratio Combining

Following the philosophy of MRC, the output variable of the kth user can be written as [4]:

$$\mathbf{Z}_{\text{MRC},k} = \sum_{m=1}^{M} Z_{m,k}\gamma_{m,k}e^{-j\phi_{m,k}}, \tag{8.14}$$

which is the superposition of the correlator outputs matched to the individual subcarriers $m = 1,\ldots,M$, weighted by the complex conjugate of the corresponding complex-valued CIR coefficient, which is expressed as $\gamma_{m,k}\cdot e^{-j\phi_{m,k}}$. Finally, the corresponding data bits b_k are decided according to the decision rule of $\hat{b}_k = \text{sgn}(\mathbf{Z}_{\text{MRC},k})$ for $k = 1,2,\ldots,K$.

8.4.2 Low-Complexity Multiuser Detection

Let us now interpret Equation 8.13 in more detail. In Section 8.3 we have divided the K number of users supported into $\mathcal{K}$ user groups, each group having N users, which

are distinguished by their time-domain spreading code $a_k(t)$. In this scenario, the system activates N time-domain spreading codes and $\mathcal{K}$ frequency-domain spreading codes. Therefore, provided that both the ith and jth user's delay is within the range of the IFW and the ith user and jth user are in the same group, the element ρ_{ij} of the correlation-matrix $\mathbf{R}[0]$ of Equation 8.13 will satisfy $\rho_{ij} = 0$. More specially, in this system each user will encounter Multiple Access Interference (MAI) imposed by a reduced number of $\mathcal{K}-1$ users, rather than K users, since all these $\mathcal{K}$ users of each of the N user groups employ the same T-domain spreading code but a different F-domain spreading code. Therefore, we have to detect a reduced number of $\mathcal{K}$ rather than K users, which facilitates the employment of low-complexity Multiuser Detection (MUD). For example, let us consider the first user in the context of supporting a total of $K = \mathcal{K}N$ users. Then the first user encounters interference inflicted by the Nth,...,$\mathcal{K}N$th user, because they share the same T-domain spreading code, but they are identified by the different F-domain spreading codes. Hence, Equation 8.13 can be simplified as:

$$\tilde{\mathbf{Z}}_m = \tilde{\mathbf{R}}[0]\tilde{\mathbf{W}}_m\tilde{\mathbf{C}}_m\tilde{\mathbf{b}} + \tilde{\mathbf{n}}_m, \tag{8.15}$$

where we have:

$$\begin{aligned}
\tilde{\mathbf{Z}}_m &= [Z_1, Z_N, \ldots, Z_{\mathcal{K}N}]^T, \\
\tilde{\mathbf{C}}_m &= \text{diag}[c_1[m], c_N[m] \ldots, c_{\mathcal{K}N}[m]], \\
\tilde{\mathbf{W}}_m &= \text{diag}[\gamma_{1,m}e^{j\phi_{1,m}}, \gamma_{N,m}e^{j\phi_{N,m}} \ldots, \gamma_{\mathcal{K}N,m}e^{j\phi_{\mathcal{K}N,m}}], \\
\tilde{\mathbf{b}} &= [b_1, b_N, \ldots, b_{\mathcal{K}N}]^T, \\
\tilde{\mathbf{n}}_m &= [n_1, n_N, \ldots, n_{\mathcal{K}N}]^T,
\end{aligned}$$

$$\tilde{\mathbf{R}}[0] = \begin{bmatrix} \rho_{1,1} & \rho_{1,N} & \cdots & \rho_{1,\mathcal{K}N} \\ \rho_{N,1} & \rho_{N,N} & \cdots & \rho_{N,\mathcal{K}N} \\ \vdots & \vdots & \vdots & \vdots \\ \rho_{\mathcal{K}N,1} & \rho_{\mathcal{K}N,N} & \cdots & \rho_{\mathcal{K}N,\mathcal{K}N} \end{bmatrix}. \tag{8.16}$$

The Maximum Likelihood (ML) decision based MUD of the mth subcarrier has to evaluate:

$$\hat{\mathbf{b}} = \arg\{\min_{\mathbf{b}}\{\| \tilde{\mathbf{Z}}_m - \tilde{\mathbf{R}}[0]\tilde{\mathbf{W}}_m\tilde{\mathbf{C}}_m\tilde{\mathbf{b}} \|^2\}\}, \tag{8.17}$$

where $\| \cdot \|^2$ denotes the Euclidean norm. Upon combining all the M subcarriers, the ML based MUD's decision function can be written as:

$$\hat{\mathbf{b}} = \arg\{\min_{\mathbf{b}}\{\sum_{m=1}^{M} \| \tilde{\mathbf{Z}}_m - \tilde{\mathbf{R}}[0]\tilde{\mathbf{W}}_m\tilde{\mathbf{C}}_m\tilde{\mathbf{b}} \|^2\}\}. \tag{8.18}$$

According to Equation 8.18, the complexity of the ML decision based MUD invoked in the context of the TF-domain spreading assisted MC DS-CDMA system is on order of $2^{\mathcal{K}}$, rather than on $2^{\mathcal{K}N}$. Let us now briefly summarize the basic features of the system considered, before we characterize the achievable system performance.

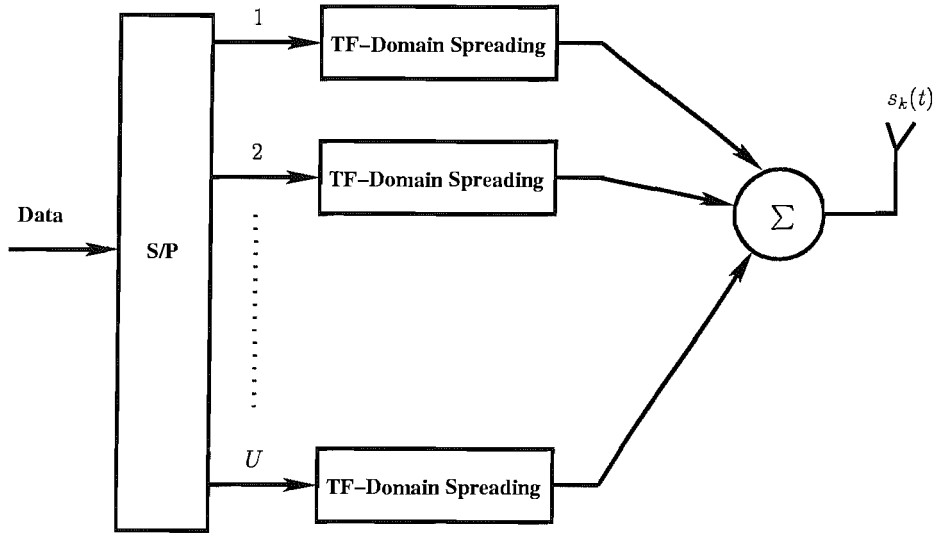

Figure 8.4: Transmitter model of MC DS-CDMA using serial to parallel conversion.

8.5 Characteristics of TF-domain Spreading Assisted MC DS-CDMA Employing Generalized Orthogonal Codes and Loosely Synchronized Codes

The system considered in Figure 8.2 of the previous section can be extended by using $U \cdot M$ number of subcarriers. Specifically, as it is shown in Fig 8.4, the original serial data stream is first subjected to serial to parallel conversion, resulting in U independent parallel data streams. Moreover, each parallel data stream is further spread to M subcarriers using the TF-domain spreading philosophy of Fig 8.2. The M subcarriers are arranged for maintaining the maximum possible frequency spacing, so that they experience independent fading and hence achieve the maximum possible frequency diversity gain. Specifically, let $\{f_1, f_2, \ldots, f_{US}\}$ be the $U \cdot M$ number of subcarrier frequencies, where each of the U parallel bits is spread according to the following $U \times M$-dimensional matrix:

$$\mathbf{F} = \begin{pmatrix} f_1 & f_{U+1} & \cdots & f_{(M-1)U+1} \\ f_2 & f_{U+2} & \cdots & f_{(M-1)U+2} \\ \vdots & \vdots & \ddots & \vdots \\ f_U & f_{2U} & \cdots & f_{MU} \end{pmatrix}. \tag{8.19}$$

Therefore, the chip rate of the MC DS-CDMA signal can be reduced by a factor of $U \cdot M$ and hence the width of the IFW can be extended by a factor of $U \cdot M$ in comparison to a DS-CDMA system, which can be expressed as:

$$\tau_{IFW,MCDS-CDMA} = U \cdot M \cdot \tau_{IFW,DS-CDMA}. \tag{8.20}$$

Based on Equation 8.20, we argue that the width of interference free window of MC DS-CDMA systems may be significantly higher than that of the DS-CDMA. This beneficial feature allows us to have significantly larger cells, which result in higher propagation delay

differences and/or allows the system to reliably operate even in case of higher absolute code synchronization errors, as long as they do not exceed the IFW width.

Another advantage of this system is that it is capable of achieving a high frequency diversity gain, because the chips of each bit are transmitted on independently fading subcarriers. Hence when the transmitted signal experiences frequency selective fading, the chances are that only some of the chips of a F-domain spreading code are corrupted and therefore the corresponding bit conveyed by the specific spreading code concerned may still be recovered. Consequently this system may be capable of achieving Mth-order F-domain diversity and benefit from a factor of $2^{\mathcal{K}N}/2^{\mathcal{K}} = 2^N$ lower multiuser detection complexity.

8.6 Simulation Results

Let us consider a system having $M = 4$ subcarriers and using different T-domain spreading codes. The F-domain spreading codes are generated by the 4×4-dimensional orthogonal Walsh code generator matrix given by:

$$\mathbf{F} = \begin{pmatrix} + & + & + & + \\ + & - & + & - \\ + & + & - & - \\ + & - & - & + \end{pmatrix}. \tag{8.21}$$

Furthermore, we considered four different T-domain spreading codes, which are the $F(16, 8, 1)$, $F(16, 4, 2)$, LS$(2, 4, 1)$ and the LS$(4, 2, 3)$ codes, where again, generalized orthogonal codes are defined with the aid of the parameters $F(L, M, Z)$, with L being the length of the code, M being the number of codes generated and Z being the IFW width. Furthermore, the LS codes are defined with the aid of the parameters LS(N, P, W), where the length of the LS code is $2NP + 2W$, the number of codes generated is $2P$, and the width of the IFW is W. Moreover, we assume that each subcarrier of each user experienced independent flat Rayleigh fading.

From Figures 8.5, 8.6, 8.7 and 8.8 we can observe that the low-complexity MUD is capable of approaching the single-user bound. By contrast, it becomes explicit from Figures 8.9, 8.10 8.11 and 8.12 that–as expected–the performance of MRC based detection is substantially worse than that of the MUD.

8.7 Chapter Conclusions

In this chapter, we employed a specific family of spreading codes which exhibit an interference free window in the context of the TF-domain spreading assisted MC DS-CDMA system considered. In this system we reduced the complexity of the MUD by a factor of $2^{\mathcal{K}N}/2^{\mathcal{K}} = 2^N$, while achieving Mth-order frequency diversity. The system is capable of significantly extending the width of the interference free window as a benefit of the

serial to parallel conversion invoked in Figure 8.4, which additionally renders the system insensitive to timing imperfections.

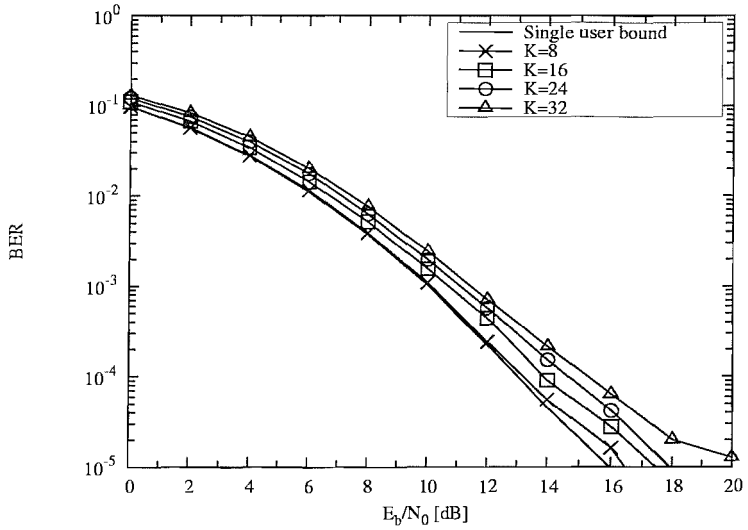

Figure 8.5: BER performance of the TF-domain spreading aided MC DS-CDMA system in conjunction with low-complexity MUD, while employing the $F(16, 8, 1)$ generalized orthogonal code as the T-domain spreading code. The F-domain spreading code was a 4×4-dimensional Walsh code, and each of the $M = 4$ subcarriers experienced independent narrowband Rayleigh fading. The MUD complexity reduction factor was $2^N = 2^8 = 512$.

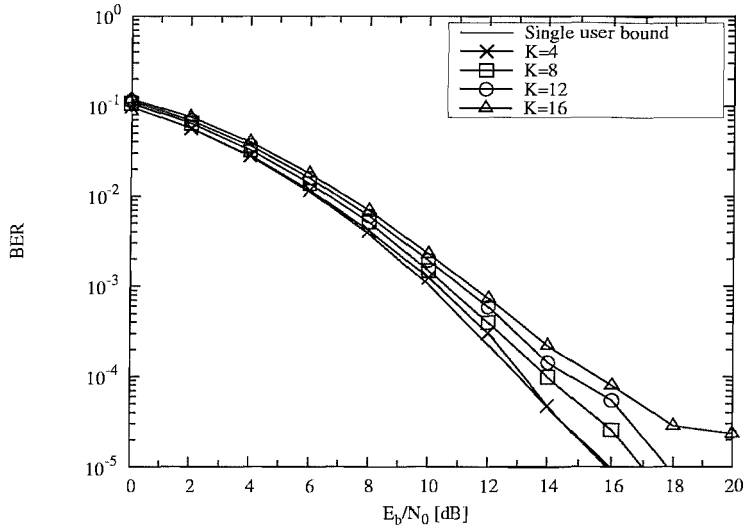

Figure 8.6: BER performance of the TF-domain spreading aided MC DS-CDMA system in conjunction with low-complexity MUD, while employing the $F(16,4,2)$ generalized orthogonal code as the T-domain spreading code. The F-domain spreading code was a 4×4-dimensional Walsh code, and each of the $M = 4$ subcarriers experienced independent narrowband Rayleigh fading. The MUD complexity reduction factor was $2^N = 2^4 = 16$.

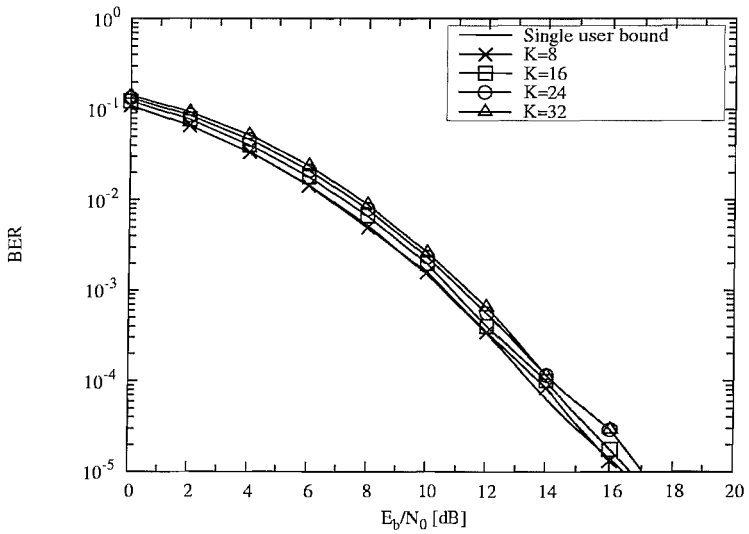

Figure 8.7: BER performance of the TF-domain spreading aided MC DS-CDMA system in conjunction with low-complexity MUD, while employing the $LS(2,4,1)$ loosely synchronized code as the T-domain spreading code. The F-domain spreading code was a 4×4-dimensional Walsh code, and each of the $M = 4$ subcarriers experienced independent narrowband Rayleigh fading. The MUD complexity reduction factor was $2^N = 2^8 = 512$.

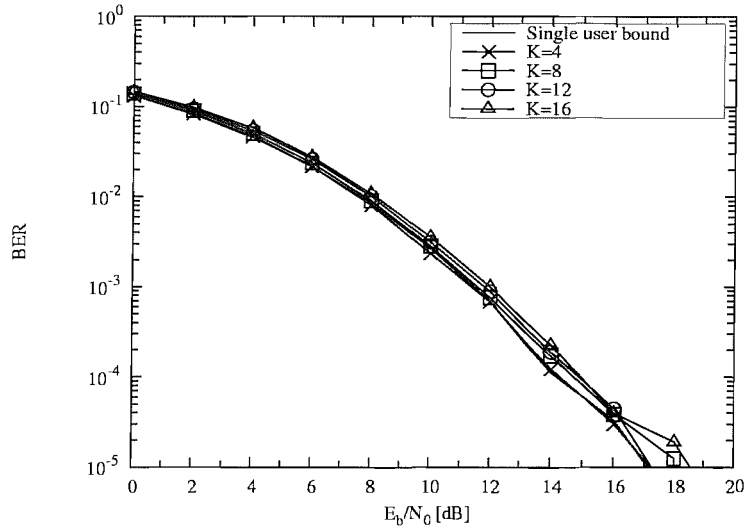

Figure 8.8: BER performance of the TF-domain spreading aided MC DS-CDMA system in conjunction with low-complexity MUD, while employing the LS$(4, 2, 3)$ loosely synchronized code as the T-domain spreading code. The F-domain spreading code was a 4×4-dimensional Walsh code, and each of the $M = 4$ subcarriers experienced independent narrowband Rayleigh fading. The MUD complexity reduction factor was $2^N = 2^4 = 16$.

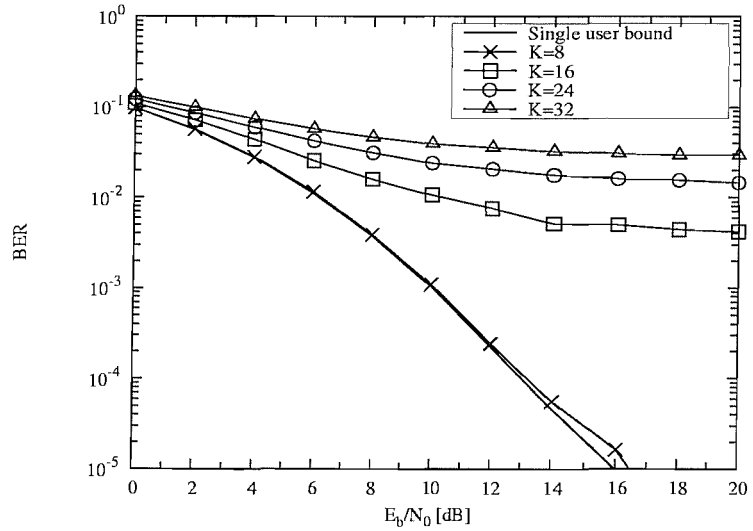

Figure 8.9: BER performance of the TF-domain spreading aided MC DS-CDMA system when MRC detection was employed, while employing the $F(16, 8, 1)$ generalized orthogonal code as the T-domain spreading code. The F-domain spreading code was a 4×4-dimensional Walsh code, and each of the $M = 4$ subcarriers experienced independent narrowband Rayleigh fading.

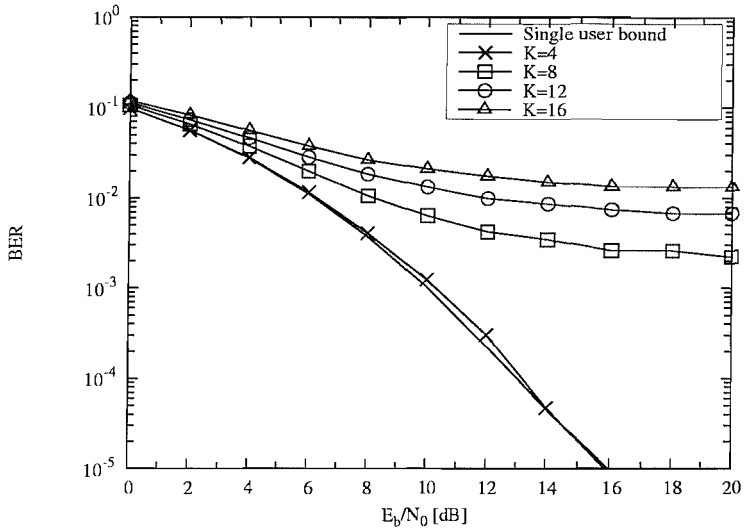

Figure 8.10: BER performance of the TF-domain spreading aided MC DS-CDMA system when MRC detection was employed, while employing the $F(16, 4, 2)$ generalized orthogonal code as the T-domain spreading code. The F-domain spreading code was a 4×4-dimensional Walsh code, and each of the $M = 4$ subcarriers experienced independent narrowband Rayleigh fading.

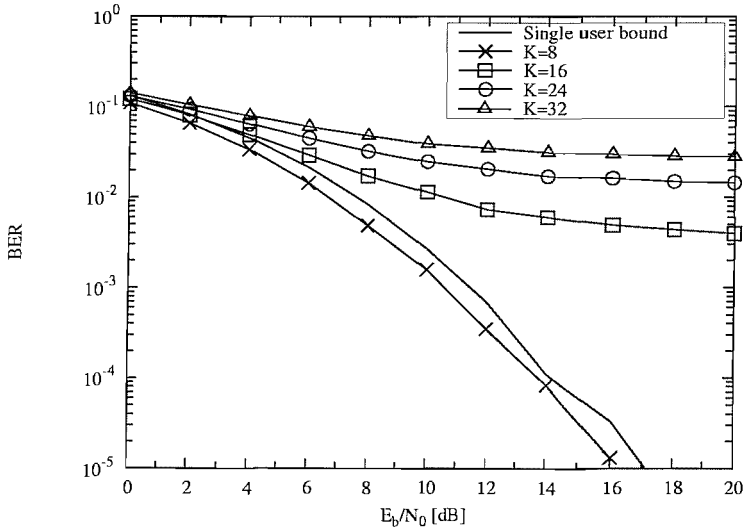

Figure 8.11: BER performance of the TF-domain spreading aided MC DS-CDMA system when MRC detection was employed, while employing the LS$(2, 4, 1)$ loosely synchronized code as the T-domain spreading code. The F-domain spreading code was a 4×4-dimensional Walsh code, and each of the $M = 4$ subcarriers experienced independent narrowband Rayleigh fading.

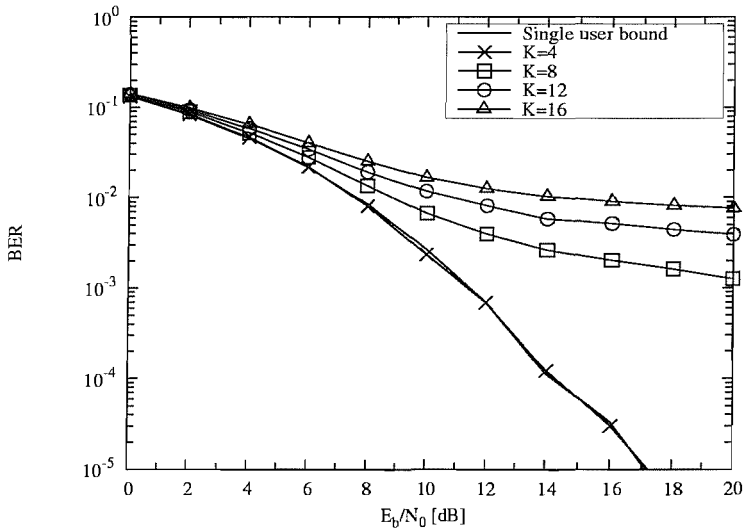

Figure 8.12: BER performance of the TF-domain spreading aided MC DS-CDMA system when MRC detection was employed, while employing the LS$(4, 2, 3)$ loosely synchronized code as the T-domain spreading code. The F-domain spreading code was a 4×4-dimensional Walsh code, and each of the $M = 4$ subcarriers experienced independent narrowband Rayleigh fading.

CHAPTER 9

Space Time Spreading Assisted MC DS-CDMA

9.1 Introduction

Broadband mobile wireless communication systems aim for supporting a wide range of services and bit rates by employing techniques capable of achieving the highest possible spectral efficiency. For example, the system is expected to support services, ranging from low bit rate speech communications at $9.6kb/s$ to high bit rate video telephony at $2Mb/s$. Furthermore, one of the basic requirements expected to be satisfied by broadband mobile wireless systems is the provision of high bit rate wireless Internet services and the delivery of high-speed multimedia services. However, the system capacity and the achievable data rate of the wireless system is limited by numerous factors, most severely by the bandwidth of the frequency-selective fading channel. In recent years, space-time coding has received much attention and as a result it has become one of the most prevalent technique of combating the time-varying characteristics of the fading channel. In order to circumvent the effects of fading, the employment of transmit diversity techniques, such as Space-Time Block Coding (STBC) [78, 154] and Space-Time Trellis Coding (STTC) [78, 154, 155] has been proposed. Both STBC and STTC incorporate channel coding, modulation, transmit diversity and optional receiver diversity. Another transmit diversity technique refraining from using channel coding is known as Space-Time Spreading (STS) [3, 25, 156–158]. References [156, 157] demonstrate that a substantial diversity gain can be achieved by STS and this typically allows the throughout of the system to be increased. In [159] an attractive STBC based transmit diversity technique has been proposed for employment in W-CDMA systems.

In this contribution, we propose a novel STS assisted Multi-Carrier Direct Sequence Code Division Multiple Access (MC DS-CDMA) system for supporting a wide range of bit rates with the aid of advantageously combining Quadrature Amplitude Modulation (QAM) [30] and Orthogonal Variable Spreading Factor (OVSF) based DS spreading codes [31]. Since OVSF codes exhibit variable *Spreading Factors* (SFs), the transmitted bit rate can be adjusted with the aid of different SFs. More specifically, when the number of activated users in a cell is low, the interference level experienced is also low, which requires a low spreading gain, and hence the users' SFs can be low. Given a fixed bandwidth and chip rate, this enables the users to support high bit rates in comparison to the scenario of having to use high SFs. Moreover, when the STS scheme of [156, 157] is invoked for spreading the signal of each subcarrier, the fading of each subcarrier is mitigated and hence the system becomes capable of significantly reducing the effects of the time-variant channel fading, provided that the number of transmit antennas is higher than one. In other words, the system will achieve a higher throughput and a higher transmitted bit rate with the advent of transmit diversity.

Finally, turbo coding [116] techniques are invoked in our system for enhancing the achievable BER versus SNR performance. As the number of turbo channel decoding iterations increases, the achievable BER versus SNR performance can be improved at the cost of an increased complexity.

Therefore, the achievable integrity and the bit rate supported by this system is determined by the following factors:

- The specific value of the SFs used, which is determined by the number of users supported within the cell considered.
- The number of transmitter antennas.
- The number of bits conveyed by the QAM scheme used on each subcarrier, which is determined by the corresponding channel transfer factor of the channel at the specific subcarrier's frequency and the corresponding transmitted power.
- The number of turbo decoding iterations, which is determined by the affordable complexity.

This chapter is organized as follows. Section 9.2 introduces the basic philosophy of OVSF spreading codes. Section 9.3 describes the schematic of this system, while Section 9.4 characterizes the receiver's structure and provides our performance analysis. Section 9.5 addresses the provision of the multirate services. Section 9.6.1 provides our simulation results characterizing the performance of this system, when no channel coding is employed, while Section 9.6.2 quantifies the performance of this system, when turbo channel coding is invoked. Finally, Section 9.9 offers our conclusions and outlines our future work.

9.2 OVSF Codes

State-of-the-art wireless communications systems are expected to support multi-rate transmissions, especially when delivering wireless multimedia communication services. More

explicitly, the system should be designed to support a variety of data services, spanning various bit rates, ranging from low to very high bit rate although the DS-spread signal bandwidth is the same for all the users. The provision of multiple rates requires the employment of multiple *spreading factors* (SFs) in the physical layer. CDMA systems may invoke OVSF spreading codes [20,31,160] for supporting multiple rates, while a constant chip rate and a constant bandwidth are maintained. The generation of the OVSF spreading codes is fairly straightforward with the aid of the modified Hadamard transformation, which has the ability of preserving the orthogonality of the codes used for supporting different bit rates R_b with the aid of different SFs, as it was originally proposed in [160].

Let C_N be an $N \times N$-dimensional matrix, which hosts a set of N binary spreading codes having a length of N chips, that are represented as: $C_{N,i}, i = 1, \ldots N$. According to [31], C_N can be recursively generated by the following equation:

$$C_N = \begin{bmatrix} C_{N,1} \\ C_{N,2} \\ C_{N,3} \\ C_{N,4} \\ \cdots \\ C_{N,N} \\ C_{N,N} \end{bmatrix} = \begin{bmatrix} C_{N/2,1} \cup C_{N/2,1} \\ C_{N/2,1} \cup -C_{N/2,1} \\ C_{N/2,2} \cup C_{N/2,2} \\ C_{N/2,2} \cup -C_{N/2,2} \\ \cdots \\ C_{N/2,N/2} \cup C_{N/2,N/2} \\ C_{N/2,N/2} \cup -C_{N/2,N/2} \end{bmatrix}, \tag{9.1}$$

where $\cup$ denotes the concatenation operation and $-C_{N,i}$ is the negated version of $C_{N,i}$. As a result, all these OVSF codes can be generated recursively using a tree structure, as shown in Figure 9.1. Starting from $C_{1,1} = 1$, a set of 2^k spreading codes having the length of 2^k chips are generated at the kth layer, which are associated with the $SF = 2^k$. Any two spreading codes found at different layers of the hierarchical structure of Figure 9.1 are also orthogonal, unless one of them is a mother code of the other, where the mother codes 'give birth' to the codes at lower layer of the hierarchy seen in Figure 9.1. Explicitly, as shown in Figure 9.2, the spreading code $C_{2,1}$ is orthogonal to the spreading codes $C_{8,4}$, $C_{8,5}$, $C_{8,7}$ and $C_{8,8}$. However, the orthogonality is destroyed, if one is the other's mother code. For example, as shown in Figure 9.3, the spreading code $C_{2,1}$ is not orthogonal to the spreading codes $C_{8,2}$ and $C_{8,3}$. In other words, once the code $C_{2,1}$ is assigned to a user, the codes $\{C_{4,1}, C_{4,2}, C_{8,1} \ldots C_{8,4}\}$ generated from this mother code cannot be assigned to other users without destroying the orthogonality amongst these codes. The number of the available spreading codes in this system is not fixed, since it depends on both the number of users supported in the cell, as well as on each user's transmission bit rate. Assuming that the spreading code $C_{N,i}$ having a length of $N = 2^n$ chips is employed in the system, which is capable of supporting the data rate of R, a spreading code having a length of 2^{n-k} chips is capable of supporting a data rate of $2^k \cdot R$.

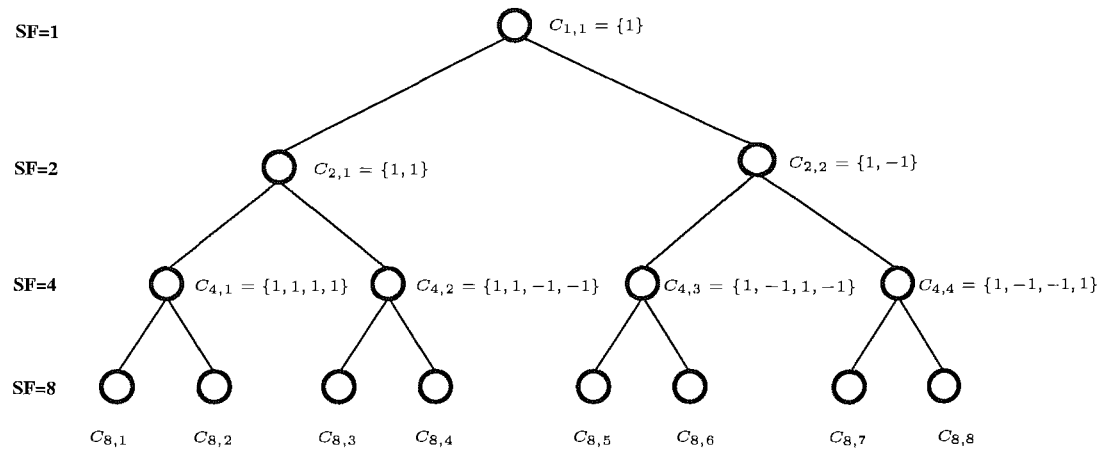

Figure 9.1: Tree structure of the OVSF spreading codes.

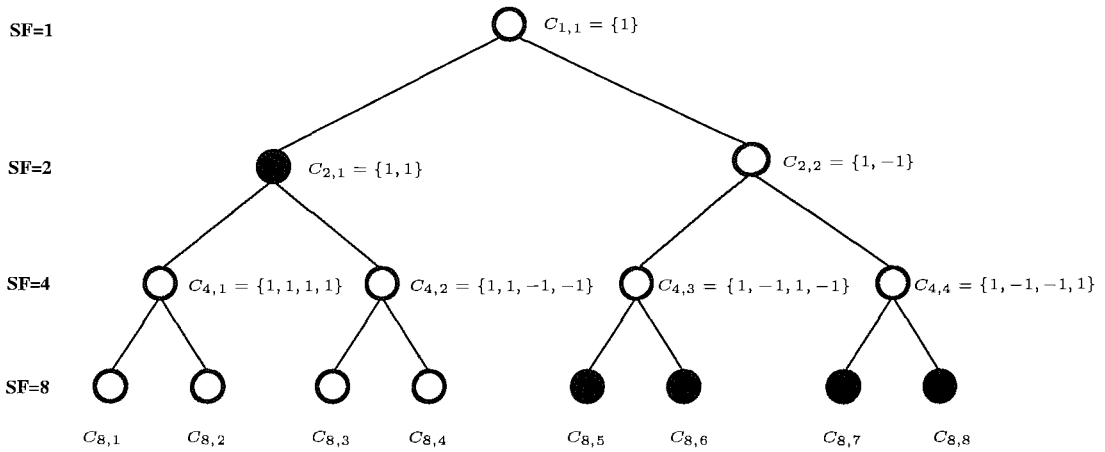

Figure 9.2: Orthogonality is maintained between the different layers' OVSF spreading codes.

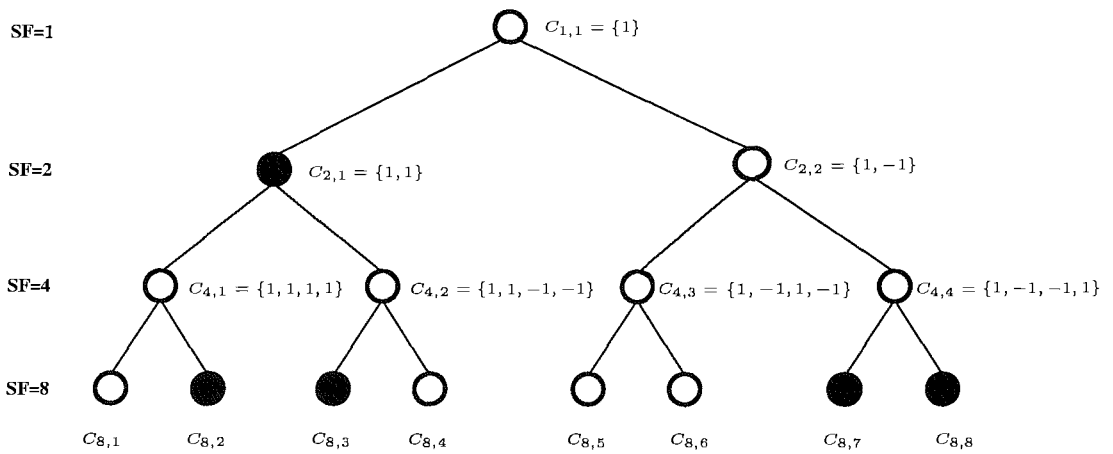

Figure 9.3: Orthogonality is destroyed between the different layers' OVSF spreading codes.

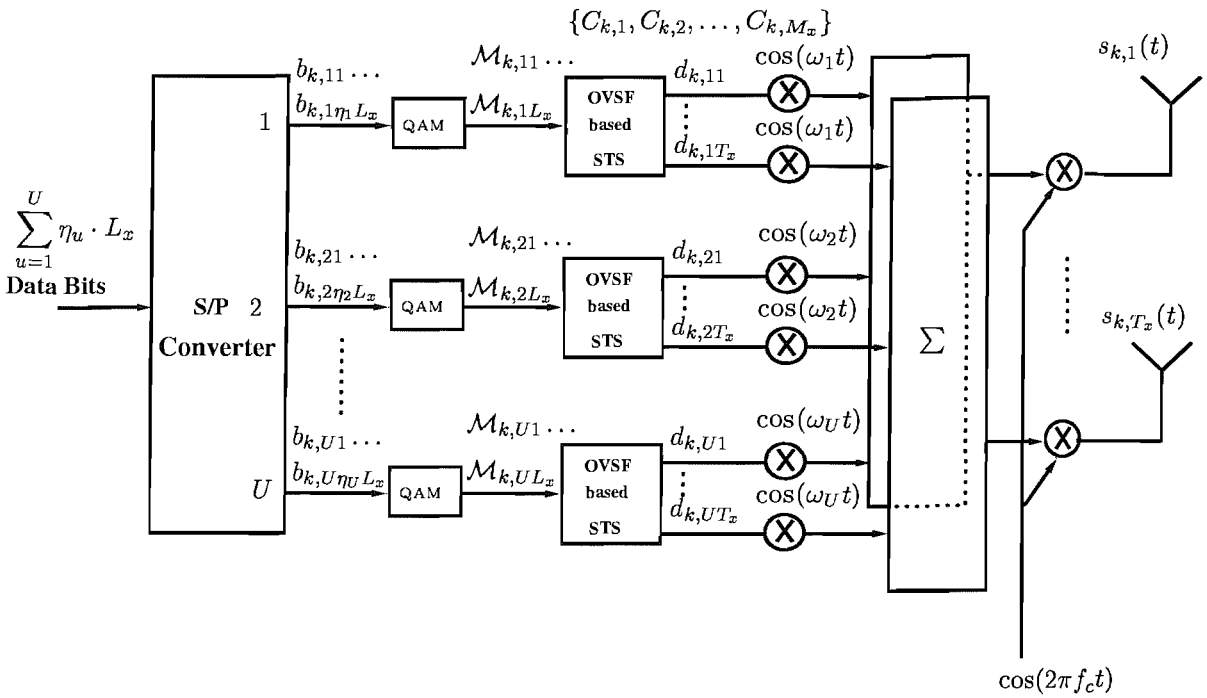

Figure 9.4: Schematic of the downlink transmitter, where the bit stream b_k is converted to the symbol stream $\mathcal{M}_k$ after the QAM block. Then the symbol stream will be mapped to the corresponding STS block d_k. Finally, each STS block will be mapped to the multiple antennas and transmitted as the signal $s_k(t)$ [3].

9.3 System Outline

The system considered in this chapter is a STS [161] assisted MC DS-CDMA scheme [3, 157] using U number of subcarriers, and the space-time spreading scheme has T_x transmitter antennas, but only a single receiver antenna is invoked. Furthermore, in this chapter a synchronous MC DS-CDMA scheme designed for the downlink channel is investigated, where K user signals are transmitted synchronously. The transmitter schematic of the kth user is shown in Figure 9.4, where the transmission of complex data symbols using QAM modulation and real-valued spreading [3, 25] were considered. As shown in Fig.9.4, at the transmitter a block of $\sum_{u=1}^{U} \eta_u \cdot L_x$ number of data bits having a bit duration of T_b is S-P converted to U parallel sub-blocks, where the η_u is the number of Bits Per Symbol (BPS) transmitted by the QAM scheme on the uth subcarrier and L_x is the number of QAM symbols per the space-time spreading sub-block. For example, if BPSK and 64QAM are invoked on the uth subcarrier, the corresponding value of η_u will be 1 and 6, respectively. Hence, each space-time spreading sub-block has $\eta_u L_x$ data bits, generating L_x modulated symbols given by $\{\mathcal{M}_{k,u1}, \ldots \mathcal{M}_{k,uL_x}\}$. These modulated symbols are space-time spread using the schemes of [3, 25, 162] with the aid of M_x number of OVSF spreading codes for example by $\{c_{k,1}(t), c_{k,2}(t), \ldots, c_{k,M_x}(t)\}$, $k = 1, 2, \ldots, K$ and mapped to T_x number of transmitter antennas. Since the bits to be transmitted are mapped to the multi-bit QAM symbols as well as to T_x number of transmit antennas, the symbol duration of the STS signals is expanded to UL_xT_b, and the number of chips of the

OVSF codes becomes $UL_xT_b/T_c = UL_xN$, where we have $N = T_b/T_c$ and T_c represents the chip-duration of the orthogonal spreading codes. The orthogonal codes assume the form of $c_{k,i}(t) = \sum_{j=0}^{UL_xN-1} c_{k,i}[j]P_{T_c}(t - jT_c)$, where $c_{k,i}[j] \in \{+1, -1\}$ and they obey the relationship of $\sum_{l=0}^{UL_xN} c_{i,m}[l]c_{j,n}[l] = 0$, whenever $i \neq j$ or $m \neq n$. Furthermore, $P_{T_c}(t)$ represents the chip waveform defined over the interval of $[0, T_c)$. Since the maximum available number of the OVSF codes having UL_xN chips is UL_xN and each user requires M_x number of OVSF codes, the maximum number of users supported by these orthogonal codes is $\mathcal{K}_{max} = UL_xN/M_x$. As seen in Fig.9.4, following STS, each STS block generates T_x number of parallel signals to be mapped to the T_x number of transmitter antennas. Finally, as shown in Fig.9.4, the Inverse Fast Fourier Transform (IFFT) is invoked for carrying out multicarrier modulation [3,4], and the IFFT block's output signal is transmitted using one of the transmitter antennas.

The kth user's transmitted signal corresponding to the T_x transmitter antennas can be expressed in a complex form as

$$\mathbf{s}_k(t) = \sqrt{\frac{2E_b}{UT_b}\frac{1}{M_xT_x}}\,[\mathbf{C}_k\mathbf{B}_k]^T\,\mathbf{w}\cos(2\pi f_c t), \tag{9.2}$$

where E_b/UT_b represents the transmitted power per subcarrier expressed as $L_xE_b/UL_xT_b = E_b/UT_b$, while the factor of M_xT_x represents STS using M_x orthogonal OVSF codes and T_x transmitter antennas. In (9.2) - where the superscript T denotes the vector or matrix transpose - $\mathbf{s}_k(t) = [s_{k1}(t)\ s_{k2}(t)\ \ldots\ s_{kT_x}(t)]^T$ represents the transmitted signal vector of the T_x transmitter antennas. Furthermore, in Eq.(9.2) $\mathbf{C}_k$ is a $(U \times UM_x)$-dimensional matrix constituted by the OVSF codes [160], which can be expressed as

$$\mathbf{C}_k^T = \begin{pmatrix} c_{k,1}(t) & 0 & \ldots & 0 \\ c_{k,2}(t) & 0 & \ldots & 0 \\ \vdots & \vdots & \ddots & \vdots \\ c_{k,M_x}(t) & 0 & \ldots & 0 \\ 0 & c_{k,1}(t) & \ldots & 0 \\ 0 & c_{k,2}(t) & \ldots & 0 \\ \vdots & \vdots & \ddots & \vdots \\ 0 & c_{k,M_x}(t) & \ldots & 0 \\ \vdots & \vdots & \ddots & \vdots \\ 0 & 0 & \vdots & c_{k,1}(t) \\ 0 & 0 & \vdots & c_{k,2}(t) \\ \vdots & \vdots & \ddots & \vdots \\ 0 & 0 & \vdots & c_{k,M_x}(t) \end{pmatrix}, \tag{9.3}$$

while $\mathbf{B}_k$ is a $(UM_x \times T_x)$-dimensional matrix mapping the U sub-blocks of QAM symbols

$\mathcal{M}_{k,ul}, u = 1,\ldots,U \quad l = 1,\ldots,L_x$ to space-time spreading symbols. According to [3,25], the STS matrix $\mathbf{B}_k$ can be expressed as

$$\mathbf{B}_k = [\mathbf{B}_{k1}^T \; \mathbf{B}_{k2}^T \; \ldots \; \mathbf{B}_{kU}^T]^T, \tag{9.4}$$

where $\mathbf{B}_{ku}$ for $u = 1,2,\ldots,U$ represents $(M_x \times T_x)$-dimensional matrices, which obey the structure of

$$\mathbf{B}_{ku} = \begin{pmatrix} a_{11}\mathcal{M}'_{k,11} & a_{12}\mathcal{M}'_{k,12} & \ldots & a_{1L_x}\mathcal{M}'_{k,1T_x} \\ a_{21}\mathcal{M}'_{k,21} & a_{22}\mathcal{M}'_{k,22} & \ldots & a_{2L_x}\mathcal{M}'_{k,2T_x} \\ \vdots & \vdots & \ddots & \vdots \\ a_{M_x1}\mathcal{M}'_{k,M_x1} & a_{U2}\mathcal{M}'_{k,M_x2} & \ldots & a_{M_xL_x}\mathcal{M}'_{k,M_xT_x} \end{pmatrix}, \; u = 1,2,\ldots,U, \tag{9.5}$$

where a_{ij} represents the sign of the element at the ith row and the jth column. More specifically, the signs a_{ij} of the matrix elements in Eq.(9.5) are determined by the STS design rule [3,25], while $\mathcal{M}'_{k,ij}$ in $\mathbf{B}_{ku}$ is the QAM symbol assigned to the (i,j)th element, which is one of the L_x number of symbols $\{\mathcal{M}_{k,u1}, \mathcal{M}_{k,u2}, \ldots, \mathcal{M}_{k,uL_x}\}$ of user k. For the specific case of $L_x = M_x = T_x = 2$ and 4, the corresponding matrix $\mathbf{B}_{ku}$ are given by [25].

$$\begin{pmatrix} \mathcal{M}_{k,u1} & \mathcal{M}_{k,u2} \\ \mathcal{M}_{k,u2} & -\mathcal{M}_{k,u1} \end{pmatrix}, \; u = 1,2,\ldots,U, \tag{9.6}$$

$$\begin{pmatrix} \mathcal{M}_{k,u1} & \mathcal{M}_{k,u2} & \mathcal{M}_{k,u3} & \mathcal{M}_{k,u4} \\ \mathcal{M}_{k,u2} & -\mathcal{M}_{k,u1} & \mathcal{M}_{k,u4} & -\mathcal{M}_{k,u3} \\ \mathcal{M}_{k,u3} & -\mathcal{M}_{k,u4} & -\mathcal{M}_{k,u1} & \mathcal{M}_{k,u2} \\ \mathcal{M}_{k,u4} & \mathcal{M}_{k,u3} & -\mathcal{M}_{k,u2} & -\mathcal{M}_{k,u1} \end{pmatrix}, \; u = 1,2,\ldots,U. \tag{9.7}$$

Finally, in (9.2) $\mathbf{w}$ represents the U-dimensional vector of QAM symbols modulating the U subcarriers, which can be expressed as:

$$\mathbf{w} = [\exp(j2\pi f_1 t) \; \exp(j2\pi f_2 t) \; \ldots \; \exp(j2\pi f_U t)]^T. \tag{9.8}$$

Equation (9.2) represents the general form of the transmitted MC DS-CDMA/QAM signals using STS, regardless of the values of L_x, M_x and T_x. However, the study conducted in [25] has shown that STS schemes using the values of $L_x = M_x = T_x$, i.e. orthogonal STS-related spreading sequences as well as transmission antennas constitute attractive schemes, since they are capable of achieving the maximal attainable transmit diversity without requiring extra STS spreading codes. Furthermore, [25] indicates that such attractive STS schemes exist for values of $L_x = M_x = T_x = 2, 4, 8$, etc. Note that for the specific values of $L_x = M_x = T_x = 2, 4$ the above mentioned attractive STS schemes have been unambiguously specified with the aid of (9.6). In this chapter, we only investigate these attractive STS schemes and our results are mainly based on MC DS-CDMA systems designed for $L_x = M_x = T_x = 1, 2, 4, 8$ number of transmitter antennas.

For the case of $L_x = M_x = T_x = 2$, the MC DS-CDMA signals transmitted by antenna 1 and 2 can be simply expressed as:

$$\begin{aligned}\mathbf{s}_k(t) &= \begin{pmatrix} s_{k1}(t) \\ s_{k2}(t) \end{pmatrix} \\ &= \sqrt{\frac{2E_b}{4UT_b}} \begin{pmatrix} \sum_{u=1}^{U} [c_{k,1}\mathcal{M}_{k,u1} + c_{k,2}\mathcal{M}_{k,u2}] \cos[2\pi(f_c + f_u)t] \\ \sum_{u=1}^{U} [c_{k,1}\mathcal{M}_{k,u2} - c_{k,2}\mathcal{M}_{k,u1}] \cos[2\pi(f_c + f_u)t] \end{pmatrix}. \end{aligned} \quad (9.9)$$

By contrast, for the case of $L_x = M_x = T_x = 4$, the MC DS-CDMA signals transmitted by antenna 1, 2, 3 and 4, respectively, can be expressed as:

$$\begin{aligned}\mathbf{s}_k(t) = \begin{pmatrix} s_{k1}(t) \\ s_{k2}(t) \\ s_{k3}(t) \\ s_{k4}(t) \end{pmatrix} &= \sqrt{\frac{2E_b}{16UT_b}} \\ \times \begin{pmatrix} \sum_{u=1}^{U} [c_{k,1}\mathcal{M}_{k,u1} + c_{k,2}\mathcal{M}_{k,u2} + c_{k,3}\mathcal{M}_{k,u3} + c_{k,4}\mathcal{M}_{k,u4}] \cos[2\pi(f_c + f_u)t] \\ \sum_{u=1}^{U} [c_{k,1}\mathcal{M}_{k,u2} - c_{k,2}\mathcal{M}_{k,u1} - c_{k,3}\mathcal{M}_{k,u4} + c_{k,4}\mathcal{M}_{k,u3}] \cos[2\pi(f_c + f_u)t] \\ \sum_{u=1}^{U} [c_{k,1}\mathcal{M}_{k,u3} + c_{k,2}\mathcal{M}_{k,u4} - c_{k,3}\mathcal{M}_{k,u1} - c_{k,4}\mathcal{M}_{k,u2}] \cos[2\pi(f_c + f_u)t] \\ \sum_{u=1}^{U} [c_{k,1}\mathcal{M}_{k,u4} - c_{k,2}\mathcal{M}_{k,u3} + c_{k,3}\mathcal{M}_{k,u2} - c_{k,4}\mathcal{M}_{k,u1}] \cos[2\pi(f_c + f_u)t] \end{pmatrix} \end{aligned} \quad (9.10)$$

In (9.9) and (9.10) we do not explicitly show the time-dependence of $c_{k,i}(t)$ for notional convenience, since in this chapter only synchronous transmissions are considered.

Assuming that K user signals expressed in the form of (9.2) are transmitted synchronously over single-path Rayleigh fading channels, the received complex-valued low-pass equivalent signal can be expressed as:

$$R(t) = \sum_{k=1}^{K} \sum_{g=1}^{T_x} \sqrt{\frac{2E_b}{UT_b} \frac{1}{M_x T_x}} \left([\mathbf{C}_k \mathbf{B}_k]^T \right)_g \mathbf{H}\mathbf{w} + n(t), \quad g = 1, \ldots, T_x, \quad (9.11)$$

where we have:

$$\mathbf{H} = \begin{pmatrix} h_{1g}\exp(j\psi_{1g}) & 0 & \ldots & 0 \\ 0 & h_{2g}\exp(j\psi_{2g}) & \ldots & 0 \\ \vdots & \vdots & \ddots & \vdots \\ 0 & 0 & \ldots & h_{Ug}\exp(j\psi_{Ug}) \end{pmatrix}, \; g = 1, 2, \ldots, T_x, \quad (9.12)$$

indicating that $\mathbf{H}$ represents the channel's complex impulse response in the context of the gth antenna and the coefficients h_{ig}, $i = 1, 2, \ldots, U$; $g = 1, 2, \ldots, T_x$ in $\mathbf{H}$ are independent

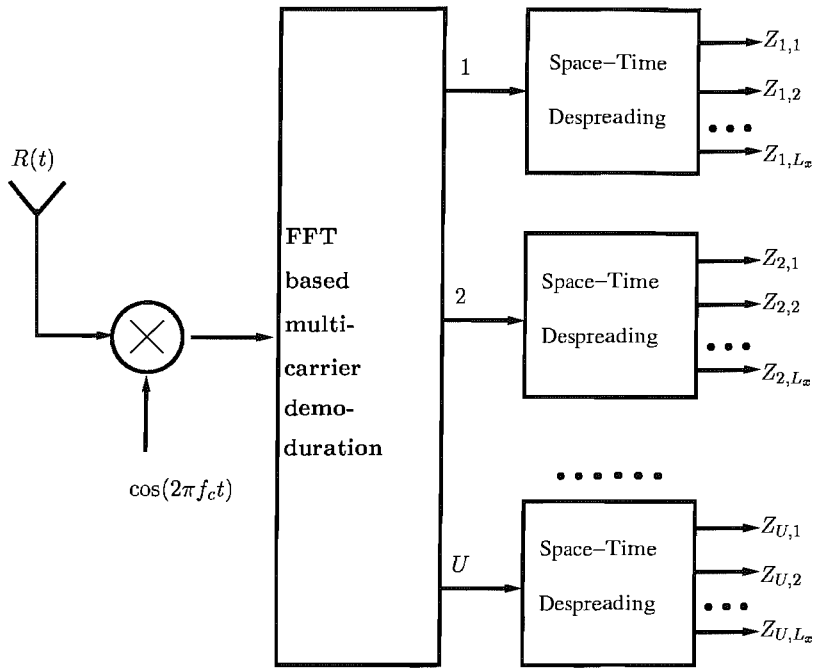

Figure 9.5: The receiver schematic of the MC DS-CDMA system using space-time spreading.

identically distributed (i.i.d) random variables obeying the Rayleigh distribution. The Probable Density Function (PDF) of the Rayleigh distribution can be expressed as:

$$f_{h_{ig}}(y) = \frac{2y}{\Omega} \exp\left(-\frac{y^2}{\Omega}\right), \; y \geq 0, \tag{9.13}$$

where $\Omega = \mathrm{E}[(h_{ig})^2]$. Furthermore, the phases ψ_{ig}, $i = 1, 2, \ldots, US$; $g = 1, 2, \ldots, T_x$ are introduced by the fading channels and are uniformly distributed in the interval $[0, 2\pi)$.

Specifically, for the case of $L_x = M_x = T_x = 2$, when the transmitted signal obeys (9.9), the received complex low-pass equivalent signal can be expressed as

$$\begin{aligned} R(t) = & \sum_{k=1}^{K} \sum_{u=1}^{U} \sqrt{\frac{2E_b}{4UT_b}} \Big(h_{u1} \exp(j\psi_{u1}) [c_{k,1}(t)\mathcal{M}_{k,u1} + c_{k,2}(t)\mathcal{M}_{k,u2}] \\ & + h_{u2} \exp(j\psi_{u2}) [c_{k,1}(t)\mathcal{M}_{k,u2} - c_{k,2}(t)\mathcal{M}_{k,u1}] \Big) \exp(2\pi f_u t) \\ & + n(t). \end{aligned} \tag{9.14}$$

9.4 Receiver Model and Bit Error Rate Analysis

Let the first user be the user-of-interest and consider a receiver employing FFT based multicarrier demodulation [4], space-time de-spreading [3, 25] as well as receiver diversity combining, as shown in Fig.9.5. The receiver of Fig.9.5 essentially carries out the inverse operations of those seen in Fig.9.4. In Fig.9.5 the received signal is first down-converted using the carrier frequency f_c, and then demodulated using FFT-based multicarrier demodulation [4]. After FFT-based multicarrier demodulation we obtain the U number of

parallel streams corresponding to the signals transmitted on the U MC DS-CDMA subcarriers, and each stream is space-time de-spread using the approach of [25], in order to obtain L_x separate complex data symbol variables, $\{Z_{u,l}, Z_{u,2}, \ldots, Z_{u,L_x}\}, u = 1, \ldots, U$, corresponding to the L_x QAM symbols $\{\mathcal{M}_{u1}, \mathcal{M}_{u2}, \ldots, \mathcal{M}_{uL_x}\}_{u=1}^{U}$ transmitted on the uth subcarrier, where we have $u = 1, 2, \ldots, U$, respectively. Following space-time de-spreading, a decision variable $Z_{u,i}, u = 1, \ldots, U; i = 1, \ldots, L_x$ is formed for each transmitted QAM symbol. Finally, the $\sum_{u=1}^{U} \eta_u \cdot L_x$ number of transmitted data bits can be decided based on the decision variables $\{Z_{u,i},\ u = 1, 2, \ldots, U;\ i = 1, 2, \ldots, L_x\}$ using the conventional threshold-detection based decision rule of the QAM scheme.

Above we have described the transmitter model and characterized the system parameters as well as the receiver model of broadband MC DS-CDMA using STS. Let us now investigate the achievable BER performance. In this section we derive the BER expression of the broadband MC DS-CDMA system using STS, which was described in Section 9.3. As an example, we derive the BER expression in detail for STS based MC DS-CDMA using the parameters of $L_x = M_x = T_x = 2$. The generalized BER expression of MC DS-CDMA using the set of attractive STS schemes of [25], i.e. using $L_x = M_x = T_x = 2, 4, 8$, etc. may then be derived from the case of $L_x = M_x = T_x = 2$ without providing the detailed derivations, since the extension of the corresponding formulae is relatively straightforward.

For the case of $L_x = M_x = T_x = 2$, the analysis can be commenced from (9.14). Let $d_{u,1}$, $d_{u,2}$ - where $u = 1, 2, \ldots, U$ - represent the correlator's output variables corresponding to the first two data bits transmitted on the uth subcarrier, where we have

$$d_{u,1} = \int_0^{2UT_b} R(t) c_{1,1}(t) \exp\left(-j2\pi f_u t\right) dt, \tag{9.15}$$

$$d_{u,2} = \int_0^{2UT_b} R(t) c_{1,2}(t) \exp\left(-j2\pi f_u t\right) dt. \tag{9.16}$$

Since orthogonal multicarrier signals, orthogonal STS codes, synchronous transmission of the K user signals as well as slowly flat-fading of each subcarrier are assumed, there is no interference between the different users and the different subcarrier signals. Therefore, when substituting (9.14) into (9.15), it can be readily shown that we arrive at:

$$\begin{aligned} d_{u,1} &= \sqrt{2UE_bT_b}\left[h_{u1}\exp(j\psi_{u1})\mathcal{M}_{1,u1} + h_{u2}\exp(j\psi_{u2})\mathcal{M}_{1,u2}\right] \\ &\quad + N_{u,1}, \end{aligned} \tag{9.17}$$

$$\begin{aligned} d_{u,2} &= \sqrt{2UE_bT_b}\left[h_{u1}\exp(j\psi_{u1})\mathcal{M}_{1,u2} - h_{u2}\exp(j\psi_{u2})\mathcal{M}_{1,u1}\right] \\ &\quad + N_{u,2}, \end{aligned} \tag{9.18}$$

where $N_{u,i}, i = 1, 2$ represents the complex AWGN expressed as

$$N_{u,i} = \int_0^{2UT_b} n(t) c_{1,i}(t) \exp\left(-j2\pi f_u t\right) dt, \tag{9.19}$$

which is a complex Gaussian distributed variable having zero mean and a variance of $2UN_0T_b$.

Assuming that the receiver has perfect knowledge of the fading parameters of $h_{ui}\exp(j\psi_{ui})$, $i = 1, 2$, the decision variables corresponding to the QAM symbols $\mathcal{M}_{1,ui}, i = 1, 2$ associated with the uth subcarrier can be expressed as

$$\begin{aligned} Z_{u,1} &= d_{u,1}h_{u1}\exp(-j\psi_{u1}) - d_{u,2}h_{u2}\exp(-j\psi_{u2}) \\ &= \sqrt{2UE_bT_b}[h_{u1}^2 + h_{u2}^2]\mathcal{M}_{1,u1} + N_{u1}, \qquad (9.20) \\ Z_{u,2} &= d_{u,1}h_{u2}\exp(-j\psi_{u2}) + d_{u,1}h_{u1}\exp(-j\psi_{u1}) \\ &= \sqrt{2UE_bT_b}[h_{u1}^2 + h_{u2}^2]\mathcal{M}_{1,u2} + N_{u2}, \qquad (9.21) \end{aligned}$$

for $u = 1, 2, \ldots, U$, and

$$\begin{aligned} N_{u1} &= N_{u,1}h_{u1}\exp(-j\psi_{u1}) - N_{u,2}h_{u2}\exp(-j\psi_{u2}), \qquad (9.22) \\ N_{u2} &= N_{u,1}h_{u2}\exp(-j\psi_{u2}) + N_{u,2}h_{u1}\exp(-j\psi_{u1}), \qquad (9.23) \end{aligned}$$

where N_{u1} and N_{u2} are both complex AWGN processes having a zero mean and a variance of $2UN_0T_b\sum_{l=1}^{T_x} h_{ul}^2$.

9.5 Provision of Multirate Services

Based on our arguments in Sections 9.2 and 9.3, the maximum number of orthogonal STS codes can be used, when all users' SF assumes the highest possible value, which is given by $SF_{max} = UL_xT_b/T_c = UL_xN$. Since each user requires M_x orthogonal STS codes, the maximum number of users supported by the UL_xN number of orthogonal STS codes is given by

$$\mathcal{K}_{max} = UL_xN/M_x. \qquad (9.24)$$

For the set of attractive STS schemes using $L_x = M_x = T_x = 2, 4, 8$, etc, the maximum number of users supported by the orthogonal STS codes is $\mathcal{K}_{max} = UN$. It can be seen that in this case the number of users supported is independent of the number of transmitter antennas, which emphasizes the advantages of the STS schemes using $L_x = M_x = T_x = 2, 4, 8$, etc. [25].

The system described in Figure 9.4 is capable of flexibly supporting multirate transmissions provided that the number of users K obey $K \leq \mathcal{K}_{max}$. Specifically, the kth user's transmission bit rate R_{kb} can be conveniently adjusted based on the following two factors:

- The users' SFs are indirectly determined by the total number of users supported in a cell, namely by K, because when the number of users K is high, the users' SFs will be inevitably increased. For example, when $K = \mathcal{K}_{max} = UN$, the users' SFs will be increased to their maximum of SF_{max}. In this scenario the achievable bit

rate R_{kb} will be the lowest in the context of a specific QAM scheme associated with a given number of bits per symbol. By contrast, if the total number of users K is very low, the SF can be adjusted to a low value, which will lead to an increased bit rate R_{kb}, while maintaining a given target integrity.

- The kth user's bit rate R_{kb} can also be adjusted by the activation of different QAM schemes. The higher-throughput modulation schemes, such as 64QAM and 16QAM, are capable of supporting a higher bit rate R_{kb}, than that of the lower-order modulation schemes, such as QPSK and BPSK. For example, the 64QAM modulation scheme is capable of supporting six times the bit rate of BPSK. However, the higher throughput modulation schemes require a higher SNR for achieving the same BER performance. In other words, for the same channel conditions, the higher-throughput modulation schemes require a higher transmitted power than that of the lower throughput modulation schemes for the sake of maintaining the same BER performance.

An interesting feature of this system is its ability of supporting multiple bit rates. Specifically, we can invoke different QAM schemes on different subcarriers, which will lead to numerous bit rate combinations. Assuming that in the full user-load scenario of $K = \mathcal{K}_{max}$ and $SF = SF_{max}$ we can employ BPSK on all the subcarriers while satisfying the target integrity requirements, the user is capable of supporting a bit rate of $R_{min}[b/s]$. If we now consider invoking a BPSK scheme on the subcarriers $1 \ldots (U-1)$ and 64QAM scheme on the Uth subcarrier, then the total supported bit rate can be expressed as:

$$R_{kb} = R_{min}/U \times 6 + (U-1) \times R_{min}/U = R_{min}(1 + \frac{5}{U}). \tag{9.25}$$

Let us investigate this scenario in little more detail. Assuming that the SF has not reached its maximum of SF_{max}, in the context of maintaining the same SNR and BER performance as before, the bit rate expressed in Equation 9.25 can be increased to:

$$R_{kb} = \frac{SF_{max}}{SF} R_{min}(1 + \frac{5}{U}), \tag{9.26}$$

by reducing the SF, provided that the BER requirements are still met. In other words, from Equations (9.25) and (9.26), we can observe that the system is capable of supporting multiple bit rates by appropriately adjusting the SF and the number of bits per QAM symbol. Hence we may conclude that we can adjust the bit rate both with the aid of the SF and also by using the most appropriate modulation schemes on the different subcarriers, depending on their subcarrier SNRs. Let us now characterize the achievable performance of the system in next section.

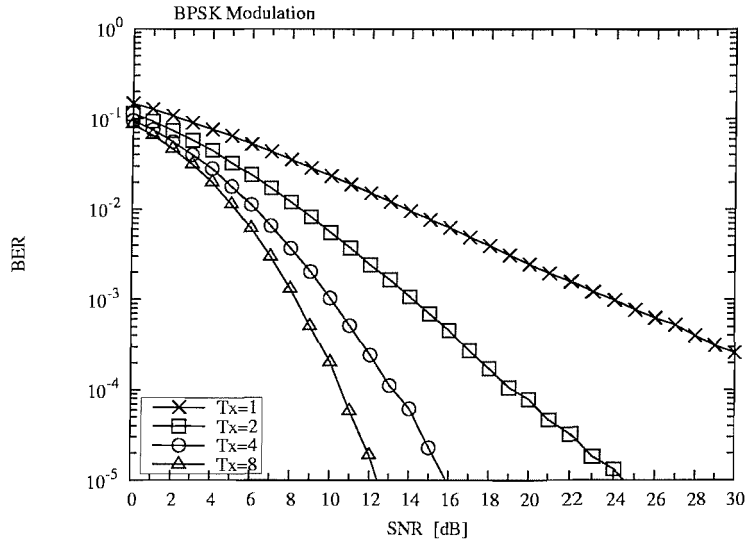

Figure 9.6: BER performance of STS-assisted MC DS-CDMA when **BPSK** modulation was invoked and the corresponding number of antennas was $T_x = 1, 2, 4, 8$, respectively. The number of subcarrier was $U = 8$, each subcarrier experienced independent flat Rayleigh fading and we used $SF = 32$.

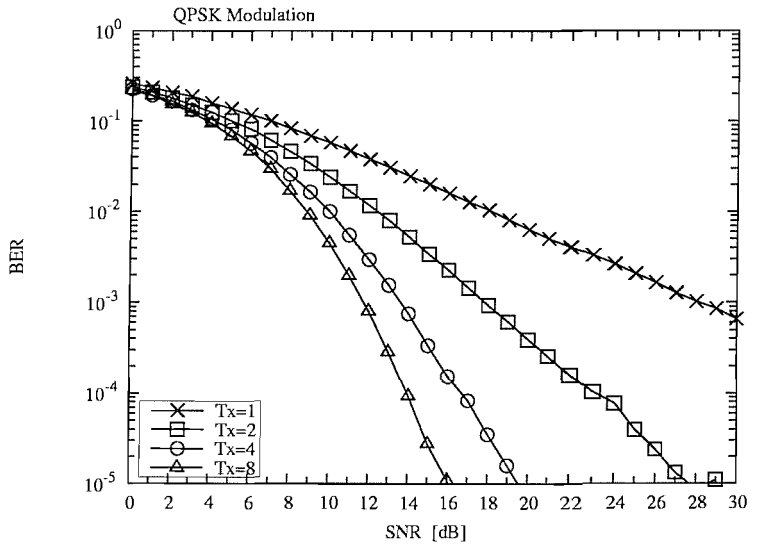

Figure 9.7: BER performance of STS assisted MC DS-CDMA when a **QPSK** scheme was invoked and the corresponding number of antennas was $T_x = 1, 2, 4, 8$, respectively. The number of subcarriers was $U = 8$, each subcarrier experienced independent flat Rayleigh fading and we used $SF = 32$.

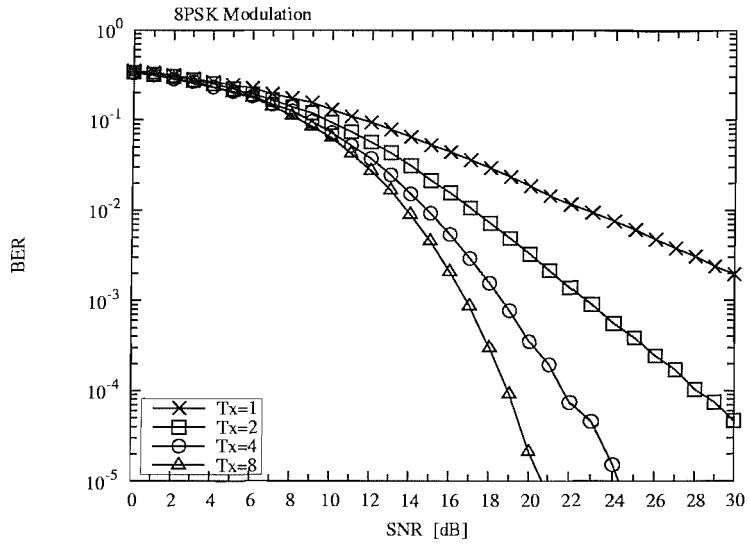

Figure 9.8: BER performance of STS assisted MC DS-CDMA, when an **8PSK** scheme was invoked and the corresponding number of antennas was $T_x = 1, 2, 4, 8$, respectively. The number of subcarriers was $U = 8$, each subcarrier experienced independent flat Rayleigh fading and we used $SF = 32$.

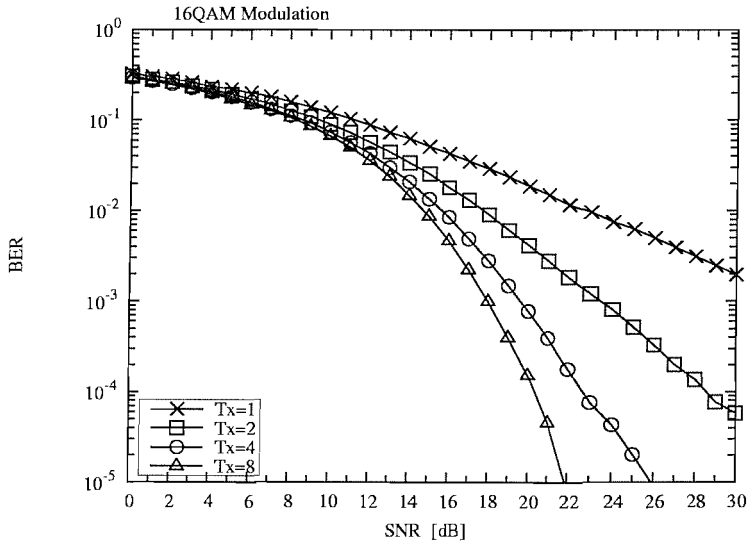

Figure 9.9: BER performance of STS assisted MC DS-CDMA, when a **16QAM** scheme was invoked and the corresponding number of antennas was $T_x = 1, 2, 4, 8$, respectively. The number of subcarriers was $U = 8$, each subcarrier experienced independent flat Rayleigh fading and we used $SF = 32$.

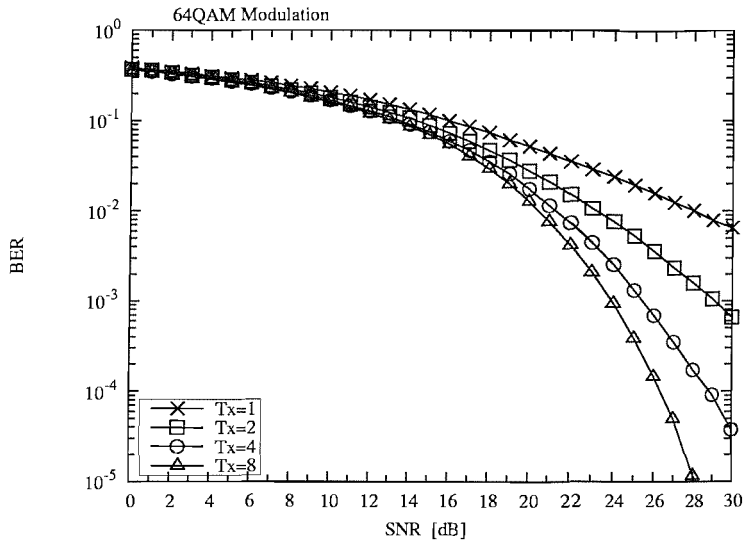

Figure 9.10: BER performance of STS assisted MC DS-CDMA when a **64QAM** scheme was invoked and the corresponding number of antennas was $T_x = 1, 2, 4, 8$, respectively. The number of subcarriers was $U = 8$ and each subcarrier experienced independent flat Rayleigh fading and we used $SF = 32$.

Modulation Scheme	$T_x = 1$	$T_x = 1$	$T_x = 4$	$T_x = 8$
BPSK SNR[dB]	24.5	14.5	10.0	8.2
QPSK SNR[dB]	28.5	17.5	13.5	12.0
8PSK SNR[dB]	33.0	23.0	19.0	17.0
16QAM SNR[dB]	32.5	23.7	19.6	18.0
64QAM SNR[dB]	38.0	29.2	26.0	24.1

Table 9.1: The SNR values required for the STS assisted MC DS-CDMA system, when different QAM schemes were invoked for achieving a BER of 10^{-3}. The number of subcarrier was $U = 8$, each subcarriers experienced independent flat Rayleigh fading and we used $SF = 32$.

9.6 Performance of Fixed QAM and STS Assisted MC DS-CDMA

9.6.1 Performance of Uncoded System

From Figure 9.6 we can observe that at a BER of 10^{-3}, the SNR required for $T_x = 1, 2, 4, 8$ transmit antennas is 24.5 dB, 14.5 dB, 10.0 dB and 8.2 dB, respectively. From this figure, the diversity gain is estimated to be about 10 dB, when the number of antennas is increased from $T_x = 1$ to $T_x = 2$. Similarly, Figures 9.7, 9.8, 9.9 and 9.10 characterized the performance of this STS assisted MC DS-CDMA system, when QPSK, 8PSK, 16QAM and 64QAM schemes were invoked. Finally, Table 9.1 summarized the SNR necessitated for achieving a BER of 10^{-3} in conjunction with different modulation schemes.

9.6.2 Performance Enhancements Using Turbo Coding

Channel coding techniques are capable of substantially improving the achievable performance of the communication systems, in particular the family of powerful turbo codes [116].

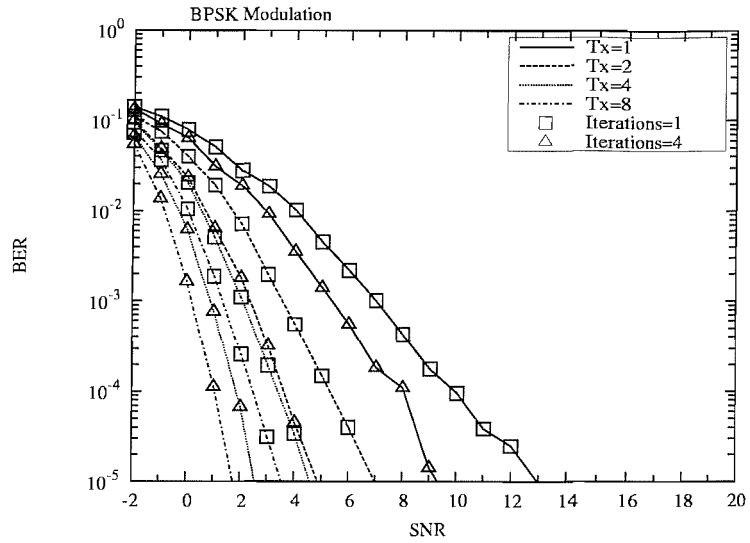

Figure 9.11: BER performance of STS assisted MC DS-CDMA when a **BPSK** scheme and **turbo coding** were employed. The number of antennas was $T_x = 1, 2, 4, 8$ and the number of turbo decoding iterations was $1, 4$, respectively. The remaining parameters are listed in Table 9.2.

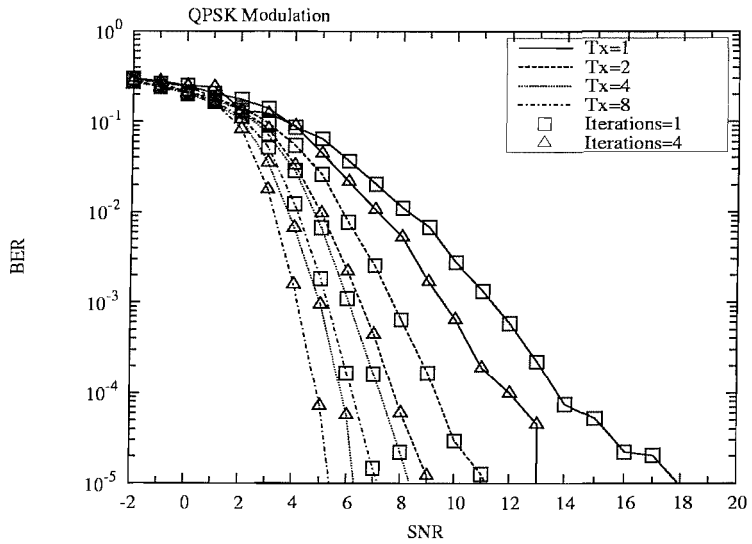

Figure 9.12: BER performance of STS assisted MC DS-CDMA when a **QPSK** scheme and **turbo coding** were employed. The number of antennas was $T_x = 1, 2, 4, 8$ and the number of turbo decoding iterations was $1, 4$, respectively. The remaining parameters are listed in Table 9.2.

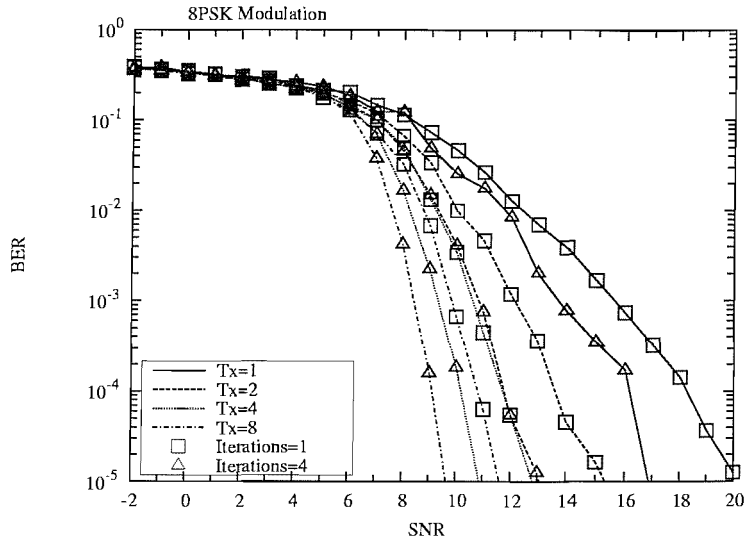

Figure 9.13: BER performance of STS assisted MC DS-CDMA, when an **8PSK** scheme and **turbo coding** were employed. The number of antennas was $T_x = 1, 2, 4, 8$ and the number of turbo decoding iterations was $1, 4$, respectively. The remaining parameters are listed in Table 9.2.

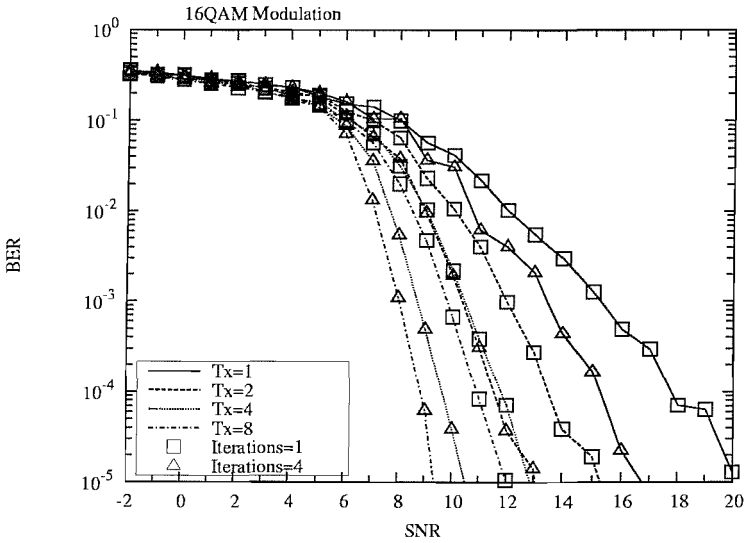

Figure 9.14: BER performance of STS assisted MC DS-CDMA, when a **16QAM** scheme and **turbo coding** were employed. The number of antennas was $T_x = 1, 2, 4, 8$ and the number of turbo decoding iterations was $1, 4$, respectively. The remaining parameters are listed in Table 9.2.

Modulation Scheme	BPSK	QPSK	8PSK	16QAM	64QAM
Symbols per burst	240				
Source bits per burst L_s	120	240	360	480	720
Coded bits per burst L_c	240	480	720	960	1440
Turbo interleaver	Random interleaver having a length of L_s				
Channel interleaver	Random interleaver having a length of $8 \times L_c$				
Memory length v of turbo code	3				
Rate of turbo code	$\frac{1}{2}$				
Terminated mode of turbo code	Yes				

Table 9.2: Turbo coding configurations for MC DS-CDMA.

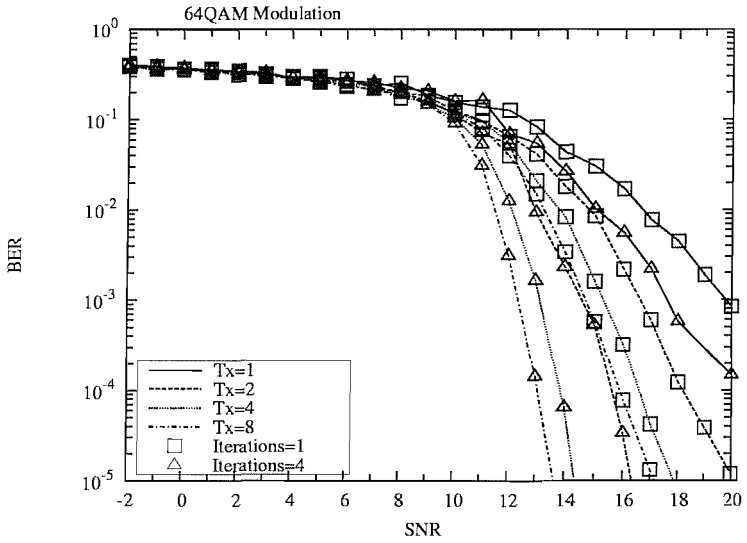

Figure 9.15: BER performance of STS assisted MC DS-CDMA, when a **64QAM** scheme and **turbo coding** were employed. The number of antennas was $T_x = 1, 2, 4, 8$ and the number of turbo decoding iterations was 1 and 4, respectively. The remaining parameters are listed in Table 9.2.

The basic configurations of the turbo codes used in conjunction with the various modems are summarized in Table 9.2. In our system, a burst-by-burst adaptive transmission scheme [137] was employed, each burst having a fixed number of symbols, namely $L = 240$. A half-rate turbo code having a memory of $v = 3$ was used in this system. When transmitting a fixed number of symbols per transmission burst by the different modulation schemes, the number of turbo coded bits per transmission burst becomes different, as seen in Table 9.2. An interesting related phenomenon is that although the higher-throughput modulation schemes are more vulnerable against channel errors, the corresponding higher turbo interleaver memory is capable of partially compensating for it. From Figure 9.11 we can observe that the performance of this system is significantly improved, when the number of antennas was increased from $T_x = 1$ to $T_x = 2$. The required SNR at a BER of 10^{-5} is 9.2dB for $T_x = 1$ antenna, when four iterations are invoked in the process of channel decoding. However, the SNR necessitated was reduced to 5dB, when the number of antennas is increased to $T_x = 2$ under the same channel conditions. Hence, the corresponding diversity gain becomes 4.2 dB, when increasing the number of antennas from

Modulation Scheme	$T_x = 1$	$T_x = 2$	$T_x = 4$	$T_x = 8$
BPSK SNR[dB]	9.2	5.0	3.5	1.8
QPSK SNR[dB]	13.0	9.0	6.2	5.4
8PSK SNR[dB]	17.0	13.0	11.0	9.6
16QAM SNR[dB]	16.8	13.0	10.5	8.2
64QAM SNR[dB]	21.0	17.2	14.4	13.8

Table 9.3: The SNR values necessitated by the STS assisted MC DS-CDMA system when different QAM schemes and **turbo coding** are invoked for achieving the performance of BER 10^{-5}. **Four turbo decoding iterations** are invoked. The other parameters are listed on Table 9.2.

$T_x = 1$ to $T_x = 2$, provided that four iterations are invoked in the process of channel decoding. Figures 9.12, 9.13, 9.14 and 9.15 portray the achievable BER performance when various modulations schemes are employed in this system. Finally, Table 9.3 summarized the SNR values required for achieving a BER of 10^{-5}, when four iterations are invoked in the process of channel decoding.

9.7 Adaptive QAM and STS Assisted MC DS-CDMA

9.7.1 Fixed Mode-Switching Threshold Based QAM

In this section, we employ a fixed threshold based adaptive QAM (AQAM) modem mode selection algorithm, which was also used in [137], adopting the AQAM techniques of [163, 164] which were first derived for serial single-carrier AQAM modems. It was assumed that the channel quality was constant for all the symbols in a transmission burst, more specifically, that the channel's fading envelope varied slowly across the transmission burst. Under these conditions, all the transmitted symbols were modulated using the same modulation mode, chosen according to the predicted SNR. Torrance *et al.* [163, 164] optimized the modem mode switching thresholds for the target BERs of 10^{-2} and 10^{-4}, which was deemed appropriate for a high-BER speech system and for a low-BER data system, respectively. The resultant SNR switching thresholds optimized for activating

System	NoTx	BPSK	QPSK	16QAM	64QAM
Target BER of 10^{-2}	$-\infty$	3.31dB	6.48dB	11.61dB	17.64dB
Target BER of 10^{-4}	$-\infty$	7.98dB	10.42dB	16.76dB	26.33dB

Table 9.4: Optimized AQAM mode switching levels quoted from [163], which were devised for adaptive modulation, when communicating over slowly-fading narrowband Rayleigh fading channels at target BERs of 10^{-2} and 10^{-4}.

a given modulation mode in a slowly Rayleigh fading narrowband channel are given in Table 9.4 for the target BERs of 10^{-2} and 10^{-4}. Specifically, a given modulation mode is selected, if the instantaneous channel SNR perceived by the receiver exceeds the corresponding switching levels shown in Table 9.4, depending on the target BER.

In conclusion, here we briefly reviewed an adaptive modulation scheme employing Torrance's switching levels, where the objective was to maximize the average BPS throughput, while maintaining the target average BER.

9.7.2 Adaptive Learning Aided Mode-Switching Based AQAM

In this section, we considered a practically-motivated AQAM mode switching approach, which is based on the philosophy of *learning* the switching thresholds [165] in an on-line fashion so that the system becomes capable of maximizing the achievable throughput expressed in terms of Bits Per Symbol (BPS). This learning schemes does not utilize the thresholds designed by Choi and Hanzo or by Torrance *et al.* [163] using Powell's optimization. More specifically, the achievable throughput was further improved by Choi and Hanzo upon realizing that the switching levels maybe reduced, when the average SNR is increased without violating the target integrity requirements. The Torrance's switching thresholds was summarized in Table 9.4. It also refrains from using analytical switching thresholds, or any other assumptions concerning the operating environment. The only necessary side information required by this scheme [165] is the current estimated BER $p_e(\gamma)$ (or the Frame Error Rate (FER)) and the target BER P_{th} of the system. The basic philosophy is that when the current BER $p_e(\gamma)$ is lower than the target BER P_{th}, this indicates that the system is capable of improving the achievable BPS throughput and hence it will reduce the switching thresholds for the sake of maximizing the throughput. By the contrast, when the current BER $p_e(\gamma)$ is higher than the target BER P_{th}, then the system is overloaded and hence the algorithm will increase the switching thresholds for the sake of reducing the system's throughput.

We considered a five mode AQAM scheme, associated with the threshold set of $s = \{s_1, s_2, s_3, s_4\}$ designed for BPSK, QPSK, 16QAM, 64QAM, respectively. For the sake of simplicity, we assumed that the AQAM threshold difference $(s_2 - s_1), (s_3 - s_1), (s_4 - s_1)$ between the different modulation schemes was the same as in Torrance's scheme, and we denoted them by $\triangle_{21}, \triangle_{31}, \triangle_{41}$, respectively. In other words, once we obtained the switching threshold s_1, we knew all the switching thresholds. Similarly, once we adjusted the switching threshold s_1, all the other switching thresholds considered were adjusted. Controlling the threshold s_1 is based on the current BER performance $p_e(\gamma)$, where the switching thresholds can be updated adaptively as follows [165]:

$$\begin{aligned} s_1(t) &= s_1(t-1) + \mu \cdot \text{sign}[p_e(\gamma) - P_{th}], \\ s_2(t) &= s_1(t) + \triangle_{21}, \\ s_3(t) &= s_1(t) + \triangle_{31}, \\ s_4(t) &= s_1(t) + \triangle_{41}, \end{aligned} \tag{9.27}$$

where $0 < \mu < 1$ is the threshold control step-size. Even though the AQAM mode-switching thresholds of Table 9.4 were originally derived for narrow-band time-domain Rayleigh fading, they were also used for frequency-domain AQAM-aided OFDM transmissions [4], since the frequency domain fading is also Rayleigh distributed Hence the

algorithm is initialized using the AQAM thresholds of Table 9.4, then producing the thresholds seen in Figure 9.16. Perfect estimation of the current BER was assumed, although in practice the accurate estimation of the short-term 'in-burst-BER' of a transmission burst is a challenging task, as it was exemplified in [137]. This issue requires further research.

9.8 Performance of AQAM and STS Assisted MC DS-CDMA

9.8.1 Performance of Uncoded System

Figure 9.16 shows evolution of the switching thresholds versus channel SNR required for maintaining the target BER of $P_{th} = 10^{-2}$, while Figure 9.17 portrays the switching thresholds derived for the target BER of $P_{th} = 10^{-4}$. We can observe that the switching thresholds are close to those proposed by Choi and Hanzo in [166] in the SNR range of $0 - 20$dB, which were summarized in Table 9.4.

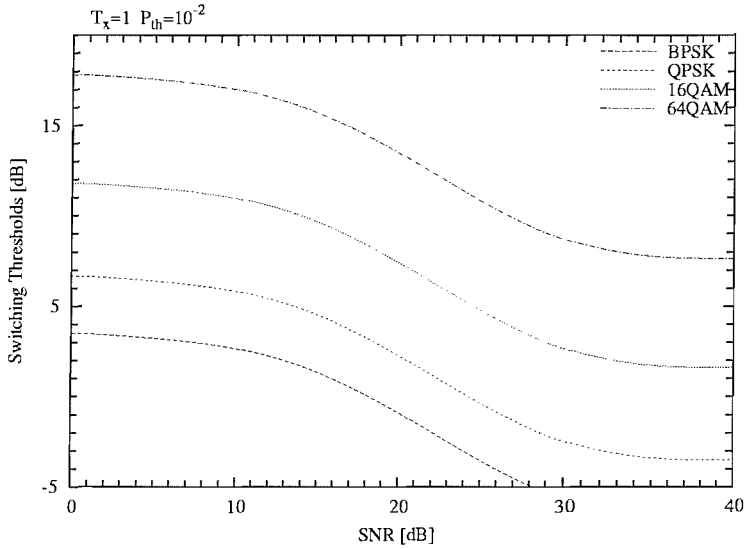

Figure 9.16: The learning based switching thresholds adjusted for maintaining the target BER of $P_{th} = 10^{-2}$, when using a step-size of μ=0.001.

Figure 9.18 and 9.19 portrays the mode selection probability of the learning-based switching threshold assisted AQAM. From these two figures, we can observe that as the average SNR increases, the high-order QAM modes are selected more often.

In this section, we will characterize the achievable performance of MC DS-CDMA system considered in conjunction with AQAM. Figure 9.20 shows the BER performance and BPS throughput of this system, when both the fixed switching thresholds seen in Table 9.4 and the adaptive thresholds of Figure 9.16 were employed for maintaining the target BER of $P_{th} = 10^{-2}$. By contrast, Figure 9.20 shows the BER performance and BPS throughput of these system, when maintaining the target BER of $P_{th} = 10^{-4}$. From these two figures, we can observe that the learning based threshold adjustment scheme exhibited a slightly better throughput than the fixed threshold based scheme of Table 9.4 in the high-SNR region. This is because at high SNRs the switching thresholds of Figure 9.16 are

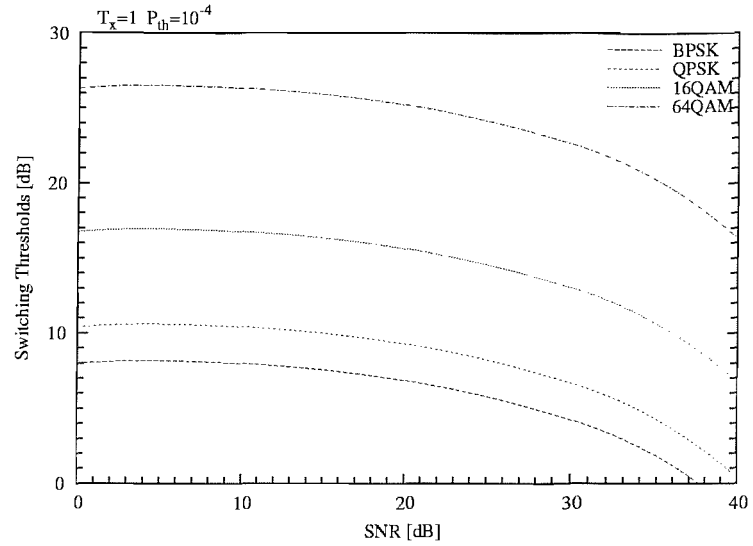

Figure 9.17: The self-learning switching thresholds adjusted for maintaining the target BER of $P_{th} = 10^{-4}$, when using a step-size of $\mu = 0.001$

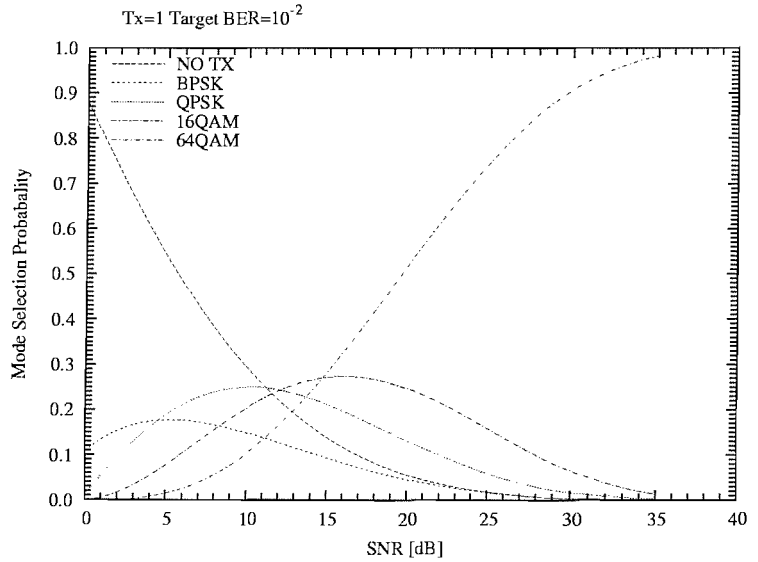

Figure 9.18: The mode selection probability of the learning-based switching threshold aided AQAM scheme at a target BER of $P_{th} = 10^{-2}$.

reduced by the algorithm for sake of increasing the achievable BPS throughput without any danger of jeopardizing the target integrity.

9.8.2 Performance of Turbo Coded System

In this section, we will consider the performance of learning-based switching thresholds in conjunction with turbo coded AQAM MC DS-CDMA techniques. Table 9.5 summarizes the configuration of the turbo codes, when the different AQAM modulation modes were invoked, and the initial switching thresholds for BPSK, QPSK, 16QAM, 64QAM were 1.46dB, 3.46dB, 7.46dB, 11.46dB, respectively. Figure 9.22 illustrates the achievable BER and BPS performance, when the system maintain a target BER of 10^{-3}. By contrast, Figure 9.23 portrays the attainable BER and BPS performance of when maintaining a

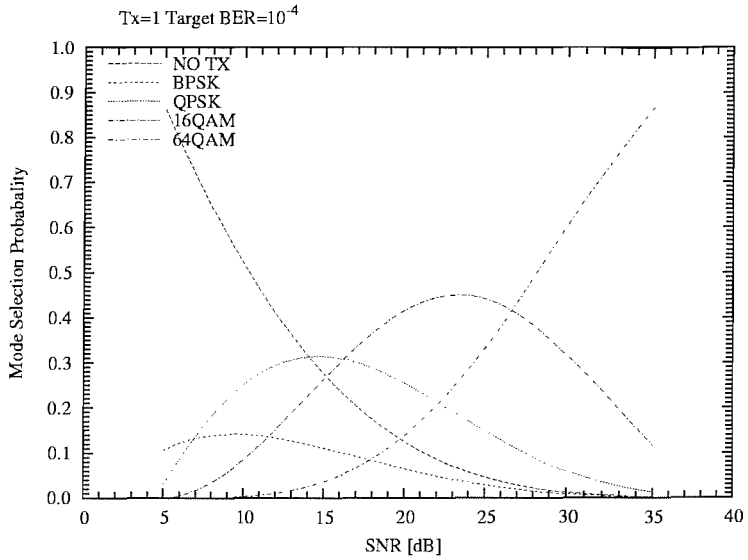

Figure 9.19: The mode selection probability of the learning-based switching threshold aided AQAM scheme at a target BER of $P_{th} = 10^{-4}$.

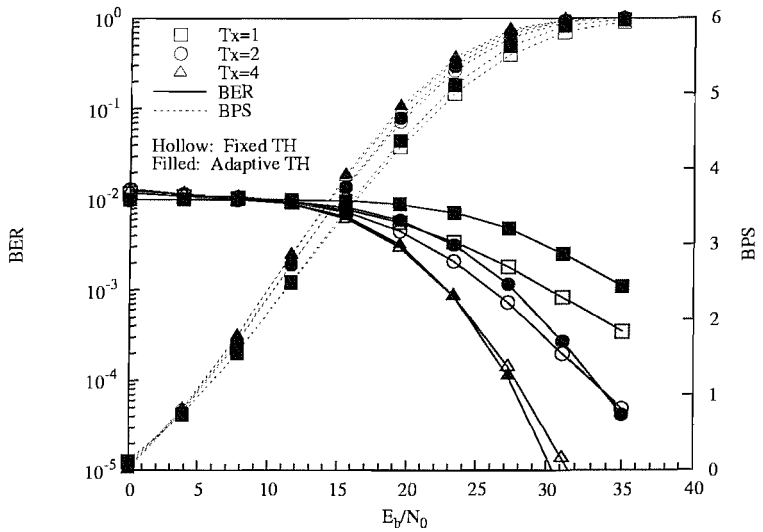

Figure 9.20: BER and BPS performance of AQAM aided MC DS-CDMA. The fixed switching thresholds (TH) used are shown in Table 9.4, while the adaptive learning-based thresholds are portrayed in Figure 9.16, which were adjusted for maintaining the target BER of $P_{th} = 10^{-2}$, and no channel coding was employed.

Configuration	BPSK	QPSK	16QAM	64QAM
Coding rate	$\frac{1}{2}$	$\frac{1}{2}$	$\frac{1}{2}$	$\frac{1}{2}$
The length of turbo interleaver L_c	120	240	480	720
Symbols per burst	240			
Channel interleaver	No employed			

Table 9.5: Configuration of the turbo codes used for AQAM-assisted MC DS-CDMA.

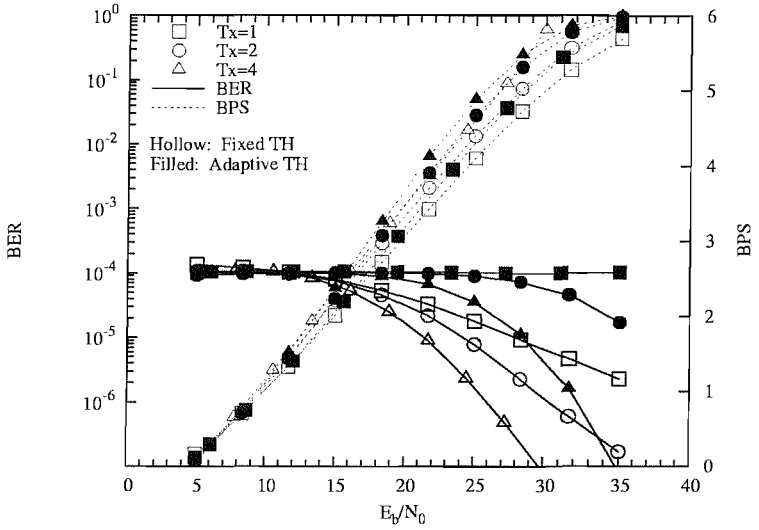

Figure 9.21: BER and BPS performance of AQAM aided MC DS-CDMA. The fixed switching thresholds (TH) used are shown in Table 9.4, while the adaptive learning-based thresholds are portrayed in Figure 9.17, which were adjusted for maintaining the target BER of $P_{th} = 10^{-4}$, and no channel coding was employed.

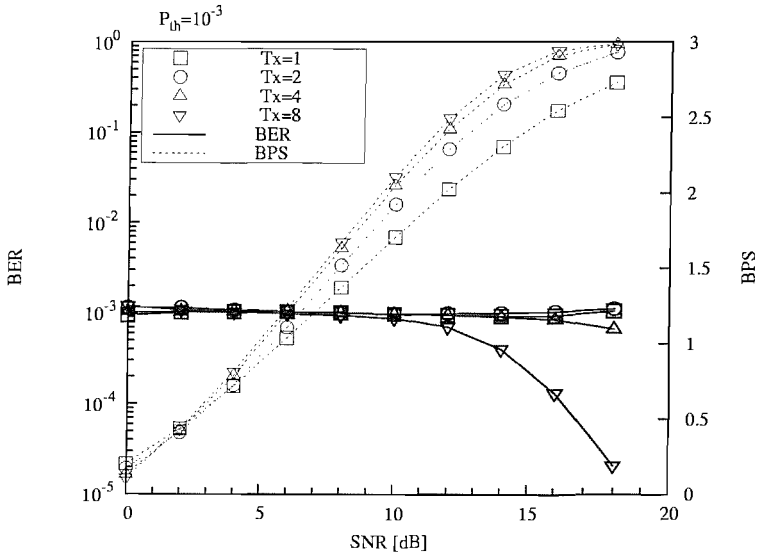

Figure 9.22: BER and BPS performance of AQAM aided MC DS-CDMA performance in conjunction with half-rate turbo channel coding, the learning based switching thresholds, which were adjusted for maintaining the target BER of $P_{th} = 10^{-3}$,

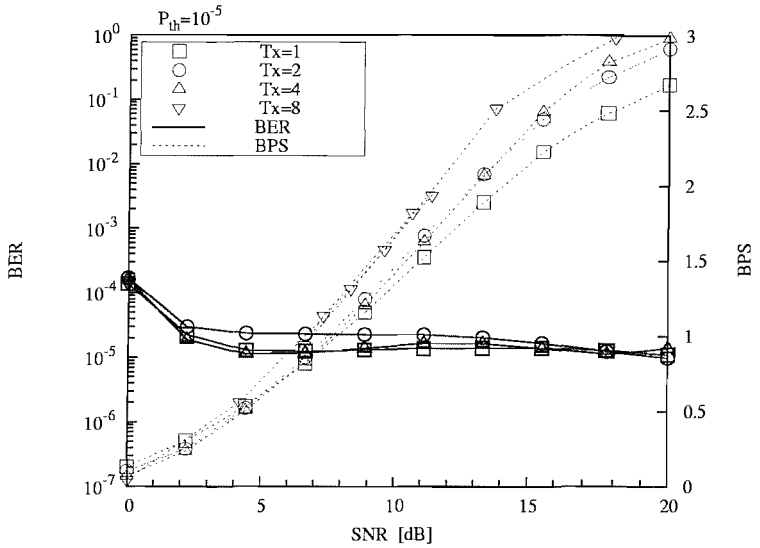

Figure 9.23: BER and BPS performance of AQAM aided MC DS-CDMA performance in conjunction with half-rate turbo channel coding, and the learning based switching thresholds are adjusted for maintaining the target BER of $P_{th} = 10^{-5}$.

target BER of 10^{-5}. From this figure we can observed that the system required an SNR of 9dB for achieving a throughput of 1 BPS, while the system maintaining a BER of 10^{-3} required an SNR only 6dB for maintaining the same throughput.

9.9 Chapter Conclusions

Number of antennas T_x	Switching Mode	**Throughput [BPS]**
$T_x = 1$	Fixed	2.6
$T_x = 1$	Learning	2.7
$T_x = 2$	Fixed	2.9
$T_x = 2$	Learning	3.0
$T_x = 4$	Fixed	3.2
$T_x = 4$	Learning	3.25
$T_x = 8$	Fixed	3.5
$T_x = 8$	Learning	3.5

Table 9.6: Throughput of AQAM assisted MC DS-CDMA at a BER of 10^{-4}.

In this chapter, we focused our attention on the achievable performance of STS-assisted MC DS-CDMA and studied its ability to support multirate communications. The system considered is capable of supporting multiple bit rates by employing both OVSF spreading codes and AQAM. Finally, Table 9.6 summarizes the system's attainable throughput for both fixed switching thresholds as well as when learning the switching thresholds of AQAM assisted MC DS-CDMA at a target BER of 10^{-4}.

CHAPTER 10

Thesis Conclusions and Future Work

This concluding chapter summarizes the results that were presented in this dissertation, and outlines a number of suggestions for future work.

10.1 Summary and Conclusions

This dissertation is concerned with the application of several interference suppression approaches devised for CDMA communication systems. Chapter 1 provided a basic overview of the family of interference suppression techniques designed for CDMA communications and introduced the basic terminology. In Chapter 2, we characterized the achievable performance of band-limited DS-CDMA in conjunction with three different time-limited and two band-limited chip-waveforms. The raised cosine waveform based DS-CDMA system exhibited the best performance among all these time-limited chip-waveforms, because its frequency-domain spectral side-lobe seen in Figure 2.2 was relatively low. When communicating in a strictly band-limited scenario having an energy containment in excess of 99.995%, the raised cosine chip-waveform exhibited more than 20dB SNR gain over the rectangular chip-waveform and 5dB gain over the half-sine chip-waveform at a BER of 10^{-2}. Furthermore, both the BRC and the optimum band-limited waveforms exhibited a better BER performance than that of the time-limited waveforms. However, when aiming for an energy containment in excess of 99%, the raised cosine waveform based DS-CDMA scheme was capable of achieving a similar performance to that of the optimum band-limited waveform based DS-CDMA arrangement.

In Chapter 3 we investigated the appropriate choice of spreading codes and demonstrated that LAS-CDMA exhibited a significantly better performance than the traditional random code based DS-CDMA system, when communicating over a quasi-synchronous

channel. Figure 3.10 suggested that LAS CDMA is capable of achieving four times the user-load in comparison to that of classic random code based DS-CDMA at the $E_b/N_0 = 15$dB. Moreover, Figure 3.9 suggested that LAS CDMA has to operate in a scenario, where the maximum time difference τ_{max} is less than $10T_c$. As the chip-rate increases, the number of resolvable paths arriving outside the IFW also increases, which imposed a performance degradation in this scenario. Hence, LAS-CDMA is most beneficial in a relatively low-chip rate scenario, where the number of resolvable paths satisfies $L_p \leq 8$. Furthermore, the limited number of available LAS codes having a certain IFW width suggests that the employment of LAS-CDMA is beneficial in a low-user load scenario, where we have $K \leq G/3$. For the MC LAS DS-CDMA system of Section 3.4, the number of subcarriers U was optimized for the sake of attaining the best possible performance trade-off between the achievable multipath diversity and the highest possible MAI as well as MPI suppression. For a 20 $Mchips/s$ system, $U = 32$ was found to be the best design option in Figure 3.13, and the LAS MC DS-CDMA system was found to be capable of outperforming the family of traditional random code based MC DS-CDMA and can dispense with the employment of multiuser detectors. We also proposed a novel LS code based STS scheme, which exhibited more than 20dB SNR gain over the traditional Walsh-code based STS scheme [25] at a BER of 10^{-3}, when the number of users supported did not exceed $G/3$.

In this dissertation, we also invoked multiuser detection techniques designed for suppressing the interference experienced in CDMA systems. In order to circumvent the complexity problem that arises, when employing optimum multiuser detection, several suboptimum multiuser detectors were investigated. In Chapter 4, we introduced a PIC assisted iterative multiuser detector, which removes the interference produced by the co-channel users accessing the channel. Since the interference is cancelled in parallel for all users, the processing delay required for completing the cancellation operation is at most a few bit durations. More specifically, a multistage iterative approach was suggested in Chapter 4, which estimated a given user's bits under the assumption that the other users' bits in the same transmission interval were correctly detected. This allowed the system to regenerate and subtract the multiuser interference based on the estimates of these bits generated during the previous cancellation iteration. We considered the employment of a range of channel coding techniques, which included convolutional coding, LDPC coding, TCM, TTCM and turbo coding, all of which are capable of achieving a near-single-user performance, as the results of Figure 4.28 demonstrate.

In Chapter 5, we concluded that the blind and group-blind multiuser detectors are capable of suppressing the MAI, and are robust to the near-far effect. Furthermore, it was shown in Section 5.2 that the group-blind multiuser detectors exhibited a better performance, when more signature waveforms were known to the receiver. The space-time blind and group-blind multiuser detectors of Section 5.3 operating in conjunction with a receiver-diversity antenna array were capable of achieving a near-single user performance with the aid of perfect knowledge of the CIR coefficients. Finally, in Section 5.4 we investigated the performance of semi-blind and group-blind multiuser detector schemes

in the context of the MC-CDMA uplink using a short cyclic prefix, which assisted us in removing both the ISI and the phase ambiguity associated with the blind channel estimation process. In the context of the blind MUD employing various spreading codes, the Walsh spreading code based MC-CDMA scheme outperformed the corresponding Gold and Zadoff-Chu code based systems.

In Chapter 6, we first comparatively studied two different algorithms, namely GAs and the MA invoked in the context of multiuser detection schemes. In our investigations, the GA performed better in the case of supporting a low number of users, and the GA exhibited a better near-far resistance. When the number of users was increased, the performance of the tree-search aided MA based multiuser detector became better in comparison to that of the GA, for example, when $K > 20$ users were supported, although they exhibited a similar complexity. It was shown in Figure 6.6 that in case of a low affordable complexity the MA is capable of outperforming the GA-aided MUD, while at a high affordable complexity, the opposite was true. In Section 6.3 a GA assisted neural network aided multiuser detector referred to as the GA-RBF MUD, was investigated, which is capable of achieving a near-optimum performance, when communicating over both non-dispersive AWGN and dispersive fading channels. In order to reduce the complexity of the conventional RBF based multiuser detector, in Section 6.3 an appropriately configured genetic algorithm was invoked for reducing the number of RBF centers.

In Chapter 7 we investigated the GA assisted MUD in the context of both synchronous and asynchronous MC-CDMA systems. The GA assisted multiuser detector designed for MC-CDMA systems was capable of significantly reducing the detection complexity imposed in comparison to Verdu's optimum multiuser detector, especially when the number of users supported was higher than $K = 15$. Specifically, in Figure 7.8 the achievable complexity reduction was approximately about 1000, when the number of users was $K = 20$. Furthermore, when channel coding techniques were employed, the GA-assisted MUD had the potential of further reducing the complexity imposed.

In Chapter 8, we studied a specific family of spreading codes, which exhibit an interference free window, namely LS codes and generalized orthogonal codes. In Section 8.3 we employed these spreading codes in the context of a TF-domain spreading assisted MC-DS-CDMA system. In this system we reduced the complexity of the optimum multiuser detector by a factor of $2^{\mathcal{K}N}/2^{\mathcal{K}} = 2^N$. The system was capable of significantly extending the width of the interference free window as a benefit of the serial to parallel conversion invoked in the MC-DS-CDMA schematic of Figure 8.4. More explicitly, the width of the IFW in this system was extended by a factor of $M \cdot U$ in comparison to that of a similar DS-CDMA system.

Finally, in Chapter 9 we considered adaptive modulation assisted MC DS-CDMA, which exhibited a flexible multirate service provision capability. The system determined the bit rate and target integrity supported by the appropriate choice of the spreading factor and modulation scheme. In Section 9.7.2 we also considered a novel practically-motivated adaptive modulation mode switching technique, which is based on the philosophy of *learning* the switching thresholds [165] in an on-line fashion, so that the system

becomes capable of maximizing the achievable throughput expressed in terms of BPS. This learning scheme does not utilize the analytical switching thresholds of [137] or any other assumptions concerning the operating environment. The only necessary side information required by this scheme [165] is the current estimated BER $p_e(\gamma)$ and the target BER P_{th} of the system. This specific AQAM scheme is capable of achieving a better throughput than that of traditional AQAM schemes in the high SNR region.

10.2 Suggestions for Further Work

In this dissertation, we have investigated numerous interference suppression techniques designed for CDMA communications systems. However, this topic still has open problems, some of which are listed below.

The performance of LAS CDMA has to be studied in conjunction with various chips-waveforms. More specifically, we may jointly consider the chip-waveform optimization and spreading-code optimization problem, and both band-limited as well as time-limited chip-waveforms may be investigated. Furthermore, owing to the advantage of LAS codes having an IFW, LAS code assisted *ad hoc* mobile networks have to be investigated.

Furthermore, we may consider slow frequency hopping and code hopping assisted MC DS-CDMA using interference rejection codes, which is promising for the future software defined radio techniques. For example, in a cell when the users' delays are in the range of the IFW, we may assign them different LAS codes, but the same frequency hopping pattern, which has the advantage of suppressing the MAI as a benefit of having an IFW. By contrast, if the users are far from the BS, and hence the IFW is insufficiently long for suppressing the MAI, we may assign them different frequency hopping patterns, but the same LAS code, which guarantees that the users are differentiated by their unique user-specific frequency-hopping patterns and hence the MAI will be suppressed, while allowing us to reuse the limited number of LAS codes.

In this dissertation, we only considered blind multiuser detectors, which were designed for the traditional DS-CDMA and MC-CDMA systems. However, it was shown in [3] that there exists an optimum subcarrier spacing in the context of MC DS-CDMA for a given system bandwidth and a given propagation environment, which results in a reduced-BER MC DS-CDMA system. This specific "spacing-optimized" MC DS-CDMA scheme is referred to as generalized MC DS-CDMA [3, 167]. The blind multiuser detection of generalized MC DS-CDMA signals [167] is promising for future research, because it may be expected to significantly improve the attainable performance characterized in [167], while retaining the advantage outlined in [167]. Furthermore, we may jointly consider transmitter optimization and blind MUD for this specific generalized MC DS-CDMA system according to the instantaneous propagation conditions. Finally, we may consider the family of space-time blind multiuser detectors specifically designed for generalized MC DS-CDMA in conjunction with smart antennas.

We only consider the iterative PIC-based multiuser detector in conjunction with channel coding techniques in Chapter 4 of this dissertation. Recently, joint source and-channel

coding techniques captured a growing interest. Hence, turbo multiuser detection in conjunction with joint source-channel coding techniques is promising for future research. The conventional turbo multiuser detector of Chapter 4 only utilizes the *aposteriori* information provided by the channel decoder, hence the iterative multiuser detectors combined with joint source-channel codecs are capable of utilizing both the *aposteriori* information of the source and the channel decoder, which will enhance the reliability of the *aposteriori* information and improve the performance of the turbo multiuser detector.

Adaptive modulation aided MIMOs may also be investigated for employment in future communication systems. The output SNR of a MIMO channel exhibits the so-called Wishart and Pseudo-Wishart distribution [168,169], which allow us to study the optimization of adaptive modulation schemes specifically designed for the MIMO channel. More specifically, we will investigate the mode-switch thresholds optimized for MIMO channels, which will allow us to achieve a higher throughput, than that of traditional fixed mode MIMO systems.

Based on the philosophy of SDMA, the spatial dimension can be also utilized for increasing the number users supported. Research on the combination of SDMA and CDMA techniques may be expected to attract substantial interests in the context of next generation mobile communications systems. Especially the combination of SDMA and SFH assisted MC DS-CDMA (SFH/MC DS-CDMA) [9,170] appears to be attractive.

Many of the GA-aided transceivers studied would also benefit from finding a reliable soft-metric for employment in channel decoding. Hence soft-input GA aided MUDs may be expected to exhibit a better performance than that of the current hard-decision GAs when used in conjunction with channel coding techniques.

Finally, Extrinsic Information Transfer (EXIT) charts have found favour in the context of iterative channel decoding techniques, especially in predicting the convergence behaviour of iterative decoders, such as turbo decoders and LDPC decoders. Hence, we may use EXIT charts as a tool for predicting the convergence behaviour and performance of PIC as well as turbo MUD aided receivers.

APPENDIX A

Glossary

2G	Second Generation
3G	Third Generation
AIC	Akaike Information Criterion
AMPS	Advanced Mobile Phone System
APP	A Posteriori Probability
AQAM	Adaptive Quadrature Amplitude Modulation
AWGN	Additive White Gaussian Noise
BER	Bit Error Ratio
BPSK	Binary Phase Shift Keying
CDMA	Code Division Multiple Access
CIR	Channel Impulse Response
DS	Direct Sequence

EEB	End Edge Bit
EM	Expectation Maximization
FDMA	Frequency Division Multiple Access
FFT	Fast Fourier Transform
FIR	Finite Impulse Response
GA	Genetic Algorithm
GSM	Global System of Mobile Communications
IFFT	Inverse Fast Fourier Transform
IFW	Interference Free Window
IS-95	Interim Standard IS-95, now known as CDMA One
ITU	International Telecommunication Union
LA	Large Area
LAS	Large Area Synchronized
LDPC	Low Density Parity Check
LLF	Log-Likelihood Function
LMMSE	Linear Minimum Mean Squared Error
LMS	Least Mean Square
LS	Loosely Synchronized
MA	M-Algorithm
MAI	Multiple Access Interference
MAP	Maximum *a posteriori* Probability

MC	MultiCarrier
ML	Maximum Likelihood
MMSE	Minimum Mean Squared Error
MMSE-BLE	Minimum Mean Squared Error Block Linear Equalizer
MMSE-BDFE	Minimum Mean Squared Error Block Decision Feedback Equalizer
MPI	Multipath Interference
MSD	Multi-Stage Detector
MSE	Mean Squared Error
PDF	Probability Density Function
PIC	Parallel Interference Cancellation
QAM	Quadrature Amplitude Modulation
QPSK	Quaternary Phase Shift Keying
RBF	Radial Basis Function
RBFN	Radial Basis Function Network
SDMA	Space-Division Multiple Access
SEB	Start Edge Bit
SIC	Successive Interference Cancellation
SINR	Signal to Interference plus Noise Ratio
SNR	Signal-to-Noise Ratio
SS	Spread Spectrum
STC	Space-Time Coding

STS	Space-Time Spreading
SVD	Singular-Value Decomposition
TCM	Trellis-Coded Modulation
TDD	Time-Division Duplexing
TDMA	Time-Division Multiple Access
TTCM	Turbo-Trellis Coded Modulation
UMTS	Universal Mobile Telecommunications System
UTRA	UMTS Terrestrial Radio Access
W-CDMA	Wideband CDMA
ZF-BLE	Zero-Forcing Block Linear Equalizer
ZF-BDFE	Zero-Forcing Block Decision Feedback Equalizer

APPENDIX B

List of Symbols

$(\cdot)^H$	Conjugate of a matrix.
$(\cdot)^T$	Transpose of a matrix.
$\|\| \cdot \|\|^2$	Euclidean norm of a vector.
λ	Eigenvalues.
Λ	The diagonal matrix which includes the eigenvalues.
$\Omega(\boldsymbol{b})$	Optimization metric function.
$\phi_k(t)$	Channel phase uniformly distributed between $[0, 2\pi)$.
ρ_{jk}	Cross-correlation of the jth user's and the kth user's signature sequence.
τ_k	Propagation delay of user k.
σ^2	Noise variance.
ι	Width of the interference free window in LS, LAS and GO codes
$\mathbf{A}$	Amplitude vector.

$b_k^{(m)}$	mth data bit of the kth user.
$\mathbf{b}$	Data bit vector.
$c_k(t)$	kth user's signature sequence.
$\mathbf{C}$	Spreading code matrix.
f_c	Carrier frequency.
G	Spreading gain.
$h_k(t)$	Complex lowpass channel impulse response associated with the kth user's signal.
K	Number of users in the system.
$\tilde{K}$	Number of users in the reference cell, whose spreading code is known to the blind MUD
$n(t)$	Zero-mean complex additive white Gaussian noise with independent real and imaginary components, each having a double-sided power spectral density of $N_0/2$ W/Hz.
$\mathbf{n}$	Gaussian noise vector.
N	Spreading factor, or the number of chips in one data bit duration T_b.
p_c	Probability of crossover in the GA-aided MUD.
p_i	Probability of selection corresponding to the ith individual in the GA-aided MUD.
p_m	Probability of mutation in the GA-aided MUD.
P	Population size in the GA-aided MUD.
$r(t)$	Received signal.
$\mathbf{R}$	User signature sequence cross-correlation matrix.

$s_k(t)$	Transmitted signal of the kth user.
T_b	Data bit duration.
T_c	Chip duration.
$\mathbf{U}_s$	Signal subspace.
$\mathbf{U}_n$	Noise subspace.
$\mathbf{w}_k$	Weight vector for the kth user's multiuser detector.
z_k	Matched filter output associated with the kth user.
$\mathbf{Z}$	Matched filter output vector.

Bibliography

[1] S. G. Glisic and P. A. Leppännen, *Wireless Communications-TDMA versus CDMA.* Kluwer Academic Publishers, August 1997.

[2] S. Glisic and B. Vucetic, *Spread Spectrum CDMA Systems for Wireless Communications.* Artech House, Inc., 1997.

[3] L. Hanzo, L. L. Yang, E. L. Kuan, and K. Yen, *Single- and Multi-Carrier DS-CDMA.* John Wiley and IEEE Press, 2003, 1060 pages.

[4] L. Hanzo, M. Münster, B. J. Choi, and T. Keller, *OFDM and MC-CDMA.* John Wiley and IEEE Press, 2003.

[5] J. Bolgh and L. Hanzo, *Third-Generation Systems and Intelligent Networking.* John Wiley IEEE Press, 2002.

[6] R. Steele and L. Hanzo, *Mobile Radio Communications.* IEEE Press-John Wiley, 2 ed., 1999.

[7] J. G. Proakis, *Digital Communications.* Mc-Graw Hill International Editions, 3rd ed., 1995.

[8] R. Prasad and S. Hara, "Overview of Multicarrier CDMA," *IEEE Communications Magazine*, pp. 126–133, December 1997.

[9] L.-L. Yang and L. Hanzo, "Software-Defined-Radio-Assisted Adaptive Broadband Frequency Hopping Multicarrier DS-CDMA," *IEEE Communications Magazine*, vol. 4, March 2002.

[10] A. Viterbi, *Principles of Spread Spectrum Communications.* ISBN 0201633744, Addison-Wesley, August 1995.

[11] R. Prasad, *CDMA for Wireless Personal Communications.* Artech House, Inc., 1996.

[12] L. Miller and J. S. Lee, *CDMA Systems Engineering Handbook.* London, UK: Artech House, 1998.

[13] ARIB/Japan, *Japan's Proposal for Candidate Radio Transmission Technology on IME-2000:W-CDMA*, June 1998.

[14] ETSI/SMG2, *The ETSI UMTS Terrestrial Radio Access (UTRA) ITU-R RTT Candidate Submission*, June 1998.

[15] TIA/US, *The cdma2000 ITU-R RTT Candidate Submission*, June 1998.

[16] CATT/China, *TD-SCDMA Radio Transmission Tehnology for IMT-2000*, June 1998.

[17] M. Saquib, R. Yates, and A. Ganti, "Power Control for an Asynchronous Multirate Decorrelator," *IEEE Transactions on Communications*, vol. 48, pp. 804–812, May 2000.

[18] S. Stańczak, H. Boche, and M. Haardt, "Are LAS-codes a Miracle?," in *GLOBECOM '01*, vol. 1, (San Antonio, Texas), pp. 589–593, November 2001.

[19] B. J. Choi and L. Hanzo, "On the Design of LAS Spreading Codes," in *IEEE VTC 2002 Fall Conference*, (Vancouver, Canada), pp. 2172–2176, September 2002.

[20] P. Fan and M. Darnell, *Sequence Design for Communications Applications.* ISBN 086380201, UK:Research Studies Press, 1996.

[21] C. S. Lee and R. Steele, "Effects of Soft and Softer Handoffs on CDMA System Capacity," *IEEE Transactions on Vehicular Technology*, vol. 47, pp. 830–841, August 1998.

[22] S. Verdú, *Multiuser Detection.* Cambridge Press, 1998.

[23] J. H. Cho and J. S. Lehnert, "An Optimal Signal Design for Band-Limited Asynchronous DS-CDMA Communications," *IEEE Transactions on Information Theory*, vol. 48, pp. 1172–1185, May 2002.

[24] D. Li, "A High Spectrum Efficient Multiple Access Code," *Chinese Journal of Electronics*, vol. 8, pp. 221–226, July 1999.

[25] B. Hochwald, T. L. Marzetta, and C. B. Papadias, "A Transmitter diversity scheme for wideband CDMA systems based on Space-time spreading," *IEEE Journal on Selected Areas in Communications*, vol. 19, pp. 48–60, January 2001.

[26] M. Wax and T. Kailath, "Detection of Signals by Information Theoretic Criteria," *IEEE Transactions on Acoustics, Speech and Signal Processing*, vol. 33, pp. 387 –392, April 1985.

[27] D. Chu, "Polyphase Codes with Good Periodic Correlation Properties," *IEEE Transactions on Information Theory*, vol. 18, pp. 531 – 532, July 1972.

[28] R. L. Peterson, R. E. Ziemer, and D. E. Borth, *Introduction to Spread Spectrum Communications.* Prentice Hall International Editions, 1995.

[29] D. G. M. Cruickshank, "Radial Basis Function Receivers for DS-CDMA," *Electronics Letter*, vol. 32, pp. 188–190, February 1996.

[30] L. Hanzo, W. Webb, and T. Keller, *Single- and Multi-carrier Quadrature Amplitude Modulation: Principles and Applications for Personal Communications, WLANs and Broadcasting.* John Wiley & Sons, Ltd, 2004.

[31] E. H. Dinan and B. Jabbari, "Spreading Codes for Direct Sequence CDMA and Wideband CDMA Cellular Networks," *IEEE in Communications Magzine*, pp. 48–54, September 1998.

[32] H. Wei and L. Hanzo, "On the Uplink Performance of RAKE-Receiver Assisted Band-Limited DS-CDMA Systems Over Nakagami Channels," in *IEE International Conference on 3G Mobile Communication Technologies (3G 2004)*, (Savoy Place, London, UK), pp. 312–316, October 2004.

[33] H. Wei and L. Hanzo, "On the Uplink Performance of Band-Limited DS-CDMA Over Nakagami-m Channels," *submitted to IEEE Transaction on Wireless Communication*, February 2004.

[34] H. Wei, L.-L. Yang, and L. Hanzo, "Interference-Free Broadband Single- and Multi-Carrier DS-CDMA," *IEEE Communication Magazine*, pp. 68–73, February 2005.

[35] H. Wei and L. Hanzo, "On the Performance of LAS-CDMA," *To appear in IEEE Transaction on Wireless Communication.*

[36] H. Wei and L. Hanzo, "Downlink Spreading Assisted DS-CDMA Using Interference Rejection Codes," *submitted to IEEE Transaction on Vehicular Technology*, February 2004.

[37] H. Wei, S. Ng, and L. Hanzo, "Coded Modulation Assisted Iterative Parallel Interference Cancellation aided CDMA," in *Proceedings of IEEE VTC 2003 Fall*, vol. 1, (Orlando, Florida, USA), pp. 1109–1113, September 2003.

[38] H. Wei and L. Hanzo, "Semi-Blind and Group-Blind Multiuser Detection for the Uplink MC-CDMA," in *Proceedings of IEEE Vehicular Technology Conference (VTC) 2004 Spring*, (Milan, Italy), pp. 1727 – 1731, September 2003.

[39] H. Wei and L. Hanzo, "Reduced-Complexity Near-Optimum Genetic Algorithm Assisted Multiuser Detection for Synchronous Multicarrier CDMA," in *Proceedings of IEEE Vehicular Technology Conference (VTC) 2004 Spring*, (Milan, Italy), pp. 1717 – 1721, April 2004.

[40] H. Wei and L. Hanzo, "Genetic Algorithm Assisted Multiuser Detection for Asynchronous Multicarrier CDMA," in *Proceedings of the IEEE Vehicular Technology Conference (VTC) 2004 Fall*, (Los Angeles, USA), October 2004.

[41] H. Wei and L. Hanzo, "Reduced-Complexity Genetic Algorithm Aided and Radial Basis Function Assisted Multiuser Detection for Synchronous CDMA," in *Proceedings of European Signal Processing Conference (EUSIPCO) 2004*, (Vienna, Austria), pp. 157–160, September 2004.

[42] L.-L. Yang, H. Wei, and L. Hanzo, "A Multicarrier DS-CDMA System using Both Time-Domain and Frequency-Domain Spreading," in *Proceedings of IEEE VTC 2003 Fall*, vol. 4, (Orlando, Florida, USA), pp. 2426 – 2430, September 2003.

[43] H. Wei, L.-L. Yang, and L. Hanzo, "Time- and frequency-domain spreading assisted MC DS-CDMA using interference rejection spreading codes for quasi-synchronous communications," in *Proceedings of IEEE Vehicular Technology Conference (VTC) 2004 Fall*, (Los Angeles, USA), October 2004.

[44] H. Wei and L. Hanzo, "A Space-Time Spreading Assisted Multicarrier DS-CDMA System Using OVSF codes and Adaptive Modulation," in *submitted to IEEE VTC'05 Fall*, October 2004.

[45] M. Mitchell, *An Introduction to Genetic Algorithms.* Cambridge, MA: MIT Press, 1996.

[46] F. Amoroso, "The Bandwidth of Digital Data Signals," *IEEE Communications Magazine*, vol. 18, pp. 13–24, November 1980.

[47] M. A. Landolsi and W. E. Stark, "DS-CDMA Chip Waveform Design for Minimal Interference Under Bandwidth, Phase, and Envelope Constraints," *IEEE Transactions on Communications*, vol. 47, pp. 1737–1746, November 1999.

[48] P. I. Dallas and F.-N. Pavlidou, "Innovative Chip Waveforms in Microcelluar DS/CDMA Packet Mobile Radio," *IEEE Transactions on Communications*, vol. 44, pp. 1413–1416, November 1996.

[49] Y. C. Yoon, "A Simple and Accurate Method of Probability of Bit Error Analysis for Asynchronous Band-Limited DS-CDMA Systems," *IEEE Transactions on Communications*, vol. 50, pp. 656–663, April 2002.

[50] L.-L. Yang and L. Hanzo, "Performance of Generalized Multicarrier DS-CDMA Using Various Chip Waveforms," *IEEE Transactions on Communications*, vol. 51, pp. 748–752, May 2003.

[51] N. C. Beaulieu and J. Cheng, "Precise Error-Rate Analysis of Bandwidth-Efficient BPSK in Nakagami Fading and Cochannel Interference," *IEEE Transactions on Communications*, vol. 52, pp. 149–158, January 2004.

[52] D. Li, "Scheme for Spread Spectrum Multiple Access Coding." US Patent, US 6,331,997 B1, December 2001.

[53] P. Fan and L. Hao, "Generalized Orthogonal Sequences and Their Applications in Synchronous CDMA Systems," *IEICE Transaction on Fundamentals*, vol. E83-A, pp. 2054–2069, November 2000.

[54] S. Verdú, "Minimum Probability of Error for Asynchronous Gaussian Multiple Access Channels," *IEEE Transactions on Information Theory*, vol. 32, pp. 85–96, January 1986.

[55] R. Lupas and S. Verdu, "Linear Multiuser Detectors for Synchronous Code-Division Multiple-Access Channels," *IEEE Transactions on Information Theory*, vol. 35, pp. 477 – 486, Jan 1989.

[56] M. Varanasi and B. Aazhang, "Multistage Detection in Asynchronous Code-Division Multiple-Access Communications ," *IEEE Transactions on Communications*, vol. 38, pp. 509–519, April 1990.

[57] S. Verdu and R. Lupas, "Near-Far Resistance of Multiuser Detectors in Asynchronous Channels," *IEEE Transactions on Communications*, vol. 38, pp. 496 – 508, April 1990.

[58] M. Honig, U. Madhow, and H. V. Poor, "Blind Adaptive Multiuser Detection," *IEEE Transactions on Information Theory*, vol. 41, pp. 944–960, July 1995.

[59] L. Wei, L. K. Rasmussen, and R. Wyrwas, "Near Optimum Tree-Search Detection Schemes for Bit-Synchronous Multiuser CDMA Systems over Gaussian and Two-Path Rayleigh-Fading Channels," *IEEE Transactions on Communications*, vol. 45, pp. 691–700, June 1997.

[60] M. C. Reed, C. B. Schlegel, P. D. Alexander, and J. A. Asenstorfer, "Iterative Multiuser Detection for CDMA with FEC: Near single user performance," *IEEE Transactions on Communications*, vol. 46, pp. 1693–1699, December 1999.

[61] D. Divsalar, M. K. Simon, and D. Raphaeli, "Improved Parallel Interference Cancellation for CDMA," *IEEE Transactions on Communications*, vol. 46, pp. 258–168, February 1998.

[62] X. Wang and H. V. Poor, "Blind Multiuser Detection: A Subspace Approach," *IEEE Transactions on Information Theory*, vol. 44, pp. 677–690, March 1998.

[63] X. Wang and A. Host-Madsen, "Group-Blind Multiuser Detection for Uplink CDMA," *IEEE Journal on Selected Areas in Communications*, vol. 17, pp. 1971–1984, November 1999.

[64] M. Reed and P. Alexander, "Iterative Multiuser Detection using Antenna Arrays and FEC on Multipath Channels," *IEEE Journal on Selected Areas in Communications*, vol. 12, pp. 2082 – 2089, December 1999.

[65] C. Ergün and K. Hacioglu, "Multiuser Detection Using a Genetic Algorithm in CDMA Communication Systems," *IEEE Transactions on Communications*, vol. 48, pp. 1374–1383, August 2000.

[66] M. Peng, Y. J. Guo, and S. K. Barton, "Multiuser Detection of Asynchronous CDMA with Frequency Offset," *IEEE Transactions on Communications*, vol. 49, pp. 952–960, June 2001.

[67] S. Chen, A. K. Samingan, B. Mulgrew, and L. Hanzo, "Adaptive Minimum-BER Linear Multiuser Detection for DS-CDMA Signals in Multipath Channels," *IEEE Transactions on Signal Processing*, vol. 49, pp. 1240–1247, June 2001.

[68] D. Reynolds and X. Wang, "Turbo Multiuser Detection with Unknown Unterferers," *IEEE Transactions on Communications*, vol. 50, pp. 616 – 622, April 2002.

[69] H. Poor and M. Tanda, " Multiuser Detection in Flat Fading Non-Gaussian Channels," *IEEE Transactions on Communications*, vol. 50, pp. 1769 – 1777, November 2002.

[70] S. Sfar, R. Murch, and K. Letaief, "Layered Space-Time Multiuser Detection over Wireless Uplink Systems," *IEEE Transactions on Wireless Communications*, vol. 2, pp. 653 – 668, July 2003.

[71] A. Kapur and M. Varanasi, "Multiuser Detection for Overloaded CDMA Systems," *IEEE Transactions on Information Theory*, vol. 49, pp. 1728 – 1742, July 2003.

[72] A. Kocian and B. Fleury, "EM-based Joint Data Detection and Channel Estimation of DS-CDMA Signals," *IEEE Transactions on Communications*, vol. 51, pp. 1709 – 1720, October 2003.

[73] M. Honig, G. Woodward, and Y. Sun, "Adaptive Iterative Multiuser Decision Feedback Detection," *IEEE Transactions on Communications*, vol. 3, pp. 477 – 486, March 2004.

[74] K. Yen and L. Hanzo, "Genetic-Algorithm-Assisted Multiuser Detection in Asynchronous CDMA Communications," *IEEE Transactions on Communications*, vol. 53, pp. 1413 – 1422, September 2004.

[75] D. Das and M. Varanasi, "Optimum Noncoherent Multiuser Decision Feedback Detection," *IEEE Transactions on Communications*, vol. 50, pp. 1974 – 1988, September 2004.

[76] Q. Li, C. Georghiades, and X. Wang, "Blind multiuser detection in uplink CDMA with multipath fading: a sequential EM approach ," *IEEE Transactions on Communications*, vol. 52, pp. 71–81, January 2004.

[77] C. Douillard, M. Jezequel, C. Berrou, A. Picart, P. Didier, and A. Glavieux, "Iterative Correction of Intersymbol Interference: Turbo-Equalization," *European Transactions on Telecommunications and Related Technologies*, vol. 6, pp. 507–511, September–October 1995.

[78] L. Hanzo, T. H. Liew, and B. L. Yeap, *Turbo Coding, Turbo Equalisation and Space-Time Coding for Transmission over Fading Channels.* John Wiley-IEEE Press, 2002.

[79] Y. Zhang, "Reduced Complexity Iterative Multiuser Detection for DS/CDMA with FEC ," in *International Conference on Universal Personal Communications*, (San Diego, U.S.A), pp. 10–14, October 1997.

[80] P. D. Alexander, A. J. Grant, and M. C. Reed, "Performance Analysis of an Iterative Decoder for Code-Division Mulitple-Access," *European Transaction on Telecommunication*, vol. 9, pp. 419–426, September/October 1998.

[81] A. Lampe, "Iterative Multiuser Detection With Integrated Channel Estimation for Coded DS-CDMA," *IEEE Transactions on Communications*, vol. 50, pp. 1217–1223, August 2002.

[82] M. J. Juntti, T. Schlosser, and J. Lilleberg, "Genetic Algorithms for Multiuser Detection in Synchronous CDMA," *IEEE International Symposium on Information Theory*, p. 492, 1997.

[83] X. F. Wang, W. S. Lu, and A. Antoniou, "A Genetic Algorithm-Based Multiuser Detection for Multiple-Access Communications," in *In the IEEE International Symposium on Circuits and System-ISCAS'98,*, (Monterey, Clifornia, USA), pp. 534 – 537, 1998.

[84] K. Yen and L. Hanzo, "Genetic algorithm assisted joint multiuser symbol detection and fading channel estimation for synchronous CDMA systems," *IEEE Journal on Selected Areas in Communications*, vol. 19, pp. 985 –998, June 2001.

[85] K. Yen and L. Hanzo, "Antenna-Diversity-Assisted Genetic-Algorithm-based Multiuser Detection Schemes for Synchronous CDMA Systems ," *IEEE Transactions on Communications*, vol. 51, pp. 366–370, March 2003.

[86] K. Yen and L. Hanzo, "Hybrid Genetic Algorithm Based Multiuser Detection Schemes for Synchronous CDMA Systems," in *Proceedings 51st IEEE Vehicular Technology Conference*, (Tokyo, Japan), pp. 1400–1404, 18 May 2000.

[87] K. Yen and L. Hanzo, "Genetic Algorithm Assisted Multiuser Detection in Asynchronous CDMA Communications," in *Proceedings of the IEEE International Conference on Communications*, vol. 3, pp. 826 –830, 2001.

[88] P. Spasojevic, X. Wang, and A. Host-Madsen, "Nonlinear Group-Blind Multiuser Detection," *IEEE Transactions on Communications*, vol. 49, pp. 1631 – 1641, September 2001.

[89] D. Reynolds and X. Wang, "Adaptive Transmitter Optimization for Blind and Group-Blind Multiuser Detection," *IEEE Transactions on Signal Processing*, vol. 51, pp. 825–838, March 2003.

[90] X. Wang and H. V. Poor, "Blind Equalization and Multiuser Detection in Dispersive CDMA Channels," *IEEE Transactions on Communications*, vol. 6, pp. 91–103, January 1998.

[91] A. Host-Madsen and X. Wang, "Performance of Blind and Group-Blind Multiuser Detection," *IEEE Transactions on Information Theory*, vol. 48, pp. 1849–1872, July 2002.

[92] M. Schnell and S. Kaiser, "Diversity Considerations for MC-CDMA Systems in Mobile Communications," in *Proceedings of IEEE ISSSTA 1996*, (Mainz, Germany), pp. 131–135, September 1996.

[93] S. L. Miller and B. J. Rainbolt, "MMSE Detection of Multicarrier CDMA," *IEEE Journal on Selected Areas in Communications*, vol. 18, pp. 2356–2362, November 2000.

[94] J. Namgoong, T. F. Wong, and J. S. Lehnert, "Subspace Multiuser Detection for Multicarrier DS-CDMA," *IEEE Transactions on Communications*, vol. 48, pp. 1897–1908, November 2000.

[95] P. Zong, K. Wang, and Y. Bar-Ness, "Partial Sampling MMSE Interference Suppression in Asynchronous MultiCarirrer CDMA System," *IEEE Journal on Selected Areas in Communications*, vol. 19, pp. 1605–1613, August 2001.

[96] Z. Yang, B. Lu, and X. Wang, "Bayesian Monte Carlo Multiuser Receiver for Space-time Coded Multicarrier CDMA Systems," *IEEE Journal on Selected Areas in Communications*, vol. 19, pp. 1625 – 1637, August 2001.

[97] D. Kalofonos, M. Stojanovic, and J. Proakis, "Performance of Adaptive MC-CDMA Detectors in Rapidly Fading Rayleigh Channels," *IEEE Transactions on Wireless Communications*, vol. 2, pp. 229–239, March. 2003.

[98] P. Kafle and A. Sesay, "Iterative Semi-Blind Multiuser Detection for Coded MC-CDMA Uplink System," *IEEE Transactions on Communications*, vol. 51, pp. 1034 – 1039, July 2003.

[99] G. Zhang, G. Bi, and L. Zhang, "Blind Multiuser Detection for Asynchronous MC-CDMA Systems without Channel Estimation," *IEEE Transactions on Vehicular Technology*, vol. 53, pp. 1001 – 1013, July 2004.

[100] P. Kafle and A. Sesay, "Performance of Turbo Coded Multicarrier CDMA with Iterative Multiuser Detection and Decoding," in *Canadian Conference on Electrical and Computer Engineering,*, vol. 1, (Montreal, Canada), pp. 105 –110, 2001.

[101] N. Nakagami, "The m-Distribution, a General Formula for Intensity Distribution of Rapid Fading," in *Statistical Methods in Radio Wave Propagation* (W. G. Hoffman, ed.), Oxford, England: Pergamon, 1960.

[102] T. Eng and L. B. Milstein, "Coherent DS-CDMA Performance in Nakagami Multipath Fading," *IEEE Transactions on Communications*, vol. 43, pp. 1134–1143, February/March/April 1995.

[103] V. Aalo, O. Ugweje, and R. Sudhakar, "Performance Analysis of a DS/CDMA System with Noncoherent M-ary Orthogonal Modulation in Nakagami Fading," *IEEE Transactions on Vehicular Technology*, vol. 47, pp. 20–29, February 1998.

[104] M.-S. Alouini and A. J. Goldsmith, "A Unified Approach for Calculating Error Rates of Linearly Modulated Signals over Generalized Fading Channels," *IEEE Transactions on Communications*, vol. 47, pp. 1324–1334, September 1999.

[105] J. H. Cho and J. S. Lehnert, "Performance of a Spatio-Temporal Matched Filter for DS/SSMA Communications with Random Quadriphase Spreading Sequences," *IEEE Journal on Selected Areas in Communications*, vol. 18, pp. 1505–1515, May 2000.

[106] M. K. Simon and M.-S. Alouini, "A Unified Approach to the Probability of Error for Noncoherent and Differentially Coherent Modulation over Generalized Fading Channels," *IEEE Transactions on Communications*, vol. 46, pp. 1625–1638, December 1998.

[107] M. K. Simon and M.-S. Alouini, "A Unified Approach to the Performance Analysis of Digital Communication over Generalized Fading Channels," *Proceedings of the IEEE*, vol. 86, pp. 1860–1877, September 1998.

[108] H. H. Chen, C. Tsai, and W. Chang, "Uplink Synchronization Control Technique and its Environment-Dependent Performance Analysis," *Electronics Letters*, vol. 33, pp. 1555 –1757, November 2003.

[109] CWTS/China, *Physical Layer Specification for LAS-2000*, June 2000.

[110] C.-C. Tseng and C. L. Liu, "Complementary Sets of Sequences," *IEEE Transactions on Information Theory*, vol. 18, pp. 644–652, Sep. 1972.

[111] R. L. Frank, "Polyphase Complementary Codes," *IEEE Transactions on Information Theory*, vol. 26, pp. 641–647, November 1980.

[112] R. Sivaswamy, "Multiphase Complementary Codes," *IEEE Transactions on Information Theory*, vol. 24, pp. 546–552, Sep. 1978.

[113] E. Geraniotis and B. Ghaffari, "Performance of Binary and Quaternary Direct-Sequence Spreading-Spectrum Multiple-Access Systems with Random Signature Sequences," *IEEE Transactions on Communications*, vol. 39, pp. 713–724, May 1991.

[114] W. C. Y. Lee, *Mobile Communications Engineering.* New York: McGraw-Hill, 2nd ed., 1998.

[115] M. B. Pursley, "Performance evaluation for phase-coded spread-spectrum multiple-access communication-Part I: System analysis," *IEEE Transactions on Communications*, vol. COM-25, pp. 795–799, August 1977.

[116] C. Berrou, A. Glavieux, and P. Thitimajshima, "Near Shannon limit error-correcting coding and encoding: Turbo-codes (1)," in *IEEE International Conference on Communications*, (Geneva, Switzerland), pp. 1064–1070, May 1993.

[117] M. C. Reed, *Iterative Receiver Techniques for Coded Multiple Access Communication System.* PhD thesis, The University of South Australia, 1999.

[118] G. Ungerböck, "Channel coding with multilevel/phase signals," *IEEE Transactions on Information Theory*, vol. 28, pp. 55–67, January 1982.

[119] D. Divsalar and M. K. Simon, "The Design of Trellis Coded MPSK for Fading Channel: Performance Criteria," *IEEE Transactions on Communications*, vol. 36, pp. 1004–1012, September 1988.

[120] P. Robertson and T. Wörz, "Bandwidth-Efficient Turbo Trellis-Coded Modulation Using Punctured Component Codes," *IEEE Journal on Selected Areas in Communications*, vol. 16, pp. 206–218, February 1998.

[121] P. Patel and J. Holtzman, "Analysis of a Simple Sucessive Interference Cancellation Scheme in a DS/CDMA System ," *IEEE Journal on Selected Areas in Communications*, vol. 12, pp. 796–807, June 1994.

[122] M. K. Varanasi and B. Aazhang, "Multistage Detection in Asynchronous Code-Division Multiple-Access Communicatons," *IEEE Transactions on Communications*, vol. 38, pp. 509–519, April 1990.

[123] P. Robertson, E. Villebrun, and P. Höher, "A Comparision of Optimal and Sub-Optimal MAP Decoding Algorithms Operating in the Log Domain," in *Preceedings of the International Conference on Communications*, (Seattle, Unites States), pp. 1009–1013, 28-22 May 1995.

[124] C. E. Shannon, "A Mathematical Theory of Communication," *The Bell System Technical Journal*, vol. 27, pp. 379–423, July 1948.

[125] R. Gallager, "Low Density Parity Check Codes," *IRE Transactions On Information Theory*, vol. 8, pp. 21–28, January 1962.

[126] R. Gallager, "Low Density Parity Check Codes," *Ph.D thesis,M.I.T,USA*, 1963.

[127] M. R. Tanner, "A Recursive Approach to Low Complexity Codes," *IEEE Transactions on Information Theory*, vol. 27, September 1981.

[128] D. J. C. MacKay and R.M. Neal, "Good error-correction codes based on very sparse matrices," *IEEE Transactions on Information Theory*, vol. 45, pp. 399–431, March 1999.

[129] D. J. C. Mackay and R. M. Neal, "Near Shannon Limit Performance of Low Density Parity Check Codes," *Electronics Letters*, vol. 33, pp. 457–458, March 1997.

[130] G. K. Woodward, *Adaptive Detection for DS-CDMA.* PhD thesis, University of Sydney, 1999.

[131] B. Yang, "Projection Approximation Subspace Tracking," *IEEE Transactions on Signal Processing*, vol. 44, pp. 95–107, January 1995.

[132] D. Reynolds and X. Wang, "Adaptive Group-Blind Multiuser Detection Based on a New Subspace Tracking Algorithm," *IEEE Transactions on Communications*, vol. 49, pp. 1135–1141, July 2001.

[133] S. Haykin, *Adaptive Filter Theory.* NJ:Prentice-Hall, 3rd ed., 1996.

[134] A. Chkeif, K. Abed-Meraim, G. Kawas-Kaleh, and Y. Hua, "Spatio-Temporal Blind Adaptive Multuser Detection," *IEEE Transactions on Communications*, vol. 48, pp. 729–732, May 2000.

[135] P. Kafle and A. Sesay, "Iterative semi-blind multiuser detection for coded mc-cdma uplink system," *IEEE Transactions on Communications*, vol. 51, pp. 1034–1039, July 2003.

[136] S. Zhou, B. Muquet, and G. B. Giannakis, "Subspace-Based (Semi-) Blind Channel Estimation for Block Precoded Space-Time OFDM," *IEEE Transactions on Signal Processing*, vol. 50, pp. 1215–1228, May 2002.

[137] L. Hanzo, C. H. Wong, and M. S. Yee, *Adaptive Wireless Transceiver.* John Wiley, 2001.

[138] S. Chen, S. McLaughlin, and B. Mulgrew, "Complex-valued Radial Basis Function Network Part II: Application to Digital Communications Channel Equalisation," *EURASIP Signal processing*, vol. 36, pp. 175–188, March 1994.

[139] S. Chen, S. McLaughlin, and B. Mulgrew, "Complex-valued Radial Basis Function Network Part I: Network Architecture and Learning Algorithms Signal Processing," *EURASIP Signal processing*, vol. 35, pp. 19–31, January 1994.

[140] R. Tanner, D. G. M. Cruickshank, S. Z. W. H. Sweatman, and B. Mulgrew, "Receivers for Nonlinearly Separable Scenarios in DS-CDMA," *Electronics Letters*, vol. 33, pp. 2103–2105, December 1997.

[141] R. Tanner and D. G. M. Cruickshank, "RBF Based Receivers for DS-CDMA with Reduced Complexity," in *Proceedings of the ISSSTA*, (Sun City, South Africa), pp. 647–651, September 1998.

[142] G. M. A. Sessler, E. Witzel, and F. K. Jondral, "Performance Evaluation of an RBF Based Receiver as Multiuser Detector for TDD-CDMA," in *Proceedings of European Wireless*, (Dresden, Germany), pp. 231–235, September 2000.

[143] S. Haykin, *Neural Networks: A Comprehensive Foundation.* 0201157675, Macmillan Publishing, 1997.

[144] C. M. Bishop, *Neural Networks for Pattern Recognition.* Oxford University Press, 1995.

[145] M. S. Yee, *Radial Basis Function Network Based Mutlilevel Channel Equalisation Techniques for Wireless Communications.* PhD thesis, University of Southampton, 2001.

[146] D. E. Goldberg, *Genetic Algorithms in Search, Optimization, and Machine Learning.* 0201157675, MA USA: Addison-Wesley, August 2001.

[147] R. Prasad and S. Hara, "Overview of multi-carrier CDMA," in *Proceedings of the IEEE International Symposium on Spread Spectrum Techniques and Applications (ISSSTA)*, (Mainz, Germany), pp. 107–114, 22–25 September 1996.

[148] J. Bingham, "Multicarrier modulation for data transmission: An idea whose time has come," *IEEE Communications Magazine*, pp. 5–14, May 1990.

[149] S. Weinstein and P. Ebert, "Data Transmission by frequency-division multiplexing using the discrete Fourier transform," *IEEE Transcations on Communications Technology*, vol. 19, pp. 628–634, October 1971.

[150] X. Gui and T. S. Ng, "Performance of Asynchronous Orthogonal Multicarrier CDMA System in Freqencey Selective Fading Channel," *IEEE Transactions on Communications*, vol. 47, pp. 1084–1091, July 1999.

[151] D. E. Goldberg, *Genetic Algorithms in Search, Optimization, and Machine Learning*. ISBN 0201157675, MA USA: Addison-Wesley, August 2001.

[152] M. Mitchell, *An Introduction to Genetic Algorithms*. Cambrdige, Massachusetts: MIT Press, 1996.

[153] L.-L. Yang, H. Wei, and L. Hanzo, "Multicarrier Code-Division Multiple-Acess Using Both Time-Domain and Frequency-Domain Spreading," *http://www-mobile.ecs.soton.ac.uk*, 2003.

[154] A. F. Naguib, V. Tarokh, N. Seshadri, and A. R. Calderbank, "A space-time coding modem for high-data-rate wireless communications," *IEEE Journal on Selected Areas in Communications*, vol. 16, pp. 1459–1478, October 1998.

[155] V. Tarokh, N. Seshadri, and A. R. Calderbank, "Space-time codes for high data rate wireless communication: performance criterion and code construction," *IEEE Transactions on Information Theory*, vol. 44, pp. 744–765, March 1998.

[156] L.-L. Yang and L. Hanzo, "A space-time spreading assisted broadband multicarrier DS-CDMA scheme: System design and performance analysis," *Submitted for Possible Publication (http://www-mobile.ecs.soton.ac.uk/lly)*, July 2001.

[157] L.-L. Yang and L. Hanzo, "Space-Time Spreading Assisted Broadband MC DS-CDMA," in *Proceedings of IEEE VTC'2002, Spring*, vol. 4, (Birmingham, Alabama, USA), pp. 1881 – 1885, May 2002.

[158] L.-L. Yang and L. Hanzo, "Broadband MC DS-CDMA using space-time and frequency-domain spreading," in *Proceedings of IEEE VTC'2002, Fall*, (Vancouver, British Columbia, Canada), pp. 1632–1636, September 2002.

[159] Proposed TDOC: 662/98 to ETSI SMG2 UMTS Standards, *Space-time block coded transmit antenna diversity for WCDMA*, December 1998.

[160] F. Adachi, M. Sawahashi, and K. Okawa, "Tree-Structured Generation of Orthogonal Spreading Codes with Different Length for Forward Link of DS-CDMA Mobile Radio," *Electronics Letters*, vol. 33, pp. 27–28, January 1997.

[161] S. M. Alamouti, "A simple transmit diversity technique for wireless communications," *IEEE Journal on Selected Areas in Communications*, vol. 16, pp. 1451–1458, October 1998.

[162] L.-L. Yang and L. Hanzo, "Performance analysis of space-time spreading assisted wideband CDMA systems communicating over multipath Nakagami fading channels," *Submitted for Possible Publication (http://www-mobile.ecs.soton.ac.uk/lly)*, May 2001.

[163] J. Torrance and L. Hanzo, "Optimisation of switching levels for adaptive modulation in a slow Rayleigh fading channel," *Electronics Letters*, vol. 32, pp. 1167–1169, 20 June 1996.

[164] J. Torrance and L. Hanzo, "On the Upper Bound Performance of Adaptive QAM in a Slow Rayleigh Fading Channel," *IEE Electronics Letters*, pp. 169–171, April 1996.

[165] C. Tang, "An Intelligent Learning Scheme for Adaptive Modulation," *In Proceedings of the IEEE Vehicular Technology Conference*, pp. 718–719, October 2001.

[166] B. Choi and L. Hanzo, "Optimum Mode-Switching-Assisted Constant-Power Single- and Multicarrier Adaptive Modulation," *IEEE Transactions on Vehicular Technology*, vol. 52, pp. 536 – 560, May 2003.

[167] L.-L. Yang and L. Hanzo, "Performance of generalized multicarrier DS-CDMA over Nakagami-m fading channels," *IEEE Transactions on Communications*, vol. 50, pp. 956 – 966, June 2002.

[168] R. K. Mallik, "The Pseudo-Wishart Distribution and its Application to MIMO Systems," *IEEE Transactions on Information Theory*, vol. 49, pp. 2761 – 2769, October 2003.

[169] P. A. Dighe, R. K. Mallik, and S. S. Jamuar, "Analysis of Transmit-Receive Diversity in Rayleigh Fading," *IEEE Transactions on Communications*, vol. 51, pp. 694 – 703, April 2003.

[170] L.-L. Yang and L. Hanzo, "Slow Frequency-Hopping Multicarrier DS-CDMA for Transmission over Nakagami Multipath Fading Channels," *IEEE Journal on Selected Areas in Communications*, vol. 19, pp. 1211 – 1221, July 2001.

Index